Multi-scale damping characterization of plant fiber composite materials

Taiqu Liu

▶ **To cite this version:**

Taiqu Liu. Multi-scale damping characterization of plant fiber composite materials. Vibrations [physics.class-ph]. Université Bourgogne Franche-Comté, 2021. English. NNT : 2021UBFCD002 . tel-03293384

HAL Id: tel-03293384
https://theses.hal.science/tel-03293384

Submitted on 21 Jul 2021

HAL is a multi-disciplinary open access archive for the deposit and dissemination of scientific research documents, whether they are published or not. The documents may come from teaching and research institutions in France or abroad, or from public or private research centers.

L'archive ouverte pluridisciplinaire **HAL**, est destinée au dépôt et à la diffusion de documents scientifiques de niveau recherche, publiés ou non, émanant des établissements d'enseignement et de recherche français ou étrangers, des laboratoires publics ou privés.

THESE DE DOCTORAT DE L'ETABLISSEMENT UNIVERSITE BOURGOGNE FRANCHE-COMTE

PREPAREE A UNIVERSITE DE FRANCHE-COMTE

Ecole doctorale n°37

Sciences Pour l'Ingénieur et Microtechniques

Doctorat de Mécanique

Par

Taiqu LIU

Caractérisation multi-échelle de l'amortissement des matériaux composites à fibres végétales

Thèse présentée et soutenue à Besançon, le 20 Janvier 2021

Composition du Jury :

M. FONTAINE Stéphane	Professeur	Arts et Métiers (Metz)	Président
M. DEÜ Jean-François	Professeur	CNAM	Rapporteur
M. BOURMAUD Alain	Ingénieur de recherche HDR	Institut IRDL	Rapporteur
M. OUISSE Morvan	Professeur	ENSMM	Directeur de thèse
M. PLACET Vincent	Ingénieur de recherche HDR	Université Franche-Comté	Co-directeur de thèse
Mme. BUTAUD Pauline	Maître de conférences	ENSMM	Co-directeur de thèse
M. GAILLARD Yves	Maître de conférences	Université Franche-Comté	Invité

PH.D. THESIS OF THE UNIVERSITY BOURGOGNE FRANCHE-COMTE

PREPARED AT THE UNIVERSITY OF FRANCHE-COMTE

Doctoral school n°37

Engineering Sciences and Microtechnologies

Ph.D. in Mechanics

by

Taiqu LIU

Multi-scale damping characterization of plant fiber composite materials

Thesis defended publicly on January 20, 2021, in Besançon

Composition of jury::

M. FONTAINE Stéphane	Professeur	Arts et Métiers (Metz)	President
M. DEÜ Jean-François	Professeur	CNAM	Reviewer
M. BOURMAUD Alain	Ingénieur de recherche HDR	Institut IRDL	Reviewer
M. OUISSE Morvan	Professeur	ENSMM	Supervisor
M. PLACET Vincent	Ingénieur de recherche HDR	Université Franche-Comté	Co-Supervisor
Mme. BUTAUD Pauline	Maître de conférences	ENSMM	Co-Supervisor
M. GAILLARD Yves	Maître de conférences	Université Franche-Comté	Invitee

Acknowledgments

Three years has been past, I still remember the first time I came to the lab. There're a lot of good memories in Besancon and France.

First of all, I want to thank my supervisors. This thesis was under the guidance of Morvan, Vincent and Pauline. I have benefited from them not only in the methodology of the research but also the writing of scientific articles.

I would like to express my heartfelt gratitude to Morvan for his constant guidance. The first time we met each other online and I was impressed by his enthusiastic for introducing the lab and tasks in the SSUCHY project to me. The opportunity to work in SSUCHY have broadened my horizon and aroused my interest in research. Thanks for his insightful comments and suggestions, which provide me with many enlightening ideas.

It's my pleasure to work with Vincent during the past three years. Thanks a lot for his helpful guidance and constant encouragement both in my research and life in France. His help makes my life and research easy and enjoyable. He has enough patience to welcome each discussion, even it's in details. I have learned a lot from him especially in cooperation, communication in SSUCHY.

I am also lucky to receive the help from Pauline. She always gives me a feeling of energetic and sunshine, which reduces my pressure and hard time. Her help makes my research and life easier and happier. It is an unforgettable three years working with her, Vincent and Morvan. Here, I would like to extend the sincerest thanks and the highest respect to all of you!

I want to thank Yves for his kindly guidance and help in the nanoindendation. Thanks again for leading me into the fascinating microscale field, the knowledge he taught me will be of everlasting significance to my future research

I would like to express my gratitude to the jury members, Stéphane Fontaine, Jean-François Deü and Alain Bourmaud, for spending time on my manuscript, and all the comments and discussions are valuable which can help my research in the future.

Thanks my colleagues in SSUCHY for their help. Xaiver, Thomas and Stani patiently and carefully helped me to start the experimental research. A lot of progress and growth in experiment during my PhD includes the advice and support from them. It's also a happy time to work with Benjamin and Fadhel, best wishes for you. Thanks to all the colleagues in SSUCHY project and team 'D-Smart', 'T2DC' for their guidance and help! It's my honor to communicate with Prof. Verpoest, Müssig, Scarpa, Aart.

Special thanks to the funding received from the Bio Based Industries Joint Undertaking under the European Union's Horizon 2020 research and innovation program.

Thanks a lot for the help in laser cutting from Gérard, Pascal and Pierre ROUX.

Thanks to Christine, Isabelle and Delphine, who let me know much better the daily work in femto-st.

It's a wonderful time with guitar, piano and music from Jason and Aflah, I hope to enjoy it again in the future. Also, all the best for your Ph.D. and the life in Besancon.

Special thanks to those who help me in my life in France. Prof. Vincent LAUDE picked me up from the train station three years ago when I arrived Besancon, which made an easy start in France. I would like to thanks Tingting, Meiling, Ning, Shaoqi, Yuxuan, Mingkai, Xiaoyu, Kaijun, Yikai, Hao, Kejun, Qingxiang, Xueyan, Mengjia ... etc. It's a nice time with them.

I want to express my gratitude to Prof. Hou, who help me a lot to do research and study abroad.

I sincerely thank my parents. I have almost not accompanied them during the past 10 years, but they have given me the best love and warmest harbor in the world. Thank you for your continuous support and encouragement.

I want to express my deep gratitude to my wife. You are extremely strong, considerate, and always supported me silently without any complaints. Maybe any words of praise are not enough to summarize your spirit. You are everything to me, and I was so blessed when god sent you for me.

There is no doubt that there are still many people who deserve to be thanked and may my gratitude warm them.

See you in the future!

Contents

Acknowledgments iii

Contents v

Preamble 1

General introduction 5

I Literature review 13

I.1 Introduction 16

I.2 Experimental techniques for the characterization of damping 20

I.2.1 Quasi-static and low frequency characterization: dynamic mechanical analysis 20

I.2.2 Low to mid-frequency characterization: modal analysis 21

I.2.3 High frequency characterization : wave number-based approaches 22

I.3 Review of studies on the damping behavior of PFCs 22

I.3.1 Meso scale parameters 22

I.3.2 Microscale parameters 25

I.3.3 Testing and surrounding conditions 32

I.3.4 Limitations of existing PFC damping studies 36

I.4 Conclusions 38

II Meso scale: dynamic mechanical analysis 41

II.1 Introduction 45

II.2 Materials and methods 46

II.2.1 Generalities on DMA 46

II.2.2 Experimental setup 49

II.2.3 Composite materials 53

II.2.4 Water aging tests 58

II.3 Results and discussion . . . 59
II.3.1 Comparision of DMA results from bending mode and tension mode . . . 59
II.3.2 Dynamic mechanical properties of GreenPoxy . . . 60
II.3.3 Damping properties of composite materials at ambient temperature . . . 63
II.3.4 Damping properties of composite materials in a wide temperatures range . . . 70
II.3.5 Evolution of damping properties as a function of frequency . . . 75
II.3.6 Influence of moisture content on UD flax reinforced composites . . . 80
II.4 Conclusions . . . 83

III Macro scale: modal analysis . . . 87
III.1 Introduction . . . 90
III.2 Materials and methods . . . 91
III.2.1 Generalities on experimental modal analysis . . . 91
III.2.2 Materials . . . 95
III.2.3 Experimental setup and post-processing . . . 96
III.2.4 Water aging . . . 98
III.3 Results and discussion . . . 99
III.3.1 Optimization of the setup in free-clamped boundary conditions . . . 99
III.3.2 Modal analysis in free-free configuration . . . 105
III.3.3 Modal analysis in free-clamped configuration . . . 111
III.3.4 Comparison of damping properties in modal analysis and DMA tests . . . 114
III.3.5 Influence of water aging in free-free boundary conditions . . . 117
III.4 Conclusions . . . 118

IV Micro scale: dynamic nanoindentation . . . 121
IV.1 Introduction . . . 124
IV.2 Materials and methods . . . 125
IV.2.1 Theory of nanoindentation and its applications . . . 125
IV.2.2 Selection of existing research on nanoindentation . . . 128
IV.2.3 Tested materials . . . 129
IV.2.4 Experimental setup . . . 129

IV.3 Results and discussion . . . 135
IV.3.1 Verification of the effect from instrument on the measurement of storage modulus and loss factor . . . 135
IV.3.2 Damping identification of GreenPoxy using CAM method . . . 136
IV.3.3 Damping identification of FGUD using CSM method . . . 139
IV.3.4 Damping identification of FGUD using CSM+CAM method . . . 144
IV.4 Conclusions . . . 149

Conclusions and perspectives . . . 151

A Appendix . . . 159
A.1 List of Symbols . . . 160
A.2 Verification of measurement in free-free boundary conditions . . . 163

References . . . 165

Figures List . . . 195

Tables List . . . 203

Preamble

The present thesis was done within the framework of the SSUCHY project (Sustainable structural and multifunctional bio-composites from hybrid natural fibres and bio-based polymers), a project which has received funding from the Bio-Based Industries Joint Undertaking Initiative (BBI JU) under European Union's Horizon 2020 research and innovation program under grant agreement No. 744349.

SSUCHY PROJECT

The project SSUCHY falls within the framework of the development and optimization of innovative and eco-efficient processes and constituents for structural and multifunctional bio-based composites. SSUCHY aims at exploiting the intrinsic and differentiating properties of plant fibres and biopolymers derived from lignocellulosic feedstock to develop fully bio-based composites with improved functionalities. The main driver behind this project is not only to substitute conventional fossil-based materials with more sustainable bio-based ones but also to achieve improved functionalities that surpasses those of fossil-based ones. Enhanced functionalities are, in addition to load-bearing resistance and weight reduction of structures, enhanced durability, vibration damping, vibro-acoustic control and fire retardancy while retaining an essentially recyclable and, for certain applications, biodegradable character. The project partners and their positioning over the value chain are shown in Figure 1.

- Université de Franche-Comté – UFC (Coordinator), University, France
- Centre National de la Recherche Scientifique - CNRS, National Center for Scientific Research, France
- EADCO GmbH, SME, Germany
- École Nationale Supérieure Arts & Industries Textiles - ENSAIT, France
- IAR, the French Bioeconomy Cluster, Non-profit organisation, France
- École Nationale d'Ingénieurs de Tarbes, France
- Katholieke Universiteit Leuven, University, Belgium
- Linificio e Canapificio Nazionale Srl (LCN), SME, Italy
- NOURYON, Industry, The Netherlands
- NPSP BV, SME, The Netherlands
- University of Stockholm, University, Sweden
- Trèves, Industry, France
- Université de Bourgogne – ICMUB, University, France
- University of Bristol, University, United Kingdom
- Università cattolica del Sacro Cuore, University, Italy
- Wilson Benesch, SME, United Kingdom

- University of Derby, United Kingdom

FIGURE 1 – Partners in SSUCHY project

As an international project in the frame of European Union's Horizon 2020 research and innovation program, many partners are working on the different aspects related to raw material supply (Università cattolica del Sacro Cuore, University of Stockholm) and transformation (CNRS, ENSAIT, École Nationale d'Ingénieurs de Tarbes, Linificio e Canapificio Nazionale Srl, Université de Bourgogne), test on bio-based composites and sandwich materials (Université de Franche-Comté, KU Leuven, NOURYON, NPSP, University of Bristol), and industry application (EADCO GmbH, Trèves, Wilson Benesch, University of Derby).

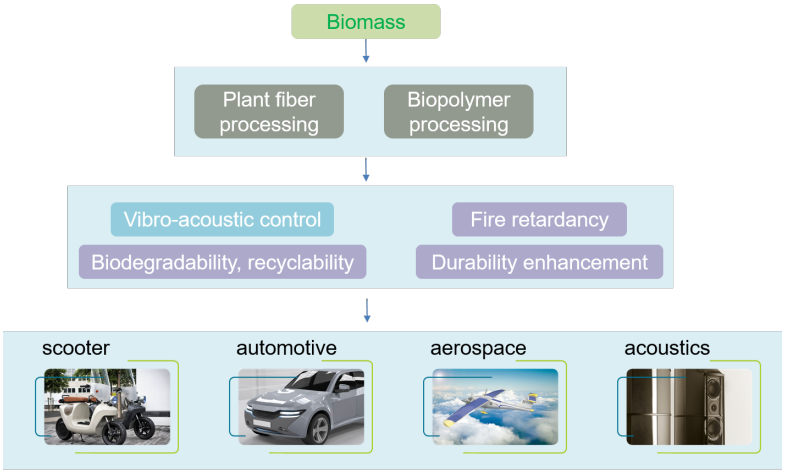

FIGURE 2 – Technology roadmap of SSUCHY project

Figure 2 shows the technology roadmap of SSUCHY project. The SSUCHY project intends to contribute to the development of bio-based composite products with advanced functionalities and high structural properties for transportation sectors and in high value market applications for bio-based composites to semi-structural and functional applications in the transportation area (ground transportation and aerospace) and create new opportunities in high value market niches such as the acoustic and electronic sectors. The core objectives are shown in Figure 3.

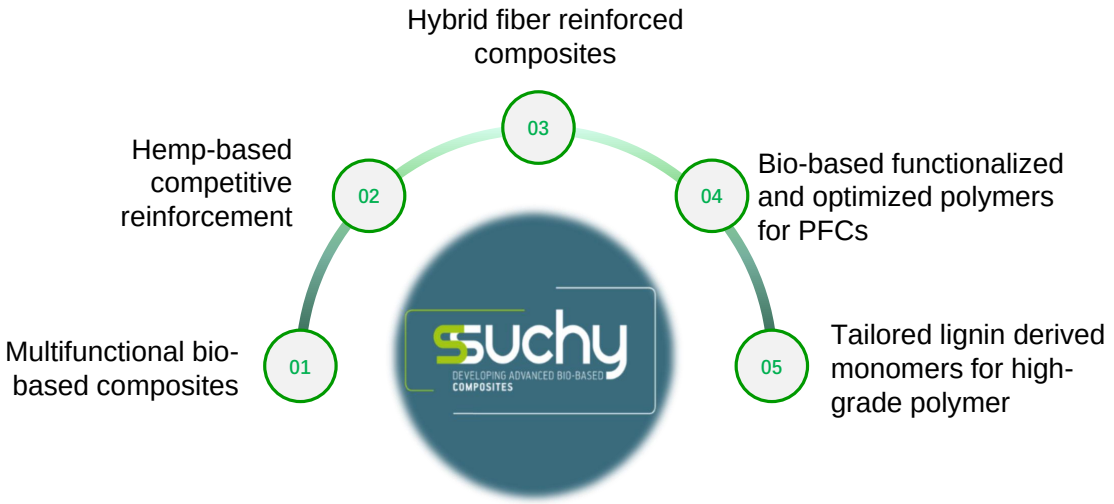

Figure 3 – Five core objectives in SSUCHY project

Among them, one of the SSUCHY objectives is to develop a Hemp-based competitive reinforcement for composite applications in order to complement the competitive flax-based reinforcements already on the market. The advantage of the availability and low cost of hemp fibers will be taken, along with their technical and environmental-friendly characteristics to market a high-performance plant fiber reinforcement for composite application at a competitive price. In this work, the performance of the newly developed hemp fabrics composites is compared to marketed flax-based reinforcements.

Tasks as part of SSUCHY project

The tasks in this thesis aim at understanding the behavior of bio-based composite materials in terms of vibration damping in order to design and manufacture efficient structures with increased damping properties without deterioration of functional properties (static, creep, temperature, fire behavior).

Considering the requirements for the product demonstrators in the field of ground transportation and aerospace, reductions in vibration and noise are expected with bio-based floor and trim panels. In addition, higher damping materials are welcome to reduce the impact of resonance on sound quality in the acoustic industry.

The first task is related to a macro analysis of bio-based composite, focused on the dynamic characterization of components and composite plates in order to qualify the mechanical properties with a specific focus on damping properties. Meanwhile, temperature and moisture effects will be investigated as they are expected to play a major role in the damping properties. However, other functional properties will be addressed in relationship to the other work packages of the project (static behavior, creep, inflammability).

Then, a novel micro-approach for the estimation of damping properties of bio-based composite will be developed. Finally, the link between geometrical, mechanical properties of interest at the micro scale and dynamical properties at the macro scale will be described by a suitable combination of experimental characterization results using various setups, numerical simulations.

General introduction

Petro-based materials have made an irreplaceable promotion effect on the progress of science and technology and the improvement of life. However, nowadays, people pay more and more attention to the effect of human activities on the environment since global warming and pollution problems are severe. Composite materials with plant fibers as reinforcement are attractive materials to contribute to the lowering of environmental impact of engineering thanks to their lightweight, high specific stiffness and also due to the recyclable and degradable character of the fibers. Thus, plant fiber composites are promising solutions to develop lightweight sustainable structures.

Challenge : understand and control the damping properties of plant fiber composites to optimize the vibratory and vibro-acoustic behaviour of sustainable structures and products

These materials, named Plant Fiber Composites (PFCs) in this manuscript, are then becoming more and more popular in many application fields. When compared to synthetic fibers, such as glass fibers, it has been observed that they seem to be good candidates to improve the damping behavior of composite materials and structures.

Indeed, classical glass or carbon fibers based composites have been developed for years for providing the highest possible stiffness/strength-to-mass ratio. High performance materials are now available on the market and their use in almost all industrial fields is now effective. However, the base materials combined through efficient manufacturing strategies, result in composite structures with poor vibro-acoustic properties. In particular, the damping properties are very low, resulting in high vibration and noise levels in operational conditions. Reducing noise and vibration levels requires curative solutions, some of them being bio-based, which finally results in an increase in the mass of the structure and in the complexity for manufacturing. Using plant fibers in composite materials constitutes a promising strategy to provide a breakthrough in the damping properties of composite structures. Indeed, most of the results presented in open literature based on experimental characterization of composite materials and structures embedding plant fibers show that high damping values can be obtained [Pinto 20, Assarar 15, Duc 14b]. In particular, in the fiber direction with continuous reinforcement, the composites

exhibit very interesting specific Young's modulus, higher than for glass fibers, while damping is in the order of 2% (with conventional thermoset resins like epoxy, polyester or acrylic), which is 10 times better than glass or carbon fibers [Shah 14]. The reasons for these good damping properties of natural fibers remain largely unexplained. One of the objectives of this thesis is to contribute to the understanding of the damping capacity of bio-based composites.

Plant fibers are complex materials. Their heterogeneous and hierarchical microstructure, complex morphology and hygroscopicity lead to specific static, dynamic and fatigue behavior, including nonlinearities and moisture activation of some mechanisms. This complex structure, involving an heterogeneous polymeric composition, various cell wall layers and their interfaces as well as a central void (called lumen) could also be at the origin of additional energy dissipation mechanisms in plant fiber composites. It makes the damping sources more complex to comprehend since these ones are associated to the ones commonly observed in synthetic fiber composites and related to the viscoelastic nature of the matrix, friction at the interface between fibers and matrix, inelastic and irreversible behaviors such as damage and/or plasticity. All these specificities of plant fibers and their composites can be perceived as weak spots. However, they offer also a great opportunity to implement new functionalities and thus to design a new family of advanced and multifunctional materials which are renewable. In particular, there are still not valued opportunities in vibroacoustic control by employing plant fibres' damping capacity within a composite to mitigate resonance.

Plant fiber

Plant fiber refers to fiber extracted from plants grown in nature, such as cotton, flax, bamboo, etc. Since the dawn of civilization, mankind has benefited from plants not only in food and oil but also in clothes, ropes and tools [Navin 94]. There are many types of plant fibers, and they are usually divided into different families based on the parts obtained from plants such as stems, leaf, seeds, and fruits, etc.

Figure 4 shows the series of some common fibers and the classification method comes from [Jawaid 11]. It is important to consider the stiffness and strength when they are using in engineering fields. Their absolute tensile properties are shown in Figure 5 (a). As shown, bast fibers such as flax, hemp and jute fiber should be the best solution when considering both tensile stiffness and strength.

In addition, the source of materials should take into account the factors such as easy access and localization. Moreover, the development of high-performance and low-cost hemp fiber is one of the core goals of the SSUCHY project. Therefore, this research will focus on the damping performance of flax and hemp fiber reinforced composites. Flax is the most developed and characterized plant fibre and is abundant in Europe. It will be considered as a reference for benchmark purpose.

The schematic representation of the flax and hemp fiber structure is shown in Figure 5 (b). It is composed of primary and secondary walls [Bourmaud 12a][Li 17a]. From the perspective of biochemistry and structure, plant fibers can be divided into two categories [Bourmaud 18]. The first type is xylan type, such as jute and

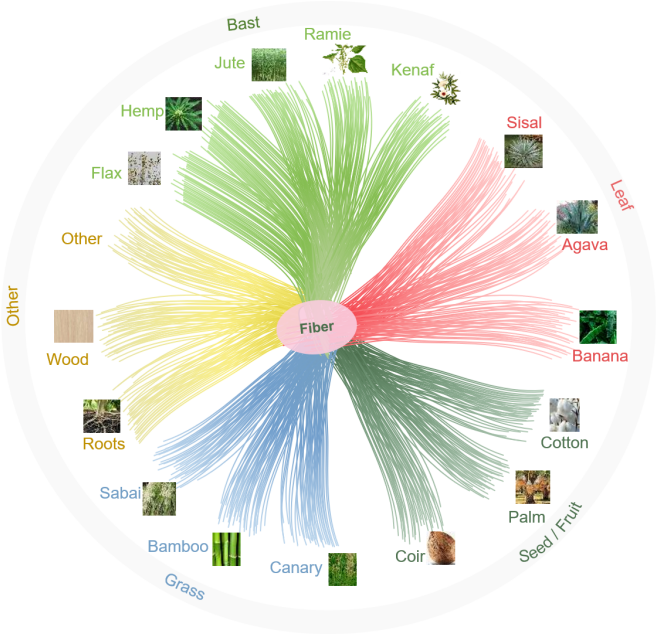

FIGURE 4 – Classification of plant fibers

kenaf fiber. These walls are characterized by high microfibrillar angle (MFA) and high lignin and xylan content. The second type is gelatinous fibers, such as flax and hemp. They are rich in galactose-based polymer and have a cellulose content of up to 85% [Gorshkova 10].

However, their MFA is small and the lignin content is very low. In particular, the distribution of cellulose in the secondary wall is generally distributed at a microhelix angle (the cellulose microfibril angle relative to the longitudinal axis of the fibre (MFA)). The main factors affecting the mechanical properties of plant fibers are cellulose content and MFA [Bourmaud 18]. High cellulose content and small MFA lead to high modulus. In addition, plant fibers are also susceptible to

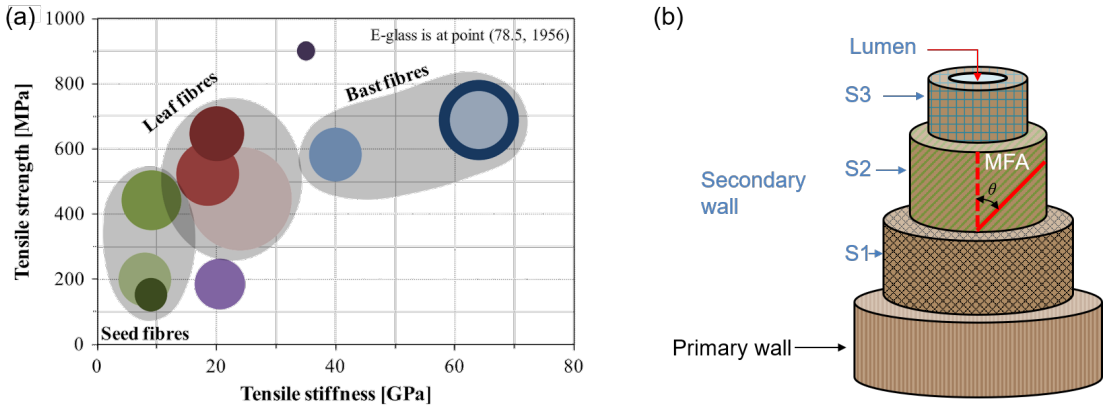

FIGURE 5 – (a) Absolute tensile properties of different series of fiber [Shah 14] (b) The schematic representation of the flax and hemp fiber structure

humidity due to the hydrophilic nature of the carbohydrates constituting the cell wall, which in turn affects the mechanical properties and the dimensions of the fibers.

Plant fiber composites

The plant fiber composites are composed of reinforcement and matrix. This is similar to other kinds of fiber-reinforced composites. The matrix mainly uses two types of polymer families : thermoset and thermoplastic. Typical thermoset matrix materials include epoxy resin, phenolic resin, saturated polyester, unsaturated polyester, etc. and typical thermoplastic matrix materials include polypropylene (PP), polylactic acid (PLA), nylon, ABS resin, polyetherimide, etc. Currently, the widely used reinforcements can be divided into short fibres, non-crimp, non-woven and woven reinforcements.

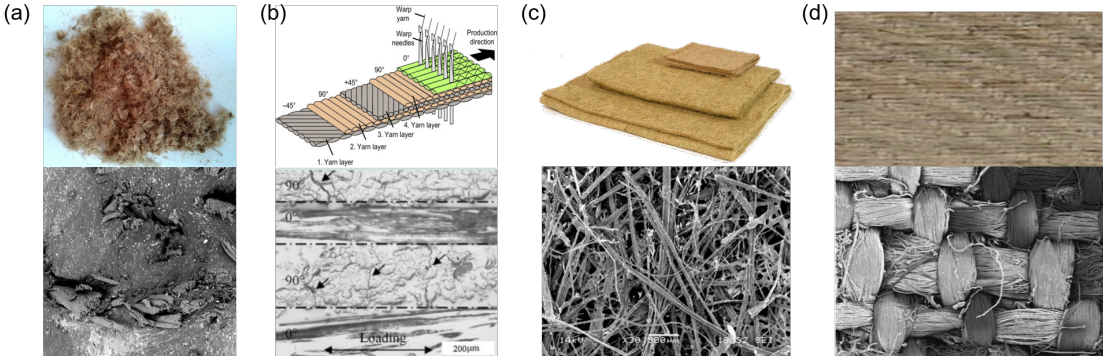

FIGURE 6 – Different reinforcements and micro-structures of (a) short fiber [Datta 17] (b) non-crimp [Schrank 17, Liang 14](c) non-woven [Reinders , Martin 16] and (d) woven fabric [Song 12, Corbin 20b]

Generally, short fibers are produced during the scutching and hackling of flax and hemp stems or using all-fibers lines. Some examples of short fibers are shown in Figure 6 (a). It can also be further processed into yarn and non-woven fabrics. Non-crimped fabric is composed of multiple layers of unidirectional fiber tapes placed in different directions, as shown in Figure 6 (b). These layers are then usually stitched into a fabric and they have obvious hierarchical micro-structure on the cross-section [Lomov 11, Liang 14]. Non-woven fabric is one kind of sheet or web-like structure made by bonding fibers together mechanically, thermally or chemically, as shown in Figure 6 (c). Their micro-structure and the difference in splitting of the bundles, shape and orientation depends largely on the manufacturing route [Martin 16]. Figure 6 (d) shows the twill woven fabric and the woven fabrics reinforcements are produced on a loom. The number, size and arrangement of the warp and weft yarns determine the weave pattern, such as plain, satin, twill, etc.

Motivation and objective of the thesis

The damping properties of plant fiber composites are considered to have a good application prospect. However, the damping mechanisms of plant fiber composites are complex and requires more research to be fully controlled and exploited in sustainable structures and products.

Up to now, researches regarding damping properties of PFCs have been focused on their damping performances at the macro scale and no clear understanding of the physical mechanisms responsible for the damping performances are available at this time. It is then also necessary to investigate the damping performance of PFCs at the microscale to provide ways and means to understand and possibly tailor the damping of these materials.

Therefore, the main objective of this thesis is to provide a better characterization and understanding of the damping behavior of several PFCs made of high-grade flax and hemp reinforcements and organic matrices. Investigations will be performed at different scales using different experimental methods to evaluate the role of the different constituents in the damping properties of PFCs and also identify the main sources of energy dissipation. Several microstructural and material parameters (including matrix types, fiber types, weave pattern) and loading/environmental parameters (temperature, frequency and moisture content) will be studied in details to evaluate their influence on damping properties based on DMA and modal analysis. One of the objective of this work is to provide an accurate description of the evolution of damping properties as a function of temperature, moisture content and frequency. The damping behavior of plant fiber composites is also expected to be known on a wide temperature and frequency ranges which can cover most of the engineering applications. One of the objectives of this thesis is also to put the focus at the microscale by measuring the in situ damping properties of the PFCs' constituents.

Thesis outline

The thesis outline is schematically presented in Figure 7. This manuscript is divided into four chapters and more details are given in the following paragraphs.

Chapter I introduces the background of the damping behavior of some common materials such as polymer, metal and composites. Then, the influence of meso and micro scale parameters as well as surrounding conditions on the damping of PFCs is reviewed. Some key points like variability, hierarchical aspects and sensitivity of the mechanical properties are thus discussed. The review provides a first reference for the factors that affect damping properties in PFCs to be used in engineering applications in various fields including automotive, aerospace, music devices. It also highlights the current shortcomings on knowledge on damping of PFCs. The Ashby diagram built from the data available in literature constitutes a first tool to

select materials considering the compromise between loss factor and stiffness that can be used for engineering design considerations, and provides a starting point for the work presented here.

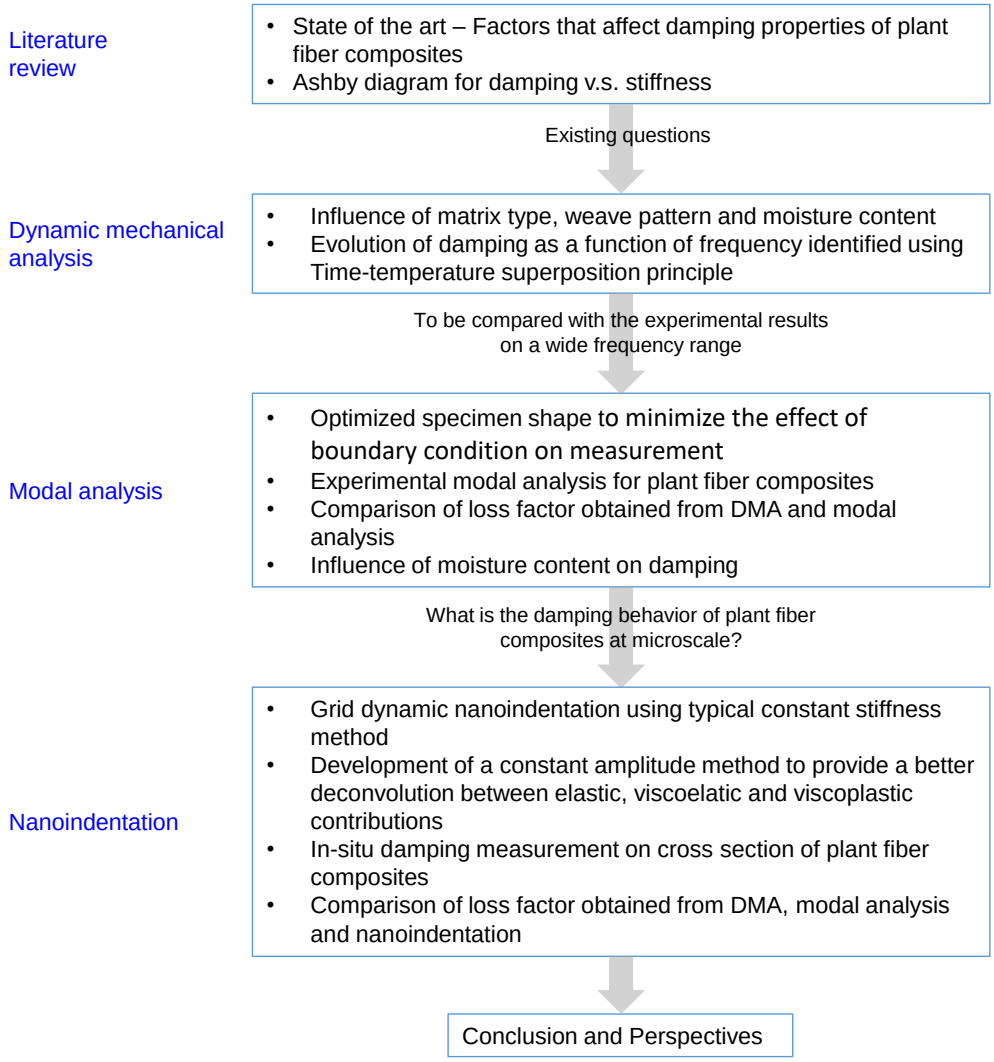

FIGURE 7 – Schematic diagram of the thesis

Chapter II states the dynamic mechanical properties of plant fiber composites at different temperatures and frequencies based on Dynamic Mechanical Analysis (DMA) tests. At first, the details of materials, which include unidirectional composites, thermoset, thermoplastic-based composites and woven fabric reinforced composites, used in this thesis are described. Relevant information, such as loss factor and storage modulus of PFCs are characterized with different matrices and fiber reinforcements. The influence of matrix type, fiber architecture, woven pattern, temperature and frequency are investigated. Also, the damping properties of flax fiber reinforced green epoxy composites under different humidity and temperature conditions are also studied considering the sensitivity of plant fibers to moisture.

Chapter III investigates the damping properties around natural frequencies of plant fiber composites using modal analysis. Optimization of the experimental setup is processed at first to minimize the influence from boundary conditions on the estimation of the damping properties according to numerical model. The damping properties of three different composites (unidirectional thermoset and thermoplastic-based composites, and woven fabric reinforced composites) are investigated. Then, the damping properties obtained by DMA and modal analysis are compared. Besides, flax fiber reinforced green epoxy composites with different moisture contents is studied by modal tests.

Chapter IV presents the dynamic properties of plant fiber composites at microscale by means of nanoindentation. An alternative technique to identify damping properties with Constant Amplitude Method (CAM) is developed and compared to the traditional Continuous Stiffness Measurement method (CSM). The verification in damping identification using CAM method is first used on neat GreenPoxy. Results are compared to that obtained from DMA method. Then, the experiments are done with CSM and CAM method on flax/GreenPoxy composites. Results point out the contribution of each component to the damping of composite materials. Furthermore, a comparison of the measured properties (storage modulus and loss factor) obtained from CAM and CSM method is proposed. Finally, the damping properties of flax fiber composites obtained using DMA, modal analysis and nanoindentation are compared.

Some parts of the chapters in this manuscript have been or will be submitted in the form of scientific articles in international peer-reviewed journals. Among them, the section on factors that affect the damping characteristics of PFCs in Chapter I was submitted in Composites Structures journal and is currently under review. Other parts of the manuscript were also extracted and compiled in other manuscripts, currently in a draft form.

Chapitre I
Literature review

I.1 Introduction 16

I.2 Experimental techniques for the characterization of damping 20

I.2.1 Quasi-static and low frequency characterization: dynamic mechanical analysis 20

I.2.2 Low to mid-frequency characterization: modal analysis . . 21

I.2.3 High frequency characterization: wave number-based approaches 22

I.3 Review of studies on the damping behavior of PFCs 22

I.3.1 Meso scale parameters. 22

I.3.2 Microscale parameters. 25

I.3.3 Testing and surrounding conditions. 32

I.3.4 Limitations of existing PFC damping studies. 36

I.4 Conclusions 38

Graphical abstract

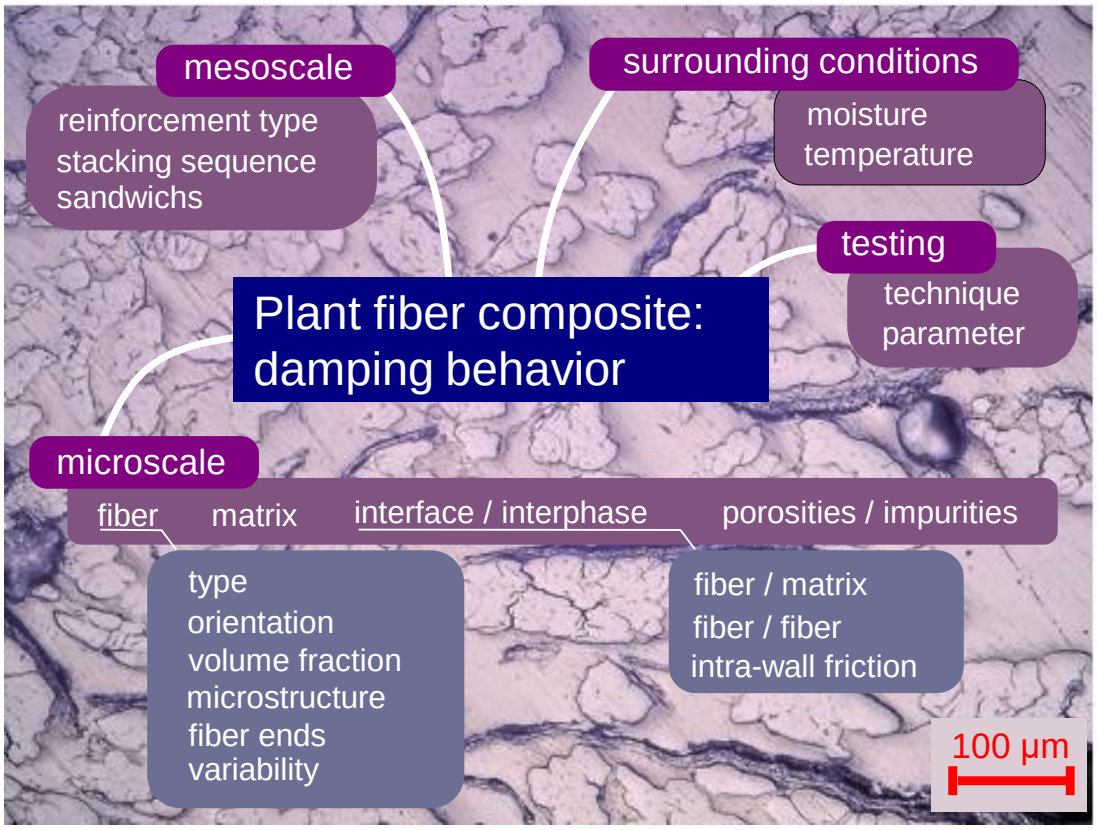

Highlights:

- ◇ Description of the damping source of the parameters that affect damping properties.
- ◇ Ashby diagram regarding stiffness and damping is built.

Résumé

Ce chapitre passe en revue les caractéristiques d'amortissement des composites à base de fibres végétales (PFC) en accordant une attention particulière à leurs performances par rapport aux composites à base de fibres synthétiques (SFC). En effet, les PFC sont de plus en plus populaires dans de nombreux domaines d'application. Leurs spécificités par rapport aux fibres synthétiques, telles que les fibres de verre, en font de bons candidats pour améliorer le comportement d'amortissement des matériaux et structures composites. L'influence des paramètres à différentes échelles ainsi que les conditions environnantes sont examinées. Des rapports contradictoires sont parfois trouvés et les connaissances existantes sur le comportement

d'amortissement des PFC sont parfois déficientes ou ambiguës. Certains points clés comme la variabilité, les aspects hiérarchiques et la sensibilité des propriétés mécaniques sont ainsi discutés. Cette étude fournit une première référence pour les facteurs qui affectent les propriétés d'amortissement des PFC utilisés dans les applications d'ingénierie dans divers domaines, y compris l'automobile, l'aérospatiale, les appareils de musique. Elle met également en évidence les lacunes actuelles dans les connaissances sur l'amortissement des PFC. Le diagramme Ashby, construit à partir des données disponibles dans la littérature, constitue un premier outil pour sélectionner les matériaux en tenant compte du compromis entre le facteur de perte et la rigidité qui peuvent être utilisés pour des considérations de conception technique.

Abstract

This chapter reviews the damping characteristics of plant fiber composites (PFCs) with particular attention regarding their performances with respect to synthetic fiber composites (SFCs). Indeed, PFCs become more and more popular in many application fields. Their specificities when compared to synthetic fibers, such as glass fibers, make them a good candidate to improve the damping behavior of composite materials and structures. The influence of meso and microscale parameters as well as surrounding conditions are reviewed. Contradictory reports are sometimes found and the existing knowledge on the damping behavior of PFCs is sometimes deficient or ambiguous. Some key points like variability, hierarchical aspects, and sensitivity of the mechanical properties are thus discussed. This review provides a first reference for the factors that affect damping properties in PFCs to be used in engineering applications in various fields including automotive, aerospace, music devices. It also highlights the current shortcomings in knowledge on the damping of PFCs. The Ashby diagram built from the data available in literature constitutes a first tool to select materials considering the compromise between loss factor and stiffness that can be used for engineering design considerations.

I.1 Introduction

Vibration and noise problems caused by mechanical equipment or vehicles have become more and more prominent. Meanwhile, the demand for modern industrial products has become more versatile, lightweight, durable, and comfortable. People have to find some effective methods, such as changing the structure or using damping materials to mitigate the impact of vibration [Chung 03, Buravalla 01]. The use of damping materials improves people's living and working conditions and creates quiet and comfortable surroundings. With the development of the petrochemical industry, the oil began to expand from the original fuel source to the use of by-products [Väisänen 17, Le Duigou 14, Zhang 05]. Resins, asphalt, and rubber began to enter the industrial field of large-scale applications, especially for reducing vibration [Zeng 01]. However, they cannot be used alone due to their low stiffness. In most cases, they are used together with wood or metal sheets in sandwich structures to make up for the shortcomings of each other. A sandwich structure has characteristics of sound insulation and vibration damping, which cannot be provided by a single material in addition to the strength properties compared with pure wood board or metal plate [Butaud 16, Li 05, Wang 00, Araújo 09].

With the development of high-strength fibers such as glass fibers and carbon fibers, attempts have been made to mix fibers and polymers in a specific ratio to manufacture fiber-reinforced composites [Mallick 07]. It has been found that this type of material has outstanding performances in specific strength, specific modulus, fatigue strength, impact resistance, damping and devisable characteristics than pure metal material or polymers [Chandra 99]. In particular, people currently want to reduce energy consumption by using some lightweight materials, and the advantages of composite materials in this respect make it a significant trend to replace traditional materials, especially in the fields of aerospace, transportation, wind power, etc. [Hine 19, Grunenfelder 17, Liu 18]. Many studies have focused on increasing strength, modulus, and enhanced crashworthiness as structural components when composite materials began to be of interest [Nguyen 16]. At present, composite materials are also intended to improve the damping performances of the structures while retaining the other primary structural functions.

However, the large-scale application of petroleum-based compounds has also brought about some adverse effects. Engineers should now consider environmental impact at each stage of the life cycle during the implementation of damping materials since petroleum-based products are difficult to be degraded by nature [Joshi 04]. Plant fibers become more and more concerned because of abundant reserves, while being renewable, low cost, quickly obtained and processed, degradable, lightweight, possess relatively high specific modulus, and other advantages [Väisänen 17, Joshi 04, Hardiman 17, Yan 14]. The properties of many plant fibers coming from hemp, flax, jute, ramie, kenaf, banana, agave, doum palm, pine cone, etc. are investigated [Thiruchitrambalam 12, Shah 14, Ramesh 19]. Compo-

sites with different types of reinforcement exhibit different mechanical properties due to the biochemical composition and structure of the cell wall, especially their cellulose content and their microfiber angle [Bourmaud 18].

The currently widely used plant fibers have a short growth cycle, are easy to survive, have low dependence with pesticides and fertilizers, and low energy consumption and chemicals during fiber extraction. Plant fibers become a sustainable material of choice for sound-insulation and damping in automotive, aerospace, musical instruments, and other applications due to their unique internal structure [Saba 16]. In particular, their role in automotive parts includes ceilings, coat racks, seatbacks, instrument panels, and some structural components such as luggage compartments, bottom guards, etc., is increasing due to weight and cost advantages [Khalfallah 14, Hagnell 19].

The development of the transportation industry is increasingly moving toward environmental impact minimization, energy use limitation and mass reduction. Plant fiber-reinforced composites (PFCs) have been mainly used, up to now, for mass saving as a low-cost and sustainable solution. As essential lightweight materials, PFCs can also overcome the mechanical and physico-chemical properties of conventional materials to a certain extent, and they could solve some critical problems that cannot be addressed by traditional materials in engineering structures. Some of their intrinsic properties, for instance their natural damping, can be exploited to implement new and advanced functionalities in structures. However, several issues, such as moisture absorption, creep, and durability, are urgently needed to be solved to support the development of these solutions for engineering structures on a large scale.

In the stiffness-loss map proposed by Lakes et al. for different material families, it can be seen that composite materials are good compromises between stiffness and loss factor [Brodt 95, Lakes 98]. A similar plot is proposed here for another set of materials: a few metals, polymers, and several PFCs and SFCs. Loss factor and storage modulus or Young's modulus at ambient temperature are collected from literatures and plotted in Figure I.1. It clearly points out that the loss factor of PFCs is generally much higher than SFCs. PFCs have reported values of loss factors comprised between 0.7% and 14%, while values are typically comprised between 0.24% and 2.5% for SFCs.

Due to their multiple components and intricate manufacturing process, composite materials exhibit different damping mechanisms when compared to conventional materials such as metals. The sources of energy dissipation in synthetic fiber reinforced polymer composites are quite well described and documented in literature [Chandra 99, Gibson 92, Gibson 91, Nelson 78]. They are mainly: (1) viscoelastic nature of the matrix and/or fiber materials, (2) damping due to interphase, (3) damping due to inelastic and irreversible behaviors such as damage and/or plasticity. By contrast, the damping behavior of PFCs, even if already documented [Duc 14b, Duc 14a] is not fully covered. Furthermore, the various effects on damping are observed when plant fibers are introduced in polymer matrices

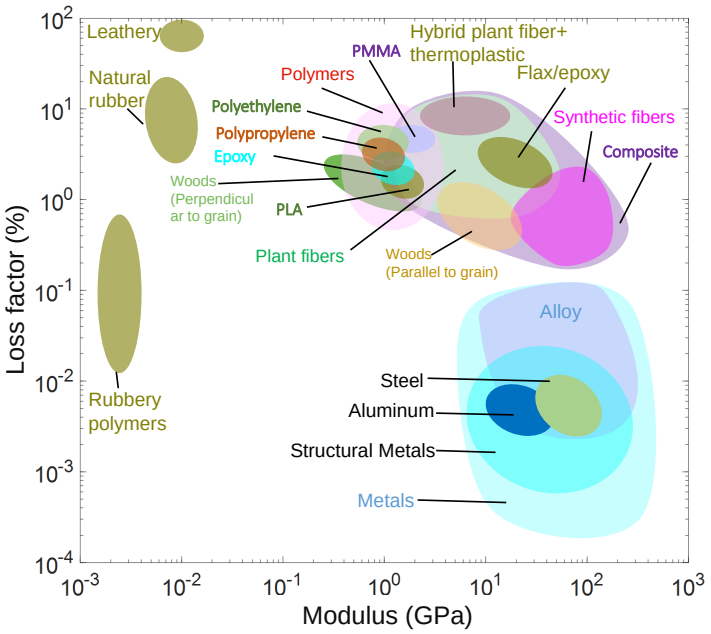

FIGURE I.1 – Ashby diagram: loss factor v.s. modulus at ambient temperature (summarized from refs.[Araújo 09, Duc 14b, Margem 10, Joseph 10, Jawaid 13, Towo 08, Saha 99, Mylsamy 11, Suresh Kumar 14, Sreenivasan 15, Ray 02, Pothan 03, Daoud 17, Shinoj 11, Karaduman 14, Mohanty 06, Etaati 14, Amenini 19, Mahmoudi 19, Li 17c, Ashworth 16, Cihan 19, Zhang 19, Essabir 13, El-Hafidi 17, Liang 10, Le Guen 16, Assarar 15, Rueppel 17, Madera-Santana 09, Mazuki 11])

depending on the nature of the polymer, stiffness, textile architecture and yarn lengths [Duc 14b]. The physics underlying their particular behavior is not yet fully understood and require additional research efforts.

Plant fiber composites differentiate from the conventional ones in terms of composition, and microstructure. These particularities lead to specific static and fatigue behavior, including nonlinearities [Jeannin 19a, Jeannin 19b], stiffening effects [Haggui 19] and moisture activation of some mechanisms [Launay 13, Zai 09, Berthelot 08]. These microstructural particularities could also be at the origin of additional energy dissipation mechanisms. Indeed, unlike most synthetic fibers such as glass and carbon fibers, plant fibers often have unique microstructures and morphologies, notably different cell wall layers and a complex cross-sectional area which varies along the fiber length [le Duigou 17, Bourmaud 16, Baley 19]. In addition to this complex morphology, plant fibers have also a very hierarchical organization with different layers and sublayers made of a mixture of carbohydrates and polyphenols [Hosseinaei 11, Goubet 02]. This polymer-based composition impart them viscoelastic properties [Keryvin 15a, Cisse 15, Van Hazendonk 96, Biagiotti 04,

Bismarck 02]. Plant fibers are also sensitive to moisture and temperature due to the hydrophilicity of some of their wall constituents and also due to their hollow morphology [Zhang 01, Péron 19, Senthilrajan 19a].

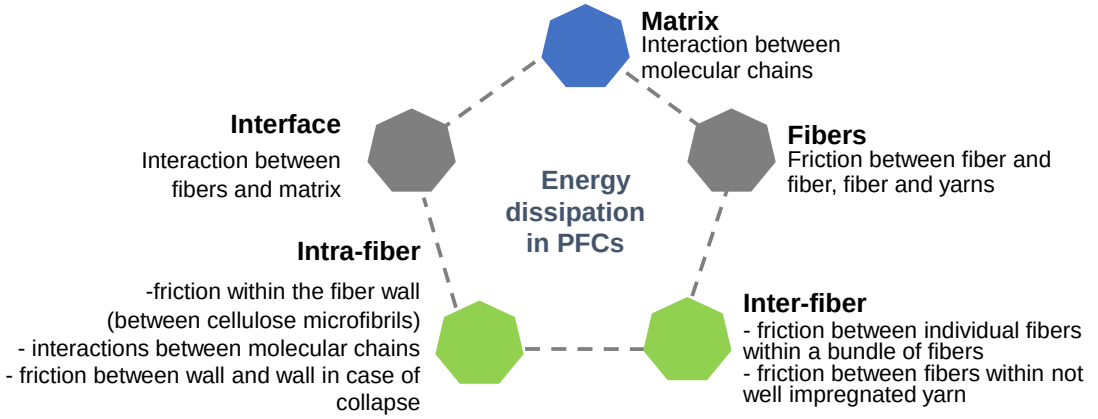

Figure I.2 – Energy dissipation in PFCs

In general, the energy dissipation in PFCs can be summarized in Figure I.2. PFCs are made of single individual fibers but also bundle of fibers. Friction at the interface between individual fibers within the fiber bundle, internal friction within fiber wall (between the heterogeneous polymers constituting the wall and particularly between the rigid cellulose microfibrils and the amorphous polymers in which they are embedded) [Duc 14b, Duc 14a, Duc 14c] are also potential sources of damping. Additionally, plant fibers have a finite length when compared with synthetic fibers. The effect of such discontinuities, even for continuous reinforcement, on the damping behavior of PFCs can be questioned and deserves to be investigated. It is proved that the mechanical and damping properties of PFCs depend on many factors, such as the chemical composition of the reinforcing fibers, fiber length and diameter, fiber orientation, sequence, and fiber/matrix interface [Sathishkumar 17]. It was previously reported that the incorporation of stiff fibers affects the damping behavior of matrices by changing the movement of polymer chains [Datta 02, Harris 93, Wingard 90, Otaigbe 91]. With certain thermoset systems, the proximity of the stiff fibers and preferential adsorption and/or absorption of diffusible constituents, in particular low molecular weight curatives, on the fiber surface or in the fiber wall may impose a relatively high crosslink density, decreasing locally the damping behavior of the resin. At the same time, this may lead to some softening of the matrix in the zone next to the interface because of the depletion of the curative [Datta 02]. This is particularly conceivable with plant fibers, which have a certain affinity and/or absorption ability with the curatives. Plant fiber reinforcements are also generally made up of yarns of elementary fibers. The friction mechanisms between fibers (intra-yarn friction) as well as the friction between the yarns (inter-yarn friction) could increase the intrinsic damping with respect to that obtained with synthetic fibers [Duc 14b]. Therefore, it is necessary

to review the current knowledge on the damping behavior of PFCs in order to draw the needs for the future research activities, and to evaluate their potentialities to improve the damping behavior of composite structures.

This chapter will start with a short description of the experimental techniques classically used for the characterization of damping, then many studies on PFCs regarding damping properties are summarized to show the root reasons from various parameters. The first section outlines the choice of the experimental method used for damping characterization. The second section introduces some mesoscale parameters including reinforcement type, stacking sequence and PFCs skins or core used in sandwich, and microscale parameters such as fiber, matrix, interface/interphase, and porosities. In addition, some issues regarding moisture effect and temperature are also discussed.

I.2 Experimental techniques for the characterization of damping

Damping, as an important physical phenomenon, is mainly used to limit or prevent the vibration of the system through the dissipation of energy. Several frequency ranges can be investigated according to the targeted application. Meanwhile, a large number of alternative approaches have been developed to characterize the damping. In this section, the most widely used damping characterization techniques (non-resonance and resonance methods) are briefly described, at first. Meanwhile, their significance and the importance of the scale regarding PFCs is discussed. At last, a comparison of the damping properties measured by the different techniques for the PFCs is proposed and discussed.

I.2.1 Quasi-static and low frequency characterization: dynamic mechanical analysis

One of the most widely used non-resonance techniques for damping characterization is Dynamic Mechanical Analysis (DMA). It is usually used to characterize viscoelastic materials with low stiffness such as polymers, or organic composite materials, and is widely used for the rheological analysis of polymers and elastomers, especially in the fields of chemistry and materials science [Menard 08]. In particular, their glass transition temperatures can be identified through temperature sweep curves at different frequencies.

The storage modulus (E'), loss modulus (E'') and loss factor ($\tan(\delta)$) are usually identified from DMA tests to describe the viscoelastic properties of materials for various temperatures [Margem 10, Mylsamy 11, Menard 08, Butaud 15a, Martínez-Hernández 07, Singh 08]. The temperature range of interest is generally investigated either through temperature ramps or temperatures steps. In the latter case, isothermal conditions are used often with a temperature stabilized stage of

several minutes to make sure that the sample has reached a homogeneous temperature distribution [Butaud 15a, Martínez-Hernández 07, Kuzak 99]. Harmonic excitation is usually set between 0.01 Hz and 100 Hz in most existing studies since DMA apparatus always exhibit mechanical resonances in the higher frequency range, that affect the measurement [Suresh Kumar 14, Placet 10a, Bhudolia 17, Wielage 03]. Indeed, Placet and Foltête achieved a straightforward model and they recommend that the experimenter should pay attention to avoiding the frequency range of the system resonance [Placet 10a]. In addition, another essential factor that needs to be considered in DMA is the ratio of the stiffness of the sample to that of the apparatus: the stiffness of the sample should be much smaller than the stiffness of the system to obtain accurate test results, especially for storage modulus [Butaud 15a]. Furthermore, the deformation of the sample should be kept in the linear viscoelastic range to meet the theoretical requirements [Menard 08]. Despite of these limitations in terms of frequency, DMA remains a popular technique for the characterization of damping, in particular because the Time-Temperature Superposition (TTS) principle, which is verified for a large set of polymers and composites, can be used to estimate their damping and stiffness properties in the higher frequency range [Menard 08, Butaud 15a].

I.2.2 Low to mid-frequency characterization: modal analysis

Modal analysis is another common method for damping identification. Natural frequencies, damping ratios, and modal shapes of composite structures are estimated at resonances by using an external excitation source within a specific frequency range [Araújo 09, Theotokoglou 15, Gibson 00]. Several excitation signals and boundary conditions can be used for resonance testing. Existing techniques on the damping measurement method with logarithmic decrement, free vibration of vibration beam are reported [Rueppel 17, Gibson 00, Mishra 12, Ouisse 19, Matter 09, Alexander 16]. The test configuration is also important. Several aspects are discussed in the literature, such as the location of the excitation, boundary conditions, adhesion of the accelerometers, and interference of the measurement [Butaud 15a, Theotokoglou 15, Gibson 00, López-Aenlle 19, Rao 97]. Specific techniques for composite structures are proposed for beams on complex shapes [AST 17, Oberst 52, Koruk 12, Viala 18].

Since there is usually no heating or cooling device used in the modal analysis tests, the samples are sometimes placed in a constant temperature oven to maintain the required test temperature [Butaud 16, Butaud 18]. However, these settings can generally not be used to reach high temperatures because most instruments cannot tolerate excessive temperatures.

I.2.3 High frequency characterization: wave number-based approaches

Marchetti et al. review several wave number based approaches used for the characterization of the dynamic properties of composite structures in frequency ranges where modal analysis approaches become unpractical as the increased modal density is too large [Ege 09, Marchetti 20]. The loss factor and storage modulus can be computed from the natural wave number obtained from the high frequency analysis.

However, this type of characterization has not been widely applied for PFCs at this time, so this frequency range is not addressed in this review paper. The works by Zhang et al. and Duval et al. can be mentioned as first inputs to be completed in future researches with additional data related to damping properties of PFCs in high frequencies [Zhang 19, Duval 15].

I.3 Review of studies on the damping behavior of PFCs

I.3.1 Meso scale parameters

This section discusses the effect of reinforcement features on damping, given the issues of fiber length and stacking sequence. Composite sandwich structures with PFCs skins are also within the scope of discussion.

I.3.1.a Reinforcement type

Plant fibers can be processed into many kinds of reinforcements such as short fibers, nonwoven, non-crimp fabrics, and woven fabrics. It leads to composite meso structures with significant differences. This part summarizes the effect of different kinds of reinforcement types on damping performances.

The fiber length effect of banana fiber-reinforced composites and sisal fiber-reinforced composites are summarized in [Senthil Kumar 14]. These two types of composites are significantly affected by the ratio of fiber length to diameter of the plant fibers. Thicker interfaces may occur with a smaller diameter of plant fiber, resulting in higher damping [Mukherjee 84, Saravana Bavan 10]. As the ratio of fiber length to diameter is relatively low, the larger is the surface contact area of the sisal fiber, the stronger is the interface [Joseph 92, Joseph 93, Geethamma 95]. The difference in inherent morphology of the fiber surface results in different trends of damping properties [Gassan 99].

In contrast, the loss factor of discontinuous synthetic fiber based composites are found to decrease as the fiber length increases, due to the long fibers that limit the movement of polymer molecules [Harris 93, Subramanian 11, Rezaei 09]. The

fiber-matrix interface is considered as a significant source of energy dissipation of discontinuous synthetic fiber based composites since short fiber increase more fiber ends and fiber-matrix interfaces [Subramanian 11].

When woven reinforcements are considered, most of the authors report a reduction of damping level compared to unidirectional (UD) reinforcements such as tapes [Duc 14b, Cihan 19, Audibert 18, Rouf 17, Alkbir 16]. Among the different weave patterns investigated, the loss factor in huckaback-type woven composites is found to be higher than that of plain, satin, twill, and basket because their performances depend on the interlace between the warp and weft directions, which increases the interaction between fiber and matrix [Rajesh 16a]. Also, twisted yarns decrease Young's modulus because of the induced crimp but increase the damping through enhanced inter-yarn friction [Duc 14c].

However, the existing reports have not found any significant effect of long fibers on damping when compared to short fibers and continuous reinforcements [Saha 99, Zhang 19]. A comparison of the effects of three types of reinforcement on damping performance is suggested in future work.

I.3.1.b Stacking sequence

The effect on damping of different stacking sequences, using some common arrangements such as 0°, 45°, and 90° are investigated by several authors. When it comes to symmetric layups, composites often show lower damping level in longitudinal direction when 90° at the outer layer and the highest for that when 0° at the outer layer [Senthilkumar 17]. The authors indicate that this is related to the flexural properties of the composite structure. In particular, the shearing effect is found to enhance resistance to fiber mobility and increase the effective load transfer between fiber and matrix in turn [Pothan 08]. The damping ratio will be higher if the layer 0^o is located close to the outer layer [Karaduman 14, Zai 09].

Stacking sequences with long UD fibers and randomly oriented short fibers are also studied. Results show the stacking sequence does not influence the dynamic mechanical properties (including storage modulus, loss factor) of the PFCs [Fiore 15].

Some research on hybrid fibers (flax and E-glass fibers) show that the best damping performance are obtained when flax fibers are distributed in the outer layer [Cihan 19]. Y. Li et al. find the damping properties in hybrid composites (flax and carbon fiber) are greatly influenced by the position of the flax fiber layers because of the slip of some microfiber layers in the S2 layer relative to adjacent microfiber layers in flax fiber, which dissipate more energy than synthetic fiber [Li 17c].

I.3.1.c Sandwich with PFCs skin or core

The source of damping in sandwich structures is complicated due to the diversity of components, including skin, core, adhesive, matrix, and diversity of behaviors regarding the frequency ranges of interest. Several hypotheses are reported from the point of view of resin, plant fiber in the skin, interfaces, and core [Monti 17, Sargianis 13, Assarar 13]. The main conclusions are as follows

a) **Resin**. Part of the energy dissipation is powered through friction mechanisms between long polymer chains as it represents most of the total volume fraction [Chandra 99].
b) **Plant fiber**. Plant fiber contains many natural polymers which show viscoelastic behavior [Yan 16]. Besides, fiber/fiber friction is also an important issue [Duc 14b].
c) **Defects**. Micro porosities, weak glue, and weak fiber/matrix interfaces increase the friction between components [Monti 16].
d) **Core**. Viscoelastic behavior of core made from plant and resin that are trapped in the core positively contributes to global damping [Monti 17, Sargianis 13, Assarar 13].

Table I.1 – Main features in mesoscale parameters

Parameters	Damping root
Fiber length	The ratio of fiber length to diameter, surface contact area
Weave patterns	Interlace between the warp and weft directions
Stacking sequence	Shearing effect, effective load transfer
Sandwich	Resin, plant fiber in the skin, interfaces, and core

The contribution of each component to the global damping of the sandwich structure is also discussed by several authors. Loss factors of sandwich structures (flax skin and balsa core) are also observed to increase with balsa core thickness increase [Monti 17]. Skins' contribution to damping becomes smaller as frequency increases due to the enhanced effect of the transverse shear in the core. On the other hand, the higher is the shear modulus of the core, the lower is the damping of the sandwich structure [Monti 17, Sargianis 13, Assarar 13]. Fiber orientations in the skin do not have a significant effect on the global damping of bending modes in sandwich structure [Monti 17, Sargianis 13, Assarar 13].

The skins in PFCs make their damping performance different from SFCs when compared to more conventional sandwich materials [Yan 16]. Finally, as for SFCs, the damping performances of sandwich structures with PFCs as core or skin are dependent on the various parameters discussed above. A hierarchy of contribution of each component on damping properties is proposed: shear modulus of the core, thickness of the core, skins, reinforcement, and thickness of the skins [Assarar 13].

In this section, the effect from reinforcement type, stacking sequence and sandwich skin have been discussed. The main features in meso scale parameters are summarized in Table I.1.

I.3.2 Microscale parameters

I.3.2.a Fiber

I.3.2.a.1 Fiber type This section summarizes the damping characteristics of composites with different types of plant fibers. Figure I.3 proposes a synthesis of the loss factor and Young's modulus values collected in literature for epoxy matrix with different unidirectional reinforcements made from different types of plant and synthetic fibers.

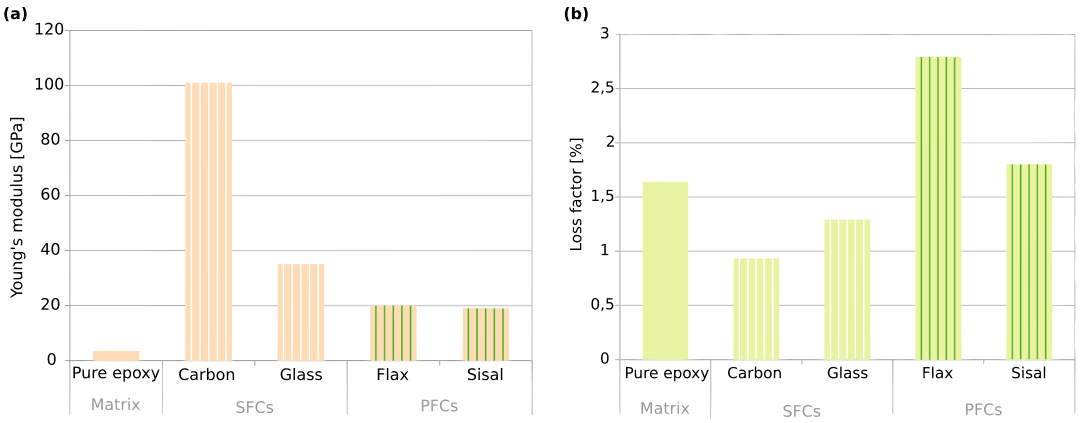

FIGURE I.3 – Mechanical properties of unidirectional (UD) fiber reinforced epoxy composites in the longitudinal direction (measured by DMA tests at 1 Hz and ambient temperature), summarized from refs. [Duc 14b, Mylsamy 11, Towo 08]

The presented results are collected using DMA tests at 1 Hz and ambient temperature. It can be observed that the fiber type does have a significant effect on the damping properties (fiber volume fraction can also be a factor, but most authors have not stated it in the literature). The addition of synthetic fibers into epoxy induces a decrease of the damping due to stress transfers from the matrix to the fibers. In addition, the presence of stiff fibers limits the chain mobility in the matrix, which implies that the friction of the intermolecular chain is reduced[Essabir 13, Pan 08, Hwang 92]. Conversely, the addition of plant fibers increases damping due to the friction at the interface but also may be due to the intrinsic damping capacity of the fibers themselves [Duc 14b, Duc 14a, Duc 14c].

In addition, some authors also show that the incorporation of ramie fiber in epoxy tends to increase the damping due to weak adhesion which indicates low interfacial shear stress [Margem 10]. Another reason that may explain the diverse damping with these plant fibers is the difference in inherent morphology of fiber surface [Senthil Kumar 14]. Besides, damping performances are strongly related

to glass transition temperature (T_g). The incorporation of plant fibers in the matrix generally induces a shift of T_g toward higher temperatures and a reduction of the loss factor peak due to the restriction of the movements of the matrix chains. This suggests an increase in stiffness of the fiber-matrix interfacial zone, however, contradictory effects have sometimes been observed [Saha 99, Ray 02, Pothan 03, Huda 06, Montazeri 12, Chua 87]. It strongly depends on the matrix type, its affinity with plant fiber and the resulting stiffness properties at the interface between fibers and matrices.

Hybrid plant fiber composites are also reported regarding with damping performance. Results show hybrid plant fiber composites, such as banana/coconut sheath, kenaf/bamboo possess higher loss factors compared to single fiber composites [Ismail 19]. Hybrid fibers combine the advantages of their components and achieve superior performances that cannot be obtained from only one type and authors also claim damping values are higher for all hybrid composites possibly due to greater energy dissipation and restricted molecular mobility at the interface [Machado 16, Senthil Kumar 16, Sathishkumar 14].

I.3.2.a.2 Fiber micro structure Plant fibers differentiate from the conventional ones in terms of composition, and micro structure. Indeed, plant fibers often have unique micro structures and morphologies, notably different cell wall layers and a complex cross-sectional area which varies along the fiber length [le Duigou 17, Bourmaud 16, Baley 19, Li 18] . In additional to this complex morphology, plant fibers have also a polymer-based composition and a very hierarchical organization with different layers and sublayers made of a mixture of carbohydrates and polyphenols [Hosseinaei 11, Goubet 02]. It imparts them viscoelastic properties [Keryvin 15a, Cisse 15, Van Hazendonk 96, Biagiotti 04, Bismarck 02]. These particularities lead also to specific static and fatigue behavior which were quite widely studied in literature, including nonlinearities [Jeannin 19a, Jeannin 19b], stiffening effects [Haggui 19] and moisture activation of some mechanisms [Zai 09, Launay 13, Berthelot 07].

It could also be at the origin of specific energy dissipation mechanisms and particular damping behavior. Only few studies investigate the viscoelastic behavior of plant fibers [Placet 09, Perrier 16, Khelfa 15] and, unfortunately, the influence of the fiber microstructure on the damping of the PFCs themselves has not been studied so far.

PFCs are made of single individual fibers but also bundle of fibers. Friction at the interface between individual fibers within the fiber bundle, internal friction within fiber wall (between the heterogeneous polymers constituting the wall and particularly between the rigid cellulose microfibrils and the amorphous polymers in which they are embedded) [Duc 14c, Duc 14b] are also potential sources of damping. Additionally, plant fibers have a finite length when compared with synthetic fibers. The effect of such discontinuities, even for continuous reinforcement, on the damping behavior of PFCs can be questioned and deserves to be investigated in the future.

I.3.2.a.3 Treatments Several investigations on the effect of pre-treatments on the plant fibers to achieve better mechanical performances in PFCs have been reported. This section summarizes the treatment methods and their effects on composite damping, including functionalization using nanotubes, chemical treatments, etc. which may change the interface state.

Carbon nanotubes (CNTs) are proposed to enhance the damping property of PFCs and SFCs [Tahan Latibari 13]. Damping is further enhanced by the stick-slip action of CNTs that takes place at the CNTs/matrix interfaces. Besides, the penetrated CNTs interact with microfibrils in the S2 cell wall of plant fibers, leading to effective stress transfer from matrix to microfibrils, which contributes to energy dissipation and enhancement of damping property [Li 17c]. In contrast, some authors also claim the presence of stiff fibers limits the chain mobility in the matrix, which implies that the friction of the intermolecular chain is reduced [Essabir 13, Pan 08, Hwang 92].

Other results report the effect of microfibers. The addition of macro/microfibers decreases the damping characteristics of PFCs and increased storage modulus, as the added fibers act as barriers to the free movement of the macromolecular chains. As a contrast, the unfilled matrix has the highest damping ratio, indicating a significant degree of mobility [Joseph 10].

It demonstrated that the improved interaction exerted by the chemical treatments makes the PFCs and SFCs more compatible and with better adhesion than the untreated fiber composites [J. George 96, Zhao 19]. Moreover, some authors claim that a high-quality interface tends to lower energy dissipation, showing a lower value of the damping peak [Fay 91, Yu 10]. The effect of chemical treatments such as acid, alkali, ethanol, and silane agents are studied. Chemical modifications cause the hemicellulose removal, which increases the number of hydrogen bonds between the modified fibers and the matrix [Zierdt 15]. The alkali and potassium permanganate treatment of PFCs leads to higher damping when compared to other earlier reports [Mohanty 06, Gassan 99]. The authors explain that the damping characteristics of heterogeneous systems is not only based on interfacial bonding but also depends on different parameters like change in interfacial thickness, bending of fibers, broken fibers, matrix cracking and formation of cavities due to the fiber pullout [Cihan 19].

Different chemical reaction times show not much difference in the height of the loss factor's peak [Saha 99]. Some authors claim that the reduction of the amplitude of the loss factor's peaks means well-combined load capacity, due to a good stress transfer between interface [Jawaid 13, Pothan 03]. Silane-treated fiber composites lead to better fiber/matrix interactions than other treatments [Berthelot 04a, Gao 11a]. Alkali and silane treated surfaces are rough, which are formed by the elimination of lignin and hemicellulose compounds. A rough surface enhances fiber/matrix adhesion and increases both the glass transition temperature and loss factor during glassy state [Dayo 18, Li 07]. This can be also explained as the combination of the shear stress concentration at the fiber end and the additional viscoelastic energy dissipated in the matrix material [Atiqah 19, Zhou 14, Zahari 15].

Besides, Yadav & Gupta find fiber coating (PLA) followed by chemical treatments can improve the damping at ambient temperature, and could also be considered as a practical approach to improve the performance of composite materials for advanced applications [Yadav 19].

I.3.2.a.4 Fiber volume fraction PFCs with a single type of reinforcement are also studied to investigate the influence of the fiber volume fraction on damping properties. The mechanical strength and damping in free vibration properties increase with the sisal fiber content (up to 50 wt%), due to the changes in inter-laminar shear at the fiber end [Senthil Kumar 14]. Sathishkumar et al. [Sathishkumar 18] report that an increase in sisal fiber content (for the specific considered range) induces an increase in the loss factors of PFCs. Nevertheless, banana fiber composites show the opposite behavior. This is attributed to the difference in inherent morphology of fiber surface [Senthil Kumar 14].

Regarding short fiber composites, it is concluded that the composite with 30 wt% noil hemp fiber shows the highest damping capacity among all investigated composites [Etaati 14]. The presence of higher fiber contents has considerably reduced damping, indicating that the composite material is more elastic at higher fiber contents [Tajvidi 10]. The interface area increases with the number of incorporated fibers, which leads to stronger interactions. Therefore, the molecular mobility of the polymer decreases and the mechanical loss that overcome intermolecular chain friction is reduced [Salleh 14]. Other reports show the dynamic characteristics are significantly influenced by the increase in fiber length and fiber loading by the changes of interface but not in a geometric progression [Sreenivasan 15].

Increasing the fraction of synthetic fibers in hybrid fiber composites (flax and carbon fiber) reduces damping [Le Guen 16], but there are also reports of increase damping [Sathishkumar 18], without clear physical explanation of this observation.

I.3.2.a.5 Fiber orientation Different fiber orientations can be used during the design of composite laminates and structures. Damping performance of PFCs with different fiber orientations has been studied in the past decades.

The loss factor of flax/GreenPoxy 56 (GP56) composites are tested from 0° to 90° fiber orientation using a modal method [Daoud 16]. Results show that the loss factor decreases as the frequency increases. This is attributed to the high internal friction between cellulose and hemicellulose caused by the flax fibers microstructure, especially at low frequency [Duc 14b, El-Hafidi 17, Assarar 15, Daoud 16]. A maximum loss factor is always found at 70° -75° fiber orientation for different frequencies. In other reports, the loss factor is found to increase at first, and then to decrease with the increasing fiber angles in flax fiber-reinforced polypropylene (PP) [Rahman 17b]. Some authors show that the maximum loss factor is obtained around 45° fiber orientation, which is similar to glass fiber composites and carbon fiber composites [Berthelot 04b, Gao 11b, Adams 03]. This phenomenon is attributed to the in-plane shear strain energy of fiber-reinforced composites which is the maximum at this fiber orientation [Hwang 92]. However, the glo-

bal trend is that the loss factor of the fiber orientation in 90° is higher than that of 0°, as shown in Figure I.4, in which (a) and (b) are measured around 500 Hz, (c) is obtained around 300-400 Hz and (d) is measured around 300 Hz [Rueppel 17, Daoud 16, Rahman 17b, Berthelot 04b].

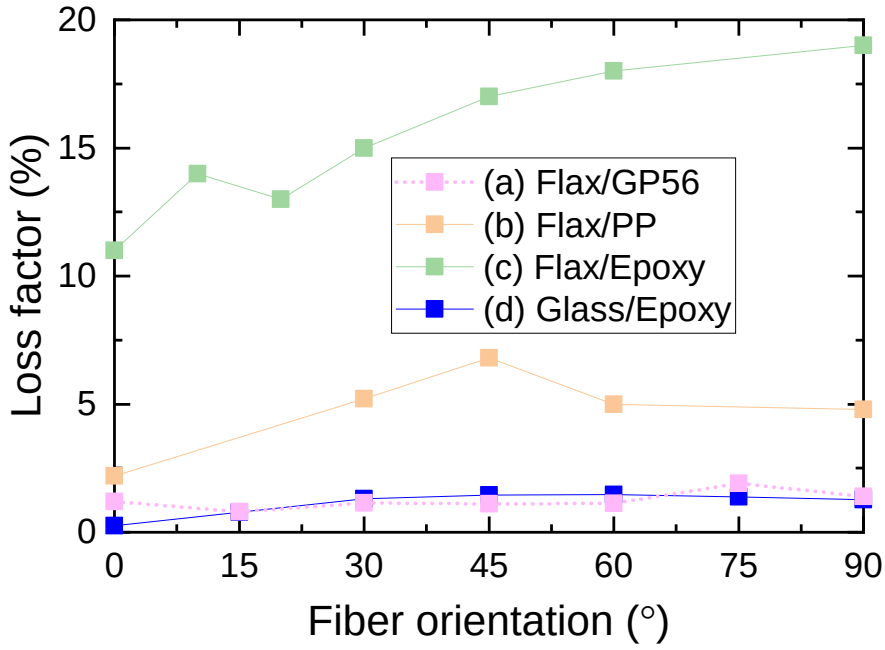

FIGURE I.4 – Variation of loss factor as function of fiber orientation in UD composites in longitudinal direction using modal tests (a) Flax/GP56, (b) Flax/PP, (c) Flax/Epoxy, (d) Glass/Epoxy [Daoud 17, Rueppel 17, Rahman 17b, Gao 11b]

The maximum damping value may also depend on the interface characteristics between different components of the composite. This performance needs to be further studied to determine the highest value of damping and it will be useful to understand why the orientation impacts the damping ratio.

I.3.2.b Matrix

Organic matrix-based PFCs and SFCs generally show a higher damping capacity due to the viscoelasticity of the polymeric matrix compared to metals [Chung 03, Treviso 15]. This section summarizes some research results on the dynamic mechanical properties of conventional polymers.

Figure I.5 summaries some dynamic mechanical properties of pure matrices, which are widely used in industrial production. Thermoset polymers, such as epoxy, are the most widely used matrix for PFCs and SFCs due to the excellent adhesion of resin and the long lifecycle. However, thermoset polymers tend to be more brittle and less tough than thermoplastics [Chung 03]. The reason is that high loss factor values are associated with ease of movement of side chains, functional

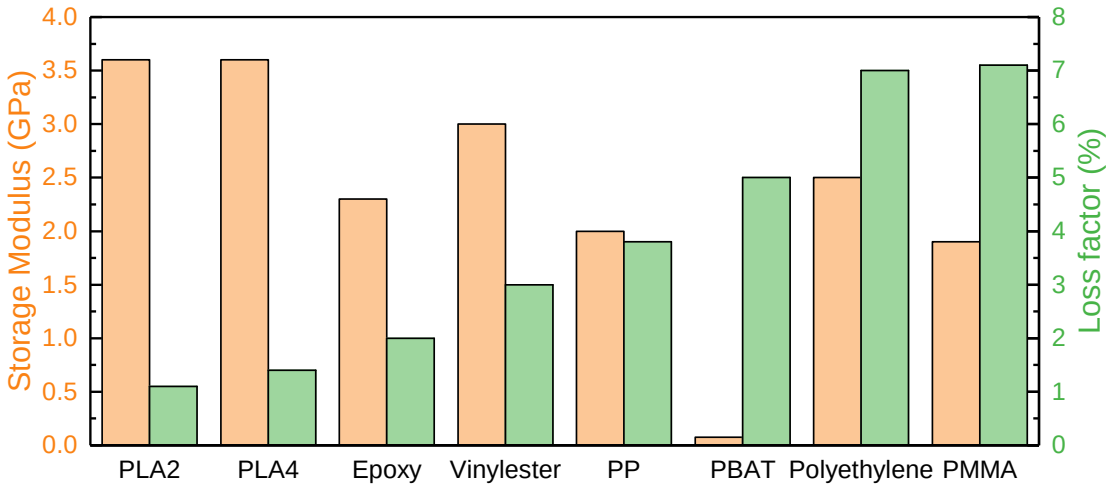

FIGURE I.5 – Loss factor and modulus of different polymers at 1 Hz and ambient temperature summarized from [Duc 14b, Margem 10, Ray 02, Shinoj 11, Madera-Santana 09, Martínez-Hernández 07, dos Santos Silva 19] (Polylactic acid 2, 4 (PLA 2, 4), and Polypropylene (PP), Polybutylene adipate-co-terephthalate (PBAT), Polymethyl methacrylate (PMMA))

groups, segments, pendant groups, and even entire molecules in the polymer. Moreover, the loss factor is reduced by the presence of negatively charged atoms (such as oxygen and nitrogen) in the molecules, which reduces the motion of hydrogen bonding [Fu 01]. This phenomenon is also interpreted as a mechanism for damping in polymer blends provided by network and interfaces [Tung 92]. Although thermoplastic polymers exhibit higher energy dissipation than thermosets, thermosets are often preferred due to their higher stiffness and better adhesion properties [Chung 03, Treviso 15].

Besides, results with particle additions are also reported. The mixture of agar particles restricts the mobility of the chains, and this performance reduces the sharpness and the maximum value of loss factor. The viscosity is substantially enhanced by fillers at a low shear rate, and in this case, the rheological behavior is utterly dependent on the composition of the polymer in the interfacial region [Liang 10]. It is also reported that the incorporation of solid fillers into the polymer matrix could increase or decrease the damping of the polymer, depending on the quality of fiber-matrix bonding [Saha 99, Wielage 03, Jonoobi 10, Landel 93]. Also, it can be observed that the damping factor decreases with the increase in bio-filler contents because the rigid particles restrain the mobility of the polymer molecules, raise the storage modulus, and reduce the loss factor [Essabir 15].

The Young's modulus and loss factor of the more widespread thermoset (epoxy), thermoplastic (Polylactic acid 4 (PLA 4), and Polypropylene (PP)) polymers used for flax composites are reported in Figure I.6 [Duc 14b], for both pure resin and UD flax composites. Although the reinforcement is the same, their global damping is quite different. The addition of plant fiber in epoxy, PLA4, and PP show a

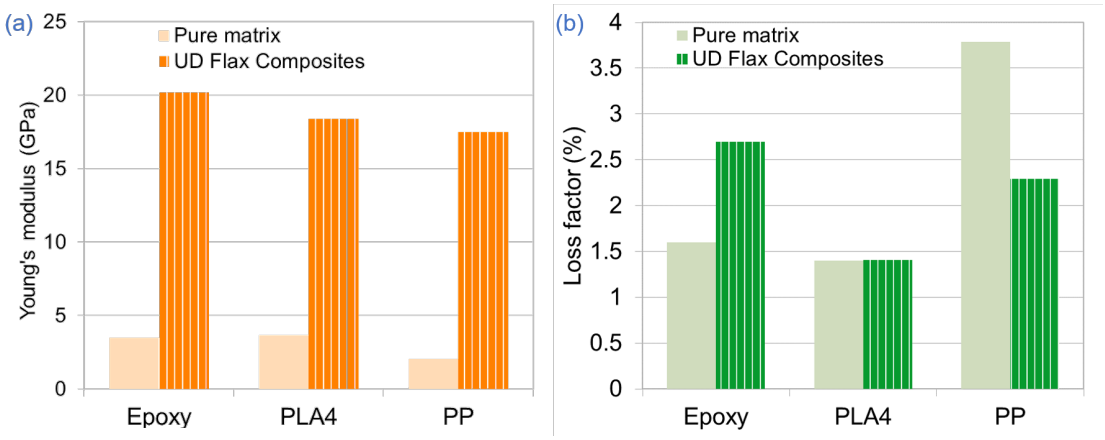

FIGURE I.6 – Young's modulus and loss factor of flax composites in the longitudinal direction and pure matrix measured by DMA at 1 Hz and ambient temperature (summarized from ref. [Duc 14b])

distinctly different trend in loss factor, but a total increase in modulus. This is because of the interactions between fiber and matrix, depending on the contribution of the internal friction in the fibers to the overall damping response [Duc 14b].

I.3.2.c Interface / interphase

As abovementioned, interfaces play a critical role in the damping properties of composites. Their properties depend not only on the manufacturing process but also on the treatments, which have been discussed in the fiber treatment section, as shown in Figure I.7. This section focuses on the original interface.

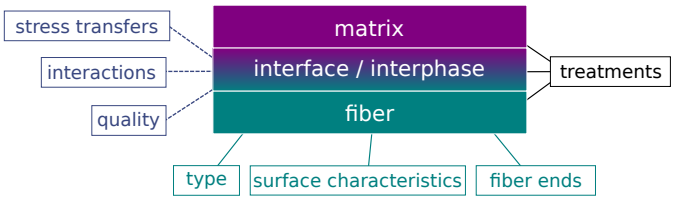

FIGURE I.7 – Parameters related to the interface properties

It is reported that a composite with weak interface bonding tends to dissipate more energy than that with good interface bonding [Essabir 13, Geethamma 05]. However, other reports show that an increased damping can be obtained often by improvement of fiber/matrix adhesion, which may activate the damping phenomena such as intra-cell wall friction between the cellulose microfibrils and the hemicellulose/lignin matrix in each cell wall and inter-cell wall friction between the cell walls [Duc 14c].

Some studies show that the loss factor and stiffness of interleaf films play an essential role in the loss factor of the interleaved laminates at the test temperature [Kishi 04].

In most cases, higher resin contents for most organic-based composites should lead to higher damping due to its viscoelastic properties. However, in some cases, the reduction of the matrix fraction increases the damping. This is due to the interface thickness and interface stiffness that also play an essential role in the damping mechanisms [Chandra 99].

I.3.2.d Porosities

Porosity is inevitable during the manufacture of composite materials. To the best of the authors' knowledge, there is no study in the open literature on the influence of porosity on the damping behavior of PFCs. A report on hybrid fiber composites (SFCs+PFCs) describes the effect of the existence of voids on damping characteristics. The damping is found to be not sensitive to the void content. This might be due to the small void content in the samples reducing the contribution [Cihan 19].

Additional research on this topic regarding different types of PFCs, such as woven pattern, matrix (thermoset or thermoplastic), etc., is necessary since not enough conclusions have been reached at this time.

As a conclusion of this sub-section, the main features in microscale parameters are summarized in Table I.2.

Table I.2 – Main features in micro scale parameters

Parameters	Damping root
Fiber type	Stress transfers, intrinsic damping capacity of plant fiber
Fiber orientation	In-plane shear strain energy
Fiber volume fraction	Increase interface or restrict the mobility of matrix
Treatments	Stress transfer, quality of interface
Matrix	Molecular structure, interactions at the interfaces
Interface	Fiber/matrix adhesion
Porosities	Not enough study in porosities

I.3.3 Testing and surrounding conditions

I.3.3.a Testing technique

The testing techniques may have an influence on the determined values of the loss factors [Butaud 18]. So, the damping results from DMA tests and modal analysis tests are compared in some studies [Rueppel 17, Butaud 15a, Butaud 18]. Regarding PFCs, Rueppel et al. describe damping measurement tests with three

different strategies: DMA, logarithmic decrement measurement method (LDM) and vibration beam measurements (VBM) [Rueppel 17]. The values obtained from DMA and VBM have a significant difference, which is attributed to air resistance effects as the amplitude of vibration is larger during VBM [Rueppel 17, Zoghaib 15]. LDM provides non-linear decay for the materials and the authors recommend to carefully consider initial parts of the displacement curve during tests, especially for high damping materials. Besides, other methods such as ultrasonic testing, nano-indentation, and scanning micro-deformation microscopy have been investigated for the damping characterization of polymer but not PFCs. Although they are also limited by frequency and temperature, they can complement the limitations of other experiments in multi-scale [Bhudolia 17, Butaud 18]. It is then essential to take into account the experimental techniques when comparing damping properties of different materials.

As mentioned before, the effect of unique microscopic characteristics of plant fibers, which are different from synthetic fibers on damping, should be studied. For the characterization of damping, a large number of reports focus on macro- and meso- scales, while studies on microscale are currently rarely seen. At last, the comparison of different test methods for specific PFCs under the same conditions to know their influential would constitute valuable analysis for future research since many other influential parameters vary from one study to another.

I.3.3.b Environmental conditions

Researchers have also paid attention to the influence of some external factors in addition to the inherent factors of PFCs components. In this section, the effects of external environment such as water aging or moisture content, temperature and various coupling conditions is summarized.

I.3.3.b.1 Moisture The environment in which PFC materials are serviced is sometimes harsh, and in most cases, the environment is accompanied by changes in moisture content.

Plant fibers are sensitive to moisture content due to their microstructure and biochemical composition [Rong 01]. Therefore, their hygroscopic properties and effects need to be studied if plant fiber composite materials are to be used in engineering fields. Many factors affect water absorption characteristics in PFCs. External factors such as temperature, manufacturing features such as fiber fraction, fiber orientation, size and percentage of voids, interface factors such as exposed area, surface treatment, component hydrophilicity, and bonding quality of interfaces between fiber-matrix are proved to be critical influencing factors [Lu 19, Saxena 11, Machado 16].

Generally, the absorption of water in PFCs is started by water entering the plant fiber through capillary transport. Materials with micro-crack defects also accelerate the diffusion of water. Plant fibers absorb water and cause the fibers to swell, leading to micro-cracks in the fiber-matrix interface area [Senthilrajan 19a, Rong 01]. Moreover, this diffusion is enhanced by the aging of the material it-

self [Machado 16], which causes the deformation and mechanical properties of the PFCs to decline [Gerald Arul Selvan 16, Hamid 12]. Many studies have shown that good interfacial properties between fiber reinforcement and matrix or better moisture absorption resistance can reduce the effect of moisture absorption on plant fiber [Gerald Arul Selvan 16].

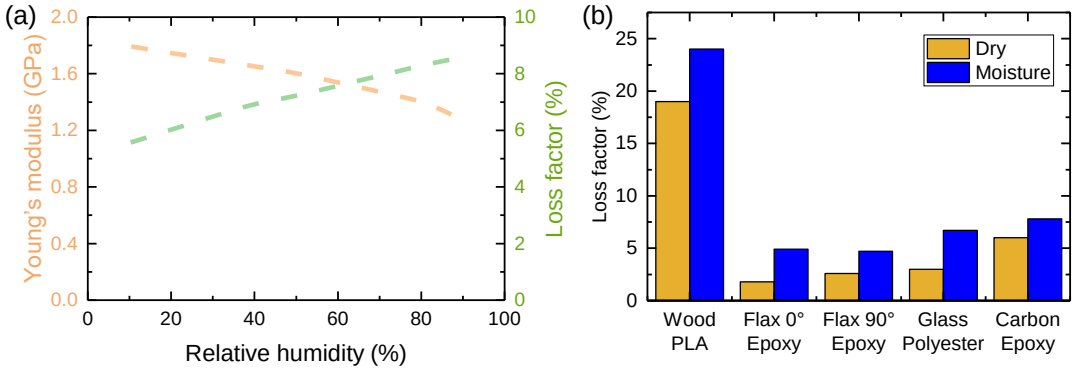

FIGURE I.8 – Different kinds of composites

FIGURE I.9 – Young's modulus and loss factor of (a) wood fiber composites and (b) different kinds of composites based on DMA tests at 1 Hz and ambient temperature with respect to relative humidity and after water absorption (summarized from ref. [Bogren 06, Gu 09, Cheour 16]

Damping is generally observed increasing with the increasing relative humidity in PFCs at the expense of Young's modulus. Damping of wood fiber composite is more sensitive to relative humidity than Young's modulus, changing by 26% and -13% from dry to humid conditions, respectively, as shown in Figure I.9 [Bogren 06]. M. Berges et al. indicate a 50% increasing of damping ratio after water vapor saturation with 20% decreasing of dynamic elastic modulus [Berges 16]. Reports on synthetic fiber composites are also available, but the effect of relative humidity on stiffness is not significant [Launay 13, Zai 09]. In addition, the matrix of a composite material usually exhibits plasticization and swelling when exposed to moisture. Damping is very sensitive to changes in stiffness of the outer layer due to the plasticization of macromolecular networks, which exacerbates energy dissipation [Fraga 03]. In addition, the moisture present in the areas at the interfaces increases friction losses [Menrad 08]. Longitudinal stiffness in UD composites is highly dependent on the strength of the fiber. In contrast, the storage modulus of synthetic fiber composites changes little because the reinforcement is hardly affected by moisture.

PFCs are not only affected by the matrix when dealing with wet environment compared to SFCs, but the changes in fiber molecules also need to be understood. The dynamic FT-IR technique can be used since the traditional macro-mechanical tests cannot provide information about the stress transfer between the fiber and the matrix [Almgren 08]. As moisture is transported from the plant fibers to the

interface between fiber and matrix, the ability to transfer stress between the fibers and the matrix is reduced [Almgren 08]. The matrix bears more loads, and the in-phase contribution of the matrix increases relatively to that of cellulose [Almgren 08]. The energy dissipation is related to the strain energy of the fiber and the friction between the different components is increased as water absorption [Berthelot 08].

The effect of fiber orientation changes has also been studied in UD composites. The sensitivity of damping in different fiber orientations to the moisture decreases gradually from 0°, 90° to 45° [Cheour 16]. The PFCs laminates with 90° outer layers are profoundly affected by moisture meaning more sensitive effect on damping [Zai 09]. Therefore, this situation should be avoided in the design of composite materials if it is intended to be used in high humidity environments. However, another reason to explain the effect of stacking sequences, is that different fiber orientations have a different amount of water absorption before the specimen reaches saturation, which are not taken into account when discussing the effect on damping. Similar research is also reported in synthetic fiber composites [Zai 09]. In this work, a dehydrated flax composites specimen after water absorption is compared with the original specimen. Although a 15% decrease in the bending modulus is observed, the author claim that the damping performance is reversible because the damping in PFCs was mainly driven by the water content in the fiber and fiber friction. The effects of cracks and interface failures are found to be negligible [Cheour 16]. Several authors claim that this behavior appears to be unrecoverable in glass fiber reinforced polymer composites because the damping of SFCs is mainly determined by the damping of the matrix and the interface [Chandra 99, Gu 09].

Damping performance under seawater or strong acids are also studied in addition to freshwater or pure water environments [Mazuki 11]. Research shows that plant fibers are more susceptible to acids than synthetic fibers [Ghasemzadeh 09]. Besides, a silane agent is proved to decrease the water absorption, which is caused by reducing the chance of hydrogen bonding between free -OH groups in cellulose and water molecules [Dayo 18]. V. Fiore et al. also claim that $NaHCO_3$ treatment show beneficial effect on damping properties of flax composites but not jute composites during exposition to salt-fog environments which is strictly related to the fiber's chemical composition [Fiore 20].

In general, many reports on the effects of moisture on SFCs behavior are available, while researches related to PFCs have focused more on monotonic mechanical behavior. The effect of water-heat coupling on the damping using different types of PFCs needs more research.

I.3.3.b.2 Temperature The dynamic mechanical properties of organic-based composites are sensitive to temperature because of the rheological properties. Temperature is the first factor that affects damping properties in various external environments [Hiroshi Mizumachi 70].

Below the glass transition temperature, the loss factor increases with temperature attributed to matrix softening [Subramanian 11]. The free volume and space of the molecule's internal movement increase when the temperature rises, which causes the storage modulus and loss modulus to decrease. An ideal damping material should have a wider transition region and higher peaks in loss factor. However, as the matrix of composite materials, the stiffness decreases significantly in the transition zone, which requires engineers to find a suitable compromise between stiffness and damping.

Besides, some results report the damping properties of flax/epoxy composites during thermal shock cycling conditions from -40 °C to 28 °C [Kollia 19]. The maximum decrease in the loss factor observed is 8%. In addition, it is reduced by about 50% for storage modulus, and dynamic mechanical properties reach an equilibrium state due to micro damage saturation after 100 thermal shock cycles. The glass transition temperature (T_g) is not affected by the thermal shock cycling conditions.

However, most of the results available up to now provide a combine effect, temperature increase and specimen drying since it is really difficult using traditional experimental methods (such as DMA tests) to maintain the moisture content equilibrium within PFCs samples while changing the temperature. Hence, more researches are suggested in the future efforts to decorrelate the effect of temperature and moisture content. At last, the main features in environmental conditions are summarized in Table I.3.

Table I.3 – Main features in surrounding conditions

Parameters	Damping root
Moisture	Friction losses caused by interface damage
Temperature	Internal movement of molecule chain, changes in micro structure of plant fiber

I.3.4 Limitations of existing PFC damping studies

Composite materials face fatigue issues during long-term service. Some effects of fatigue on damping performance are also reported. The loss factor shows a substantial drop in the first cycles then it slightly decreases, then it stabilizes before the final failure [Haggui 19]. The author claims this refer to stiffness degradation in the state of the composite [Su 09]. The effect of various coupling conditions such as fatigue, moisture, temperature, etc. on the damping properties of PFCs should be studied in the future. Besides, different parameter configurations during the composite manufacturing process also have an impact on the damping

performance. A study finds that higher pressures appear to reduce the damping ratio due to alterations in the fiber-matrix bond [Ashworth 16]. The influence of parameters in the manufacturing process can be considered in the future.

(1) **Porosity** - The influence of porosity level has been recently investigated for PFCs made of non-woven fabrics and thermoplastic polymer [Hadiji 20]. However, results remain poor in literature in particular for short fibre composites as well as woven fabric based composites. Additional research on this topic regarding different type of PFCs with different matrices (thermoset or thermoplastic) is necessary since not enough conclusion has been reached at this time. In addition to the porosity level, the influence of the size and distribution of porosities should be investigated.

(2) **Environmental conditions** - The effect of hygrothermal coupling on the damping using different types of PFCs needs more research. At present time, the influence of environmental conditions is generally investigated using DMA tests, involving moisture content variation when sweeping temperature. The use of vibration tests is also recommended in the future to obtain direct measurements in a mid-frequency range.

(3) **Characterization at the microscale and multi-scale approach** - For the characterization of damping, a large number of reports focus on macro- and meso- scales, while studies on microscale are currently rarely seen. However, this is required to map the damping in the different constituents: plant fiber wall, surrounding matrix and its interface, to better understand the influence of microscale parameters on the damping at the macroscale.

(4) **Wideband frequency and experimental technique effects** – Evolution with frequency – Most of the results obtained for non-woven composites as well as non-crimp and woven composites show that the loss factor varies slightly with the frequency [Amenini 19, Hadiji 20]. Based on these results, it is however sometimes difficult to derive a trend. The combination of data collected using different experimental techniques on a same PFCs is suggested to observe the trend of the loss factor over a wide range of frequencies. Comparison of experimental techniques - The comparison of different test methods for specific PFCs under the same conditions to know their influential would also constitute valuable analysis for future research since many other influential parameters vary from one study to another. Use of additional techniques – In parallel to the classical DMA and vibration techniques, other methods such as ultrasonic testing, nano-indentation, and scanning micro-deformation microscopy have been investigated for the damping characterization of polymer [Ismail 19]. These techniques could also be used for PFCs. Although they are also limited by frequency and temperature, they can complement the limitations of other experiments in multi-scale [Butaud 15a, Butaud 18]. Wave number-based approaches can be an optional method to deal with high frequency range issues.

(5) **Fiber length and microstructure** - Even if the influence of fiber length on the damping properties has been already investigated for short-fiber composites, a more in-depth study is necessary to better comprehend the

influence of fiber length, fiber ends and discontinuities on the damping behavior, in particular in non-crimp fabric composites. For such composites, the influence of fiber type and fiber microstructural features should also be studied.

(6) **Stress level effect** - Since most of the PFCs exhibit a nonlinear static behavior as a function of the stress level, it would be also interesting to verify the linearity of the damping behavior as a function of the stress level.

(7) **Other factors** - Composite materials face fatigue issues during long-term service. Some effects of fatigue on damping performance are already reported. The loss factor is shown to decrease substantially in the first cycles, then it slightly decreases, then it stabilizes before the final failure [Haggui 19]. This deserves to be explained since one may expect an increase of the damping capacity with the damage creation and propagation. The effect of various coupling conditions such as fatigue, moisture, temperature, etc. on the damping properties of PFCs should be studied in the future. Besides, different parameter configurations during the composite manufacturing process also have an impact on the damping performance. A study finds that higher pressures appear to reduce the damping ratio due to alterations in the fiber-matrix bond [Ashworth 16]. The influence of parameters in the manufacturing process can be considered in the future.

I.4 Conclusions

This chapter introduces some experimental methods to determine damping and many reviews factors that affect the damping properties of PFCs in mesoscale parameters, microscale parameters, surrounding conditions, etc. based on recent research reports.

Literatures show that PFCs have values of loss factor comprised between 0.7% and 14%, while values are comprised between 0.24% and 2.5% for SFCs, as shown in Figure I.10. The damping capacity of PFCs is generally much higher than SFCs but PFCs have also a more complex behavior. The literature review points out also sometimes contradictory results. This is attributed to the wide variety of plant fiber composites studied, involving various types of plant fibers organized in different reinforcement architectures embedded in a very broad set of polymer matrices. This variety prevents sometimes from reaching a consensus and establishing generic conclusion.

The main conclusions are the following:

(a) The damping characteristics of PFCs are unique because of their microstructural and morphological properties, linked to their polymeric nature, moisture sensitivity, complex interface, finite length when compared to SFCs. Quantitative analysis of the influence of microstructure on damping performance is rarely seen, although there have been many studies on static mechanical properties.

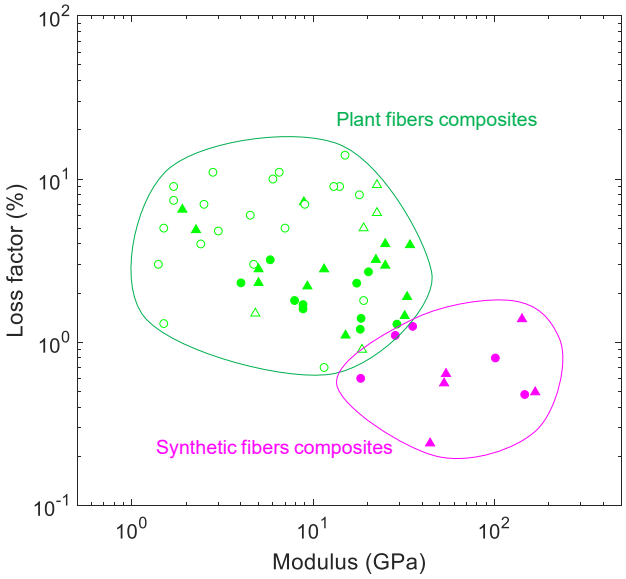

FIGURE I.10 – Ashby diagrams of PFCs and SFCs: loss factor v.s. modulus (triangles are measured by modal tests at first mode and ambient temperature, circles are measured by DMA tests at 1 Hz and ambient temperature, empty symbols and full symbols mean horizontal axis are using storage modulus and Young's modulus, respectively. (summarized from refs. [Shah 13, Araújo 09, Duc 14b, Margem 10, Joseph 10, Jawaid 13, Towo 08, Saha 99, Mylsamy 11, Suresh Kumar 14, Sreenivasan 15, Ray 02, Pothan 03, Daoud 17, Shinoj 11, Karaduman 14, Mohanty 06, Etaati 14, Amenini 19, Mahmoudi 19, Li 17c, Ashworth 16, Cihan 19, Zhang 19, Essabir 13, El-Hafidi 17, Liang 10, Le Guen 16, Assarar 15, Rueppel 17, Madera-Santana 09, Mazuki 11])

(b) The diameter-length ratio of plant fiber has a significant effect on the damping of PFCs and different reinforcement types have different trends. The outer layer in the stacking sequence has a considerable effect on damping.

(c) Interface properties between fibers and matrices have a significant effect on damping performance with sometimes contradictory interpretations. Additional studies and knowledge are necessary to shield light of this complex issue.

(d) The effect of plant fibers on the enhancement of damping is mainly due to intra-cell and inter-cell wall friction, intra-yarn, and inter-yarn friction, and fiber/matrix sliding. The effect of treatments on composite damping is caused by the change of interfacial properties between fiber and matrix.

(e) Plant fiber composites are more sensitive to moisture content than synthetic fiber composites because of the mismatch of the moisture expansion coefficients between the matrix and the fiber, which would induce a modification of the interfacial properties.

(f) Future work can expand on these issues regarding the effect on damping properties such as comparison of multiscale experimental method, different reinforcement type, surrounding conditions, parameters in the manufacturing process, etc.

Chapitre II
Meso scale: dynamic mechanical analysis

II.1 Introduction 45

II.2 Materials and methods 46

II.2.1 Generalities on DMA 46

II.2.2 Experimental setup 49

II.2.3 Composite materials 53

II.2.4 Water aging tests 58

II.3 Results and discussion 59

II.3.1 Comparision of DMA results from bending mode and tension mode 59

II.3.2 Dynamic mechanical properties of GreenPoxy 60

II.3.3 Damping properties of composite materials at ambient temperature 63

II.3.4 Damping properties of composite materials in a wide temperatures range 70

II.3.5 Evolution of damping properties as a function of frequency 75

II.3.6 Influence of moisture content on UD flax reinforced composites 80

II.4 Conclusions 83

GRAPHICAL ABSTRACT

- Influence of matrix type on the damping behavior of UD composites

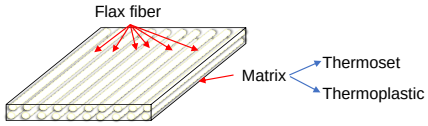

Damping behavior of UD composites is mainly driven by fiber in L direction and by matrix in T direction

The loss factor of flax fiber is around 2% and 4% in L and T direction, respectively, according to back calculation from composite measurements

- Influence of woven pattern on the damping behavior of composites

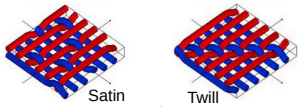

GreenPoxy based composites reinforced with hemp woven fabrics have comparable loss factor (2%) when compared to cross-ply flaxtape laminates

Fiber waviness induced by crimp makes woven hemp slightly higher damping than cross-ply

DMA Tests

- Evolution of damping as a function of frequency identified using TTSP

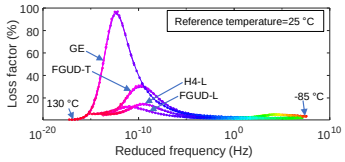

Non-constant and non-linear evolution on a measured frequency range (10^{-2}-10^{2} Hz) and 15 decades of reduced frequency owing to T_g (<0°C) for thermoplastic based composites and secondary transition (-50°C) for thermoset based composites

- Influence of water aging on damping properties of PFCs

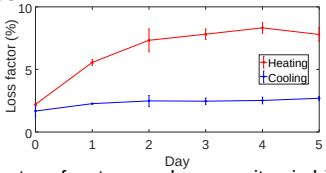

Loss factor of water aged composites is higher than that of unaged composites

Moisture is the most influential parameter among the ones studied in this chapter (matrix type, woven pattern, fiber type, lay-up, frequency)

RESUMÉ

Ce chapitre est dédié à l'étude des propriétés d'amortissement des PFCs à l'échelle mésoscopique. Une méthode expérimentale classique, l'analyse mécanique dynamique (DMA), est utilisée pour mesurer les propriétés viscoélastiques sur une large gamme de fréquences (0,01 - 100 Hz) et de températures (-100 - 160 °C).

Tout d'abord, l'influence de différents types de matrices sur les propriétés d'amortissement est étudiée en comparant les données mesurées sur des composites renforcés de fibres de lin unidirectionnelles (UD) à matrices thermodurcissable et thermoplastique (Flax fiber reinforced composites, FFRC). Par ailleurs, l'effet de l'ajout de fibres de lin dans la matrice pure sur les propriétés mécaniques dynamiques est introduit. Les résultats montrent que le comportement en amortissement des composites UD est principalement piloté par celui des fibres dans la direction longitudinale et celui de la matrice dans la direction transversale, à température ambiante comme à la température de transition vitreuse. Ce premier volet de l'étude a également permis d'identifier par méthode inverse le facteur de perte de la fibre de lin. Il est d'environ 2 % dans le sens longitudinal et de 4 % dans le sens transversal.

Dans un deuxième temps, le facteur de perte des composites renforcés de tissus de chanvre (Hemp fabric reinforced composites, HFRC) avec différents types de motifs tissés est déterminé. Les résultats montrent des facteurs de perte comparables (environ 2 %) pour les composites à base de GreenPoxy fabriqués à partir de

tissus de chanvre à ceux mesurés pour des stratifiés croisés de lin. L'amortissement est légèrement supérieur pour les tissés de chanvre, ceci est attribué à l'ondulation des fibres dans le renfort tissé.

Dans un troisième temps, les propriétés mécaniques dynamiques des composites FFRC et HFRC sont estimées dans une large plage de fréquences en utilisant l'equivalene temps-température. Les propriétés d'amortissement du unidirectional flax/GreenPoxy composites (FGUD) et du HFRC sont non constantes sur la plage de fréquences étudiée. Leur évolution est non linéaire sur la plage de fréquences mesurées (0,01 - 100 Hz) et également sur la plage de fréquences réduites associée. Ce constat est valide tant pour les composites à base thermodurcissable que thermoplastique. Cette tendance est expliquée par la présence de la transition vitreuse à basse température pour les thermoplastiques et la présence de transitions secondaires et de la transition vitreuse dans la plage d'intérêt pour les thermodurcissables.

Enfin, l'effet de la teneur en humidité sur les propriétés d'amortissement du FFRC est étudié dans les deux directions matérielles principales des a une température et une fréquence données, UD lin/époxy. Le facteur de perte des composites vieillis en immersion est significativement plus élevé que pour le matériau non vieilli en équilibre avec les conditions ambiantes. L'humidité apparait clairement comme le paramètre le plus influent parmi ceux étudiés dans ce chapitre (type de matrice, type de fibre, architecture de renfort, nappage).

ABSTRACT

This chapter is dedicated to the investigation of the damping properties of PFCs at meso-scale. A typical experimental method, dynamic mechanical analysis (DMA), is used to measure the visco-elastic properties in low frequency range (0.01 - 100 Hz) and wide temperature range (-100 - 160 °C).

First, the influence of different matrices on the damping properties are studied by comparing the results of thermoset and thermoplastic based flax fiber reinforced composites (FFRC). Meanwhile, the effect of the addition of flax fiber into pure matrix on dynamic mechanical properties is discussed. The results show that the damping behavior of UD composites is mainly driven by that of fiber in longitudinal direction and matrix in transverse direction. This is valid both at ambient temperature and T_g. The loss factor of flax fiber is also back-calculated using these measurements at the scale of the UD laminates. Values of approximately 2 % in longitudinal direction and 4 % in transverse direction are determined for flax fibers.

Then, the loss factor of hemp fabrics reinforced composites (HFRC) with different kinds of woven patterns are considered. Results show that GreenPoxy based composites made from hemp woven fabrics and cross-ply flaxtape laminates have comparable loss factors (around 2%). The slightly higher value for woven hemp composites can be attributed to the fiber waviness induced by crimp in woven fabrics.

Third, the dynamic mechanical properties of FFRC and HFRC under wide frequency range are obtained using Time-Temperature Superposition Principle (TTSP). The damping properties of unidirectional flax/GreenPoxy composites (FGUD) and HFRC are non-constant and non-linear on a the measured frequency range (0.01 - 100 Hz) as well as on the corresponding reduced frequency range. For both thermoset and thermoplastic based composites considered in this work, this is due to the presence of glass transitions at low temperature for thermoplastics and secondary transitions and glass transitions for thermosets.

At last, the effect of moisture content on the damping properties of FFRC are investigated in both material directions for UD flaxtape laminates. The loss factor of aged sample is significantly higher than for unaged sample, equilibriated with ambient conditions. For a given frequency and temperature, , moisture is clearly the most influential parameter among the ones studied in this chapter (matrix type, fiber type, reinforcement architecture, lay-up).

II.1 Introduction

For the organic matrix-based PFCs, several parameters, such as matrix type, reinforcement type and moisture content, are proved to have a significant influence on damping properties. This was reviewed in details in the previous chapter (Sections I.3.1-I.3.2). For instance, the loss factor of different pure matrices was measured between 1 - 8 % [Margem 10, Shinoj 11, Madera-Santana 09]. Moreover, the energy dissipation of thermoplastic- and thermoset-based PFCs at 1 Hz and ambient temperature was compared in literature [Chung 03, Duc 14b]. Another important parameter is the reinforcement type. It was sometimes investigated to evaluate the effect of weave patterns on the damping and monotonic mechanical properties [Rajesh 16b]. In addition, the influence of moisture content has also been paid attention since plant fibers are sensitive to humidity [Berthelot 08, Mazuki 11]. However, the comparison in the existing literature is usually mixed with multiple parameters such as fiber type, reinforcement type, and matrix and it is difficult to clearly understand which component plays the main role in damping performance.

Therefore, the main objective of this chapter is to get a better insight into this issue. The study in this chapter mainly focuses on four parameters: matrix type, reinforcement type and lay-up, frequency and moisture content. Different matrices in unidirectional flax fiber composites are studied to evaluate the contribution of fiber and matrix in damping properties both in fiber and transverse directions. Then, different weave patterns in hemp-fibre reinforced composites with balanced or unbalanced yarn densities in warp and weft directions are investigated. Furthermore, visco-elastic properties under specific frequency and temperature ranges are obtained at meso scale. In addition, the coupling effect on dynamic mechanical properties from moisture and temperature is also investigated.

This chapter gives, at first, a brief introduction for the theory of DMA method. The configuration of the experiments are then detailed as well as the precautions to make sure that all the tests are processed in a linear visco-elastic range. To make sure that the manufacturing process is reliable, the curing status of PFCs after manufacture with thermoset resins are also verified. Then, the DMA tests are carried out on specific temperature and frequency ranges using a piece of sample from the whole composite plate. Damping properties at low frequency (0.01 - 100 Hz) at ambient temperature in different kinds of flax or hemp composites are compared. Subsequently, the master curve of storage modulus and loss factor are built using the results at different temperature stages based on Time–Temperature Superposition Principle. Therefore, the visco-elastic properties on a wide frequency range and the reference temperature (T_{ref}) is obtained. This serves as a supplement to the multi-scale (including frequency and temperature scale) properties and will be further compared with the macro-scale and micro-scale results obtained in the following chapters. At last, the changes in damping properties after water aging are discussed for UD flax/epoxy laminates.

II.2 Materials and methods

The brief description and state of the art for DMA method has been detailed in the previous chapter. This section will focus on the mechanism of DMA method including the theoretical basis of visco-elastic mechanics and the principle of experimental measurement. The advantages and application of DMA method and the dynamic mechanical parameters collected by this method will be also discussed. Moreover, the details of the DMA tests as well as selected raw materials, composite production process and experimental setup will be described in this section.

II.2.1 Generalities on DMA

DMA, which is one of the non-resonance methods for damping identification, is usually used to study the viscoelastic materials in low stiffness such as polymer, organic composite materials, etc. It was widely used in the early years for the rheological analysis of polymers, especially in the fields of chemistry and materials science [Menrad 08]. Currently, many researchers use it to determine the dynamic mechanical properties of the materials in a certain range of temperatures and frequencies under periodically changing stress (or strain) [Margem 10, Mylsamy 11, Menard 08, Butaud 15a].

The mechanical response of an elastic material is instantaneous. The response of stress and strain, under the action of dynamic alternating stress, has the same frequency and phase without any difference. As one kind of viscoelastic materials, the mechanical response of flax or hemp reinforced polymer based composites is time-dependent, and the response of strain lags behind that of stress as shown in Figure II.1 (a). The hysteresis curve of the strain lags behind the stress in the viscoelastic material is shown in Figure II.1 (b). The area converted by the curve represents the energy dissipated within a vibration period.

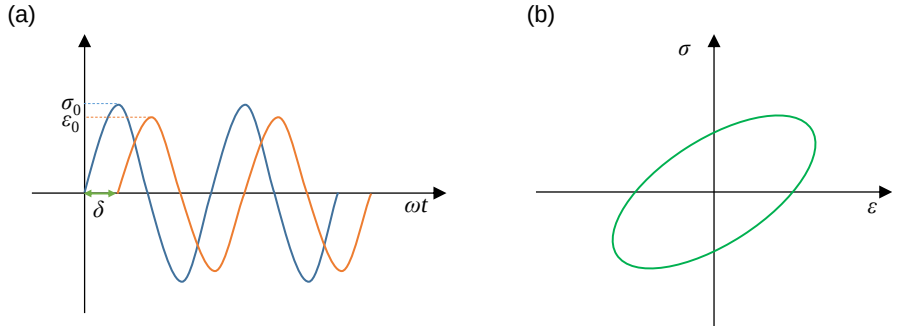

Figure II.1 – Mechanics of viscoelastic material under alternating stress: (a) Stress and strain curve, (b) Hysteresis loop

Generally, the mechanism of hysteresis is due to the internal frictional resistance of the intra-molecular and inter-molecular interactions when the chain segments of the molecular chain move, so that the segment movement cannot keep up with

the change of external force and the strain lags behind the stress. The greater is the internal frictional resistance, the more difficult is the movement of the chain segment, and the greater is the lag phase angle. Hysteresis strongly depends on external conditions, such as the frequency, external forces, and temperature.

Stress and strain can be expressed as,

$$\sigma(t) = Re(\bar{\sigma}e^{i\omega t}), \tag{II.1}$$
$$\varepsilon(t) = Re(\bar{\varepsilon}e^{i\omega t}), \tag{II.2}$$

where $\bar{\sigma} = \sigma_0$, $\bar{\varepsilon} = \varepsilon_0 e^{-i\delta}$, $i = \sqrt{-1}$, σ_0 and ε_0 refers to amplitude of stress and strain, ω means angular speed, t is the time and δ is the phase difference between stress and strain.

The phase angle δ is equal to 0° for elastic materials. An ideal viscous materials have a large lag between stress and strain, and the phase angle is close to 90° [Chang 19]. The ratio of stress (σ) to strain (ε) under dynamic load is defined as the complex Young's modulus of the material (E^*), which can be expressed as:

$$E^* = \frac{\bar{\sigma}}{\bar{\varepsilon}} = \frac{\sigma_0}{\varepsilon_0}e^{i\delta} = E^{'} + iE^{''}. \tag{II.3}$$

Three important parameters in DMA tests, storage modulus ($E^{'}$), loss modulus ($E^{''}$) and loss factor (tan δ), are usually used to describe the viscoelastic properties of polymer or organic-based composite materials. Other dynamic mechanical parameters can be also expressed as shown in Table II.1.

Table II.1 – Dynamic mechanical parameters in DMA tests

Parameters	Equation
Stress	$\sigma(t) = \sigma_0 \sin(\omega t)$
Strain	$\varepsilon(t) = \varepsilon_0 \sin(\omega t + \delta)$
Complex modulus	$E^* = \frac{\bar{\sigma}}{\bar{\varepsilon}} = E' + E''$
Modulus value	$\lvert E^* \rvert = \frac{\sigma_0}{\varepsilon_0}$
Storage modulus	$E' = \frac{\sigma_0}{\varepsilon_0} \cos\delta$
Loss modulus	$E'' = \frac{\sigma_0}{\varepsilon_0} \sin\delta$
Loss factor	$\eta = \tan\delta = \frac{E''}{E'}$

The dynamic mechanical properties of organic-based composites are sensitive to temperature and frequency. Temperature is one of the most important factors that affects damping properties among the various external environments [Mizumachi 70]. DMA testing is one of the techniques for measuring the damping properties that change with temperature.

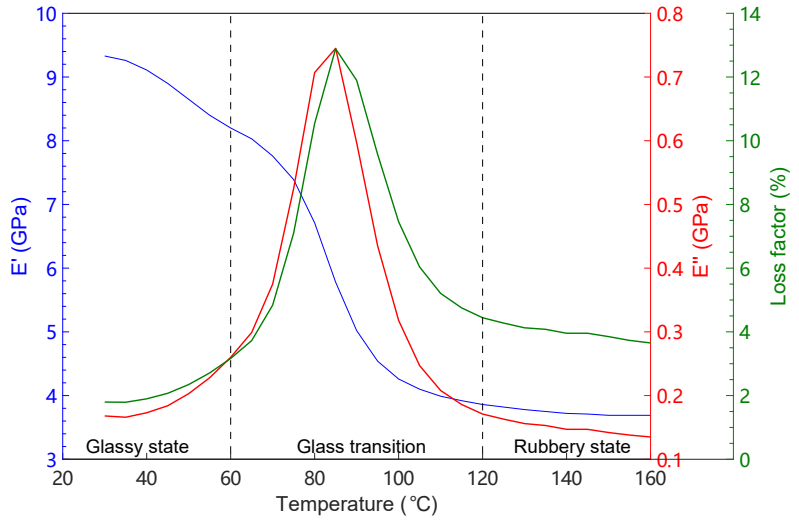

FIGURE II.2 – Typical dynamic mechanical properties of epoxy based composites

It is well known that the storage modulus (E') is usually related to the stiffness of the material, which represents the ability of the material to store the applied energy. The loss modulus (E'') is proportional to the energy dissipated in a loading cycle. The loss factor indicates the ability of a material to dissipate energy.

A typical dynamic mechanical curve of epoxy based composites is shown in Figure II.2. It can be observed that the loss factor increases from ambient temperature to T_g. This is attributed to the matrix softening, and the associated increase in molecular mobility [Subramanian 11]. The storage modulus shows a decrease from glassy state to rubbery state. After that, the movement of the molecular chain begins to be active, and the polymer exhibits viscous behavior. At glass transition, the internal loss reaches its maximum value. The loss factor usually varies by orders of magnitude in the glass transition zone. An ideal damping material for the application of vibration absorption should have a wide transition region and high peak in loss factor. However, the stiffness decrease in the transition zone generally requires engineers to find a suitable compromise between stiffness and damping. In addition, many meaningful dynamic mechanical information can be obtained in the glass transition zone. The temperature corresponding to the peak of the loss factor curve is considered as the T_g for the specified frequency in this thesis but other definitions may be used [Ehrenstein 12].

The above content regarding rheology forms the basis of DMA for characterization of the damping mechanisms. The analysis of subsequent experimental results in this chapter will analyze the time delay characteristics especially damping properties of the materials of interest of this thesis, including pure epoxy, flax and hemp fiber composites based on these principles.

II.2.2 Experimental setup

II.2.2.a DMA test system

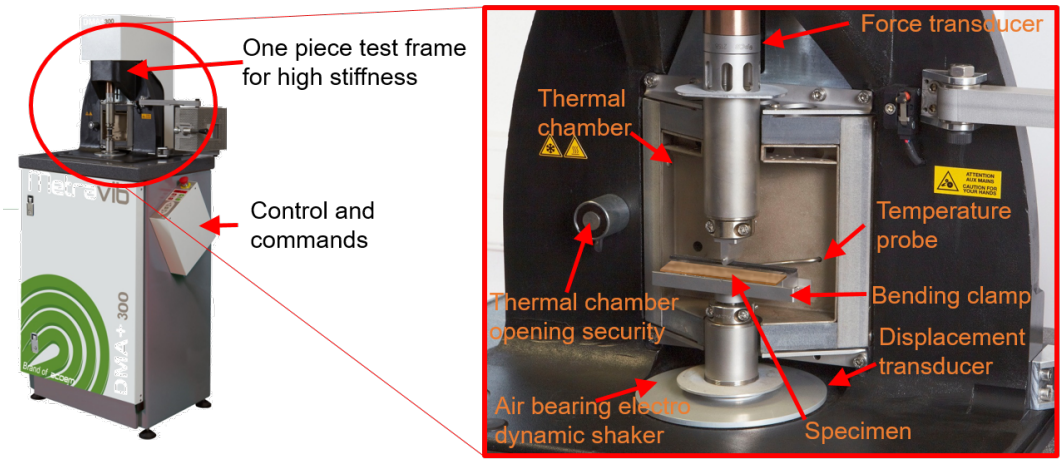

FIGURE II.3 – Main assets in Metravib® DMA+300

The apparatus used to process DMA tests in this work was METRAVIB® DMA+ 300 as shown in Figure II.3. It can be used for typical DMA tests under tensile, bending, or shear mode using different kinds of clamps. The sinusoidal stress was generated by the electro dynamic shaker and applied to the specimen. Specimens were solicited under tensile and bending modes. Many parameters such as storage modulus, loss modulus and loss factor are directly calculated by the software 'Multitest'.

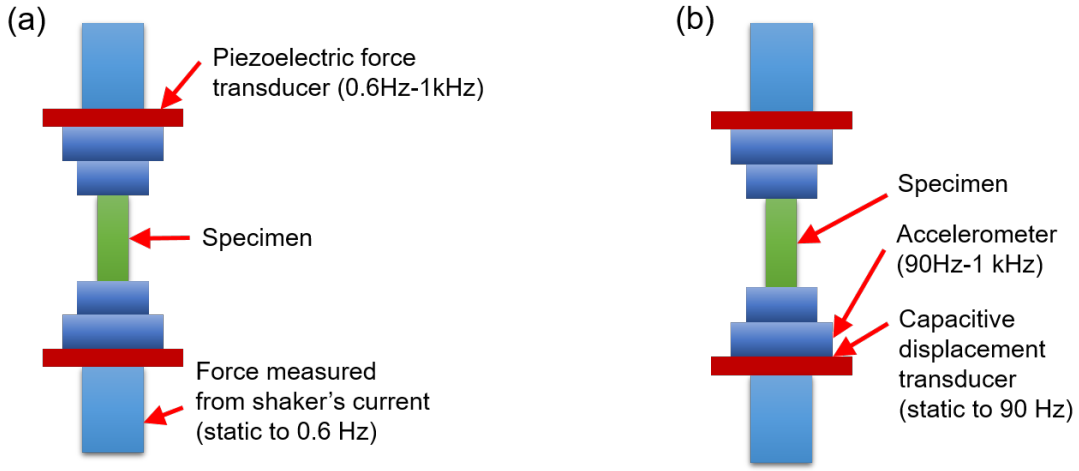

FIGURE II.4 – (a) Force measurement and (b) displacement measurement technologies in the used device

Figure II.4 shows that the measurement sensors used to record force and displacement depend on the frequency range in the experimental setup. The force transducer is fixed between the high stiffness frame and the upper clamp to measure the sinusoidal force. The stiffness of each component in the system should be much greater than the stiffness of the specimen. Using the DMA+300, it is recommended to test specimens with a stiffness comprised between 1 N/m to 10^7 N/m. 10^6 N/m at a maximum is finally recommended according to my experience. The maximum displacement which can be applied is 12 mm from peak to peak, respectively. The frequency and temperature ranges in which it can operate is 10^{-5} Hz to 200 Hz and -150°C to 500°C. These limits in terms of stiffness, loading, displacements and frequencies may be different from those reported in the apparatus data-sheet. Practically speaking, the measurement below 0.01 Hz always meets the problem of sinus distortion due to creep or relaxation and studies at high frequency (beyond 200 Hz) in DMA tests have not been reported due to limitations in instrument technology [Assarar 15], and also due to resonance problems [Placet 10a]. Furthermore, the deformation of the sample should be kept in the linear viscoelastic range to meet the theoretical requirements.

Another essential factor that needs to be considered in DMA is the ratio of the stiffness of the sample to that of the apparatus. The stiffness of the sample should be much smaller than the stiffness of the system to obtain accurate test results, especially for storage modulus. For composite specimens, in particular for UD composites tested in the fiber direction, it is sometimes difficult to ensure that the specimen stiffness is substantially lower than the frame stiffness. Indeed, when defining the size of the specimen to be tested, a compromise has to be reached between a representative elementary volume and a low stiffness. The specimen size has to be large enough to guarantee that the tested specimen is representative of the material and the section has to be the small to ensure low specimen stiffness. It is recommended by the DMA provider that the specimen stiffness is at least ten times lower than the frame stiffness. For some of the tested specimens, this could not be respected. In this case, the absolute value of the rigidity which was measured is erroneous. The parameters with this problem will marked with a symbol $*$ on the right top of the value. Only its relative evolution using normalized values as a function of temperature and frequency can be considered reliably.

II.2.2.b Experimental configurations

Complex modulus was measured during the experimental procedure to obtain the dynamic mechanical properties of the sample. The experiments using DMA method in this work were based on non-resonance method take reference of ISO and ASTM standard [ISO 01, D5026 13]. The tests in this study are expected to be processed in the linear elastic range of the material. The dynamic force is used as feedback with a static force to avoid the compression during the test, as shown in Figure II.5. Figure II.6 (a) shows the response of the flax/Petro based epoxy composites in transverse direction under different static and dynamic forces. As shown, the curve fitting between static stress and static strain was quite linear.

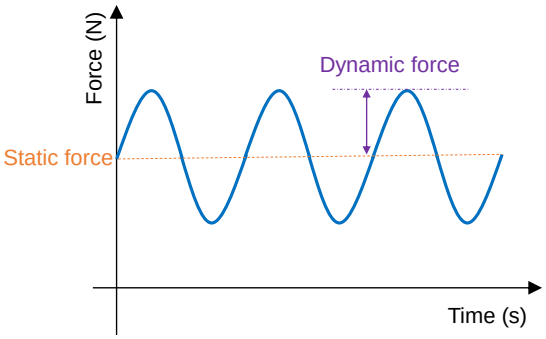

FIGURE II.5 – Excitation in DMA tests

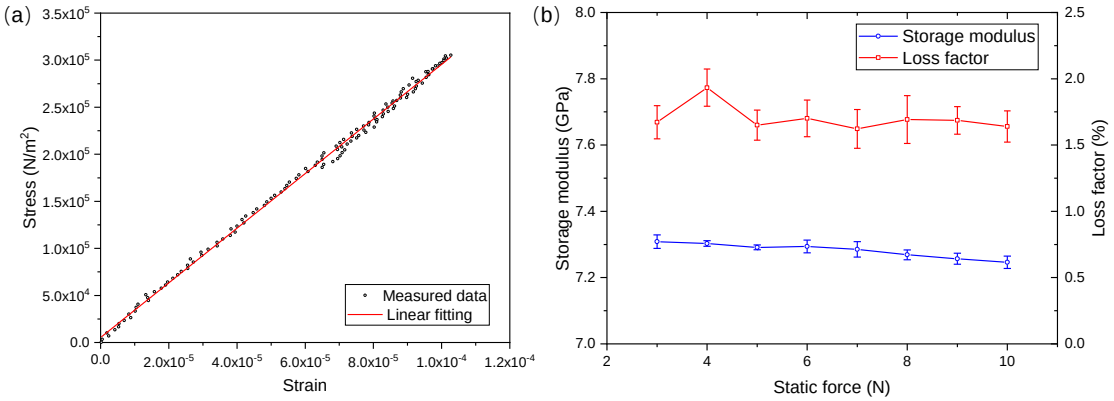

FIGURE II.6 – Verification of the excitation setup in DMA tests (a) Response of stress-strain under quasi-static tension (b) Storage modulus and loss factor with different static and dynamic forces under tension mode

The results of storage modulus and loss factor under different setups can be seen in Figure II.6 (b). The coefficient of variation for storage modulus and loss factor is less than 1 % and 10 %, respectively. It shows a stable dynamic mechanical response in the range of 5-10 N for static force.

Hence, the static force and dynamic force were selected as 6 N and 3 N, respectively. The verification for other kinds of composites and material directions was processed in the same way and will not be detailed here. The control of temperature and frequency in DMA tests can be divided into two situations: one keeping a constant temperature while the frequency is scanned, and the dynamic properties of different frequencies are measured at the specified temperature. The other one consists in keeping a constant frequency while the temperature changes and the dynamic properties under different temperatures are measured at the specified frequency. For the temperature sweep, the setup of the temperature pathway is configured with a monotonic ramp of with dwells (which allow measurement in isothermal condition) according to the researcher's intention and the characteristics

of the tested specimen. In our case, each step included a dwell at temperature for several minutes to make sure the sample has reached a homogeneous temperature distribution.

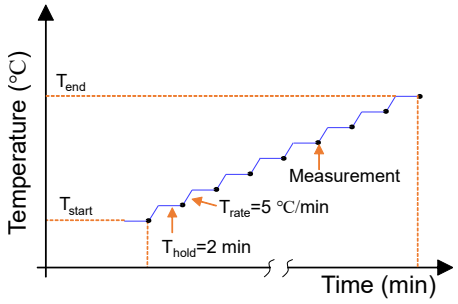

FIGURE II.7 – Protocol changes during temperature sweep in DMA tests

Figure II.7 shows the typical temperature pathway used in the DMA tests. T_{start} and T_{end} refer to the first and the last measured temperature values, respectively. The heating rate (T_{rate}) was set to 5 °C/min with a 2 minutes hold (T_{hold}) for each ramp to make sure a homogeneous temperature in the sample. Meanwhile, the relative humidity was not controlled during the tests since it was not within the function of the Metravib device.

TABLE II.2 – Configrations for each materials in DMA tests (D_{DMA}: Dimension, F_{sta}: Static force, F_{dyn}: Dynamic force, T_{DMA}: temperature range, f_{DMA}: frequency range, FGUD: UD Flax/GreePoxy composites, FPGE: Flax/Petro-based epoxy composites, FPPC: Flax/Polypropylene composites, HFRC: Hemp fabric composites, H4: Hemp4/GreenPoxy composites, L and T refer to longitudinal and transverse direction)

Material	D_{DMA} (mm^3)	F_{sta} (N)	F_{dyn} (N)	T_{DMA} (°C)	f_{DMA} (Hz)
FGUD	65*10*3.6	6	3	30 - 160	1 - 50
FPGE	65*10*3.5	6	3	30 - 160	1 - 50
FPPC	65*10*1.8	6	3	30 - 160	1 - 50
HFRC	65*10*2.0	6	3	30 - 160	1 - 50
Pure matrix	65*10*2.4	6	3	30 - 160	1 - 50
FGUD-L, H4-L	-	20	10	-20 - 160	0.7 - 50
FGUD-T, H4-T	-	10	5	-20 - 160	0.7 - 50
Pure epoxy	65*10*2.4	10	5	-85 - 160	0.7 - 50

The frequency and temperature ranges used for all the tested materials are detailed in Table II.2. Five values were inserted into the tested frequency range at logarithmic intervals. The dynamic mechanical properties were measured every 5 °C. All the tests were performed using a load feedback under tension mode. A static force of 20 N and 10 N for FGUD in longitudinal direction and pure epoxy, respectively, was set considering a low strain when the test was processing below 0 °C. At least three samples were tested for each material type following ASTM standard D5026.

II.2.3 Composite materials

In this work, three types of plant fiber reinforcements, made of flax and hemp fibers, were used to manufacture composites as shown in Figure II.8, namely non-crimp fabrics, woven fabrics and commingled fabrics. They are described in this Chapter which is focused on DMA testing, however, they will also be used in the next Chapters.

The first non-crimp fabric is a fully unidirectional flax fiber tape (FlaxTape™ 110 supplied by LINEO®, France), as shown in Figure II.8 (a). The number '110' stands for its areal mass was 110 g/m^2. A density of 1.45 g/cm^3 for flax fiber was measured using Archimedes' principle [Cadu 18].

The hemp reinforcements used in this study were woven fabrics produced in the frame of the SSUCHY project. They were manufactured by ENSAIT using hemp rovings supplied by Linificio e Canapificio Nazionale™, Italy. The rovings were fully made of hemp fibers [Corbin 20b]. The woven structure in satin (Hemp4 and 5) and twill (Hemp6 and 7) types are shown in Figure II.8 (b), respectively. The density of the rovings in weft and warp directions are shown in Table II.3. Among them, Hemp4 and 6 were balanced woven fabric in both directions with a density of 6.5 yarns/cm. Hemp 5 and 7 were unbalanced fabric with 9.5 yarns/cm in weft direction and 6.5 yarns/cm in warp direction.

Table II.3 – Hemp fabric with different woven patterns

Name	Woven pattern	Density in weft and warp (yarns/cm)
Hemp4	Satin	6.5 × 6.5
Hemp5	Satin	9.5 × 6.5
Hemp6	Twill	6.5 × 6.5
Hemp7	Twill	9.5 × 6.5

A woven commingled fabric was also used. It is labelled H4/PA12 and is made of Hemp4 and PA12 using commingled method detailed in Ref. [Corbin 20a] as shown in Figure II.8 (c). The woven fabric reinforced composites had a obvious different micro structure compared to UD or quasi-UD PFCs. The warp and weft yarn can be seen clearly on the cross-sectionnal views from Figure II.8 (b).

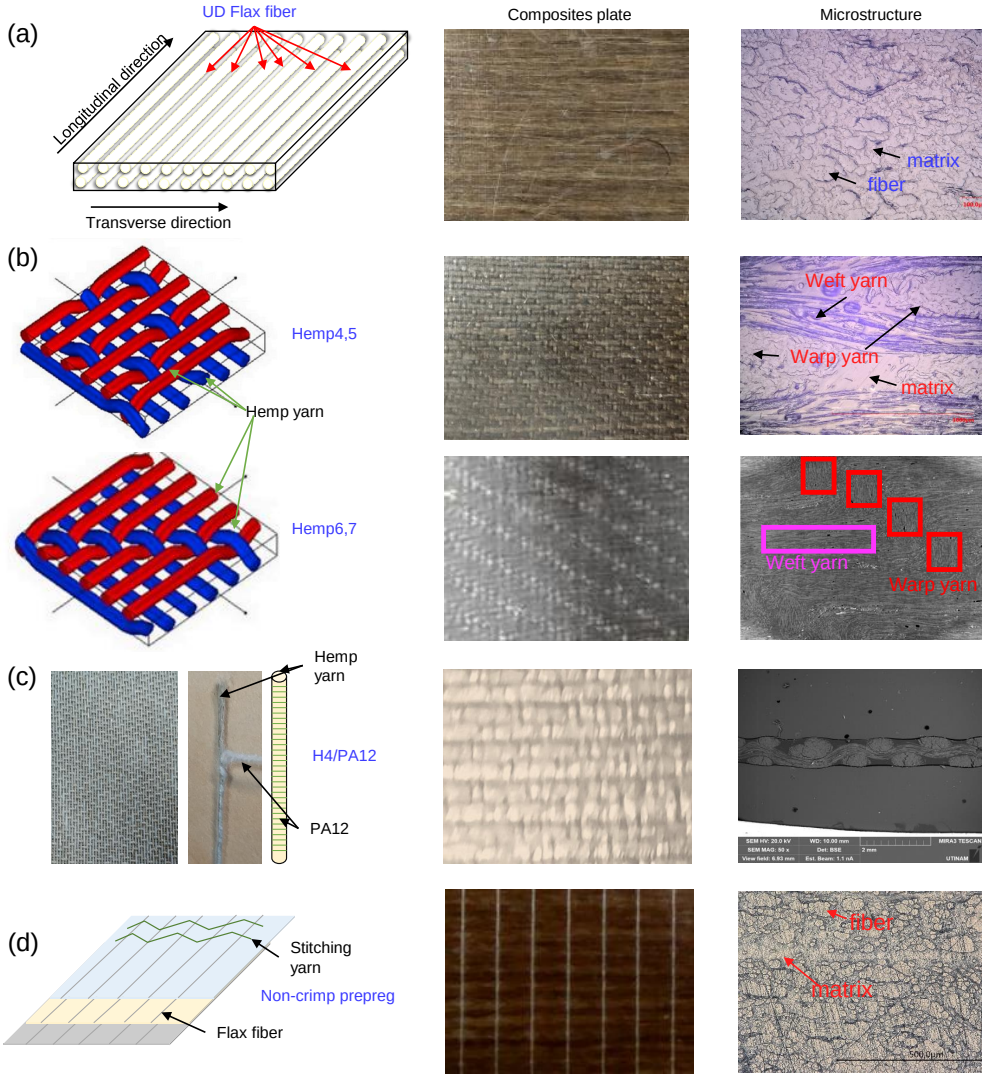

FIGURE II.8 – Reinforcements used in this work: (a) Unidirectional flax tape, (b) Hemp4 - Satin fabric and Hemp6 - Twill fabric [Corbin 20b], (c) non-crimp flax/PP prepreg, (d) H4/PA12 prepreg (H4/PA12 refers to Hemp4 reinforced Polyamide 12 composites)

The last reinforcement, a non-crimp flax/PP prepreg, was provided by 'Terre de lin®'. It is a quasi-unidirectional reinforcement, which includes stitched yarns in the transverse direction, as shown in Figure II.8 (d). The areal weight of flax fiber was around 200 g/cm^2 in the prepreg.

Table II.4 – Components in each product

Product	Reinforcement	Matrix	Hardener	Fabrication
Pure GreenPoxy (GE)	-	SR Greenpoxy 56	SD 7561	II.9 (a)(1)
Pure Polypropylene (PP) [Duc 14b]	-	Molpen HP500V	-	[Duc 14b]
Pure petro-based epoxy (PE)	-	SR 8500	SZ 8525	II.9 (a)(2)
Flax/GreenPoxy composites (FGUD)	UD FlaxTape™ 110 ($[0]_{20}$)	SR Greenpoxy 56	SD 7561	II.9 (a)(1)
Cross-ply flax/GreenPoxy composites (FGCR)	UD FlaxTape™ 110 ($[0/90]_{10}$)	SR Greenpoxy 56	SD 7561	II.9 (a)(1)
Hemp/GreenPoxy composites (HGEC)	Woven Hemp Fabric (4 plies)	SR Greenpoxy 56	SD 7561	II.9 (a)(1)
Flax/Petro based epoxy composites (FPEC)	UD FlaxTape™ 110 (20 plies)	SR 8500	SZ 8525	II.9 (a)(2)
Flax/Polypropylene composites (FPPC)	Prepreg (6 plies)	Polypropylene	-	II.9 (b)
Hemp4/Polyamide 12 composites (H4PA12)	Prepreg (2 plies)	Polyamide 12	-	II.9 (b)

The constituents for each composite manufactured and characterised in this work are detailed in Table II.4 and Figure II.9. The thermoset based composites and FPPC were manufactured by myself, and H4PA12 was made by the partner from ENSAIT in the frame of SSUCHY project. For the matrices, all the thermoset prepolymers and the hardeners are provided by Sicomin®, in France. The weight ratio of SR 8500 (density 1.17 g/cm^3) and SZ 8525 (density 0.94 g/cm^3) was 4:1, and that of SR Greenpoxy 56 (density 1.198 g/cm^3) and SD 7561 (density 0.971 g/cm^3) was 3:1. The curing parameters in this work were set using the data-sheet provided by the supplier. Pure matrix, also sometimes called neat matrix or pristine matrix in this work, describes the polymer without the reinforcement.

All the composite materials were manufactured by thermo-compression using the plant fiber reinforcements and the matrices, as detailed in Table II.4. This table also report the acronyms used all over the manuscript to refer to the materials in the text.

The thermoset-based composites were manufactured using hand impregnation and lay-up. The process starts with the preparation of the mold.

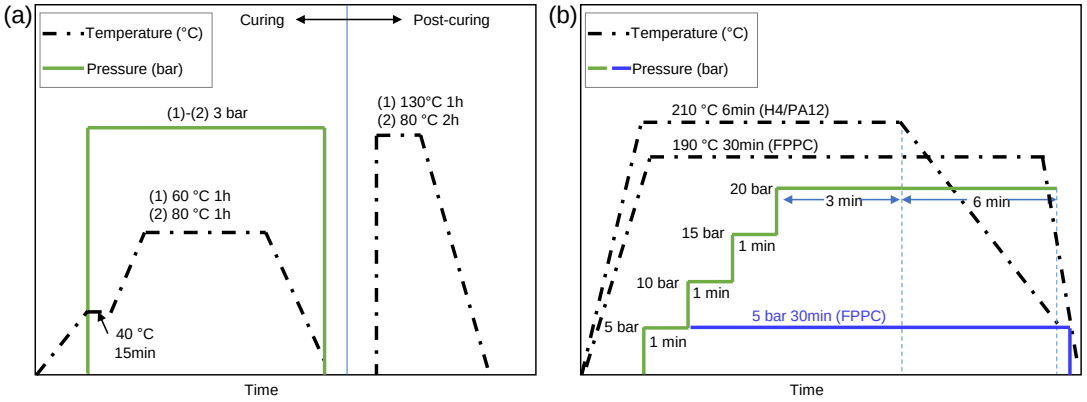

FIGURE II.9 – Temperature and pressure during fabrication of (a) (1) pure GreenPoxy and plant fiber/GreenPoxy composites (2) Pure petro-based epoxy and plant fiber/petro-based epoxy composites, (b) Hemp/PA12 composites

First, the rectangle mold (Length 300 mm, width 200 mm) is cleaned to ensure that its surface is flat without protrusions, so that a high-flatness composite material can be obtained. A little resin was scattered on the Teflon film. The reinforcement was placed in the specified direction, and then small amount of resin was scattered on the surface of the reinforcement again. This step was repeated until the predetermined number of plies was reached.

For unidirectional flax fibers, the resin can be placed directly in the center of the mold and it will diffuse and flow along the fiber direction under pressure by thermo-compression. The FGCR was manufactured following the sequence of [0/90] (0, 90 refers to longitudinal and transverse direction, respectively) and repeated 10 times. However, for hemp fiber woven fabrics, the resin was recommended to be evenly distributed on the surface of the reinforcement using a roller since the network-like fibers may restrict its flow compared with unidirectional fibers.

The control of temperature and pressure for the composites was guided by Ref. [Cadu 18]. The composite laminates were cured in a 'Fontjine Grotnes TPC 321' hot press device after the hand lay-up process. The pressure was applied when the temperature reaches 40 °C and the temperature was maintained for 15 minutes to optimize the impregnation of the matrix to the reinforcement as much as possible. The GreenPoxy 56 based composites were cured at 60 °C under a pressure of 3 bar for 1 hour, and then it was post-cured at 130 °C for 1 hour (130 °C, 1 h). This is a compromise choice considering the curing condition and time, and it will be discussed in the later section. The Petro-based epoxy based composites were cured at 80 °C under a pressure of 3 bar for 1 hour, and then post-cured at 80 °C for 2 hours. For the thermoplastic based prepreg, flax/Polypropylene composites were manufactured at 190 °C under a pressure of 5 bar for 0.5 hour. The hemp4/PA12 composites were produced by a SSUCHY partner (ENSAIT) using the temperature and pressure setup in Figure II.9 (b).

The pure matrix plates were made by pouring epoxy and hardener into the mold and then started the thermo-compression without pressure. Subsequently, post-curing was carried out for the thermoset matrix in the oven at the specified temperature and time to make sure they are fully cured.

The pure matrix and plant fiber reinforced composite plates were finally formed and then cut into rectangular shape specimens with a size of 65 mm × 10 mm for length and width using laser cutting, respectively. The thickness was dependent on the layers of reinforcement and the pressure, and its value were detailed in the section of experimental setup. All the samples were stored in a climate chamber with 23±1°C and 50±1 % RH for at least 4 weeks after cutting to ensure that they reached their moisture content equilibrium.

The calculation for the volume fraction of fiber, matrix and porosity was refereed from ASTM 3171 [ASTM-D3171 09]. The mass of each product was determined by a balance with 0.1 g precision. The length (L_c) and width (W) of the specimens are measured using a scaled ruler and the thickness (t_c) was measured using a vernier caliper with a precision of 0.01 mm. At last, the following equations are used to calculate the volume fraction of fiber, matrix and porosity:

$$\mathrm{Vol}_c = L_c \times W \times t_c, \tag{II.4}$$

$$M_m = M_c - M_f, \tag{II.5}$$

$$V_f = \frac{M_f}{\rho_f} \times 100\%, \tag{II.6}$$

$$V_m = \frac{M_m}{\rho_m} \times 100\%, \tag{II.7}$$

$$V_p = 100\% - V_f - V_m, \tag{II.8}$$

where, Vol_c was the volume of the composite plate; M_c, M_f and M_m are the mass of composite plates, fiber and matrix, respectively; ρ_f, ρ_m was the density of fiber (1.45 g/cm^3) and matrix (1.19 g/cm^3), respectively; V_f, V_m and V_p are the volume fraction of fiber, matrix and porosity, respectively. The average fiber volume fraction of FPEC, FGUD, FGCR and Hemp4/GreenPoxy composites (H4) were finally determined to be around 48 %, 47 %, 44 % and 48 %, respectively.

Table II.5 shows the static mechanical properties of flax and hemp reinforced composites obtained by quasi-static tensile test, where E and σ_f refer to Young's modulus and stress at failure, respectively . H4PA12 was manufactured at ENSAIT by Anne-Clémence Corbin and the characterization was part of another PhD thesis performed by Benjamin SALA in the frame of the SSUCHY project [Sala 20]. The Young's modulus do not show significant difference in flax reinforced composites with two different types of matrix and the values are around 30 GPa and 4 GPa for longitudinal and transverse direction, respectively. Hemp4 reinforced composite was balanced in the two main directions. Static properties are comparable to the ones obtained in flaxtape cross-ply laminates.

TABLE II.5 – Static mechanical properties of different type PFCs (mean value + standard deviation)

Material	Direction	V_f (%)	V_p (%)	E (GPa)	σ_f (MPa)
FPEC	L	48±1	2.5±0.7	31.4±0.6	320 ±32
	T			4.3±0.3	21±5
FGUD	L	47±1.3	3.2±0.9	30.1±0.6	310 ±20
	T			4.6±0.38	19 ±3
FGCR	L	44±1	2±2	17±1	177 ±17
H4	T	48±2	0.3±0.1	19±1	176 ±3
H4PA12	T	54±1	-	11±1	104±9
FPPC	L	44±2	-	24.2±3.3	155±8

II.2.4 Water aging tests

Figure II.10 shows the whole process of the water aging test. The flax/GreenPoxy 56 composites was selected in this study to investigate the influence of water aging time on dynamic properties of PFCs.

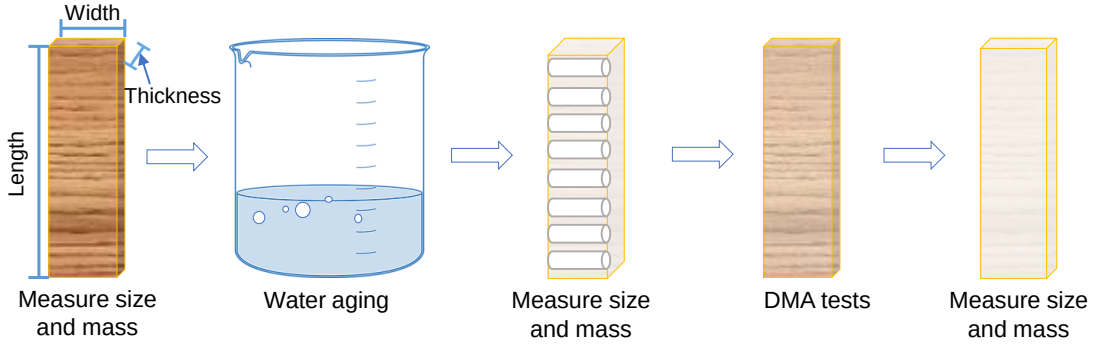

FIGURE II.10 – Water aging test process

Three samples in fiber direction and three samples in transverse direction were tested in DMA tests for each ageing time. 5 N and 1.25 N were set to the static and dynamic force, respectively. The samples were tested in 3-point-bending mode in longitudinal direction and tension mode in transverse direction, respectively.Bending mode is preferred for longitudinal direction to know the changes of storage modulus and this is discussed in the section II.3.1. The temperature range for DMA was distributed from 30 °C to 160 °C and the heating rate (T_{rate}) was set for each steps.

The flax/GreenPoxy composite samples with a size of 65×13×3.5 mm^3 were used and the samples were weighted and their dimensions in the three main directions measured after being removed from the climate chamber (23 °C and 50 % RH). Then, the samples were dropped into tap water and maintained for 1 to 5 days at ambient temperature. The sizes and mass were then measured before and after the DMA tests.

II.3 Results and discussion

In this section, the test mode and the dynamic mechanical properties of GreenPoxy are introduced at first. Then, the damping properties of FFRC and HFRC are described at ambient temperature. Meanwhile, the influence of fiber architecture and matrix type on damping is studied. The dynamic mechanical properties of FGUD and H4 as well as GE are obtained at wide frequency according to TTSP based on DMA tests at wide temperature range.

II.3.1 Comparision of DMA results from bending mode and tension mode

DMA tests in 3-point-bending and tension mode were processed for FGUD-L to evaluate the influence of the loading mode on the measured viscoelastic properties. Hereinafter, 3-point-bending mode will be referred to as bending mode. The configuration in bending mode are the same as in tension mode except the value of excited force: 5 N and 1.25 N were set to the static force and dynamic force, respectively.

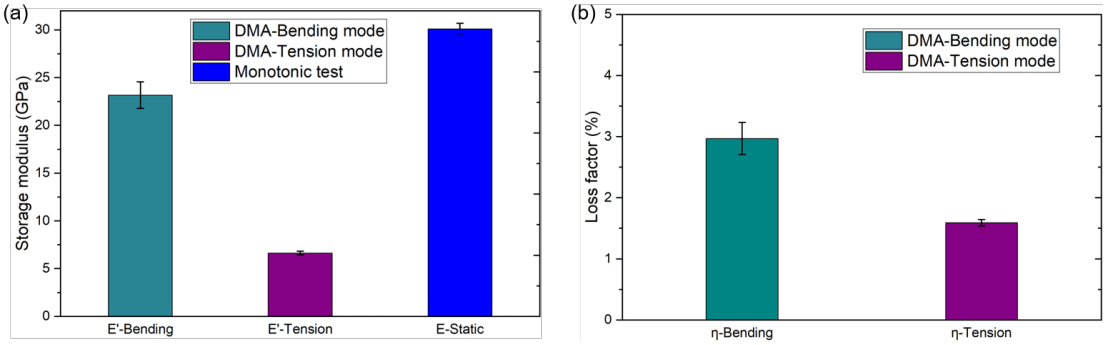

Figure II.11 – (a) Storage modulus and (b) loss factor of FGUD-L obtained from DMA test in bending and tension mode at 1 Hz (E-Static refers to monotonic test in tension)

Figure II.11 shows the results of storage modulus and loss factor for FGUD-L at 1 Hz. The storage modulus obtained in bending mode (storage modulus: 23.6 GPa, stiffness: 5.3×10^5 N/m) is significantly higher than the one determined

in tension mode (storage modulus: 6.6 GPa, stiffness: 5.4×10^6 N/m). This is due to the stiffness frame limitation in tension mode. It can be seen that the value of E′ determined in bending mode have less difference than that in tension mode compared with the value from monotonic test. The loss factor obtained in bending mode (2.9 %) is higher than that obtained in tension mode (1.59 %). This was already observed in literature [Duc 14b] and is attributed to the friction between the sample and clamp in bending mode. Based on these results, it was decided to prefer the tension mode in the following experiments. Indeed, the main focus of this PhD thesis is to investigate the damping behavior, the static behavior of these materials being investigated accurately in other works. An exception is made in the last section of this chapter (influence of moisture) where the bending mode was preferred to minimize the problems related to clamping in tension mode for specimens which shrinked when temperature sweep is applied.

II.3.2 Dynamic mechanical properties of GreenPoxy

II.3.2.a Verification of the curing conditions

The curing process is one of the important parameters during the manufacture of thermoset based PFCs. GreenPoxy 56 works as a new type of epoxy family compared to traditional DGEBA-based epoxy. Some curing protocols are proposed by the provider for the neat resin and some others can be found in the existing literature for composites [Perrier 16, Perrier 17, Pertegás 16]. The curing time generally varies between 8 and 48 hours depending on the temperature conditions. This is time-consuming in particular for industrial production. Therefore, it was decided to verify the curing condition of GreenPoxy based composites after manufacturing in order to try to minimize the curing time.

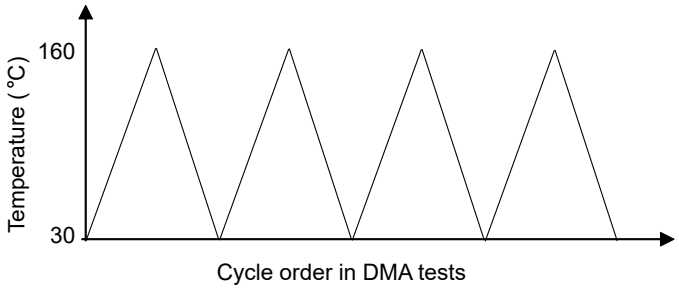

Figure II.12 – Temperature cycle during DMA test

Samples cut from FGUD in transverse direction were then tested in DMA after curing and post-curing steps. 8 loops with increasing and decreasing temperature ramps, as shown in Figure II.12 were applied to study the changes in T_g of FGUD. Different post-curing conditions (95 °C 1h, 95 °C 8h, 130 °C 1h, 130 °C 8h) were compared after curing at 60 °C during 1h. Table II.6 shows the evolution of T_g over

the heating/cooling cycles for the different post-curing protocols. The difference in T_g is decreasing obviously as the increase of curing temperature and time. A stable value, which means a fully cured condition, is obtained using 130 °C.

TABLE II.6 – T_g of FGUD-T as a funtion of temperature cycle in DMA tests (T_g 1: T_g in the first loop, T_g 8: T_g in the last loop, difference=T_g 8 - T_g 1)

Post-curing	95 °C 1h	95 °C 8h	130 °C 1h	130 °C 8h
T_g 1	79	89	93	99
T_g 2	87	89	94	97
T_g 3	90	92	96	99
T_g 4	91	92	95	97
T_g 5	94	95	98	100
T_g 6	94	94	95	98
T_g 7	95	96	98	100
T_g 8	95	96	96	98
Difference	16	7	3	-1

The dynamic mechanical properties at 1 Hz of FGUD using post-curing protocol of 130 °C and 1h are shown in Figure II.13.

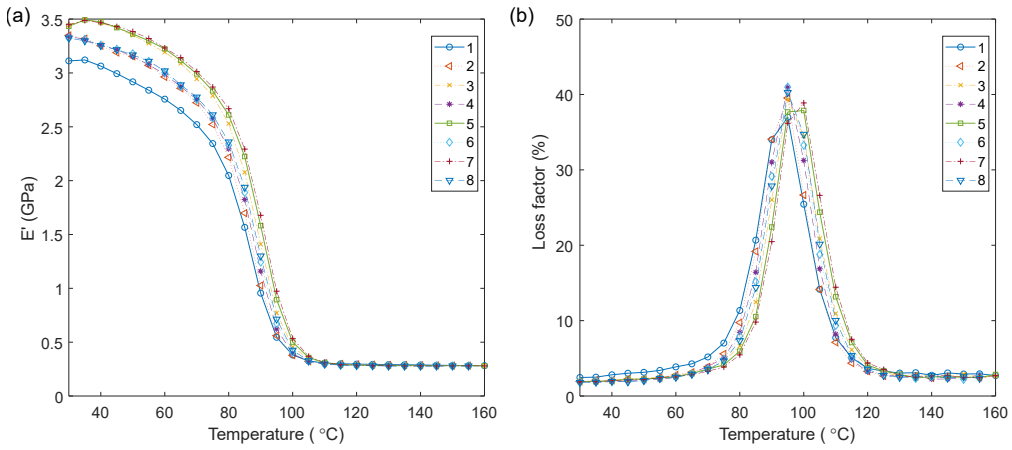

FIGURE II.13 – (a) Storage modulus and (b) loss factor of FGUD (post-curing at 130 °C and 1h) in transverse direction for each temperature cycles at 1 Hz

Figure II.13 (a) shows the evolution of the storage modulus as a function of temperature for each heating/cooling cycle. The difference of E' observed at 30 °C between the different cycles is attributed to the moisture loss due to the successive heating phases. The loss factor curves do not show significant difference for the

different cycles and show regular trend. A difference of 3 °C from the first to the last loop is observed when the T_g is determined from the curve of loss factor. This difference is low and shows that the post-curing protocol was well adapted. As the best compromise between curing level and time, 130 °C and 1h is selected as the final setup in the post-curing process.

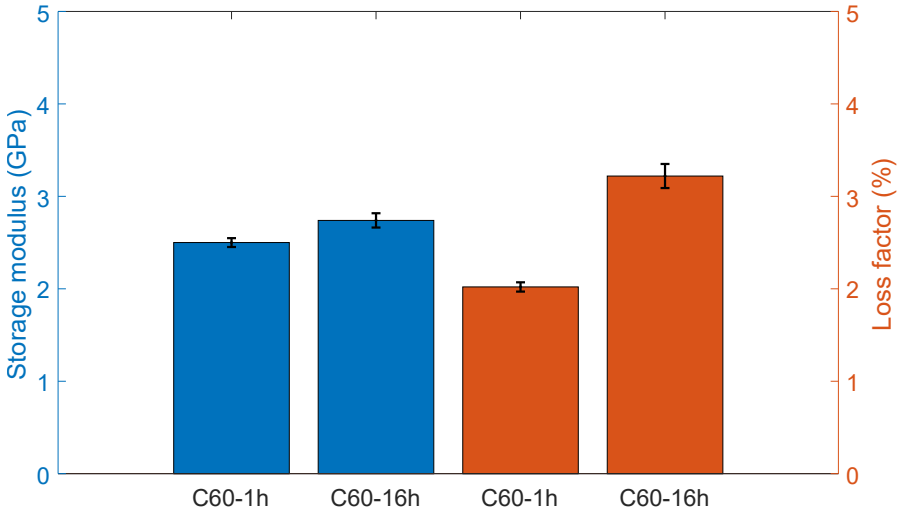

FIGURE II.14 – Comparison of storage modulus and loss factor of pure GreenPoxy at 1 Hz and ambient temperature using the optimized curing time and the datasheet from Sicomin® (C60-1h refers to sample curing at 60 °C and 1 hour with post-curing at 130 °C and 1 hour, C60-16h refers to sample curing at 60 °C and 16 hour with post-curing at 100 °C and 1 hour)

Based on the optimized curing condition, the GreenPoxy curing at 60 °C and 1 hour with post-curing at 130 °C and 1 hour is compared with that curing at 60 °C and 16 hour with post-curing at 100 °C and 1 hour using DMA tests. The storage modulus and loss factor at 1 Hz and ambient temperature are presented in Figure II.14. As it can be observed, there is no significant difference on storage modulus between our optimized curing condition (C60-1h) and that suggested by Sicomin® (C60-16h). However, the loss factor of optimized curing condition (C60-1h) is around 37 % lower than that the one measured with the curing protocol suggested by Sicomin® (C60-16h). This attributed to the different cross-linking state.

II.3.2.b Glass and secondary transitions

The dynamic mechanical properties of traditional epoxy family were widely studied and it has been observed that the secondary transition usually occurred below 0 °C except the glass transition (around 110 - 135 °C) [Hassan 16]. DMA tests between -100 °C and 160 °C were processed at 5 Hz on the pure GreenPoxy specimens. The storage modulus, loss modulus and loss factor were measured every

5 °C as shown in Figure II.15. The curve of loss factor shows two peaks, corresponding to the glass transition and secondary transition. The main transition, the glass transition, is found around 86 °C. A secondary transition is seen -50 °C.

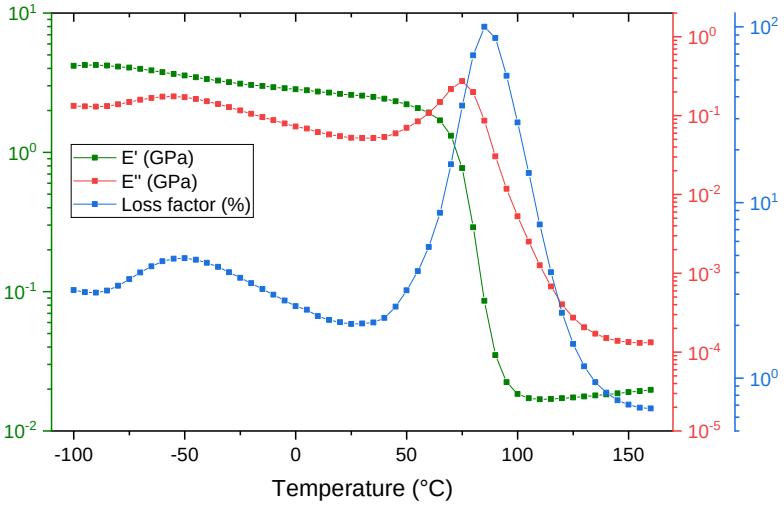

FIGURE II.15 – Dynamic mechanical properties of GreenPoxy from -100 to 160 °C at 5 Hz

II.3.3 Damping properties of composite materials at ambient temperature

In this section, experimental results from DMA tests at ambient temperature and 1 Hz on FFRC and hemp fabric reinforced composites (HFRC) are first described. The effect from different reinforcements and matrix will then be discussed to show their influence on damping properties.

II.3.3.a Damping properties of FFRC at 1 Hz

In this section, pure PE, GE, PP matrices and associated flax fiber based composites (FPEC, FGUD, FPPC). For FPEC, the two types of laminates (unidirectional and cross-ply) were considered. The dynamic mechanical properties of all these materials were measured using DMA tests. Results are shown in Figure II.16, where 'L' and 'T' means 'Longitudinal direction' and 'Transverse direction' of the UD composite materials, respectively. The error bar refers to the standard deviation measured from at least 3 samples for each material.

The behaviour of the UD composites is analyzed at first. The value of the storage modulus of the neat epoxy matrices and flax reinforced composites determined experimentally are given in Figure II.16 (a). The values for pure polypropylene were collected from Ref. [Duc 14b]. As shown, the highest values of storage modulus for FPPC are obtained in longitudinal direction. Table II.7 shows the comparison of storage modulus at 1 Hz from DMA tests and Young's modulus from monotonic mechanical tests.

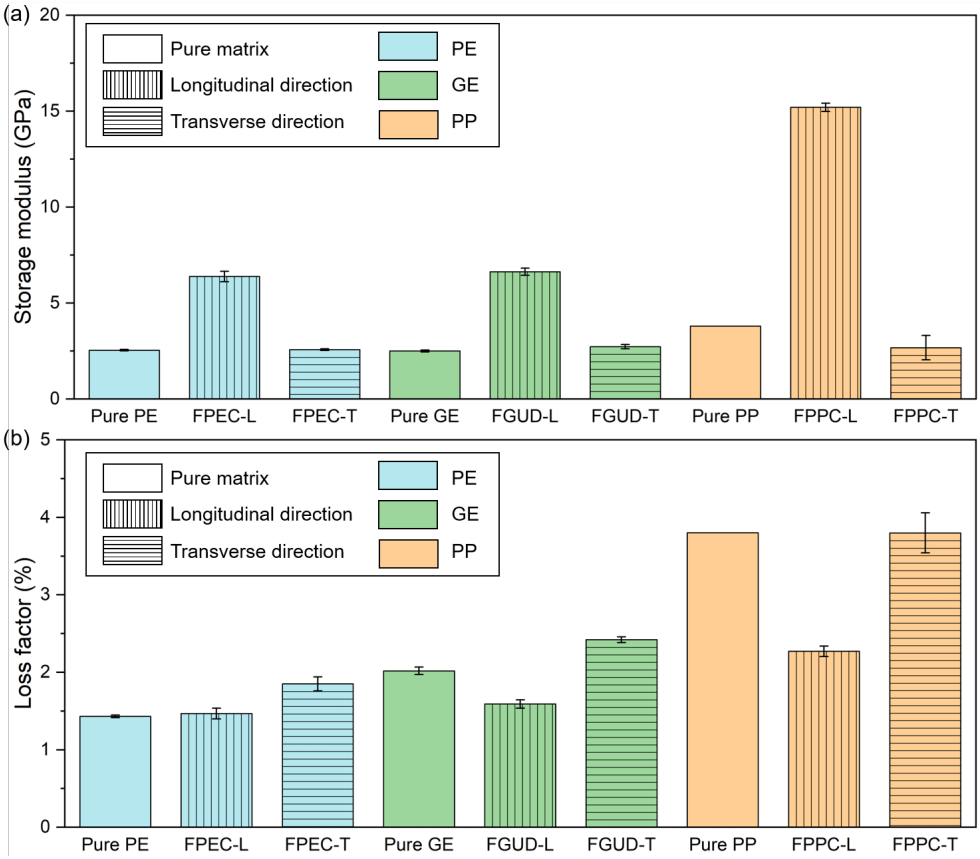

FIGURE II.16 – (a) Storage modulus and (b) loss factor of pure matrix and Flax reinforced composites measured by DMA tests at 1 Hz and ambient temperature (value of Pure PP is refer to [Duc 14b])

A large difference can be observed for most of the tested specimens, in particular in the fiber direction of the UD composites. Although the difference in manufacturing process and the measurement method needs to be considered, the main influencing factor here is that the stiffness of FPEC and FGUD in longitudinal direction is close to the limit value of the test system. The strain measurement of the specimen is overestimated due to the frame contribution and then the storage modulus is under-estimated. This is a well-known effect in DMA experiments, even if a better behavior was expected with this apparatus.

Indeed, the new DMA+ series instruments from Metravib are dynamic testing machines based on a one-piece high rigidity test frame. Given the relatively low stiffness of the pure matrix and FFRC in transverse direction, the difference between the storage modulus and Young's modulus is lower but still significant. Additional measurements have shown that this difference is due to the strain determination. Indeed, when strain in DMA tests is measured with contact extensometers (instead of determined from the displacement of the actuator), the values of the storage modulus are similar to the ones determined using monotonic tests.

TABLE II.7 – Values of storage modulus (E′) determined at 1 Hz using DMA tests and Young's modulus determined using monotonic tests (E_{static}) (FGCR refers to cross-ply flax/GreenPoxy composites)

	FPEC-L	FPEC-T	FGUD-L	FGUD-T	FGCR	FPPC-L
E′ (GPa)	6.4*	2.6	6.6*	2.7	7.4*	15.2
E_{static} (GPa)	31	4.3	30	4.6	17	24

* The value is not accurate due to the stiffness of the sample which is closed to the one of the frame of the test system

Based on these measurements, it is recommended not to consider the absolute value of the storage modulus determined at the composite scale in the fiber direction. Only their relative variation as a function of frequency and temperature will be considered in the next sections.

However, as expected, it is observed that the addition of flax fiber into pure matrix cause an increase in storage modulus and these results are similar to those reported by F. Duc [Duc 14b].

The damping properties of pure matrix and FFRC measured by DMA tests at 1 Hz and ambient temperature are shown in Figure II.16 (b). This allows quantitative comparison and description the influence of different kinds of matrices including thermosets and thermoplastics on the damping properties of FFRC.

Longitudinal direction

In longitudinal direction, it can be observed that the loss factor of the flax/epoxy composites in the fiber direction is of the same order of magnitude than the neat epoxy matrices. The mean values are approximately 1.4 % for the FPEC and 1.5 % for the FGUD, when 2 % are measured for the neat resins, respectively. For the PP, it can be observed that the addition of high-strength fibers induces a strong decrease in loss factor (from 4% for the pure PP to 2.3 % for the composite). The integration of fibers probably restricts the movement of the matrix so that the energy cannot be dissipated by the matrix [Senthil Kumar 16].

As for the traditional glass and carbon fiber composites, it can be hypothesized that for PFCs, in the fiber direction, the damping behavior is also mainly driven by the damping of the fiber themselves. However, and to the best of the author's knowledge, no damping values were measured using direct method on flax fibers. A value of 4 to 4.5 % was reported recently for cellulose fibers (viscose and bleached softwood kraft) by Elsayad et al. [Elsayad 20] using Brillouin spectroscopy. Values comprised between 1 and 10 %, depending on the loading frequency and path, for hemp fibers, in the longitudinal direction using DMA on single fibre were also reported by Placet [Placet 10b].

It is proposed here to estimate the value of the loss factors of the fiber using inverse method and a homogenization model with several assumptions as follows:

(1) Total energy is dissipated in the fibers and matrix.
(2) Fiber and matrix are linear viscoelastic elements.
(3) No porosity in the composites.

The loss factor can be calculated based on the model developed by Ungar and Kerwin[Ungar 62],

$$\eta = \frac{\sum_{i=1}^{n} (\eta_i W_i)}{\sum_{i=1}^{n} W_i}, \tag{II.9}$$

where η_i is the loss factor for ith element, W_i is the strain energy stored in ith element, n is the total number of elements. The flax fiber composites can be divided into two components of fiber and matrix, then

$$\eta_L = \frac{\eta_f W_{fl} + \eta_m W_m}{W_{fl} + W_m}, \tag{II.10}$$

where $\eta_L, \eta_{fl}, \eta_m$ is the loss factor of the composites, fiber in longitudinal direction and matrix, respectively, W_{fl}, W_m is the strain energy stored in fiber in longitudinal direction, matrix. The W_i can be calculated based on their strain energy,

$$W_i = \frac{1}{2} \int_{V_i} \sigma_i \varepsilon_i dV, \tag{II.11}$$

where V_i is the volume fraction of ith components and among them,

$$W_{fl} = \frac{1}{2} E_{fl} \varepsilon_{fl} \varepsilon_{fl} V_{fl}, \tag{II.12}$$

$$W_m = \frac{1}{2} E_m \varepsilon_m \varepsilon_m V_m, \tag{II.13}$$

Therefore, the damping properties of the fiber in longitudinal direction can be estimated using the following model:

$$\eta_L = \frac{\eta_{fl} E_{fl} V_f + \eta_m E_m V_m}{E_{fl} V_f + E_m V_m}, \tag{II.14}$$

where $\eta_L, \eta_{fl}, \eta_m$ refer to loss factor of the composites and the fiber in longitudinal direction, and matrix. E_{fl}, E_m is the Young's modulus of the fiber in longitudinal direction and matrix, respectively.

The estimated values of the loss factor in the fiber direction for the flax fibers are approximately 1.6 % and 2.2 % when back-calculated from FGUD and FPPC results, respectively. The effect of yarn in the transverse direction of FPPC as well as the crimp of the fiber bundles in the longitudinal direction should be taken into account.

The values identified in this work by inverse method are consistent with the ones reported in literature. It can be concluded also that more effort should be put in the future on the determination of the damping properties of plant fibers by direct method to evaluate the relevance of the values determined by back-calculation.

In particular, such investigations could help to understand the role of the interface between the matrix and the fibers in the damping profermances. This will be discussed later in the manuscript. Whatever their physical origin, the values measured for PFCs are still higher than that of composites reinforced by synthetic fibers such as carbon fiber and glass fiber (around 0.5 - 0.9 %) [Duc 14b], which shows wide potential of plant fibers in application where damping plays a major role.

Transverse direction

In transverse direction, results show an increase in the damping by approximately 20-28 % when flax fiber are added into the thermoset matrices. This phenomena can be caused by the damping potential of flax fibers in the transverse direction, as well as energy dissipation at the interface between matrix and fibers. Again, damping properties of flax fibers in the transverse direction are also lacking sorely.

The damping properties of PP based flax fiber composites are radically different from that of PE and GE. A higher range of loss factor (3.8%) is obtained in FPPC in transverse direction and this is similar to the existing literature, which shows a higher damping capability than thermoset based PFCs [Chung 03].

Similarly, the damping properties of the fibers in transverse direction can be estimated using the following model:

$$\eta_T = \frac{\eta_{ft} E_m V_f + \eta_m E_{ft} V_m}{E_{ft} V_m + E_m V_f}, \tag{II.15}$$

where η_T, η_{ft} refer to loss factor of the composites and the fiber in transverse direction, and matrix. E_{ft} is the Young's modulus of the fiber in transverse direction. For transverse direction, 3.4 % and 4 % are identified for the loss factor of flax fiber in transvserse direction from FGUD and FPPC, respectively. The differences can be explained by the fact that the FPPC is made with a quasi-UD fabric (including stitching yarns in the transverse direction) while FGUD is made from a pure UD composite. The damping properties of this composite in the transverse direction are very similar to the ones of the pure matrix. So, it can be underlined that the behavior is mainly driven by the matrix in this material direction. It could be also an effect from weaker interactions between flax fiber and PP compared to flax fiber and PE or GE, which lead to a lower stress transfer to flax fibers. In this case (weak interface), a higher energy dissipation at the interface could also be expected. The large uncertainty in FPPC-T values is attributed to the presence of yarns in the transverse direction. Indeed, as mentioned just above, this composite material is made of a non-crimp fabric including stitching yarns.

Regarding the cross-ply laminates (FGCR), a loss factor equal to approximately 1.89 % is measured in the two main directions. It is comprised between the values measured in the fiber and transverse directions of the UD laminates, FGUD-L and FGUD-T (1.6 and 2.4 %, respectively).

II.3.3.b Damping properties of HFRC at 1 Hz

Woven hemp fabrics with different weave patterns including satin and twill and different matrices were also tested. The dynamic mechanical properties of hemp/GE composites and H4/PA 12 composites measured by DMA tests at 1 Hz and ambient temperature are shown in Figure II.17, where the 'longitudinal direction (L)' and 'transverse direction (T)' of the composite materials correspond to 'warp direction' and 'weft direction' of the reinforcement, respectively. The error bar refers to the standard deviation measured from at least 3 samples for each tests.

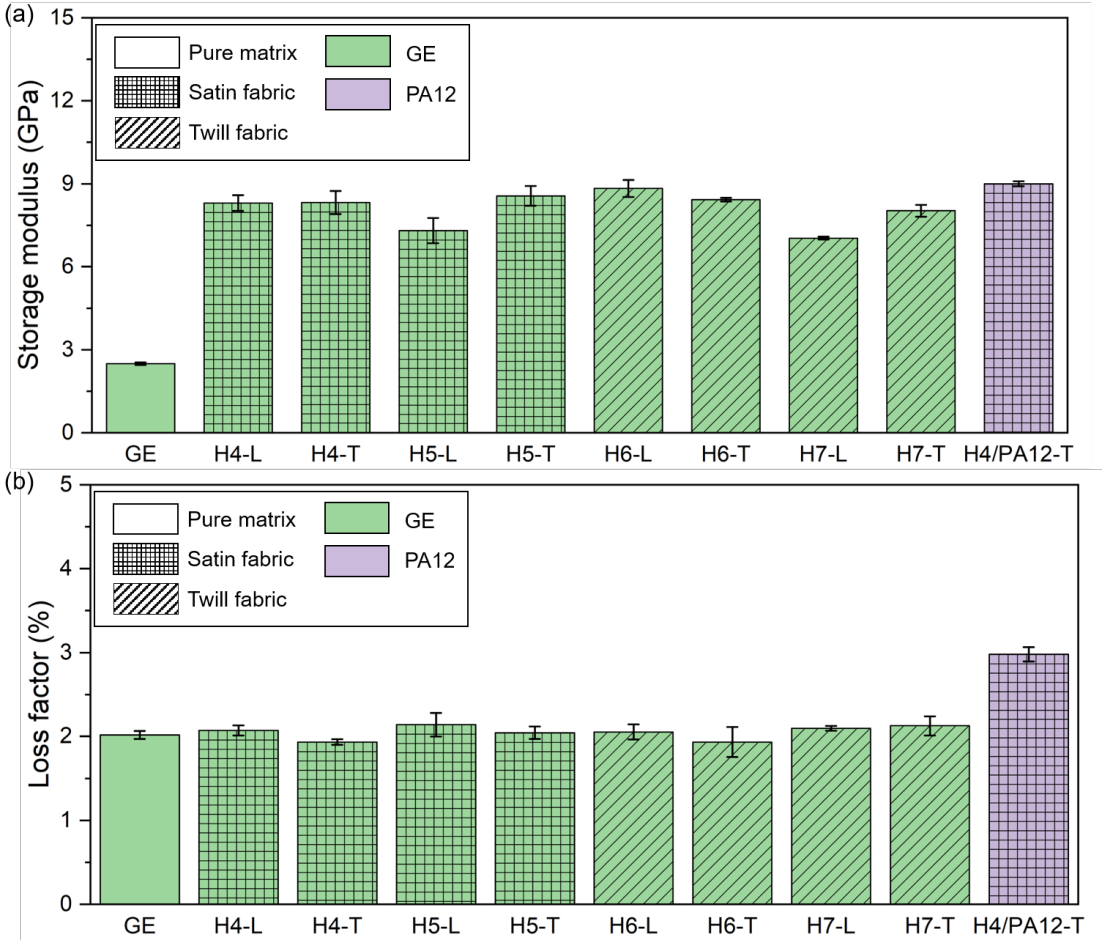

FIGURE II.17 – Loss factor of hemp fiber reinforced composites measured by DMA tests at 1 Hz and ambient temperature

Figure II.17 (a) shows the storage modulus of the HFRC with different weave patterns. It can be seen that the storage modulus among H4-H7 including thermoset (epoxy) and thermoplastic (Polyamide 12, PA12) based hemp fabric composites do not show a large difference. Indeed, the fiber density of the hemp fabric reinforcement in longitudinal and transverse direction used in this section has a closed value. This is in contrast with the unidirectional reinforcements described in the previous section. For the balanced fabrics (satin (H4) and twill (H6)), the sto-

rage modulus of GreenPoxy based H4 and H6 composites in both directions is approximately equal to 8.5 GPa. This is close to the storage modulus (9 GPa) of the thermoplastic based composites (H4/PA12). H5 and H7 are unbalanced hemp fabric reinforced composites. The density of yarn in transverse direction is higher than longitudinal direction. This caused the storage modulus to be around 15 % higher in transverse direction. Again, the storage modulus (8-9 GPa) of HFRC measured using DMA tests is far from that in monotonic tests (around 11-18 GPa) due to the higher stiffness of the sample (around 3.3×10^6 N/m).

The loss factors of thermoset and thermoplastic-based HFRC are shown in Figure II.17 (b). For the thermoset-based composites, no significant differences can be observed among the tested materials, whatever the woven pattern and material directions are. All the values are around 2 %. For these woven fabric composites, the damping is indeed mainly driven by the fiber damping in both main directions. This result would be consistent with a loss factor of hemp fibers of approximately 2 %. The values of approximately 2 % measured at the hemp composite scale are also comparable to that of cross-ply flax/GE composites (FGCR, mean value of 1.85 %, Figure II.18). The slight difference, if significant when considering measurement uncertainties, could be attributed to the fiber waviness induced by crimp in the woven fabric. This slight disorientation of the fiber when compared to loading axis could provide additional energy dissipation.

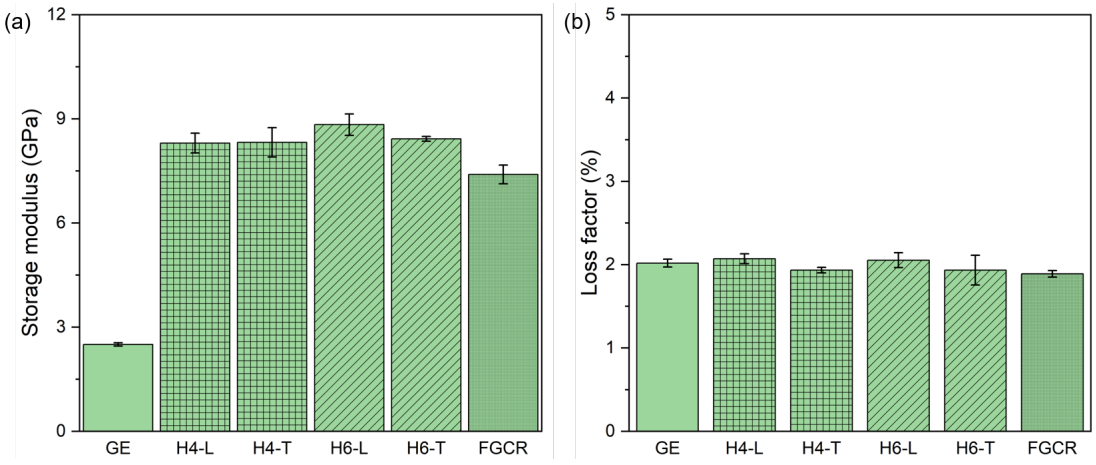

FIGURE II.18 – Comparison between balanced hemp fabric/GreenPoxy composites and FGCR in (a) storage modulus and (b) loss factor at 1 Hz and ambient temperature

At last, the damping properties in H4/PA12 composites are higher with a loss factor equal to approximately 3 %. This value can be explained by the meso structure of the composite, as shown in Figure II.19. Indeed, in this composite made from a commingled fabric, it can be observed that the yarns are not well impregnated by the polymer. They were highly compacted when the hydrid wrapped spun yarns were manufactured. Under tensile loading in the wrap and weft direc-

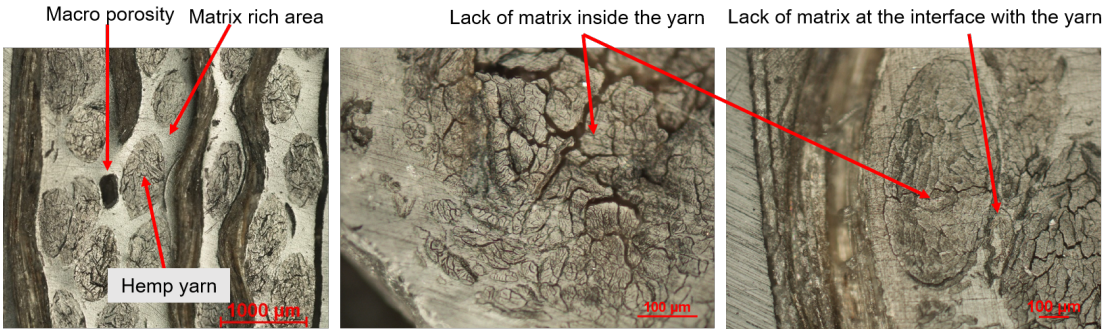

FIGURE II.19 – Mesostructure of H4/PA12

tions, friction can occur between the fibers within the rovings. This is an additional source of energy dissipation that could explain, at least partly, the higher damping loss factor measured when compared to the epoxy-based composites.

II.3.4 Damping properties of composite materials in a wide temperatures range

The damping properties regarding matrix type and fiber architecture have been investigated at ambient temperature. This section will focus on their damping properties in a wide temperature range.

II.3.4.a UD Flax reinforced composites

The dynamic mechanical analysis of FFRC was carried out with specific frequency and temperature ranges using DMA tests. The researches in this section regarding the dynamic mechanical properties of FFRC materials are mainly aimed at three objectives. The first is to study the dynamic mechanical response as a function of frequency and temperature. Then the influence from reinforcement will be studied. At last, the master curve will be built to obtain the damping properties on a wide frequency range.

The results of the storage modulus, loss modulus and loss factor sweep with temperature at 1 Hz are shown in Figure II.20. The curves of storage modulus are normalized using the measured value divided by the value measured at 30 °C.

In the glassy state, the molecular structure in the polymer is almost frozen. As the temperature increases, the molecular chain starts to relax, which is manifested in a slight decrease in the storage modulus.

(1) For GreenPoxy (GE)-based composites, the storage modulus of FGUD-L decreases by approximately 45 % from ambient temperature to T_g. The behavior of E′ in FGUD-T is similar to that of Pure GE and their value decrease by about 77 % -96 % from ambient temperature to T_g.

(2) For Petro(PE)-based composites, their T_g is around 115 °C so the decrease of E′ occurs at higher temperature than for GE-based composites and the value of decrease (about 24 % for FPEC-L) is also smaller than that of

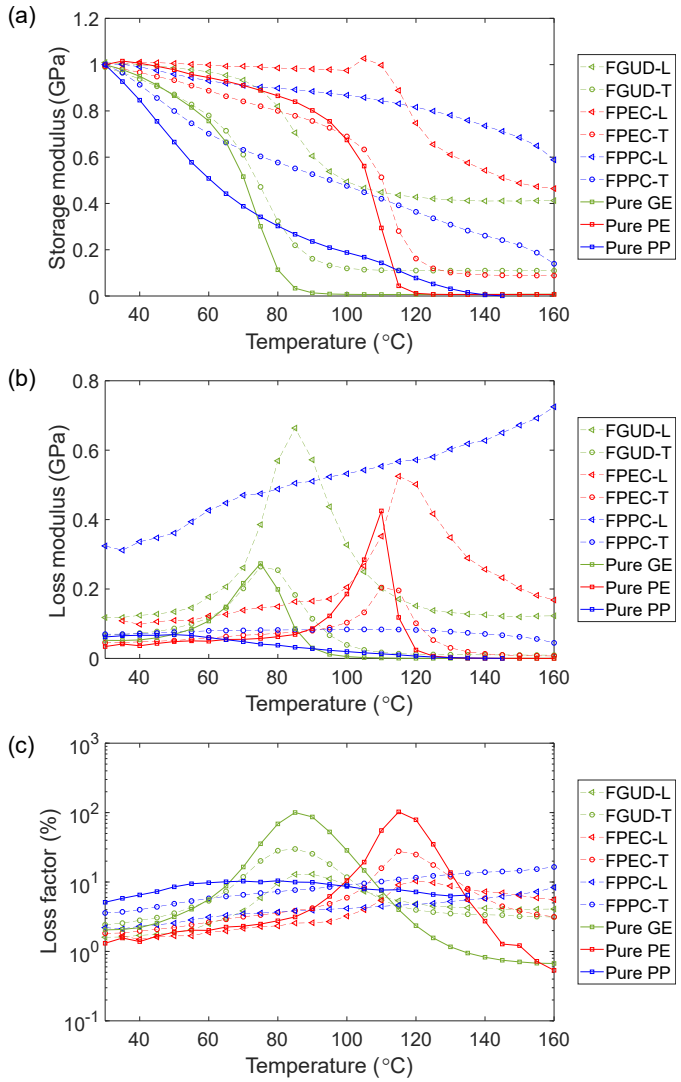

FIGURE II.20 – (a) Normalized storage modulus, (b) loss modulus, (c) loss factor of FFRC and pure matrix at 1 Hz and 30 - 160 °C

FGUD-L. However, the performance of E′ in FPEC-T and PE (with a decrease of 70 % to 96 %) is similar to that of FGUD-T and GE from ambient temperature to T_g.

(3) For PP-based composites, the decrease of FPPC-L and FPPC-T is around 11 % and 40 %, respectively, and that value of PP is about 72 % from ambient temperature to the T_g at secondary transition (75 °C), which is close to the value reported by Ref. [Mofokeng 12].

During the heating before T_g, the internal friction of the matrix increases while the loss factor and loss modulus begin to rise gradually. the increase of E″ is around 3.1 to 4 times and 3.5 to 4 times for FGUD and FPGE, respectively, from ambient temperature to T_g. For FPPC, that value at secondary transition temperature is around 0.8 to 1.7 times of that at ambient temperature. An order of magnitude increase is observed for the loss factor of thermoset based composites (FGUD and

FPEC): the value at the peak is around 7.2 times and 12 times of that at ambient temperature for longitudinal and transverse direction, respectively. In addition, the peak value of loss factor in thermoset-based composites is about 0.1 and 0.4 times of that of pure matrix in fiber and transverse direction, respectively. For PP based composites, an increase of 40 % - 56 % are found from ambient temperature to the T_g at secondary transition for FPPC and Pure PP, respectively.

When it comes to glass transition zone, a large decrease in storage modulus with the increasing temperature will be seen. This is due to long range cooperative mobility in amorphous regions at T_g zone [Pothan 03]. The movement of macromolecules is beginning to increase and the space of molecules are also becoming larger in this temperature range and it triggers the movement of the chain segment. Damping is produced due to this form of movement in polymer materials. Since the internal frictional damping of the molecules is still relatively large, the external mechanical energy is dissipated in the form of thermal energy through the internal friction of the molecules. This part of the converted energy cannot be returned, which is manifested as a sharp increase in loss modulus and loss factor. Considering the addition of flax fiber into matrix, the visco properties inside flax fiber and shear stress caused by the fiber ends will also produce additional energy dissipation in the composite material.

In this process, the stiffness of the tested composites decrease the fastest with temperature, and the loss factor reaches a maximum value. When the temperature exceeds T_g, the movement of the molecular chain is more free and its shape begins to change, resulting in a gradually decreasing loss modulus. Finally, the composites enter the rubbery state and exhibit higher elasticity and their storage moduli, loss moduli and loss factor will not change significantly. In addition, the loss factors of FPPC shows a continuous increasing trend since the T_g of PP is below 0 °C as shown in II.24 (b). Therefore, a peak value of loss factor is not observed between 30 and 160 °C.

It can be clearly seen that the pure matrix has higher peaks than FFRC. It is also found that incorporating plant fibers into the matrix slightly changes the T_g. This means that the interaction between the fiber and the matrix in the composite is different. Moreover, the addition of fibers increases the load-bearing capacity in the high-temperature region and reduces the molecular mobility in the polymer chain resulting in a low damping peak. In the longitudinal direction, FPEC has a higher damping peak than FGUD due to the relatively poor fiber/matrix adhesion, which results in higher inter-link movement in the glass transition zone [Rajesh 16a].

II.3.4.b Hemp fabric reinforced composites

Figure II.21 shows the results of the storage modulus, loss modulus and loss factor of HFRC sweep with temperature at 1 Hz. It can be seen that the dynamic mechanical behavior of thermoset based HFRC is similar with that of thermoset based FFRC shown in II.20 (a-c). Hence, the physical mechanisms associated to the behavious shown in these figures are similar to those presented for in FFRC.

In addition, the value of changes in this kind of curve at ambient temperature and T_g is also similar with FFRC and it can be found in Table II.8 so they will not be detailed here.

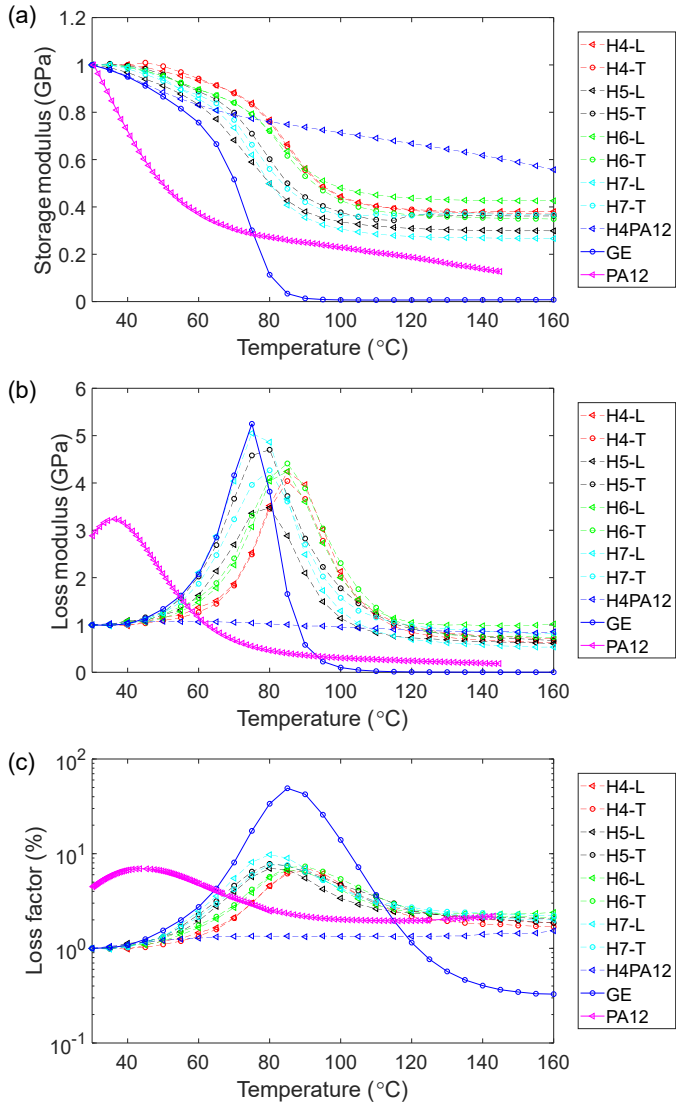

FIGURE II.21 – (a) Normalized storage modulus, (b) loss modulus, (c) loss factor of HFRC at 1 Hz and 30 - 160 °C (PA12 is collected from Ref. [Liao 18])

In figure II.21 (c), the influence of weave pattern on the damping properties of hemp fabrics reinforced composites can also be analyzed. The T_g of hemp reinforced GE composites (HGEC) is around 83±3 °C and there is no significant difference in the peaks. It is also found that incorporating hemp fabrics induces a decrease in the loss factor peaks due to the limitation of the molecular mobility in GE. It can also be observed that the weave pattern has no significant effect on damping properties of HGEC. No significant peak is found in the loss factor of H4/PA12 from 30 °C to 160 °C, which is similar to the behavior of FPPC.

II.3.4.c Comparison of dynamic properties between FFRC and HFRC on a wide temperature range

Table II.8 shows the dynamic properties of all types of material in longitudinal and transverse directions. It can be seen clearly that a decrease in orders of magnitude of the storage modulus of thermoset based composites occurs when increasing the temperature from 30 °C to T_g.

TABLE II.8 – Dynamic mechanical properties at 1 Hz, 30 °C and T_g (E′ and loss factor are measured at 30 °C, E′_T_g and loss factor-T_g are measured at T_g)

	E′ (GPa)	E′_T_g (GPa)	T_g (°C)	η (%)	η-T_g (%)
GE	2.55	0.03	85	2	100
FGUD-L	8*	4	87	1.7	12.2
FGUD-T	2.7	0.6	84	2.5	31.1
FGCR	7.4*	5	88	1.9	15
FPPC-L	11.8*	5	-	2	-
FPPC-T	2	0.5	-	3.5	-
H4-L	7.9*	5.2	88	1.9	13.8
H4-T	9*	4.9	90	1.9	13
H5-L	7.4*	5	80	2	14.4
H5-T	8.3*	5	80	2	14.3
H6-L	8.3*	5.1	86	1.8	12.5
H6-T	7.7*	4.9	87	1.8	13.4
H7-L	7.1*	4.6	80	2	16
H7-T	7.8*	4.4	82	1.9	14.7

* The value is not accuracte due to the stiffness of the sample which is closed to the one of the frame of the test system

For the UD thermoset based composites, the peak value of loss factor is around 12 % and 31 % in fiber and transverse directions, respectively. Although the addition of the fiber into matrix enhanced the damping in transverse direction at ambient temperature, it also restrict the chain mobility of the polymer. It can be seen the peak loss factor for FGUD-L (12 %) and FGUD-T (31 %) at T_g is smaller than GE (100 %). For woven fabric composites, the peak value of loss factor is always close to that of FGUD-L. This indicates that the peak of loss factor in fiber direction is mainly driven by the presence of fibers into matrix.

II.3.5 Evolution of damping properties as a function of frequency

II.3.5.a Direct measurements on the 0.01-100 Hz frequency range at ambient temperature

As mentioned before, DMA tests have the advantage of operation at low frequency (less than 100 Hz) and on a wide range of temperatures. Therefore, FGUD, FPPC and H4 were selected to study their damping properties on a frequency range from 0.01 to 50 Hz. Among them, FGUD and FPPC are thermoset and thermoplastic based composites, respectively. H4 was also selected on behalf of the thermoset based HFRC since previous measurements have shown that all HFRC have similar damping properties at ambient temperature.

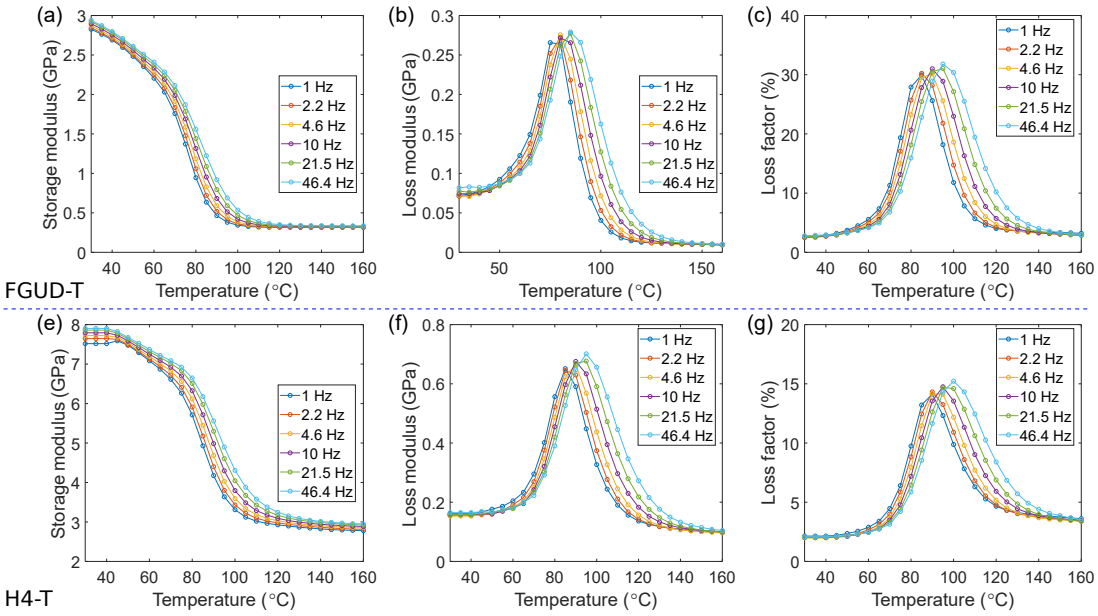

FIGURE II.22 – (a) Storage modulus, (b) loss modulus, (c) loss factor of FGUD-T at 1-50 Hz and 30 - 160 °C, (e) Storage modulus, (f) loss modulus, (g) loss factor of H4-T at 1-50 Hz and 30 - 160 °C

It can be seen from Figure II.22 that the storage modulus, loss modulus and loss factor are all highly frequency-dependent in both FFRC and HFRC. The storage modulus increases with the increasing frequency. When the frequency is low, the time required for the material to complete a cycle of vibration is longer, which exceeds the relaxation time of the macro-molecule, and the movement time of the chain segments is sufficient to make adjustments to keep up with the changes in excitation. Therefore, the movement of the chain segments can be kept consistent with the vibration force at all times. This means the material will try to minimize the localized stresses by rearrangement of molecular chain [Pothan 03].

Figure II.22 (c) shows the loss factor of FGUD in transverse direction on the 1-50 Hz. Similarly, the loss factor will first rise slightly in the extremely low frequency range (equivalent to extremely high temperature), and it will enter a peak area as the frequency increases. As the frequency continues to increase (equivalent to decrease the temperature), the damping of the thermoset based FFRC starts to decrease. With the increase of frequency, the T_g will move to the high temperature direction because the relaxation of the molecular chains needs a higher temperature. The behavior of other types of composites will not further be described since they have similar performance and they will be detailed in the section of 'Master curve'.

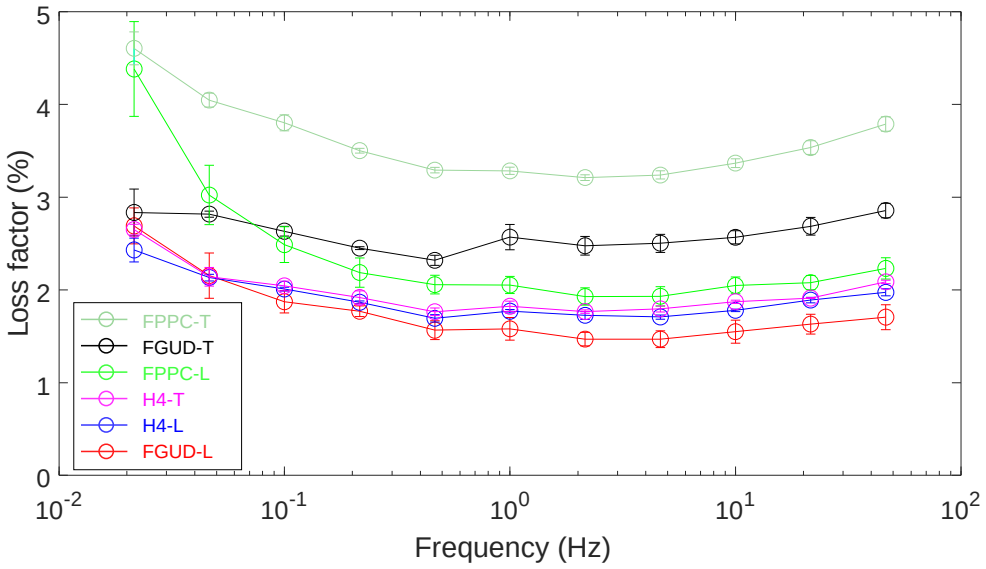

FIGURE II.23 – Loss factor of FGUD, FPPC and Hemp4 at 0.01-100 Hz and ambient temperature

Figure II.23 shows the loss factor of the three different materials in both material directions. As shown previoulsy, it can be observed that the damping level is highly dependent on the material and the direction for this whole frequency range. It is confirmed here that the PP matrix provides higher damping than the Green-Poxy one on the whole frequency range studied here. For all the materials, the loss factor show the same evolution as a function of frequency. A slight decrease trend from 0.01 Hz to 1 Hz is observed, at first. This is due to the motion of the chain segments of the matrix which decrease as the frequency increases. The slight perturbation in trend near 1 Hz is due to the change of sensor in the DMA device used, as indicated in Section II.2.2.

For all the tested materials and material directions, the maximum value of loss factor over temperature tends to increase from this level of frequency up to the last tested frequency. It is well known that, in this frequency range, measurements are sometimes disturbed by resonances of the whole system and that the measurement of the phase difference could not be reliable.

However, many precautions in the design of the set-up have been taken to avoid it. If DMA results beyond this frequency range may be questionable, modal tests is an interesting alternative method that will be used in the next chapter. Another reason to explain this evolution as a function of frequency is the temperature transitions of the considered polymers.

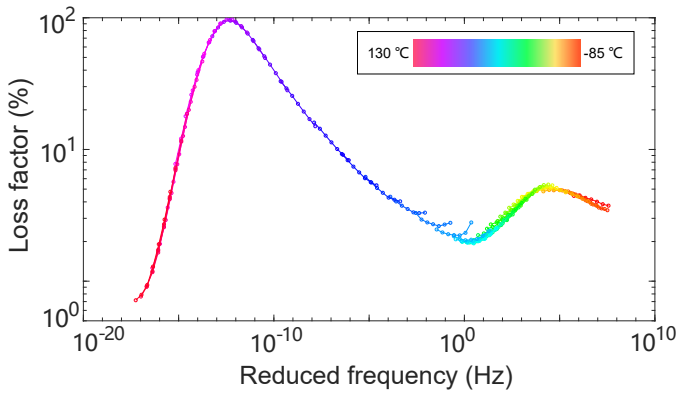

FIGURE II.24 – Master curve of loss factor for pure GE (reference temperature = 25 °C)

The secondary transition of GE is shown in Figure II.24. It will close to the second peak of loss factor near the secondary transition range when the frequency is higher than 10 Hz. On the other hand, the T_g of pure PP is lower than GE so the glass transition peak in master curve for pure PP will shift to higher frequency than that of GE. This can explain the different slop of FPPC and FGUD from 0.01 Hz to 1 Hz in Figure II.23.

The damping properties of these materials will be also further investigated at higher frequency range with modal analysis in the next chapter.

II.3.5.b Evolution on a broader frequency range using TTSP

The dynamic properties of PFCs are expected to be known in a wide frequency range. This range depends directly of the targeted application. However, it will be difficult to perform a frequency sweep beyond 100 Hz using DMA directly due to the limitation of the instrument. Thanks to Time–temperature superposition principle described by JD. Ferry [Ferry 80], the dynamic properties of visco-elastic material under lower and higher frequencies can be obtained by plotting the master curve from experimental data collected in a restricted frequency range but on wide range of temperature. [Menrad 08]. According to this principle, the changes in material properties when lowing (or increasing) the temperature are the same as those obtained when increasing (or lowing) the frequency.

Master curves are produced using the curves of dynamic properties under different temperature stages on a specific frequency range.

To illustrate this, the shift factor α obtained by the TTS principle can convert the single curve of dynamic mechanical properties (storage modulus and loss factor) at different temperatures into the single curves of the dynamic mechanical function at a reference temperature, so that the storage modulus or loss factor in a wider frequency range can be obtained.

Typically, logarithmic coordinates are used to describe the time-temperature conversion algorithm for viscoelastic mechanical behavior. The curves of viscoelastic properties at different temperatures are built according to shift the experimental curve in a certain shift factor in the horizontal direction under the reference temperature. The shift factor is only related to temperature and two calculation methods are often used namely WLF (Williams, Landel & Ferry) and Arrhenius formula in order to describe the evolution of the shift factor over temperature. The calculation of shift factor in this work is based on the principle of least squares inspired by Ref. [Butaud 15a].

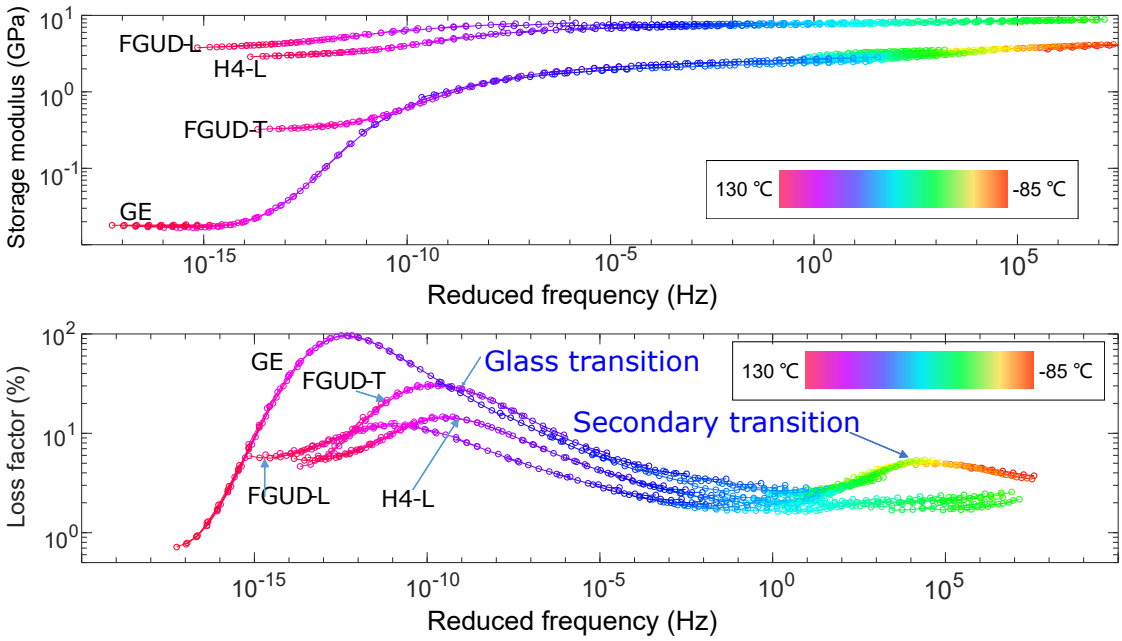

FIGURE II.25 – Master curves of storage modulus and loss factor for GE, FGUD and H4 with T_{ref} = 25 °C

Figure II.25 shows the master curves of storage modulus and loss factor for the FGUD and H4. As shown, the frequency range has been extended to [10^{-10}, 10^5] Hz for the reference temperature 25 °C. This can make up for the shortcomings of DMA test in ultra-low frequency (less than 10^{-2} Hz) and high frequency (higher than 10^2 Hz) ranges. These results also provide a basis for comparison with data obtained using other experimental techniques. It will be further analyzed in the following chapters. The master curves of other materials can also be obtained using the same method and will not be described in detail here.

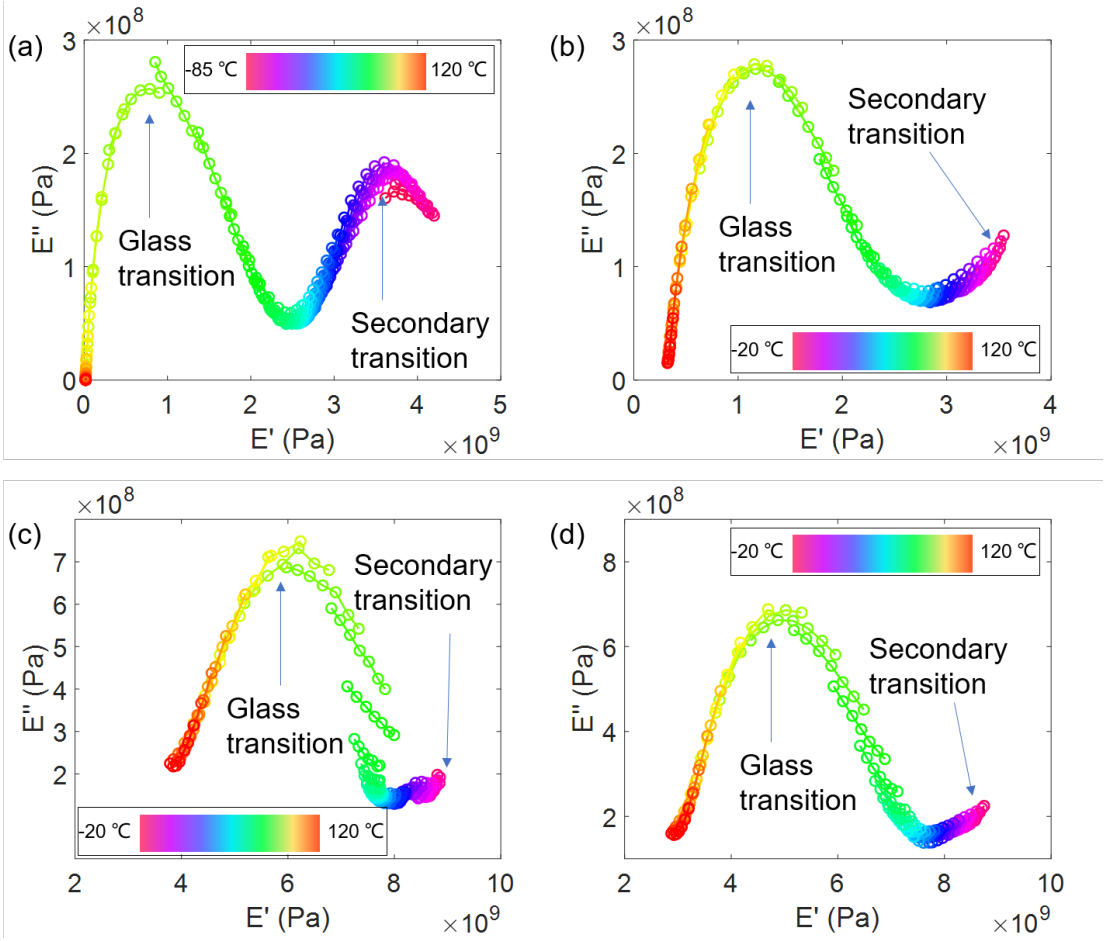

FIGURE II.26 – Cole-cole curve of (a) GE, (b) FGUD-T, (c) FGUD-L and (d) H4-L

The Cole-Cole plots are shown in Figure II.26 by plotting loss modulus against storage modulus. It is clear that the composites show approximately two semi-circles related to the glass transition and the secondary transition as mentioned before. This provides the information about the validity of TTS and TTS is usually observed for neat polymers but it seems also work on composite materials.

II.3.6 Influence of moisture content on UD flax reinforced composites

Although plant fiber composites have many advantages as described above, existing studies have shown that humidity coupling with hot environments have a great influence on the stiffness and damping properties of PFCs [Li 16]. Plant fiber is a hydrophilic material due to its hollow shape and chemical properties, and its moisture absorption is higher than that of resin matrix and synthetic fiber. This section will study in details the influence of aging time in water-immersed conditions on the dynamic mechanical properties of flax fiber reinforced composites.

II.3.6.a Influence of aging time on mass change

The changes of mass (D_m) are calculated as follows,

$$D_m = \frac{m_i - m_0}{m_0}, \tag{II.16}$$

where m_i refers to the mass after water aging i days. m_0 is the original value of the above mass before aged.

Figure II.27 shows the changes in mass of specimens cut in longitudinal and transverse directions. The error bar refers to the standard deviation measured from at least 3 samples for each tests. As shown, the mass of samples increases from 5 % to 10 % as the increasing of water aging days from 1 to 5 days for longitudinal specimens and of 15 % for transverse specimens at the end of aging day. This difference in moisture absorption after 5 days between the two material directions can be explained by the difference in the sorption kinetic, directly dependent on the quantity of fibers exposed on the lateral faces of the specimens.

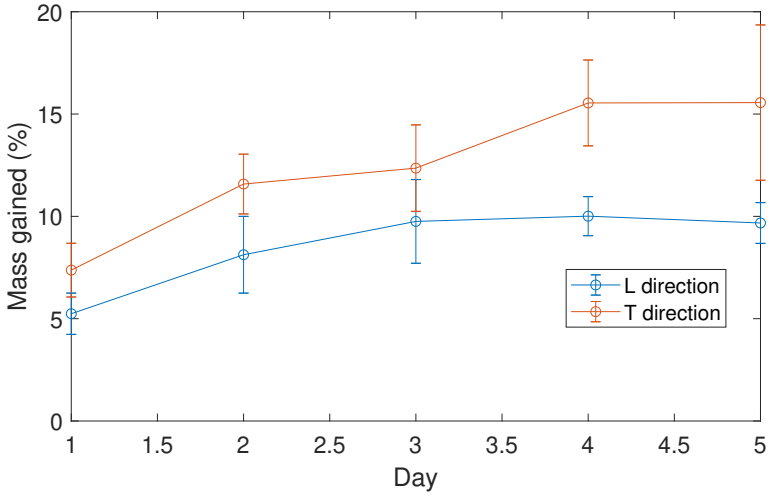

FIGURE II.27 – Mass gained versus water aging time in longitudinal and transverse direction

II.3.6.b Influence of aging time on damping properties

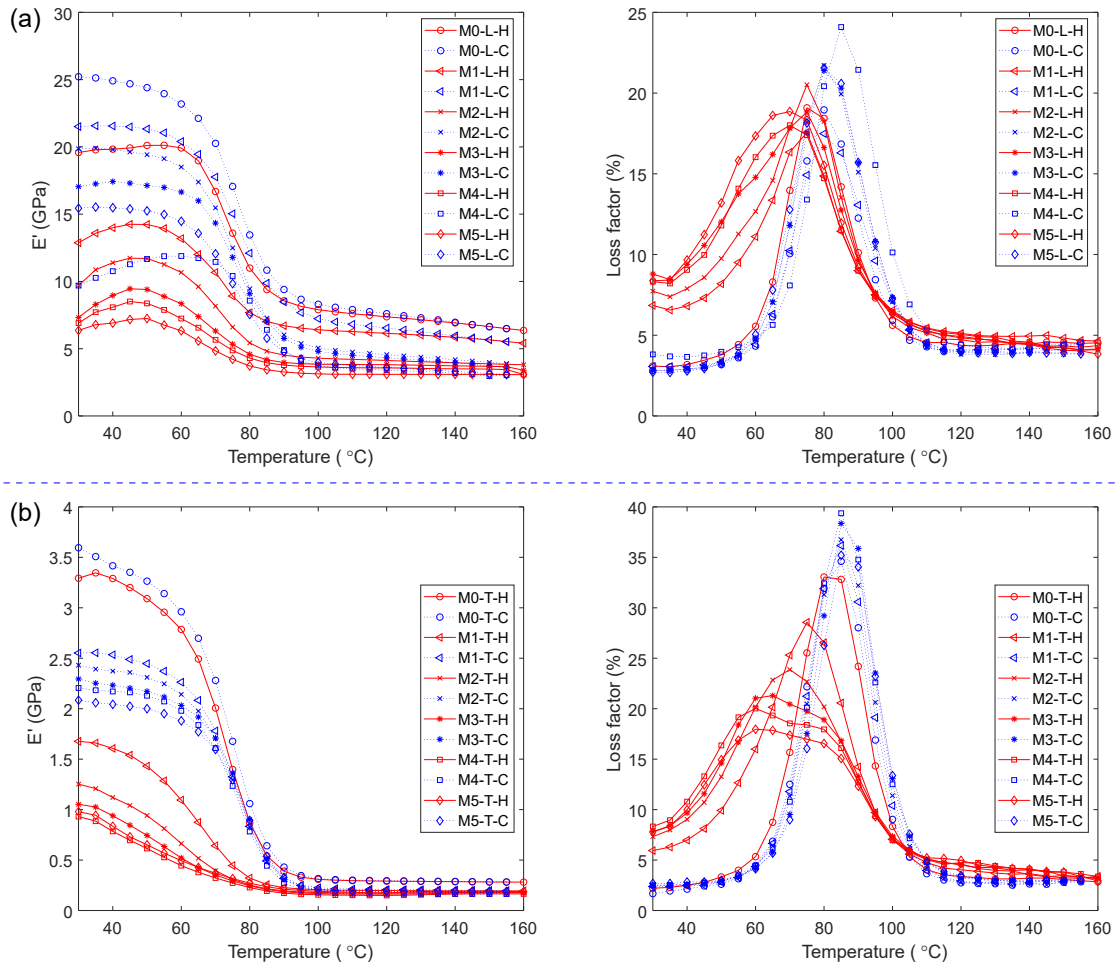

FIGURE II.28 – Mean curve of storage modulus and loss factor versus water aging time in (a) longitudinal direction(L) and in (b) transverse direction(T) 'M*i*-L(T)-1(2)', '*i*' refers to water aging day,'H' and 'C' means the heating and cooling process in DMA tests, respectively

Figure II.28 shows the storage modulus and loss factor of FGUD, i the two main material directions, as a function of their water aging time. For each heating and cooling cycle, it can be observed that the viscoleastic properties as a function of temperature do not follow exactly the same path in the cooling phase than in the heating phase. During the heating phase, the classical behaviour described in the previous section is observed. When cooling, the same path is followed until 100 °C. Below this temperature, the storage modulus is observed to be higher than in the heating phase. This is attributed to the drying of the specimen during the test. It is well known that water has a plasticizing effect. So, the removal of water during drying induced an increase in stiffness.

It can also be noticed obviously that the storage modulus of FGUD in the glassy region drops significantly during exposure to water by comparing the dynamic mechanical properties before and after water aging. The storage modulus decreases from 20 GPa to 6.2 GPa and 3.3 GPa to 1 GPa in fiber and transverse directions, respectively after the water aging. This is again directlty linked to the plasticizing effect of water. The irregular change of the storage modulus on the 4th day may be caused by the internal defects of the samples so it also has a larger uncertainty in Figure II.29.

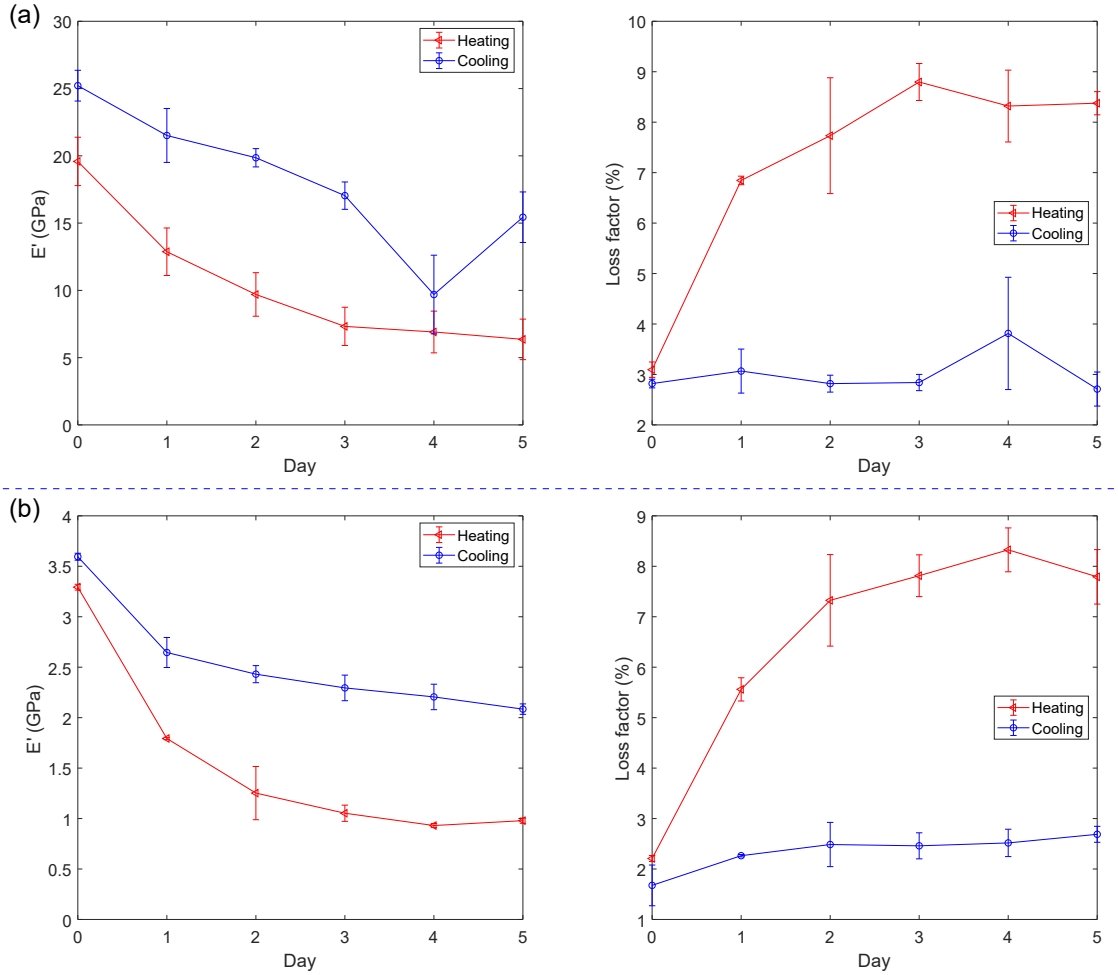

FIGURE II.29 – Changes in storage modulus and loss factor versus water aging time at 1 Hz and 30 °C in (a) longitudinal direction(L) and in (b) transverse direction(T)

For the loss factor, a significant increase is seen at ambient temperature and the width of the peak of loss factor is increasing as the water aging time increases. For each heating and cooling phase, a shift of the T_g toward the higher temperatures is observed during cooling. A more acute and tightened peak of loss factor is also observed. This is again consistent with the plasticizing effect of water. For all these measurements, it is also important to mention that tests are done in a transient

regime since most of the specimens are not at the equilibrium moisture content before DMA test. Therefore, moisture content is certainly heterogeneous within the sample. Heating during DMA tests also induces a drying which causes also an inconstant moisture content during the test.

When considering the values of storage modulus at the end of the cooling phase, a decrease can be observed as a function of the ageing time. This can be due to the damage of the composites and the damage level is increasing with the aging time. In addition, it can be seen from the peak value of damping that the sample after water absorption always shows a lower peak value, which indicates the damage effect of water aging caused by the plasticizing effect. The water aged sample has a lower T_g and wider damping peak than the unaged sample due to the softening of the fiber and matrix and the microfiber of flax obtains local fluidity, which is beneficial to the transition to a lower temperature. [Wang 19].

Figure II.29 shows the trends of storage modulus and loss factor compared with unaged sample (day 0). The error bar refers to the standard deviation measured from at least 3 samples for each tests. Moisture has a significant effect on the storage modulus measured by FGUD at 30 °C. As the water content in the composite material increases, the dynamic stiffness decreases significantly. The storage modulus in longitudinal and transverse direction are reduced by about 70 % and 57 %, respectively on the 5th water aging day during heating. The mechanical properties in the longitudinal direction are more susceptible to moisture due to the reinforcing fiber working as the main load-bearing component compared to the transverse direction. Although part of moisture inside the samples is lost during the DMA tests, the storage modulus at the 5th aging day in both directions is still reduced by about 40 %. This can indicate that water aging will irreversibly damage the mechanical properties of FGUD.

The loss factor gradually increases by around 2.1 and 2.5 times in longitudinal (from 3 % to 8.4 %) and transverse direction (from 2.2 % to 7.8 %) from unaged to 5th aging day, respectively. The slight increase in loss factor determined at ambient temperature at the end of the cooling phases as a function of aging time reflects the damage increase induce by drying. This section shows a most influential parameter on the damping properties at ambient temperature among the whole studied parameters in this chapter. Furthermore, a long time water aging test will be described in the chapter III.

II.4 Conclusions

The researches for damping performance of PFCs at meso-scale using DMA tests are divided into four parts, matrix type, woven pattern, frequency range and water aging, which can cover most working conditions for engineering applications and the gap in current literature.

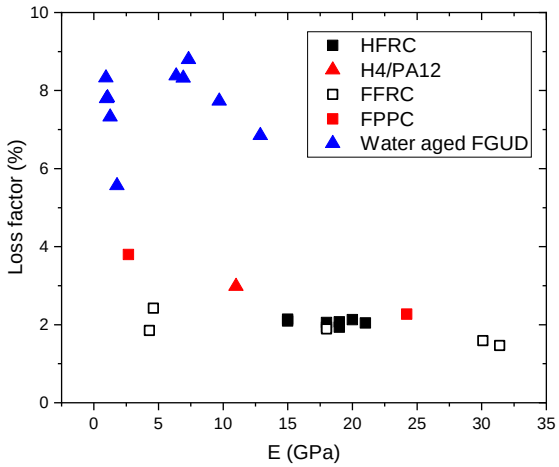

FIGURE II.30 – Ashby diagram using loss factor and Young's modulus measured at 1 Hz in this thesis (black, red and blue points are thermoset, thermoplastic based composites and water aged FGUD, respectively)

Regarding the behaviour of flax-based composites at ambient temperature, the loss factor in thermoplastic based PFCs (2.3 %-3.8 %) have a better capacity than that in thermoset based PFCs (1.4 %-2.6 %) in both directions, as shown in Figure II.30. The addition of flax fiber into matrix has a significant influence on damping performance in longitudinal and transverse directions. It is proved that the damping properties in longitudinal direction are mainly driven by the fiber and the matrix plays a major role in the loss factor in the transverse direction whatever the damping properties of the matrices. Moreover, the loss factor of flax fiber in longitudinal (1.6 - 2.2 %) and transverse direction (3.4 - 4 %) is obtained using back calculation.

Regarding the behaviour of hemp-based composites at ambient temperature, results have shown that the weave pattern is not influential on the damping properties. The loss factor of HGEC is always around 2 % in both directions even if the yarn density is different. In addition, HGEC and FGCR have comparable loss factors. The slightly higher value for woven hemp can be attributed to the fiber waviness induced by crimp. For the wide temperature range, FPEC, FGUD and HGEC have shown similar trend in dynamic mechanical behavior with their matrix. In general, the loss factors of FFRC and HGEC in this study are higher than that of SFCs, which indicates a bright application prospect of SSUCHY materials. The master curve of neat resin, FGUD and H4 are built to obtain the storage modulus and loss factor in a wide frequency range and they will be compared with the results measured with other experimental techniques in the next chapters.

Regarding the damping properties in a specific reduced frequency range, a non-constant and non-linear evolution is found for both thermosets and thermoplastic based composites owing to the presence of T_g at low temperature for thermoplastics and secondary transition (around -50 °C) and T_g at higher temperature.

At last, the effect from water aging is studied using FGUD. Storage modulus decreases of more than 50 % after 5 days of water-immersed aging and it can not recover to that in unaged condition even after drying the moisture. Loss factor increases of about 4 times after 5 days aging. It can be seen clearly from Figure II.30 that moisture content is the most influential parameter at ambient temperature among all the parameters studied in this chapter (matrix type, fiber type, reinforcement architecture, lay-up, frequency) .

Chapitre III
Macro scale: modal analysis

III.1 Introduction 90

III.2 Materials and methods 91

III.2.1 Generalities on experimental modal analysis 91

III.2.2 Materials 95

III.2.3 Experimental setup and post-processing 96

III.2.4 Water aging 98

III.3 Results and discussion 99

III.3.1 Optimization of the setup in free-clamped boundary conditions 99

III.3.2 Modal analysis in free-free configuration 105

III.3.3 Modal analysis in free-clamped configuration 111

III.3.4 Comparison of damping properties in modal analysis and DMA tests 114

III.3.5 Influence of water aging in free-free boundary conditions . 117

III.4 Conclusions 118

GRAPHICAL ABSTRACT

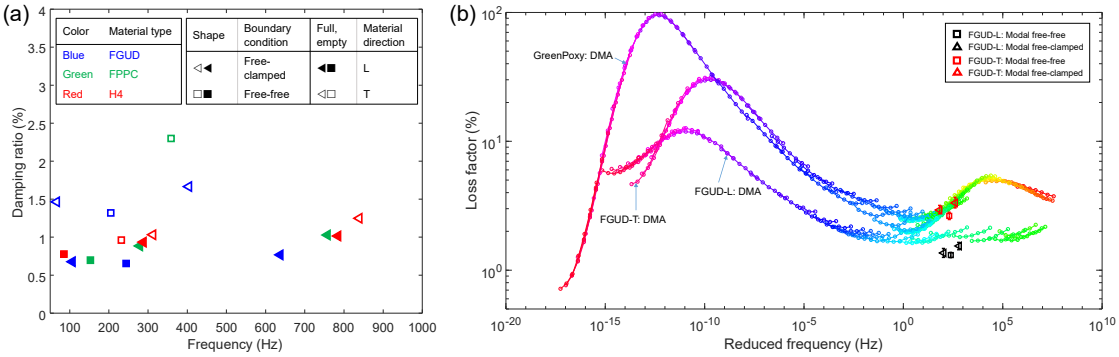

- An optimized specimen shape is designed using numerical simulation to minimize the effect of clamping on material damping identification in free-clamped configuration.
- Loss factors in L and T directions identified from modal tests in free-free and free-clamped conditions at ambient temperature for FGUD, FFPC and H4 materials are in good agreement with the ones determined with DMA tests
- The storage moduli identified by inverse method from modal tests are similar to the E-modulus determined using quasi-static tests
- The loss factors identified from modal tests in the two main directions of FGUD over the frequency range are well superimposed to the master curve built by TTSP from DMA data
- The damping behavior of FGUD material is significantly affected by water ageing

RÉSUME

Dans ce chapitre, les matériaux composites renforcés de fibres de lin et composites renforcés de tissus de chanvre sont caractérisés sur une large bande de fréquences (de 50 Hz à 1 kHz) en utilisant l'analyse modale afin d'identifier leurs propriétés dynamiques à l'échelle macroscopique. L'analyse modale est effectuée dans deux configurations, libre-libre et encastré-libre. La géométrie et la configuration expérimentale des essais encastré-libre sont préalablement optimisées par simulation numérique de manière à minimiser l'effet de l'encastrement sur la mesure de l'amortissement des composites. Les mesures expérimentales réalisées dans les deux configurations montrent que le facteur d'amortissement mesuré en encastré-libre reste légèrement supérieur à celui mesuré en libre-libre. Les valeurs d'amortissement mesurées dans les deux configurations pour les trois matériaux sont similaires à celles déterminées en DMA, et ce pour les deux directions matérielles principales. Les modules de stockage identifiés par méthode inverse à partir des essais modaux sont également comparables aux modules d'élasticité mesurés sous chargement quasi-statique. Les valeurs de facteur de perte identifiées à partir des essais modaux pour les unidirectionnels lin/GreenPoxy sont également en bon accord avec les courbes maîtresses construites par équivalence temps-température à partir des données DMA. Le comportement dynamique en libre-libre est fortement influencé par la teneur en eau des composites lin/GreenPoxy. Les mesures sont néanmoins

parfois altérées par les déformations de la plaque provoquées par la sorption d'eau et les relaxations de contrainte induites.

ASTRACT

In this chapter, FFRC and HFRC are characterized on a wide frequencies band (50 Hz to 1 kHz) using modal analysis to identify their dynamic properties at the macroscale. Modal analyses are carried out under two different boundary conditions, namely free-free and free-clamped conditions. An optimized specimen shape and experimental configuration is determined for the free-clamped configuration using numerical simulation to minimize the influence of the boundary conditions on the measurement of the damping of the tested materials. Damping ratio obtained in free-free and free-clamped boundary conditions for the three selected materials are compared. The results show that the values of damping ratio identified from the free-clamped configuration is slightly higher than the one from the free-free configuration. The loss factors identified from the modal tests for the three types of composites and in the two main directions are of the same order of magnitude than the one determined using DMA tests. Storage moduli identified by inverse method from the modal tests are also comparable to the one obtained under quasi-static loading. The loss factor values determined from the modal tests on the UD flax/Greenpoxy composite over the frequency range are also in good agreement with the master curve built using time–temperature superposition principle from DMA data. The dynamic behavior of the FGUD plates characterized under free-free conditions is also strongly influenced by the moisture content. Measurements are however disturbed by the plate distortion induced by moisture sorption and the associated internal stress relaxation.

III.1 Introduction

The previous chapter has investigated the viscoelastic behavior of different PFCs selected or developed in the frame of the SSUCHY project using DMA at the scale of small coupons. The results have shown the advantages of this method but also some limitations, in particular regarding the frequency range. The objective of this chapter is to characterize some of these materials using modal tests, a usual technique dedicated to the analyis of structures. In the literature, several investigations on the damping properties of thermoset and thermoplastic-based plant fiber composites using modal analysis are available [Rajeshkumar 14, Rahman 17a, Gopalan 19, Della 07]. Although this technique is quite widely used for damping identification of plant fiber composites, the results of damping properties from literature are mixed under different mode shapes including flexural and torsional. It is difficult to classify the longitudinal and transverse damping ratios clearly since the organic based fiber reinforced composites are anisotropic materials. It is also sometimes difficult to compare it accurately with the results from DMA tests. Therefore, this chapter is dedicated to the investigation of the damping properties of UD and woven fabric composites on a wide frequency range (50 - 1000 Hz). The modal response is analyzed through the mode shapes to identify the damping properties under the different loading modes and then in the different material directions. This gives an opportunity to compare the damping properties at macroscale from modal analyses from the one collected at the mesoscale using DMA tests, in particular using the master curves obtained by time–temperature superposition principle. In addition, free-clamped boundary conditions are commonly used in experimental modal analysis in many studies [Munde 19, Gopalan 19]. However, the study of effect of boundary conditions on damping identification is rarely reported. Hence, this work also proposes to investigate the influence of boundary conditions on the identified damping properties using numerical model. The final objective is to optimize the experimental configuration to minimize the effect of boundary conditions on the damping.

Moisture content is also one of the influential parameters on the damping properties, as pointed out at the mesoscale in chapter II. Several results regarding the influence of water aging on the damping of plant fiber composites, characterized using modal tests, are also found in the existing literature [Berges 16, Senthilrajan 19b, Cheour 16]. In these works, composite beams, which are cut from a whole plate, are always used as testing samples. In this work, the effect of water aging on the damping is also studied using plates to provide a better understanding of these properties at the macroscale.

This chapter follows a plan similar to the one proposed in the previous chapter. At first, the materials and methods are described. Some generalities on modal testing are also presented as well as the model and methodology used to analyze the influence of boundary conditions on damping. After this, a second part is dedicated to results and discussion. The optimized shape of specimens to minimize the effect of boundary conditions is described. Then, the damping properties of

FGUD, FPPC and H4 are investigated under free-free and free-clamped conditions. A comparison between the loss factors determined from DMA tests and those determined by modal tests under free-free and free-clamped conditions is proposed to highlight the influence of frequency and matrix types on damping properties at macroscale. At last, the influence of moisture content on damping properties on wide frequency range is investigated. A conclusion summarizes the main outcomes of this chapter.

III.2 Materials and methods

III.2.1 Generalities on experimental modal analysis

Modal analysis consists in vibration testing of an object in which the natural frequencies, modal damping ratios and mode shapes of the object under test are determined. There are several ways to do modal tests. In forced vibration tests, energy is supplied to the system with a known frequency content. Modal analysis involves the acquisition of vibration excitation and response signals from a measurement point or a grid of measurements points on the surface of a structure and the subsequent analysis of the measurement data. The structural behaviour is characterized through a set of transfer functions between excitation and measurement points. The transfer functions (or frequency response functions (FRFs)) are often fitted to identify the modal parameters. There are many methods of modal parameter estimation. In this work the PolyMAX frequency-domain method has been used [Peeters Bart 04]. This section provides a short description on the experimental configurations generally used for modal analysis.

III.2.1.a Boundary conditions, excitation and measurement

Boundary conditions

There are two types of boundary conditions which are commonly used in the experimental setups of modal analysis of simple composite structure. The first one is free-free boundary conditions, which means that all the boundaries are fully free, or more exactly almost free since most of the time the specimen or structure is supported by elastic strings. The second one is free-clamped boundary conditions which means that one side of the sample is fixed in a clamp and the other side is free.

Excitation

The excitation in the experimental modal analysis can be various depending on the type of instruments and the signal applied on the excitation apparatus. Several commonly used methods are as follows.

- **Free response**. A static displacement is imposed on the structure, and released instantaneously. The time response of the structure is then a combination of decreasing oscillatory movements corresponding to the modes of the structure. This technique may be useful to measure the eigenfrequency and modal damping of the first mode, however it is very difficult, even impossible, to operate for the other modes.
- **Shaker**. A shaker is connected with the tested sample directly using a rigid rod to transfer the specific excitation signal. Ideally, a sensor is used between the connector of the shaker and the tested sample to measure the response of force or acceleration. However, the effect of the shaker on the sample behavior can be important due the rigid connection.
- **Acoustic source**. It is one kind of non-contact excitation method. The excitation can be applied using a loudspeaker by the acoustic wave acting on the tested sample. As this excitation is contact-less, there is no impact of the excitation device on the structure. However, as the force is distributed on the structure, and since no measurement of the input force is possible, the comparisons with numerical FRFs is impossible. A reference signal issued from the loudspeaker may be used for transfer identification, but its comparison with numerical results is tricky.
- **Electromagnetic magnets**. Excitation can also be performed with a magnet and a coil. The excitation is applied by the movement of the magnet caused by electromagnetic force. The effect of excitation device on the measurement is weaker than with a shaker as this is a contract-less technique, however an additional mass need to be considered on the structure (magnet or coil). The input force can be measured, but fine positioning of the excitation device and levels to avoid nonlinearities is required.
- **Impact method**. Impacts can also be used. They are applied with an impact hammer or other impact devices. A transient excitation is then applied on the tested sample resulting on a wide frequency bandwidth excitation. The advantage of the impact method is that the instrument is simple and will not affect the dynamic characteristics of the specimen without additional mass. However, it is easy to cause nonlinear problems since its energy is concentrated in a short period of time. The measurements are also more difficult to operate because of the rigid body movements.

Measurement

The dynamic response can be measured in the following ways.

- **Accelerometers**. Accelerometers are electromechanical devices used to measure acceleration. They convert the acceleration into electrical changes. The accelerometer needs to be connected with the tested sample so the effect of its presence on the measurement must be considered during modal analysis.

- **Laser vibrometer**. It is a non-contact method of measurement based on Doppler effect. It measures the velocity of the surface using 1D or 3D measurement systems. Due to the cost of the corresponding setup, most of the time the measurements on the structure are obtained by scanning a mesh, meaning that it is not straightforward to deal with transient responses as soon as they are not fully repeatable.
- **Full-field techniques** High-speed cameras are used for measuring vibration fields of displacement and strain combining the resulting images with Digital Image Correlation techniques for modal analysis and dynamic properties identification. Compared with traditional accelerometers, this method avoids the problems of the debonding or damage of the sensor during the experiment, the influence of the mass of the sensor on the specimen. Compared with 1D vibrometer, full field strain and deformation are automatically generated along with frequency. Compared with scanning laser vibrometer, the amplitude does not affect the acquisition time even on large structures with large amplitudes. However, these techniques can only be applied to visible parts of the structures, and are limited to relatively low frequency analysis, due to the sampling frequency of cameras and decreasing vibration displacement when the frequency increase.

III.2.1.b Calculation of the damping ratio

Damping ratio is one of the important parameters in modal analysis. It can be calculated by various ways.

Logarithmic decrement method

In the case of a free response, the damping ratio can be calculated in the time domain using logarithmic decrement method based on the measured amplitude as shown in Figure III.1 (a). The logarithmic decrement (ψ) can be expressed as:

$$\psi = \frac{1}{n} \cdot \ln\left(\frac{x_1}{x_{n+1}}\right), \tag{III.1}$$

where n is the number of selected periods, x_1 and x_{n+1} are the amplitude of the first and $n+1$ period, T_d is one period of vibration. The damping ratio (ζ) is obtained using the following equation:

$$\zeta = \frac{\psi}{\sqrt{4\pi^2 + \psi^2}}. \tag{III.2}$$

Half-power bandwidth method

For simple forced case where resonance are well separated in frequency, the modal damping ratio can be calculated in the frequency domain with half-power bandwidth method (-3dB method). Its processes are as follows:

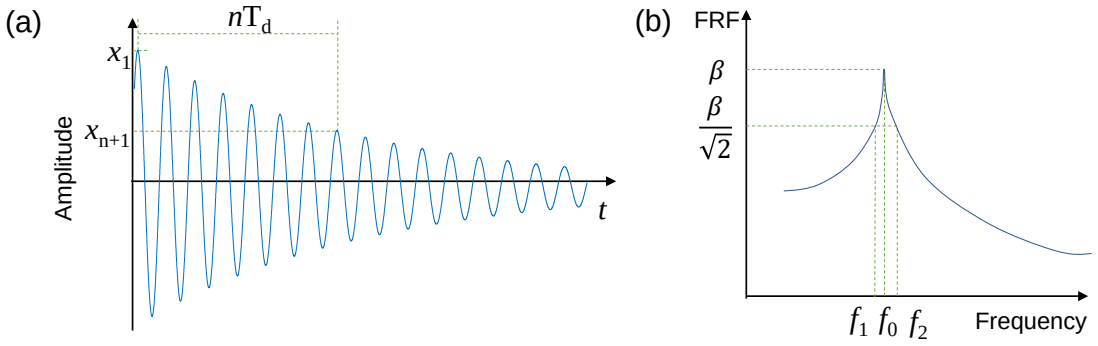

FIGURE III.1 – Method of damping calculation using (a) logarithmic decrement (b) half-power bandwidth

- the amplitude of the frequency response function curve of the sample is plotted as a function of frequency,
- the peak value (β) of the corresponding resonance frequency (f_0) is localised as shown in Figure III.1 (b),
- the value of $\beta/\sqrt{2}$ and the two corresponding frequencies (f_1, f_2) are calculated,
- the damping ratio can be obtained using the following equation by

$$\zeta \simeq \frac{f_2 - f_1}{2f_0}. \tag{III.3}$$

Complex method

For complex structures, the identification of the eigen frequencies requires the use of advanced techniques like the PolyMAX approach [Peeters Bart 04]. It consists in finding the stable poles of models when the model order increases. These pole provide the values of the complex eigen frequencies λ_i, (λ_i^*=-$\zeta_i\omega_i \pm j\sqrt{1-\zeta_i^2}\omega_i$) from which the modal damping ratio can be deduced. In the case of low damping ($|\zeta| \ll 1$) the relation writes:

$$\zeta_i \simeq \frac{real(\lambda_i)}{imag(\lambda_i)}, \tag{III.4}$$

Relationships

In order to compare the value of damping ratio with loss factor from DMA test, the relationship of parameters related to damping, based on the assumption of a linear behaviour and isotropic material, is: [Carfagni 98],

$$\eta = \tan\,\delta = \frac{E''}{E'} = 2\zeta, \tag{III.5}$$

where η is the loss factor, tan δ is the tangent value of the phase δ between the stress and strain, E'' and E' are the loss and the storage modulus, respectively, ζ is the damping ratio.

III.2.2 Materials

Damping properties of different kinds of PFCs selected within the SSUCHY project have been studied using DMA tests at the mesoscale in the previous chapter. Some representative materials were selected for experimental modal analysis in this chapter according to the results from chapter II. Unidirectional flax/GreenPoxy based composites and flax/Polypropylene composites as representatives of thermoset and thermoplastic based composites, respectively, were selected at first. H4 was also selected as one of the hemp fabric/GreenPoxy composites. Indeed, it was previously shown that the weave pattern has no significant effect on damping properties. So, only one pattern was chosen for further investigation. Therefore, three types of plant fiber composites (FGUD, FPPC and H4) were tested in this chapter and the details of manufacturing have been described in chapter II.2. At least three samples of each kind of composite, and each aging time, were prepared for modal analyses. The composite plates were cut into rectangular shapes and the dimensions for modal tests in free-free condition and free-clamped condition are shown in Figure III.2.

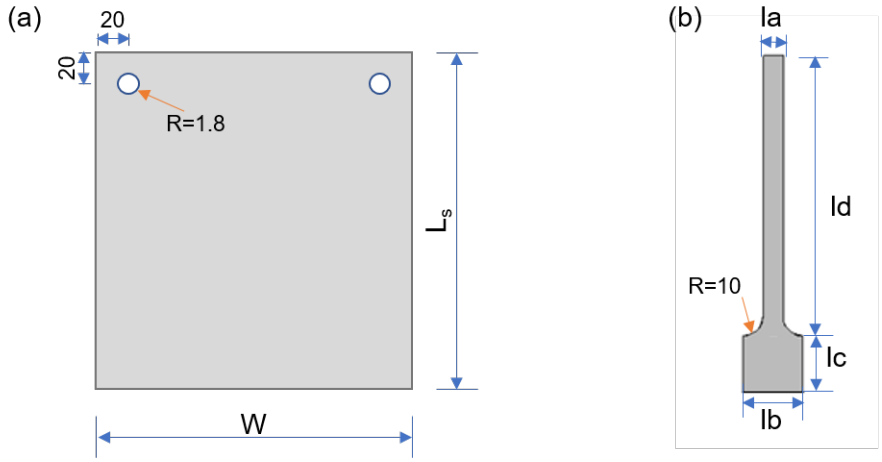

FIGURE III.2 – The shape of the sample for modal test in (a) free-free and (b) free-clamped boundary conditions (unit: mm) (Values are given in the Table III.3.2.a)

For modal tests in free-free boundary conditions, a rectangular composite plate is used with two holes (diameter: 1.8 mm) near the corner of the plate to support it on the frame with nylon strings. The dimensions of length (L_s), width (W) and thickness (t_c) for each material are shown in Table III.3.2.a. For modal tests in free-clamped boundary condition, an optimized shape is used to minimize the effect of clamp on the damping as shown in Figure III.2 (b). The details for optimization of

the sample shape in free-clamped condition are described in the section III.3.1. The small differences in dimensions of FGUD plates are due to difficulties encountered during the laser-cutting of the sample.

TABLE III.1 – Dimensions of the different plates and specimens used for modal tests in free-free and free-clamped configurations (Unit: mm)

Materials	L_s	W	t_c	la	lb	lc	ld
FGUD-1	286	185	3.9	4	40	50	168
FGUD-2	283	192	3.4	4	40	50	168
FGUD-3	279	179	3.5	4	40	50	168
FPPC	237	92	1.9	4	40	50	169
H4	277	177	2	4	40	50	163

III.2.3 Experimental setup and post-processing

The experimental modal analysis was carried out at ambient temperature. The two kinds of experimental setups, involving free-free and free-clamped boundary conditions, are shown in Figure III.3 (a). For the free-free configuration, the composite plate was hung on the frame using two nylon strings and the frame was fixed on the desk. The experiment was repeated several times using the same composite plate. For free-clamped configuration, the sample was fixed using a clamp as shown in Figure III.3 (b), and the experiment was repeated with different composite beams. The measurement point on the surface of the sample was covered with a reflecting patch to enhance the vibrometer response.

The schematic diagram of modal analysis tests in free-free and free-clamped boundary conditions are shown in Figure III.4. First, modal analysis started with a sweep sine signal produced by MATLAB software at a specific frequency range (50 - 1000 Hz). Then, the signal was amplified by an amplifier after sent by NI acquisition system (Data Acquisition (DAQ)-NI). The sample was excited through a non-contact acoustic excitation method by a loudspeaker (supplier MONACOR®). The velocity of the sample was measured by a 1D laser vibrometer (Polytec OFV-505). After that, the data was sent back to computer to do the post-processing. All the steps mentioned above were repeated at least 3 times and the mean value was used as final data.

The Frequency Response Function (FRF) was obtained using the output measured by 1D vibrometer as the reference of input on the loudspeaker. The eigenfrequency and damping ratio were analyzed by the PolyMAX method [Peeters Bart 04] using the Modan software (developed by Department of Applied Mechanics, FEMTO-ST [Piranda 94]).

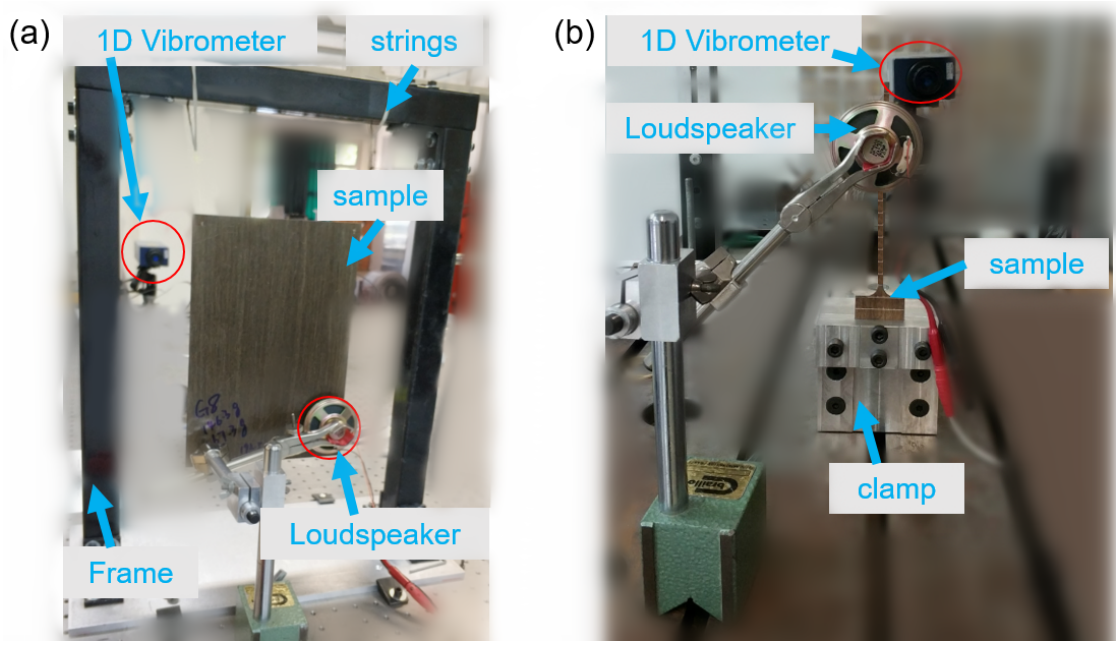

FIGURE III.3 – Experimental setup in (a) free-free and (b) free-clamped boundary condition

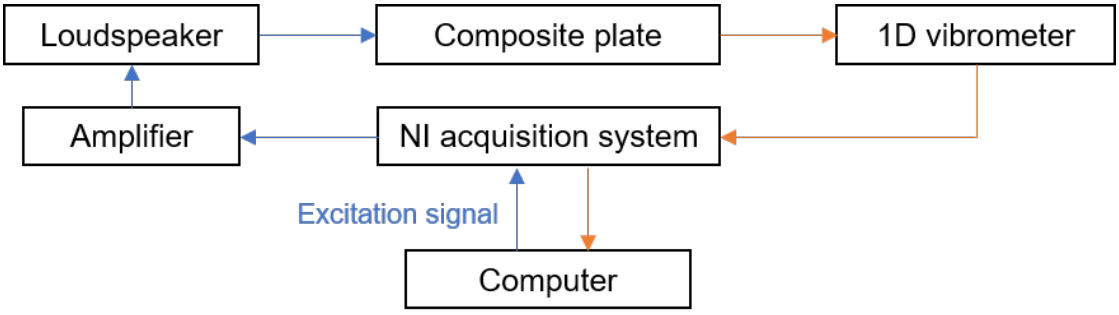

FIGURE III.4 – Schematic diagram of the experimental system

When a specific mode mainly involves a particular direction, the corresponding material parameter may be easily identified using simple model updating procedures [Butaud 15b]:

$$E' = E_{num} \times \left(\frac{f_{exp}}{f_{num}} \right)^2, \tag{III.6}$$

where the E_{num} is the Young modulus set in the numerical model, f_{exp} and f_{num} are the eigenfrequencies of the modes identified from experiment and numerical model. For more complex situations where the various components of the constitutive law are inolved in the response, advanced techniques are required [Viala 18]. The values provided in this chapter are identified on specific mode where the contribution of

the modulus of interest plays the major role in the response. The finite element models is used to identify the storage modulus by equation III.6 and associated text.

III.2.4 Water aging

The samples used for water aging tests were cut into 279 × 178.5 × 3.34 mm^3 plates from FGUD material (manufacturing process is similar to the one detailed in chapter 2). The plates were then stored in a climatic chamber with 50 % RH and 23 °C for at least 4 weeks to reach the moisture equilibrium. Its dimensions and mass were measured using a ruler and mass balance. The first state was labeled water aging 0 days (unaged sample).

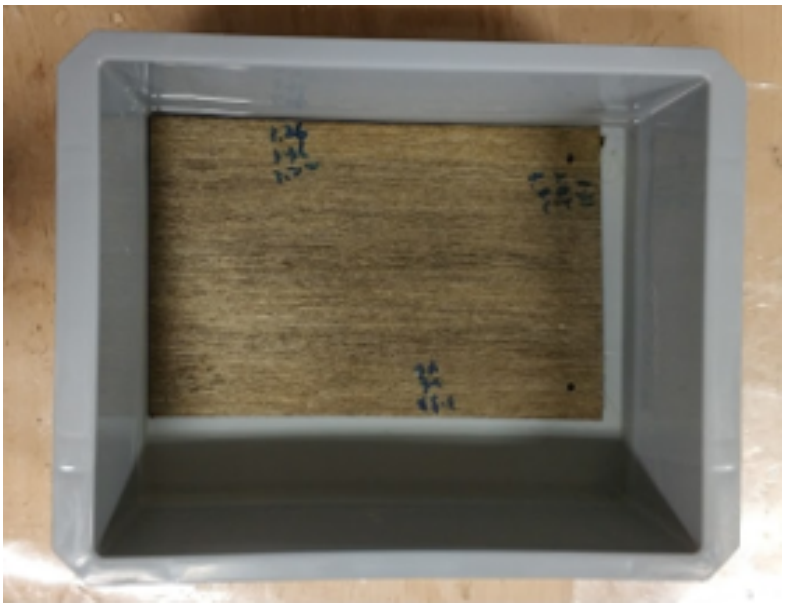

FIGURE III.5 – Water aging test at ambient temperature

Plates were then immersed in a box with tap water at ambient temperature as shown in Figure III.5. Experimental modal analysis was carried out on each aging days under free-free boundary condition at 50 - 1000 Hz and ambient temperature after measuring the mass gained (M_g) using the following equation:

$$M_g = \frac{m_i - m_0}{m_0} \times 100\%, \tag{III.7}$$

where m_i is the mass measured on water aging after i days. m_0 is the mass of unaged sample. The tests were stopped when the plates reached the saturation state.

III.3 Results and discussion

III.3.1 Optimization of the setup in free-clamped boundary conditions

Experimental modal analysis using free-free boundary conditions has several advantages when compared to free-clamped ones. The effect of the surroundings is as low as possible since only elastic strings touch the plate when non-contact excitation and measurement systems are used. Hence, it can minimize the dissipation which is not directly due to the structure itself. Free-clamped configuration has also many advantages (no rigid body movements and higher amplitude can be used) and can be used reliably if the influence of the clamping on the damping identification is minimized. In addition, experimental modal analysis is expected to be carried out in the linear viscoelastic range of the samples. The excitation amplitude and measurement point have to be calibrated and well selected to respect this hypothesis. These details are shown in Annex A.2 since they are prelimilar to the experiment. This section will focus on the effect of boundary conditions.

Boundary conditions can have a strong impact on the identification of the damping, in particular for clamped beams or plates, as the coupling between the structure and the hosting system cannot be perfect. Some dissipation occurs in the clamp due to non-perfect geometry and mounting. However, a clamped configuration allows precise measurement of the input force, which provides additional confidence in the values obtained from the measurement. An optimization of the clamping configuration has been performed numerically, in order to minimize the effect of the dissipation inside the clamp. The experimental modal analyses in free-clamped boundary conditions were then realized in the configuration numerically optimized to reduce the influence of the clamp on the damping measurement.

As dissipation occurs in the clamp, the value of the damping properties identified in the modal analysis process results from a combination of the losses in the material to be measured and the losses in the clamp which are unknown. The proposed methodology aims at defining the geometry of the sample and the clamp so that the dissipation at the junction has the minimum impact on the identified value of the damping. To that end, the numerical model uses a virtual material made of the same material as the clamp but with a very large loss factor. The geometry is then optimized so that the global loss factor of the model including the clamp is close to the one of the material. After optimization, a check on the effect of uncertainties on geometry and material parameters will qualify the robustness of the design.

In the free-clamped configuration, the beam is fixed by the clamp at one side and the other side is free. For the numerical simulations, isotropic and orthotropic constitutive behavior's laws were considered for the clamp and composite materials, respectively. The coupling between the clamp and the part of the sample which is inside the clamp was described using a virtual material as shown in Figure III.6. The loss factor of the sample (η_{sample}), virtual material ($\eta_{virtual}$) and

clamp (η_{clamp}) are respectively set to 2 %, 200 % and 200 %, which is expected to minimize the impact of boundary conditions as much as possible based on a higher damping ratio of clamp with a factor of 100 than the sample.

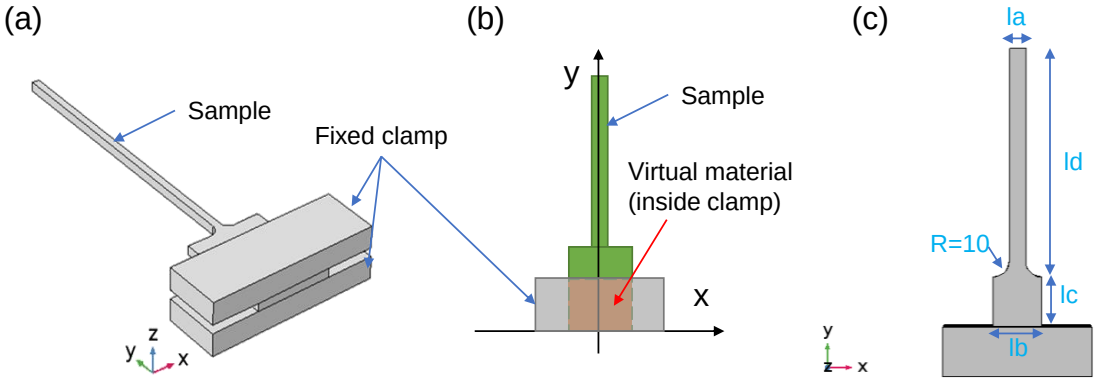

FIGURE III.6 – Geometry of the sample for clamped boundary conditions (Unit: mm)

The effect of the boundary conditions on the measurement of damping was studied using COMSOL®, which is a cross-platform finite element analysis, solver and multiphysics simulation software [Multiphysics 98]. The structure including the sample and the clamp in the numerical model is shown Figure III.6 (a) and (b). Details of numerical modeling are expounded in the following steps.

(1) The first step consists in building the geometry for each specimen shape. The considered dimensions are named la, lb and lc, as shown in Figure III.6 (c). The total length (lc+ld=200 mm) is fixed by the dimension of the mold during the manufacturing process. The width of the clamp is changed accordingly.

(2) Isotropic and orthotropic constitutive laws are set up to represent the mechanical behavior of the clamps and composites. The values of composite material, such as elastic modulus, are wrote as $\{E_x, E_y, E_z\}$ for the three different directions and are representative of the materials of interest. Their basic mechanical parameters are shown in Table III.2.

TABLE III.2 – Mechanical properties of different materials

	Density (kg/m^3)	Young's modulus (Pa)	Poisson's ratio
Clamp	2700	69e9	0.33
Composites	1200−1500	$\{E_x, E_y, E_z\}$	{0.04,0.32,0.04}

(3) All deformations are supposed in a linear elastic stage.

(4) The excitation is done by imposing a the pressure (p) on one of the sample sides with

$$p = \frac{e^{ikR}}{R} \quad (i = \sqrt{-1}), \tag{III.8}$$

$$\text{with } k = \frac{\omega}{c} \quad (c = 340 \text{ m/s}), \tag{III.9}$$

$$\text{and } R = \sqrt{(x - x_0)^2 + (y - y_0)^2 + (z - z_0)^2}, \tag{III.10}$$

where x, y, z is the three-dimensional coordinates on the sample and x_0, y_0, z_0 is the three-dimensional coordinates of the excitation (location of the transducer). This model is not representative of the real excitation, as the real acoustic field is not spherical and has a frequency-dependent amplitude, and the interaction occurs on the whole surface of the sample, however, it provides a distributed force corresponding to an acoustic excitation that can be used to verify the values of the stiffness and damping of the materials.

(5) Complex eigenvalue analysis is selected to investigate its modal frequency and damping characteristics. Loss factor of the structure (η_{str}) is obtained using equation III.11:

$$\eta_{str} = 2 \times \frac{\text{imag(solid.freq)}}{\text{abs(solid.freq)}}, \tag{III.11}$$

where imag(solid.freq) refers to imaginary part of the complex frequency, abs(solid.freq) refers to the real part of the complex frequency.

(6) The difference (err) between the computed loss factor of the structure (including the composite and the clamp) and the input value (2 %) is calculated using the following equation,

$$err = \frac{\eta_{str} - 2\%}{2\%} \times 100\%, \tag{III.12}$$

and the err is expected below 10 % to be considered as acceptable, taking into account all the other sources of uncertainties.

The value ranges of the investigated parameters are shown in Table III.3.

Table III.3 – Mechanical properties of different materials

Parameters	Range (mm)
la	[4, 24]
lb	[30, 90]
lc	[0, 60]

To provide a clear representation of the results, 2D plots are used. The objective is to select the best set of parameters (la, lb and lc).

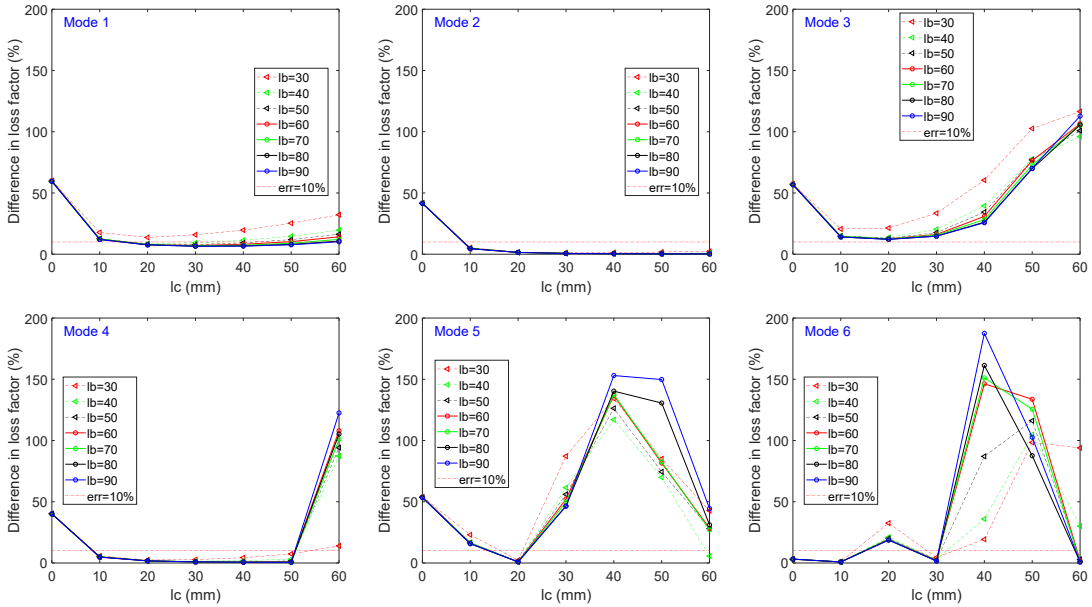

FIGURE III.7 – The influence of lb and lc on modes 1-6 when la=4 (Different curve refers to different value of lb)

Figure III.7 shows the influence of lb and lc values on the loss factor for modes 1 to 6 when la is equal to 4 mm. It can be seen that the difference (err) is mainly driven by lc and the changes in lb has less effect on the difference in loss factor compared with lc. The optimized values of lc are summarized in Table III.4 considering that the difference between numerical results and input value of loss factor are expected less than 10 %.

TABLE III.4 – Selected lc for modes 1-6 when la=4

Mode	1	2	3	4	5	6
lc-selected	20-40	10-60	20*	10-50	20	10 ; 30

* The value of difference is around 16 % when lc=20 mm and it can not be optimized more.

TABLE III.5 – Selected la for modes 1-6 when lb=40

Mode	1	2	3	4	5	6
la-selected	4	4 ; 8	4	4-18	4 ; 8	4

Figure III.8 shows the influence of la and lc on the loss factor for modes 1 to 6 when lb is equal to 40 mm. The difference within 10 % in loss factor can be found when lc is in the range of 10 - 30 mm whatever the values of la and in this case the optimized values of la are summarized in Table III.5.

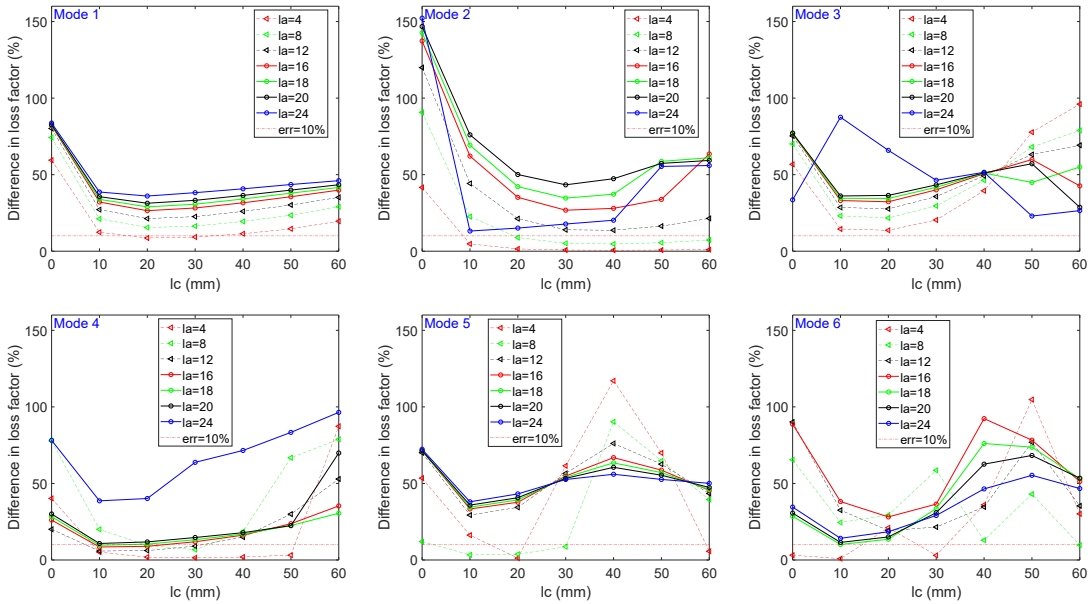

FIGURE III.8 – The influence of la and lc on mode 1-6 when lb=40 (Different curve refers to different value of la)

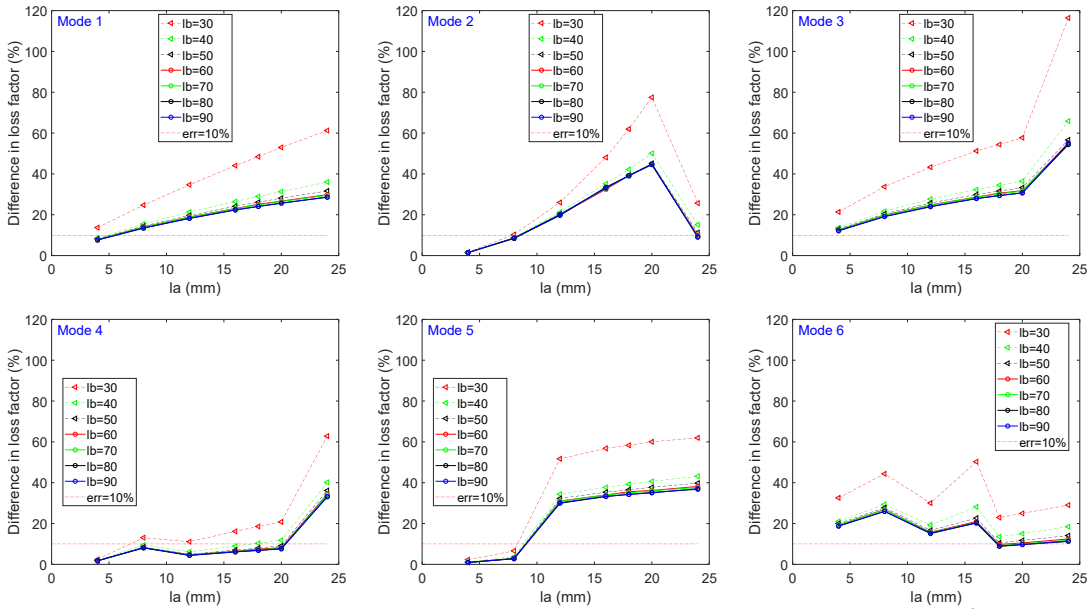

FIGURE III.9 – The influence of la and lb on modes 1-6 when lc=20 (Different curve refers to different value of la)

Figure III.9 shows the influence of la and lb on the loss factor in modes 1 to 6 when lc is set equal to 20 mm.

It can be clearly seen that the difference loss factor will not have a significant changes when lb is larger than 30 with a specific value of la. However, the difference in loss factor is beyond 12 % in mode 3 even the lb changes from 30 to 90. The

influence of la is similar with previous description. Based on this, the optimized values of la are summarized in Table III.6, and lb is suggested a vlalue larger than 30.

TABLE III.6 – Selected range of la for modes 1-6 when lc=20

Mode	1	2	3	4	5	6
la-selected	4	4 ; 8	4*	4-18	4 ; 8	18

* The value of difference is around 17 % when la=4 mm and it can not be optimized more.

Although the 2D plots are convenient to observe the influence of the parameters individually, they do not constitute a relevant tool to select the optimized set of parameters since we need to fix one of the parameters. Another way to plot the difference is using a color marker in 3D plot to show the difference of loss factor using different colors as shown in Figure III.10.

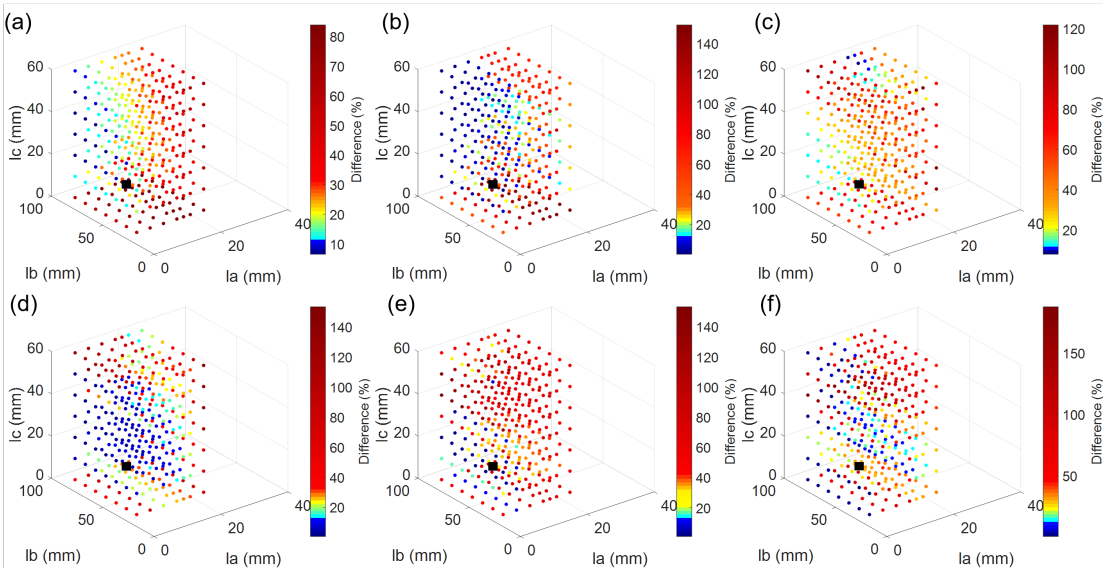

FIGURE III.10 – Difference of loss factor under various values of la, lb and lc in modes 1-6 ((a)-(g)) (the blue points refer to difference (*err*) is less than 10 %, ■ refers to the final selected value)

However, it is difficult to find a set of values of la, lb and lc which can meet the expected difference for all the modes. In this case, we try to make the maximum number of modes meet this condition (at least 5 modes less than 10 %) and a compromise was found for a set of la, lb and lc parameters equal to 4, 40 and 20, respectively, considering both the optimized shape and the constraints related to the manufacturing of the plate.

Using this selected set of values, the influence of slight variations (5 %) in dimensional and mechanical parameter on the damping of the modes 1-6 was studied. Results are shown in Figure III.11 and the maximum value is around 0.27 % which means these slight changes representing potential uncertainties do not have a significant influence on the identified value of loss factor.

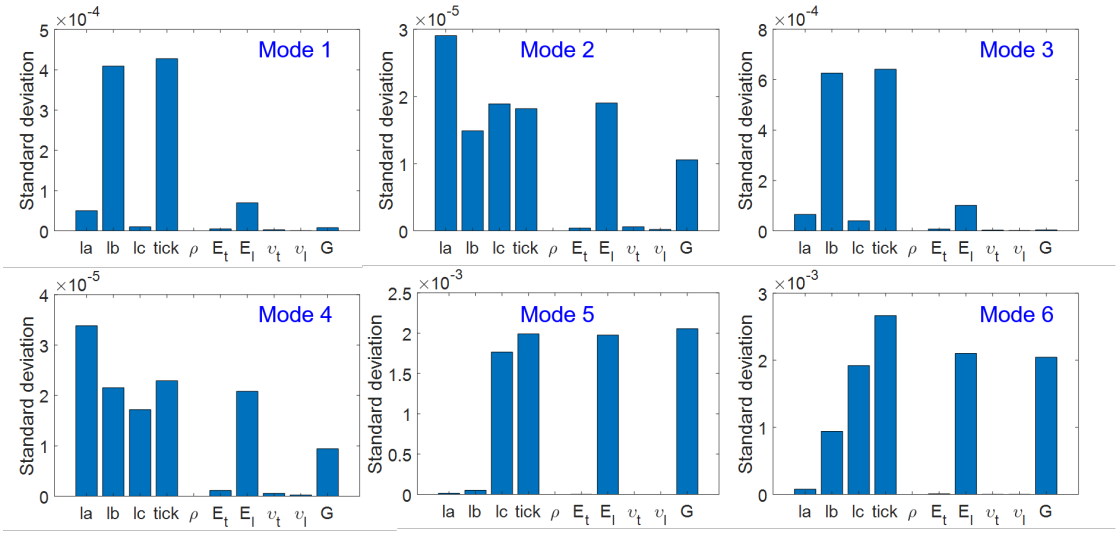

FIGURE III.11 – Standard deviation on loss factor obtained 5 % variation around the nominal value of the parameters in experimental setup (tick: thickness of the sample, ρ: density of the composites, E_t and E_l: Young's modulus in transverse and longitudinal direction, υ_t and υ_l: Possion's ratio in transverse and longitudinal direction, G: shear modulus)

The dimensions considered later for free-clamped boundary condition always use this optimal configuration.

III.3.2 Modal analysis in free-free configuration

III.3.2.a Damping identification of FGUD

The modal response of FGUD is shown in Figure III.12. Different curves (FGUD-1, FGUD-2, FGUD-3) corresponding to repeated measurements on 3 different plates are presented. It allows the quantification of uncertainties related to the experimental set-up, in particular related to the mounting and unmounting of the plate, as well as to the material itself to be characterized. The different natural frequencies observed in the experimental results are due to the difference in dimensions between the three tested plates (see Table). Despite these differences, the flexural mode always appeared in second position for the transverse direction and in third position for the longitudinal direction. These modes (flexure in L and T directions) will be used in this work to determine the damping ratio in L and T directions, respectively.

The geometric dimension of the sample used in numerical model have been mentioned in section III.2 and mechanical parameters are refer to the value introduced in chapter II. As already mentioned, the modal of the excitation does not aim to be representative of the acoustic pressure radiated by the loudspeaker. The FRFs are shown to illustrate the resonaces and qualitatively check the damping levels. The amplitudes of the numerical and experimental FRFs can not be compared.

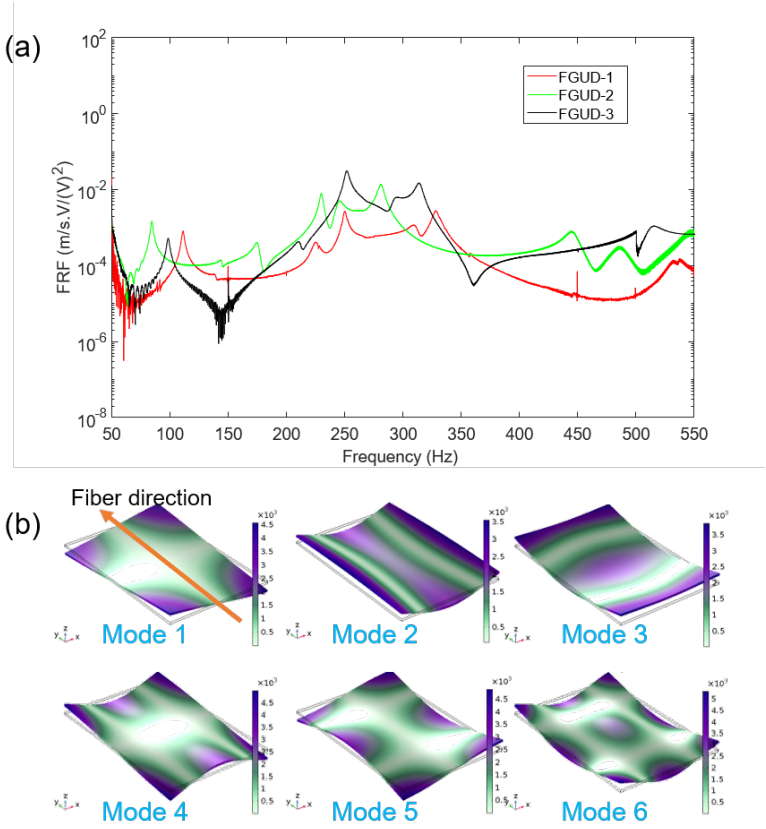

FIGURE III.12 – (a) FRF results of numerical model and experiment, and (b) modal shape simulated by numerical model for FGUD in free-free conditions

The damping ratios and natural frequencies measured for the 3 different FGUD plates at each natural frequency are summarized in Table III.7. The minimum value of damping ratio (0.67 %) is found at 250 Hz with a flexural mode in L direction and the maximum value of damping ratio (1.33 %) is found at 225 Hz with a flexural mode in T direction. The damping ratio determined from torsion mode varies between 0.74 % and 1.2 % . These values are between that of flexural modes in L and T direction.

TABLE III.7 – Results of modal analysis of FGUD in free-free conditions (f_{exp} and f_{num} refers to natural frequency from experiment and numerical model, respectively, 'Tor' and 'Fle' refer to torsion and flexural mode, L and T refer to longitudinal and transverse direction, respectively)

Mode	1	2	3	4	5	6
$f_{exp} - 1$ (Hz)	111	225	250	311	329	531
$f_{exp} - 2$ (Hz)	83	173	230	244	281	445
$f_{exp} - 3$ (Hz)	98	209	250	292	313	514
f_{num}-mean (Hz)	93	208	235	283	298	494
ζ (%)	0.92	1.33	0.67	1.2	0.74	1.09
E'-mean (GPa)	-	4.65	34.6	-	-	-
Mode shape	Tor 1	Fle 1-T	Fle 2-L	Tor 2	Tor 3	Tor 4

The average values of the loss factor in the two main material directions were then calculated from the measurements made on the three plates. Results are synthetized in figure III.13. It can be observed that the scattering is quite low with a coefficient of variation less than 1 % for the longitudinal direction and about 9.9 % for the transverse direction. The higher uncertainty in the transverse direction compared to the longitudinal direction is attributed to the natural frequency variation from 173 to 225 Hz for the different tested plates. The mean loss factor is equal to 1.31 % in the longitudinal direction and 2.64 % in the transverse direction. These values are comparable to the one determined in DMA tests (1.59 % and 2.42 % in the respective directions).

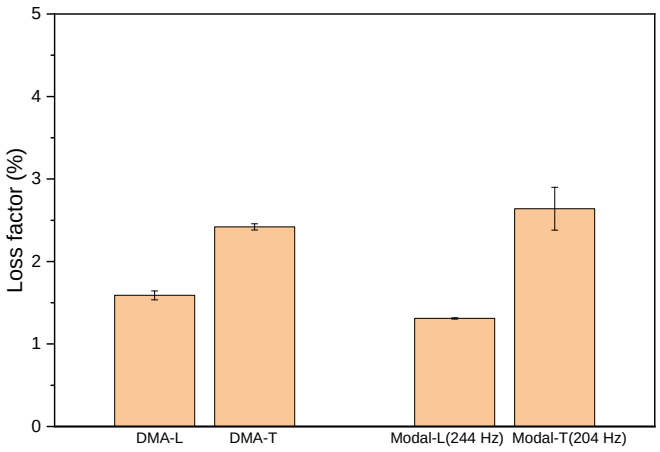

FIGURE III.13 – Comparison of the loss factor values determined for FUGD material in DMA and modal tests. (The resutls from DMA test is at 1 Hz and modal tests are obtained from the flexual modes in longitudinal direction (around 244 Hz) and transverse direction (204 Hz))

The storage modulus was also identified by inverse method from these experimental results. A value of 4.65 GPa and 34.6 GPa (with standard deviation: 0.15 and 2.1) were obtained in the transverse and longitudinal directions, respectively. These values are close to the ones determined using quasi-static tests (4.5 and 30 GPa, respectively). As explained in chapter II, the comparison with the storage modulus determined using DMA tests is not relevant since it is under-estimated due to the frame stiffness limitation in DMA instrument.

III.3.2.b Damping identification of FPPC

The modal response of the FPPC plate is shown in Figure III.14. The different curves presented correspond to repeated measurements on a single plate. The first mode, a torsion mode, is around 100 Hz. Mode 2 and mode 4 are flexural modes in L and T directions, respectively. Their natural frequencies are around 153 Hz and 358 Hz, respectively.

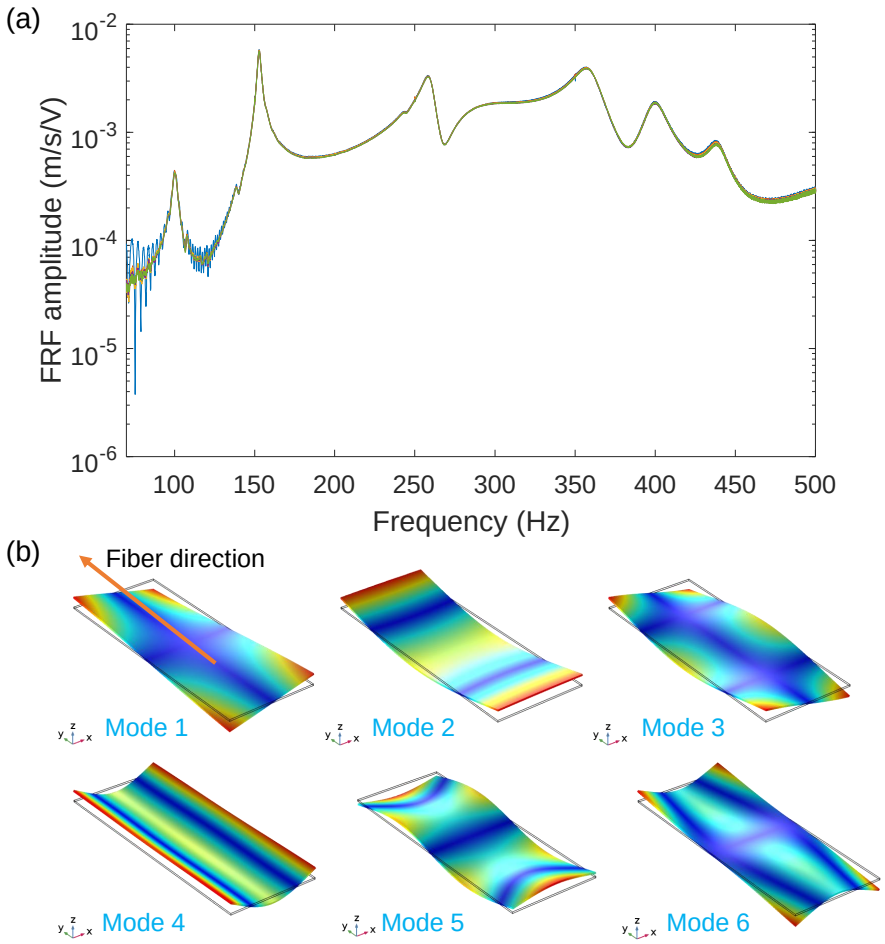

FIGURE III.14 – (a) FRF from numerical model and experiment, and (b) modal shape in numerical model for FPPC in free-free conditions

The average damping ratio values are reported in Table III.8. The minimum value of damping ratio (0.7 %) is found at 145 Hz with a flexural mode in L direction and the maximum value of damping ratio (2.3 %) is found at 378 Hz with a flexural mode in T direction. These values of loss factor in L (1.4 %) and T (4.6 %) direction from modal analysis are around 18 - 67 % difference compared with those of DMA at 1 Hz in L (2.3 %) and T (3.8 %) direction at 1 Hz since the difference of frequency is quite large. The damping ratio determined from torsion mode is between 1.4 % and 1.7 %. The storage modulus value back-calculated in longitudinal and transverse directions are equal to 20 GPa and 5.4 GPa, respectively. The storage modulus of FPPC in longitudinal direction by back calculation is also closed to the Young's modulus from static measurements (24 GPa).

TABLE III.8 – Results of modal analysis of FPPC in free-free conditions (f_{exp} and f_{num} refers to natural frequency from experiment and numerical model, respectively)

Mode	f_{exp} (Hz)	f_{num} (Hz)	ζ (%)	E' (GPa)	Mode shape
1	100	100	1.54	-	Torsion 1
2	152.8	145	0.7	20	Flexure 1_L
3	259.3	250	1.6	-	Torsion 2
4	358.4	378	2.3	5.4	Flexure 2_T
5	399.4	396	1.68	-	Torsion 3
6	438.7	431	1.46	-	Torsion 4

III.3.2.c Damping identification of H4

The modal response of H4 is shown in Figure III.15. Results are given for repeated tests on a single plate. The first mode is still a torsion mode at a frequency of approximately 85 Hz. The flexural modes in a single material direction are used to determine the damping ratio values in L or T directions. It can be seen from the numerical simulations that mode 1 and mode 3 are flexural modes in T and L directions. Their natural frequencies are around 85 Hz and 232 Hz, respectively. The mode at around 258 Hz observed experimentally is a mix of two modes, the one obtained at the two natural frequencies 247 and 253 Hz with the numerical model.

The average values of the damping ratio from the repeated measurements on the same plate at each natural frequencies are summarized in Table III.9. The minimum value of damping ratio (0.78 %) is found at 85 Hz with a flexural mode in T direction and the maximum value of damping ratio (0.96 %) is found at 232 Hz with a flexural mode in L direction. These values of loss factor (1.6 - 1.9 %) are comparable to the loss factor (2 %) measured using DMA at 1 Hz. The damping

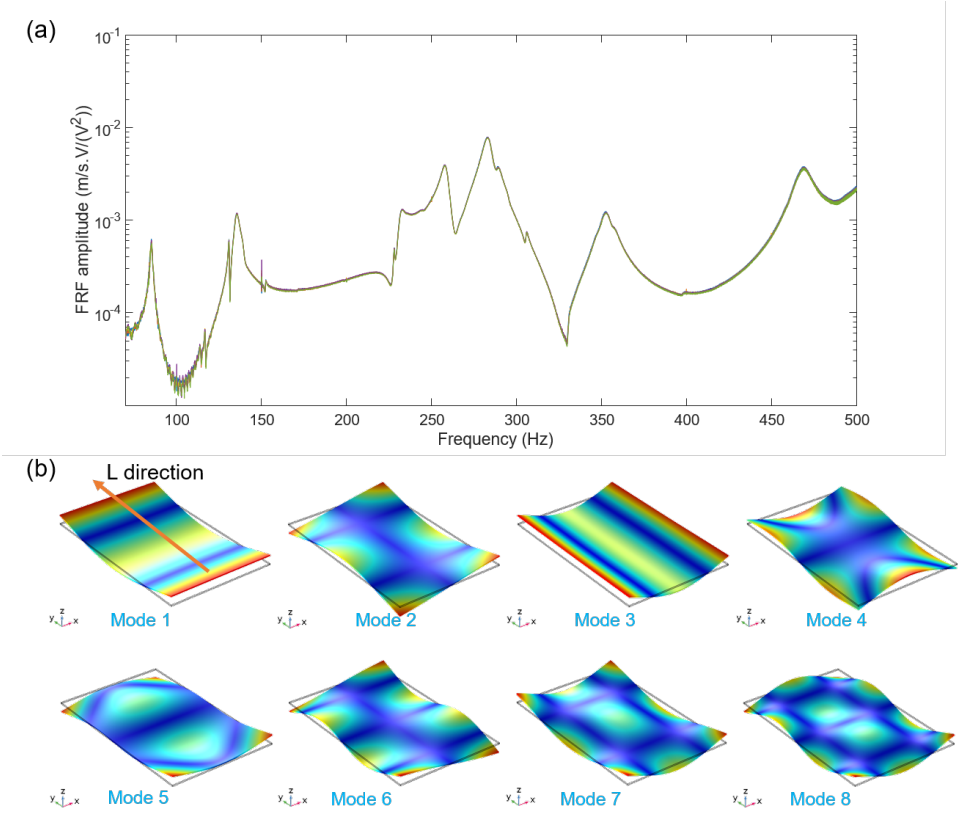

FIGURE III.15 – (a) FRF from numerical model and experiment, and (b) modal shape in numerical model for H4 in free-free condition

TABLE III.9 – Results of modal analysis of H4 in free-free conditions (f_{exp} and f_{num} refers to natural frequency from experiment and numerical model, respectively)

Mode	f_{exp} (Hz)	f_{num} (Hz)	ζ (%)	E' (GPa)	Mode shape
1	85	90	0.78	14.3	Flexure 1_T
2	135	134	1	-	Torsion 1
3	232	230	0.96	15.3	Flexure 2_L
4	-	247	-	-	Torsion 2
5	258	253	0.87	-	Torsion 3
6	283	289	1.04	-	Torsion 4
7	352	316	1	-	Torsion 5
8	467	451	1	-	Torsion 6

ratio determined from torsion mode is between 0.8 % and 1.04%. The storage modulus are around 14.3 GPa and 15.3 GPa in the longitudinal and transverse directions, and they are close to the value from static tests (around 18 GPa).

III.3.3 Modal analysis in free-clamped configuration

III.3.3.a Damping identification of FGUD

The modal response of FGUD in longitudinal and transverse directions under free-clamped boundary conditions is shown in Figure III.16. The different experimental curves were measured on different samples. Figure III.16 (a) shows the first and second modes of FGUD-L. All of them are flexural modes in L direction. They are at frequencies around 107 and 637 Hz. The natural frequencies determined by experiment are close to that obtained by numerical simulation. Figure III.16 (b) shows the first and second modes of FGUD-T and both of them are again flexural mode in T direction, with frequencies around 65 and 404 Hz. The natural frequencies in transverse direction determined by experiment are also close to that of the numerical model. The modal shapes in the experiment under free-clamped are all corresponding to flexural modes, from 50 to 1000 Hz. In addition, a resonance frequency is found at around 280 Hz in both directions with a damping ratio of 10 %. This may be the damping from the support of clamp or the vibrometer.

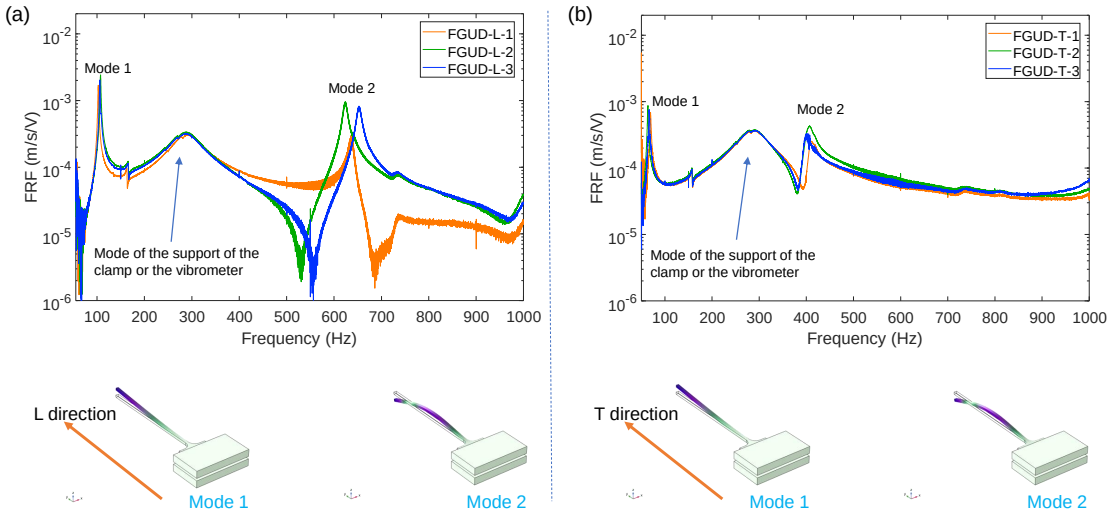

FIGURE III.16 – Modal response of FGUD in (a) longitudinal direction, and (b) transverse direction

The average values of the damping ratio under free-clamped boundary conditions at each natural frequency are summarized in Table III.10. The value of damping ratio in longitudinal direction increases from 0.68 % to 0.77 % as the frequency increases from 107 Hz to 656 Hz and the value of damping ratio in transverse direction increases from 1.47 % to 1.67 % as the frequency increases from 65 Hz to 400 Hz. The storage modulus is around 32 GPa and 4.6 GPa with standard deviation of 1.2 and 0.8 in the longitudinal and transverse directions on the frequency range 60-700 Hz.

TABLE III.10 – Results of modal analysis of FGUD in free-clamped conditions (f_{exp} and f_{num} refers to natural frequency from experiment and numerical model, respectively) (The results from experiment are using the average values of three samples, std refer to their standard deviation)

f_{exp} (Hz)	f_{num} (Hz)	ζ (%)	std	E' (GPa)	Modal shape
FGUD-L					
107	107	0.68	0.03	32	Flexure 1_L
637	656	0.77	0.06	30.2	Flexure 2_L
FGUD-T					
66	65	1.47	0.05	4.6	Flexure 1_T
404	399	1.67	0.09	4.6	Flexure 2_T

III.3.3.b Damping identification of FPPC

Figure III.17 shows the results of FRF for FPPC in longitudinal direction. One curve from experiment corresponds to one sample. The modal response of FPPC in transverse direction is missing because of the limitation in the dimensions of the plate. The modal shapes obtained from numerical model around 278 and 758 Hz are flexural modes in longitudinal direction.

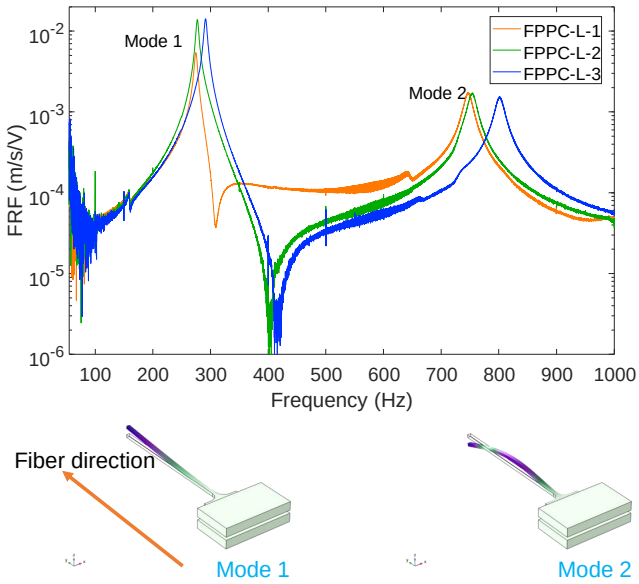

FIGURE III.17 – Modal response of FPPC in longitudinal direction

The results including natural frequency, damping ratio, storage modulus and mode shapes of FPPC-L from modal test under free-clamped boundary conditions are summarized in Table III.10. A slight increasing trend of damping ratio (from

0.89 % to 1.03 %) in the longitudinal direction is found with the frequency increasing from 278 Hz to 758 Hz. The storage modulus is around 20 GPa with standard deviation of 0.92 in the longitudinal direction at 271 and 745 Hz.

TABLE III.11 – Results of modal analysis of FPPC in free-clamped conditions (f_{exp} and f_{num} refers to natural frequency from experiment and numerical model, respectively). (The results from experiment are using the average values of three samples, std refer to their standard deviation).

f_{exp} (Hz)	f_{num} (Hz)	ζ (%)	std	E' (GPa)	Modal shape
278	271	0.89	0.02	20	Flexure 1_L
758	745	1.03	0.06	19.7	Flexure 2_L

III.3.3.c Damping identification of H4

The results of experimental modal response and the FRF from numerical model of H4 in longitudinal and transverse directions are shown in Figure III.18. As previous, one experimental curve corresponds to one sample. Figure III.18 (a) shows the mode shapes for the first (around 288 Hz) and second mode (around 784 Hz) and it can be seen that they are both flexural modes in longitudinal direction. Figure III.18 (b) shows the modal shape of H4-T from numerical model at around 312 and 839 Hz and they are flexural mode in T direction. This allows to calculate the storage modulus and loss factor in L and T directions.

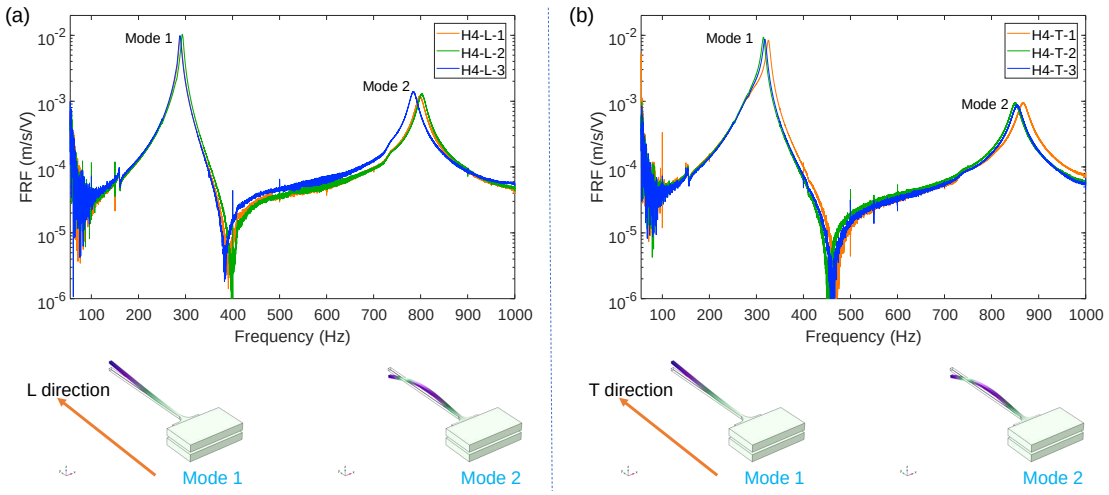

FIGURE III.18 – Modal response of H4 in (a) longitudinal direction, and (b) transverse direction

Table III.12 summarizes the dynamic properties of H4 such as the natural frequency from both numerical model and experiment, damping ratio and storage modulus. For the longitudinal direction, the damping ratio shows a slight increase from 0.94 % to 1.02 % as the frequency increasing from 288 Hz to 784 Hz. For

transverse direction, the damping ratio increases by around 20 % (from 1.03 % to 1.25 %) as the frequency increases from 312 Hz to 839 Hz. Although the density of the yarn in longitudinal and transverse direction is the same, the damping properties show an effect from the frequency range. In addition, the storage modulus is identified at approximately 16 GPa and 18 GPa in the longitudinal and transverse directions using back calculation from 280-900 Hz, it is close to the value obtained in static measurements.

TABLE III.12 – Results of modal analysis of H4 in free-clamped conditions (f_{exp} and f_{num} refers to natural frequency from experiment and numerical model, respectively) (The results from experiment are using the average values of three samples, std refer to their standard deviation)

H4-L					
f_{exp} (Hz)	f_{num} (Hz)	ζ (%)	std	E' (GPa)	Modal shape
288	288	0.94	0.03	16	Flexure 1_L
784	793	1.02	16	Flexure 2_L	
H4-T					
312	288	1.03	0.04	19	Flexure 1_T
839	793	1.25	18	Flexure 2_T	

This section shows the results of modal analysis for three representative plant fiber composites (FGUD, FPPC and H4) independently, and their damping properties are investigated at around 50 - 1000 Hz. Furthermore, the length of the beam can be shorter to achieve damping measurement in higher frequency range and this work is in progress. In addition, it is better to do the comparison of damping properties between these three materials measured from modal analysis under free-free and free-clamped boundary condition as well as the results from DMA tests.

III.3.4 Comparison of damping properties in modal analysis and DMA tests

Figure III.19 shows the damping ratio of the three types of plant fiber composites tested in this study, both in longitudinal and transverse directions and under free-free conditions as well as free-clamped boundary conditions. The reported values of the damping ratio were all determined from flexural mode shapes.

For longitudinal direction (full symbol ◀, ■), the damping ratios of the different types of plant fiber composites are comparable, with values comprised between 0.7 % and 1 %. It indicates that the damping properties in the longitudinal direction is also mainly driven by the fiber behavior at the macroscale. For transverse direction (empty symbol ◁, □), the maximum value of the damping ratio is obtained for the FPPC-T (2.3 %) and then followed by the thermoset based

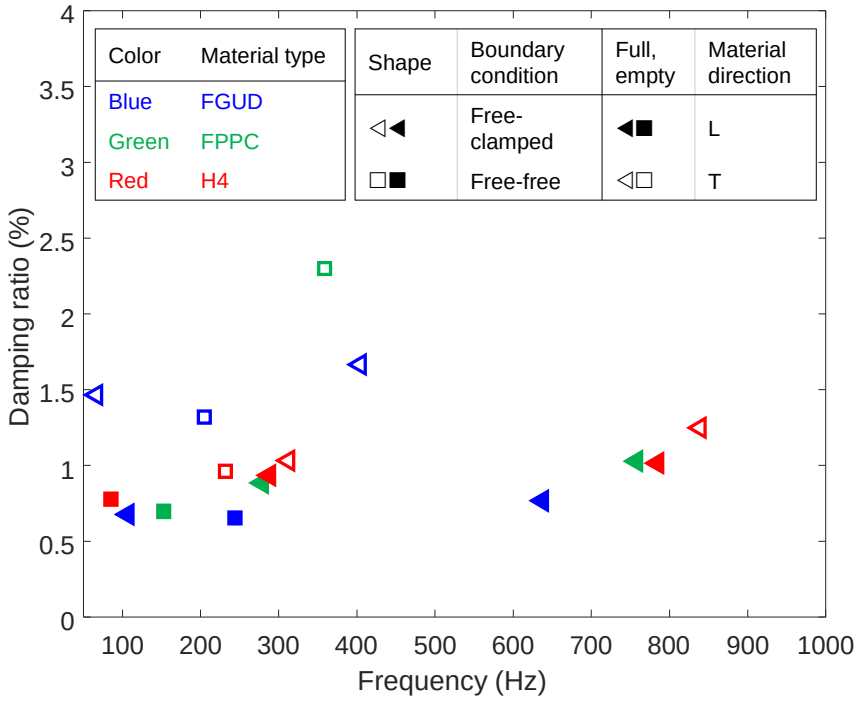

FIGURE III.19 – Damping ratios measured under free-free and free-clamped boundary conditions.

composites (FGUD: 1.67 %, H4: 1.25 %). It leads to the same conclusions that the one drawn from DMA results. At the macroscale, the damping properties in the transverse direction of unidirectional plant fiber composites are also mainly driven by the matrix' behavior. The damping ratio of H4-T is lower than FGUD-T because H4 in transverse direction is also reinforced by fibers in this woven fabric composite.

In addition, it can be seen that the damping ratio measured under free-free boundary conditions (square symbol) are lower than the ones determined under free-clamped boundary conditions (triangle symbol), which indicates that the influence from boundary conditions can not be ignored even if using optimized sample shapes.

Figure III.20 compiles the loss factors determined from DMA and modal tests as a function of frequency. The damping ratios from modal tests are converted to loss factor using a factor of 2 since the damping ratios are determined by the flexural mode in longitudinal and transverse directions of the composites. The difference in loss factor between DMA and modal tests at 40 - 100 Hz is attributed to the uncertainty of measurements in this frequency range in DMA tests.

In addition, the damping ratios of thermoset based composites from modal tests also show a slight increasing trend for the frequency beyond 200 Hz. This can be explained by the secondary transition of the GreenPoxy as shown in Figure III.21. It clearly shows the obvious increase in loss factor from 100 Hz to 10 kHz in the master curve. This figure also shows a good agreement between the damping

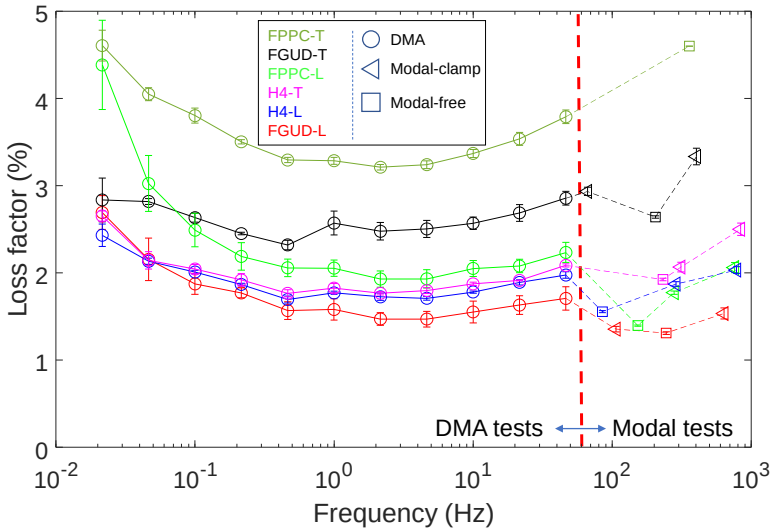

FIGURE III.20 – Loss factor in Modal and DMA tests. (Modal-clamp and modal-free refer to modal tests under free-clamped and free-free boundary conditions)

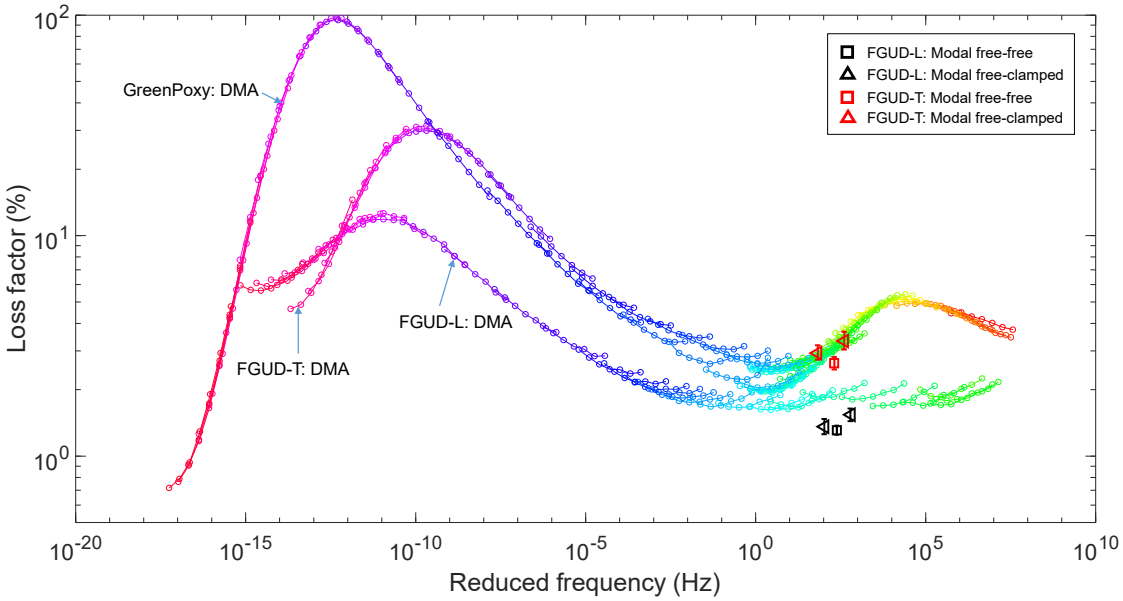

FIGURE III.21 – Superimposition of the loss factor master curves identified from DMA tests and loss factor values identified from modal tests for FUGD

values measured at the mesoscale using DMA and the one obtained using modal analysis at the macroscale. For instance, a difference of approximately 19 % in loss factors is obtained between the two techniques in FGUD-L.

Regarding the ability of the modal approach, experiment under free-free boundary conditions seem to provide more confident values of loss factors compared to those under optimized free-clamped boundary conditions. The modal approach shows slight lower values of loss factors when compared to DMA, which leads to

conclude that the modal approach is providing more precise results. However, we have to be very careful when doing the experiment as any dissipation in the setup will result in increased estimation of the loss factor.

III.3.5 Influence of water aging in free-free boundary conditions

As mentioned in chapter 2, the moisture content is one of the most influential parameters among the studied ones using DMA tests for a given temperature and frequency. The damping properties of FGUD were also studied at the macroscale and ambient temperature using modal tests in this section.

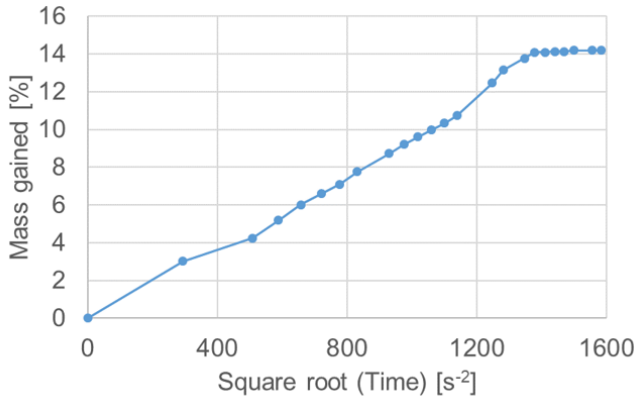

FIGURE III.22 – Results of water aging tests for gained mass as a function of square root of time

Figure III.22 shows the water absorption as a function of the water aging time. The mass gained at saturation is around 14.2 %. This value is closed to that from existed literature (11.9 %, 13.5 %) [Jeannin 19a, Chilali 17]. The small difference observed between this work and literature may be due to the different types of material produced, fiber volume fraction etc.

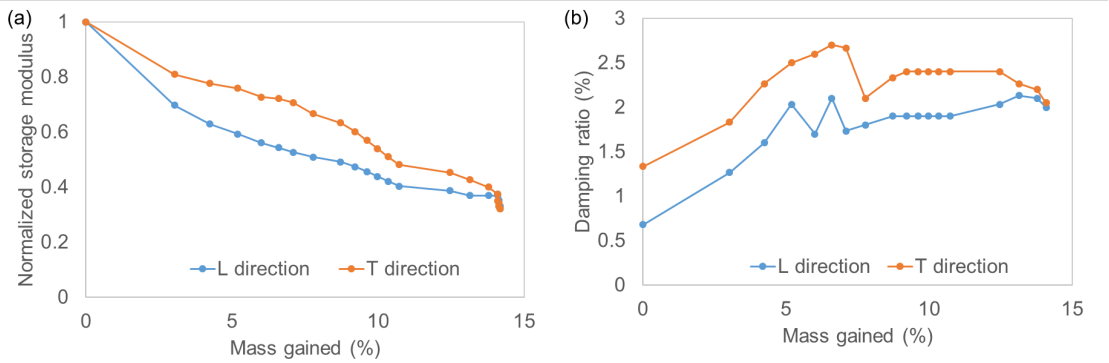

FIGURE III.23 – Results of water aging tests for (a) normalized storage modulus and (b) loss factor as a function of gained mass in L and T direction

The changes in normalized storage modulus (as a reference of unaged state) identified by inverse method from modal tests as a function of mass gained of water is plotted in Figure III.23 (a). The storage modulus is obviously decreasing as the moisture content increases. A decrease of around 68 % in both direction is found in storage modulus at the equilibrium moisture content state compared to unaged state. The decreasing value in modal tests (mass gained around 14 %) is slight higher than that from DMA tests (60 %, 65 % in transverse and longitudinal direction) due to the not enough aging time in DMA tests (mass gained around 10 - 15 %).

FIGURE III.24 – The deformation of the tested plate during water aging

The evolution of the damping ratio as a function of mass gained is presented in Figure III.23 (b). Between the dry state and 6.5 % of mass gain, the damping ratio is increasing almost monotonically from 0.68 % to 2.1 % and from 1.4 % to 2.7 % in longitudinal and transverse directions of the FUGD, respectively and the changes in transverse direction from modal test is closed to that obtained in DMA tests with an increases of damping ratio from 1.2 % to 2.75 %. The measurements are varying quite significantly at around 6.5 % of mass gain. This was attributed to the deformation of the FGUD plate as shown in Figure III.24. This deformation are certainly due the internal stress relaxation induced by the activation of viscoelastic properties (plasticizing effect of water). As shown, an obvious warpage (around 1 cm of height) is found at the corner of the plate. It may have an effect on the modal shape of FGUD. Therefore, the damping ratio determined after the appearance of this deformation of the plate is certainly not reliable, and the apparent stabilization of the damping properties with the increasing moisture content in the second part of the curve should be confirmed by additional measurements. At last, the damping ratio comes to around 0.5 - 2 times in longitudinal and transverse directions at the saturated state compared to unaged samples. This can be compared to the results from literature on quasi-UD flax composites in longitudinal and transverse direction (0.8 - 1.25 times [Cheour 16]). The difference can be attributed to the pattern of the flax reinforcement (pure UD versus qusi-UD). This needs to be further studied with more samples and under free-clamped boundary conditions.

III.4 CONCLUSIONS

In this chapter, researches related to the identification of damping properties at the macroscale were proposed. The damping properties of SSUCHY materials (FGUD, FPPC, H4) have been studied using modal analysis under free-free and

free-clamped boundary conditions. Their resonance responses were compared to those obtained using numerical simulations, allowing identification of the mode shapes. An optimized shape is designed using the numerical model to minimize the influence of clamping in the free-clamped configuration on the damping identification. The damping properties of these materials for the first 6 modes are given. The longitudinal and transverse properties are identified from the shapes of the eigenmodes. The loss factors of FGUD and FPPC composites are comprised between 1.3 % - 3.3 % and 1.4 % - 4.6 % on the frequency range of 40 Hz – 1000 Hz, respectively. These results show better damping capacities of unidirectional flax composites with thermoplastic matrix (PP) than the thermoset matrix (Greenpoxy) in transverse direction.The loss factor of H4 is between 1.5 %-2.5 % on the frequency range of 40 Hz – 900 Hz. There is no significant difference between warp (L) and weft (T) directions. Although the shape of sample is optimized, the damping ratio determined from free-clamped boundary conditions is still higher (maximum 20 %) than that from free-free boundary conditions.

Loss factors from DMA and modal tests were also compared using the plot of master curve. A good corresponding is found in FGUD-T and a maximum 19 % difference is obtained in FGUD-L when compared to loss factor using master curve. The damping ratio of aged FGUD is around 2 % in both longitudinal and transverse direction at the saturated mass (14.2 %). Influence of moisture has to be more thoroughly studied in the future, in particular at different temperatures.

Chapitre IV
Micro scale: dynamic nanoindentation

IV.1 Introduction 124
IV.2 Materials and methods 125
IV.2.1 Theory of nanoindentation and its applications 125
IV.2.2 Selection of existing research on nanoindentation 128
IV.2.3 Tested materials 129
IV.2.4 Experimental setup 129
IV.3 Results and discussion 135
IV.3.1 Verification of the effect from instrument on the measurement of storage modulus and loss factor 135
IV.3.2 Damping identification of GreenPoxy using CAM method 136
IV.3.3 Damping identification of FGUD using CSM method 139
IV.3.4 Damping identification of FGUD using CSM+CAM method 144
IV.4 Conclusions 149

GRAPHICAL ABSTRACT

- Development of a new method (CAM: Constant Amplitude Method) with constant mean and dynamic amplitude after unloading to provide a better deconvolution between elastic, viscoelatic and plastic contributions.
- Good consistency between DMA and Dynamic NanoIndentation (DNI) measurements for the loss factor of neat GreenPoxy on the 30-65 °C and 1-40 Hz ranges.
- Values of loss factor identified at the microscale are strongly dependent on the DNI method
- Using CAM method, a loss factor of 4% is measured in the flax fiber wall. This is consistent with the values back-calculated from DMA tests on composites.

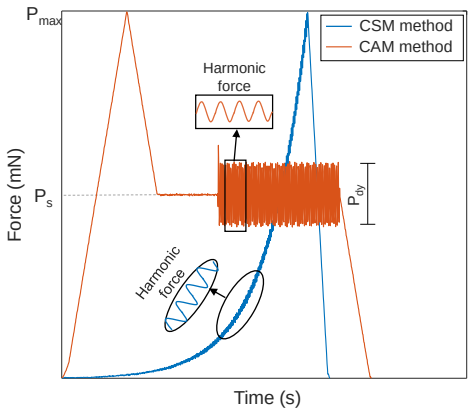

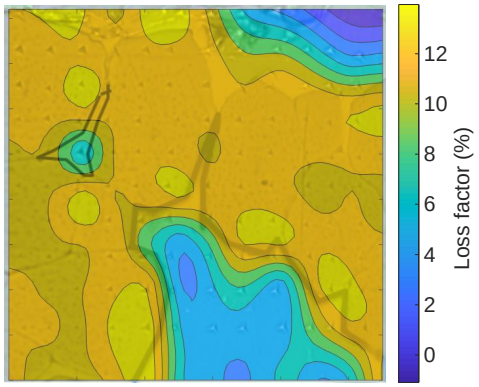

RESUME

Dans les chapitres précédents de cette thèse de doctorat, l'identification des propriétés d'amortissement est réalisée à l'échelle macroscopique. Compte tenu de l'organisation complexe et hiérarchique des composites de fibres végétales, il est nécessaire d'étudier leur comportement viscoélastique à l'échelle microscopique. De plus, il est important de connaître les spécificités des mécanismes de dissipation dans les composites de fibres végétales à l'échelle microscopique afin de comprendre et de prévoir les propriétés d'amortissement à l'échelle macroscopique. Ainsi, le but de ce chapitre est d'identifier l'amortissement à l'échelle microscopique à l'aide de mesures de champs des propriétés viscoélastiques par nanoindentation dynamique (DNI). Une amélioration de la technique de nanoindentation dynamique et son utilisation pour la caractérisation des composites de fibres végétales à l'échelle microscopique sont proposées. Cette méthode vise à mesurer les propriétés viscoélastiques des parois de fibres végétales, de la matrice et de leurs interfaces dans le matériau composite en utilisant la nanoindentation dynamique dans des conditions environnementales contrôlées, grâce à des mesures de champs. La valeur du facteur de perte de la résine époxy pure mesurée grâce à cette méthode montre une bonne adéquation avec celle obtenue en DMA sur des plages de fréquences et de températures comprises entre 1 et 40 Hz, et 30 et 65 °C. Les valeurs de facteur de perte mesurées dans la section transverse des composites UD lin/GreenPoxy sont étroitement dépendantes de la méthode de nanoindentation dynamique utilisée. En utilisant la méthode d'amplitude constante, une valeur moyenne de 4 % est

mesurée dans la paroi des fibres de lin. Cette valeur est similaire à celle identifiée dans la direction transverse des fibres par méthode inverse à l'aide des essais DMA sur composites. La méthode proposée permet également d'accéder à la mesure du champ des propriétés viscoélastiques dans la section transverse du composite, ceci permet d'évaluer la contribution respective des différents constituants à l'amortissement global du composite. Enfin, les mesures réalises à l'échelle microscopique en nanoindentation dynamique sont comparées aux résultats obtenus par DMA et analyses modales.

ABSTRACT

In the previous sections of this PhD thesis, the identification of damping properties has been carried out at the macro scale. Considering the complex and hierarchical organization of plant fiber composites, it is also necessary to study their viscoelastic behavior at the micro scale. Furthermore, it is important to find out the specificities of dissipation mechanisms in plant fiber composites at micro scale in order to understand and to predict damping properties at the macro scale. So, the purpose of this chapter is to identify the damping at the microscopic scale using dynamic grid nanoindentation. The dynamic nanoindentation (DNI) technique with constant mean and harmonic amplitudes after partial unloading and its use for characterization of plant fiber composites at the microscale are proposed. This method provides the viscoelastic properties of plant fiber walls, matrix and their interfaces in composite using environment-controlled dynamic nanoindentation, through full-field measurements. The loss factor of neat resin shows good consistency using the improved dynamic nanoindentation technique with that from DMA tests on a frequency range from 1 to 40 Hz and a temperature range from 30 to 65 °C. The loss factors identified on the cross-section of UD flax/GreenPoxy laminates are highly dependent on the DNI method. Using the constant amplitude method, a mean value of 4 % is measured in the fiber wall. This is consistent with the value back-calculated in the transverse direction from DMA tests on composites. Grid dynamic nanoindentation provides also a very interesting map of the viscoelastic properties at the microscale in the cross-section of the composite. It clearly shows the damping contribution of the various components such as fibers, matrix and their interfaces. At last, these measurements at the microscale are compared to results from DMA and modal analysis at the macroscale.

IV.1 Introduction

Currently, the hierarchical organization and complex micro-structure of plant fibers and their composites drive many researchers to study their morphology, mechanics, biological characteristics in order to better establish the structure-behavior links. When it comes to micro- and nano-scale, nanoindentation appears as a very powerfull and commonly used method. If the application of nanoindentation in the characterization of traditionnal polymer composite materials and their constituents has been a particularly fast growing research area since the early 2000s, it can be underlined that it has been relatively little experienced with PFCs. The review of literature shows that the existing studies were realized mainly using quasi-static loading such as the traditional loading-unloading curves. As an example, the reduced modulus and hardness of flax fiber walls and PFCs have been measured by Arnould et al. and Bourmaud et al. [Arnould 17, Melelli 19, Bourmaud 12b]. Similarly, in-situ measurement of the static mechanical properties of the PFCs constituents has also be done using nanoindentation by Perrier et al. [Perrier 16, Li 17b]. To the best of the author's knowledge, the existing literature working on the dynamic nanoindentation measurement with plant fibers and their composites are rarely seen. However, dynamic nanoindentation testing, generally realized through continuous stiffness measurement (CSM), is a really powerful method to measure simultaneously the elastic properties of the tested material as well as its damping.

So, the main objective of this Chapter is to use dynamic nanoindentation to map the damping properties of PFCs in controlled environments. First, a dynamic nanoindentation with constant amplitude method is proposed. When compared to CSM, which involves the superposition of a small high frequency oscillatory load on the larger monotonically increasing indenter load during the loading portion of the indentation test, it is proposed here to apply a protocol similar to the one classically used in DMA at macroscale. It consists in applying a steady state harmonic loading with constant mean amplitude after loading and partial unloading to provide a better deconvolution of the elastic, viscous and plastic contributions (Section 3.1). The verification of the proposed CAM method is made on neat resin. Then, the damping properties in FGUD are measured and mapped with both the CAM method and the typical CSM method to provide a comparison (Section 3.2, 3.3). The results showing damping contribution from fibers and matrix zone are then compared with the ones measured and/or back-calculated from DMA tests. At last, all the results from DMA, modal and nanoindentation tests are compared (section 3.3).

IV.2 Materials and methods

IV.2.1 Theory of nanoindentation and its applications

Nanoindentation technology, also called depth-sensitive indentation technology, is one of the usual methods to test the micro mechanical properties of materials. With the development of modern microelectronic and material sciences, the size of specimens is becoming more and more miniaturized, and the traditional indentation measurement method has gradually exposed its limitations. Nanoindentation instrumented technology has solved some drawbacks of traditional measurements. It controls the load which increases monotonically through a computer program, and measures the indentation depth in real time. Because of the ultra-low load applied, the monitoring sensor has a displacement resolution lower than 1 nm. It is also suitable for measuring the mechanical properties of thin materials such as films and coatings. The mechanical properties of materials that can be measured from the loading-unloading curves are the elastic modulus and hardness. Fracture toughness, strain hardening effect, viscoelasticity etc. can also be investigated.

The advantage of nanoindentation technology is that it can characterize the mechanical properties of materials at very small scale. It has the characteristics of convenient instrument operation, non-destructive experiments, high positioning accuracy and has become an important tool for testing materials at nanoscale. However, nanoindentation technology is affected by several factors during the measurement process, related to the instrument (indenter defect, contact point), sample surface (roughness), material properties (dents, bumps, plastic range), measurement environment (temperature, vibration). These parameters have to be taken into account when designing and exploiting such experiments.

The typical mechanical properties (elastic modulus and hardness) of the tested material can be obtained from the loading-unloading curve of force as a function of penetration depth (IV.1 (a)). The sample generally undergoes both elastic deformation and plastic deformations during the loading process, resulting in the nonlinearity of the loading curve. Then, the unloading curve reflects the elastic recovery process of the sample. Figure IV.1 (b) is a schematic diagram of indentation profile by an indenter during loading and unloading. As shown, the indenter press into the sample resulting in an indentation depth h and a contact depth h_c.

Oliver and Pharr et al. [Oliver 92] proposed an indentation experiment analysis method based on the elastic contact theory that can effectively characterize the reduced modulus of materials. This technique requires the evaluation of the contact stiffness. To this end, the unloading part of the nanoindentation curve is selected to fit the following equation:

$$P = B_1(h - h_f)^m, \tag{IV.1}$$

where, P is the load acting on the sample, B_1 and m are the fitting parameters, h is the penetration depth. The elastic contact stiffness (S) can be calculated as:

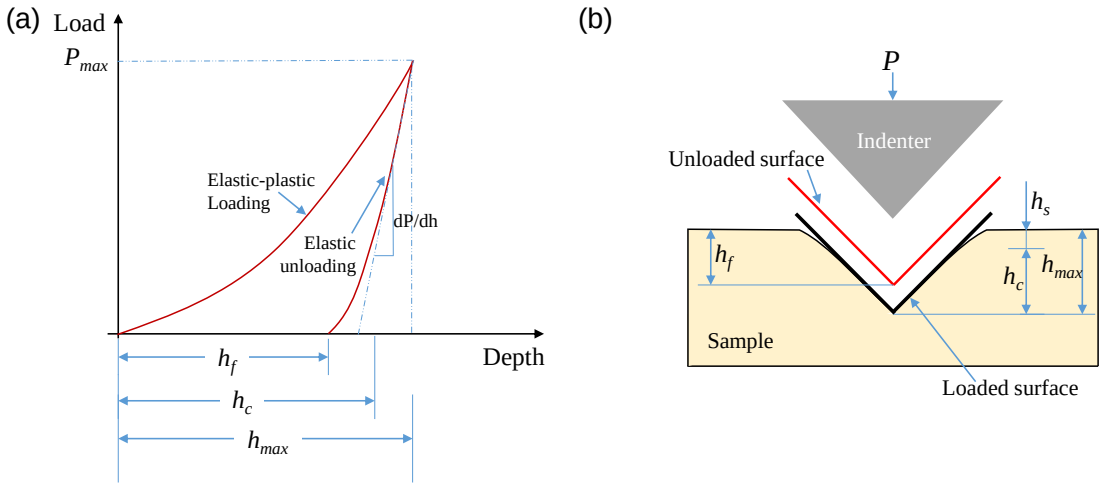

FIGURE IV.1 – (a) Typical loading-unloading curves (P_{max} is the maximum load during nanoindentation, h_f is the depth of the residual indentation, h_{max} is the depth from the original sample surface at load P_{max}) (b) Profile change after indentation (h_s is the distance from the edge of the contact to the surface, $h_s + h_c = h_{max}$, h_c is the contact depth measured from maximum depth h_{max})

$$S = \left(\frac{\mathrm{d}P}{\mathrm{d}h}\right)_{h=h_{\max}} = \alpha m \left(h_{\max} - h_f\right)^{m-1}. \tag{IV.2}$$

Most of the time, the error obtained by fitting the entire unloading curve is relatively large, so only 25% to 50% of the curve from the top is generally used. The projected area of the contact surface under the action of P must be known in order to calculate the hardness and modulus of the sample.

The projected area of the contact surface (A) can be calculated according to an empirical formula $A = f(h_c)$. For an ideal Berkovich indenter, this can be expressed by:

$$A = 24.56 h_c^2, \tag{IV.3}$$

where h_c is the contact depth.

Oliver and Pharr obtained the relationship between the contact depth (h_c) of the indenter and the total indentation depth (h):

$$h_{\mathrm{c}} = h - B_2 \frac{P_{\max}}{S} \tag{IV.4}$$

where, B_2 is a constant value related to the shape of the indenter (for a spherical or pyramidal (Berkovich) indenter the value is 0.75).

The hardness (H) and reduced modulus (E_r) can finally be defined as:

$$H = \frac{P_{\max}}{A}, \tag{IV.5}$$

$$E_{\mathrm{r}} = \frac{\sqrt{\pi}}{2\beta}\frac{S}{\sqrt{A}}, \tag{IV.6}$$

where, P_{max} is the maximum load at any indentation depth, A is the projected area of the contact surface under the action of P_{max}, β is a constant value related to the shape of the indenter (β=1.034 for Berkovich indenter). The elastic modulus of the tested sample can be obtained from the following formula based on isotropic considerations:

$$\frac{1}{E_r} = \frac{(1-{\nu_I}^2)}{E_I} + \frac{(1-{\nu_S}^2)}{E_S} \tag{IV.7}$$

where E_I and ν_I are Young's modulus and Poisson's ratio of the indenter, E_S and ν_S are the Young's modulus and Poisson's ratio of the sample, respectively. It should be noted that E_r is not sensitive to the value of ν_I for most materials and it will only produce an error of 5% on E_r when ν_I is equal to 0.25±0.1 [Fischer-Cripps 11].

Nanoindentation has been widely used to characterize mechanical properties at microscale during the past few decades [Li 02, Gibson 14], in particular to investigate the linear elastic properties of thin films, modified surfaces, individual phases in alloys or carbon and glass fiber composites. Attempts to characterize viscoelastic solids have been far fewer. Most have focused on strain-rate sensitivity [Shen 04, Alkorta 08]. Others investigated the transient properties of the response during creep or relaxation tests [Huang 06, Shen 12]. In this kind of NI creep (or relaxation) tests, the force (or displacement) increases rapidly to reach a specified value of force (or displacement) and then is maintained during a certain time, as shown in Figure IV.2 (a).

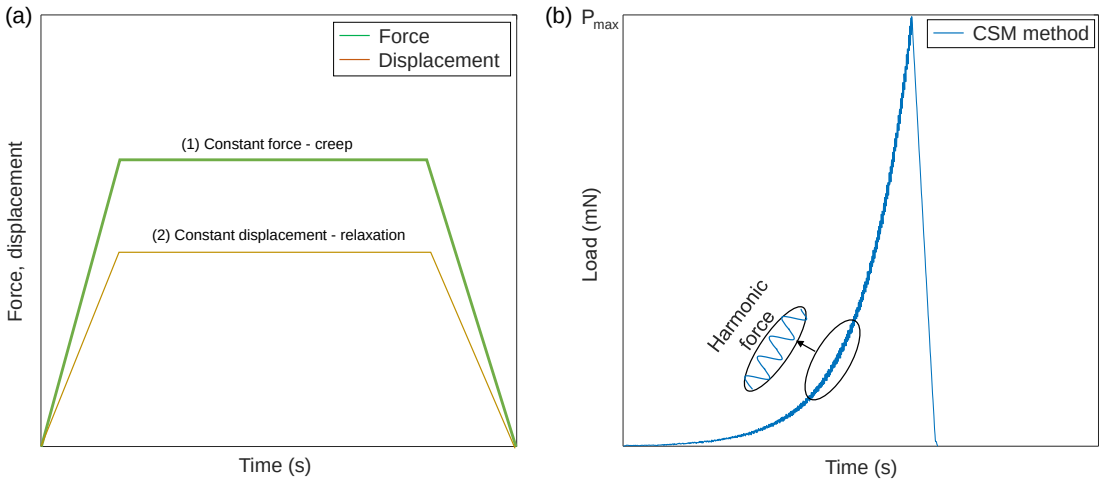

FIGURE IV.2 – Protocols for viscoelastic properties measurement from (a) creep and relaxation tests (b) CSM method

The use of dynamic nanoindentation was more recent and applied to polymer and wood cell walls. The continuous stiffness measurement (CSM) technique offers a direct measure of dynamic contact stiffness during the loading portion of

an indentation test [Oliver 92, Pethica 88]. CSM involves the superposition of a small high frequency oscillatory load on the larger monotonically increasing indenter load during the loading portion of the indentation test, as shown in Figure IV.2 (b). Continuous contact stiffness and contact damping can be obtained by the ratio of amplitude and phase difference in the feedback circuit, respectively [Li 02], and with a simple mathematical model for a single-degree-of-freedom spring-mass-damper system. However, the accuracy of the results depends on the precise dynamic response of the system [Oliver 92]. It was shown by Herbert and Oliver that nanoindentation can accurately measure the dynamic mechanical properties of linear viscoelastic solids under the premise of calibrating the cut-off frequency, dynamic stiffness and damping of the instrument [Herbert 08]. While the technical implementation of this oscillation is current in the state-of-the-art, there is still an ongoing debate on whether this superimposed signal influences the mechanical properties of materials [Leitner 17].

IV.2.2 Selection of existing research on nanoindentation

IV.2.2.a Dynamic Nanoindentation

Measurements of local dynamic properties have been investigated for different materials. As an example, Y. Lu and D. M. Shinozaki have developed a precisely controlled piezoelectric microindenter to measure the storage modulus (E') and loss factor ($\tan\delta$) of thin film materials [Lu 97, Shinozaki 97]. Herbert et al. compared the complex modulus of highly plasticized polyvinyl chloride (PVC) measured by nanoindentation with that of DMA and results show that the difference is less than 15 %. The measured quantities such as storage modulus and loss modulus (E'') are also shown to be influenced by many parameters such as the material properties and the experimental setup. Density is found to be a sensitive factor on the measured E' and E'' of polyethylene. The harmonic amplitude was shown to have a limited influence on E' and E'' of high-density polyethylene (HDPE) from 5 -50 Hz [Odegard 05]. Kramer suggested that the penetration depth should be less than 10 % of the thickness of the sample to avoid the effect of deformation from the substrate [Kramer 01]. Besides, J. Deuschle emphasized that the preparation of the surface has a significant impact on the accuracy of the test results [Deuschle 07].

IV.2.2.b Nanoindentation on plant fiber composites

During the past few decades, many studies regarding the static mechanical properties of plant fiber composites had been done using nanoindentation technology [Poon 08]. To the best of the author's knowledge, there is no existing literature using dynamic nanoindentation for the characterization of plant fibers and plant fiber composites. Arnould et al. and Bourmaud et al. explored the mechanical properties in the cross-section of flax fiber and its composites, and the static parameters such as reduced modulus and hardness were given for the fiber walls [Arnould 17, Melelli 19, Bourmaud 12b]. Similarly, in-situ measurement of the sta-

tic mechanical properties of the constituents of hemp/GreenPoxy composites were realised using grid nanoindentation by Perrier et al. [Perrier 16, Li 17b]. Wood cell walls have also been quite widely characterized using nanoindentation in different environments [Gindl 04b, Tze 07, Eder 13]. When it comes to time-delayed properties, Keryvin et al. [Keryvin 15b] determined the viscoelastic properties of flax fibers using nanoindentation creep tests.

It can be seen that the existing literature mostly focus on static mechanics of plant fiber composites at the micro scale, while the research on dynamic mechanical properties is rarely seen. Therefore, the present study fills the gap by identifying the damping performance in micro scale, which clearly characterize the damping contribution of each component in plant fiber composites.

IV.2.3 Tested materials

Two kinds of materials (neat resin and FGUD) were studied in this chapter. Neat resin was made from GreenPoxy 56 and SD 7561 (3:1) with curing at 60 °C 16 hours and post-curing at 100 °C 1 hour. This curing/post-curing process was different to the one used for pure GE in chapter II. Before nanoindentation testing, the neat resin and FGUD materials were stored in a climatic chamber with 23 °C and 50% RH for at least 4 weeks. Then, samples were cut for neat resin (20 × 10 × 2.5 mm^3) and FGUD (20 × 10 × 3.5 mm^3) and they were embedded in a fast curing acrylic at ambient temperature. Meanwhile, a thermocouple was embedded between the acrylic and neat resin to measure the temperature, as shown in Figure IV.3 (a) and (b). FGUD was mounted following the vertical direction with its fiber direction as shown in Figure IV.3 (c). After the curing of embedding acrylic, their surfaces were polished with 40 nm aluminum suspension.

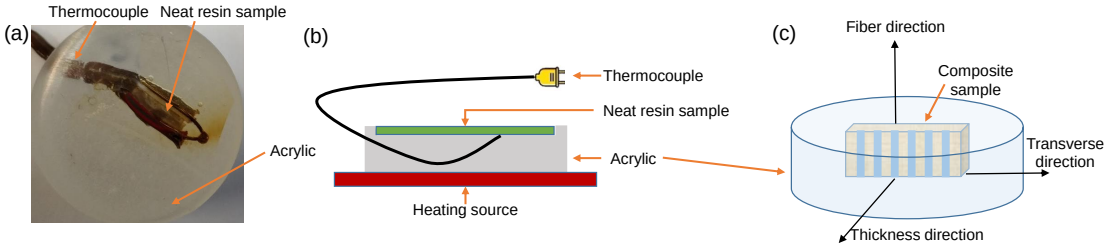

FIGURE IV.3 – Sample for nanoindentation tests of (a),(b) neat resin and (c) FGUD

IV.2.4 Experimental setup

IV.2.4.a Instrument

All the nanoindentation tests in this chapter were carried out in a UNHT System (Ultra nanoindentation tester) supplied by Anton Paar, as shown in Figure IV.4 (a). It can be used to characterize the mechanical properties of polymers,

films and bio materials at the nanoscale on a temperature range from ambient temperature up to 200 °C and at relative humidities up to 90 % at ambient temperature thanks to the heating source and climatic chamber. The maximum load of UNHT system is 50 mN with a 3 nN resolution and it can perform a test within 50 μm in depth with a resolution of 0.1nm. The indenter used in the system was a three-sided pyramid Berkovich tip with a half angle of 65.3 ° measured from the axis to one of the pyramid flats, as shown in Figure IV.4 (c). The Young's modulus and Poisson's ratio of the used indenter are 1141 GPa and 0.07, respectively.

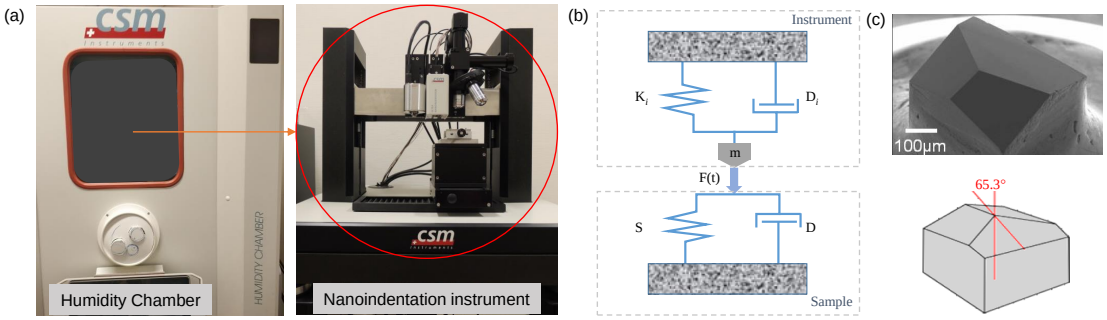

FIGURE IV.4 – (a) Anton Paar Nanoindentation Instrument (b) Dynamic mechanical model of viscoelastic material in the test system (c) Shape of Berkovich indenter [Fischer-Cripps 11]

For the dynamic loading, as mentioned in chapter II, the tangent value of the phase difference between stress and strain can be used to determine the loss factor. When considering a homogeneous isotropic material with a linear viscoelastic behaviour, the nanoindentation system can be represented by a simple mathematical model for a single-degree-of-freedom spring-mass-damper system as shown in Figure IV.4 (b). It is important to note that the indentation head should be represented by these two spring mass damper system (the indentation head and the reference head). A simplified model take into account only the indentation head. The calculation of storage modulus and loss modulus are determined as follows [Herbert 08]:

$$\frac{E'}{1-\nu^2} = (\frac{F_0}{h_0}\cos\delta + m\omega^2 - K_i)\frac{\sqrt{\pi}}{2}\frac{1}{\beta}\frac{1}{\sqrt{A}} \tag{IV.8}$$

$$\frac{E''}{1-\nu^2} = (\frac{F_0}{h_0}\sin\delta - D_i\omega)\frac{\sqrt{\pi}}{2}\frac{1}{\beta}\frac{1}{\sqrt{A}}, \tag{IV.9}$$

where K_i and D_i are the stiffness and damping ratio of the instrument, ν is the Poisson's ratio, β is 1.034 for a Berkovich, m is the mass of the indenter (For the instrument used in this thesis, the value of K_i, m and D_i is 2346 N/m, 1.9 g and 0.0364 Ns/m, repectively), A is the projected contact area, F_0 and h_0 are force and displacement and δ is the phase difference between force and displacement, $\omega = 2\pi f$ and f is the frequency of the sinusoidal loading.

Therefore, the investigation for the effect of dynamic stiffness and damping of the testing system is important to quantify the impact of the instrument on the measurement of dynamic mechanical properties.

IV.2.4.b Protocols for the determination of the viscoelastic properties

Loading paths

Dynamic nanoindentation is usually performed with a sinusoidal harmonic force which is usually superimposed to the monotonic force ramp (CSM method). It should be noted that the quantities measured with CSM method result from elastic, viscoelastic and viscoplastic properties at the same time.

Therefore, a constant amplitude method for damping identification, labeled CAM method, is proposed. The loading path is represented in Figure IV.5. It consists in first applying loading and partial unloading phases. The unloading phase is stopped at a certain load level which is then maintained for a given time after what a sinusoidal load with constant dynamic and mean amplitudes is superimposed. After the desired number of harmonic periods at the selected frequency, the load is then monotonically decreased down to zero. This load-path is similar to the one used in most of the DMA protocols and prevent the measured viscoelastic properties to be interfered by plastic strains.

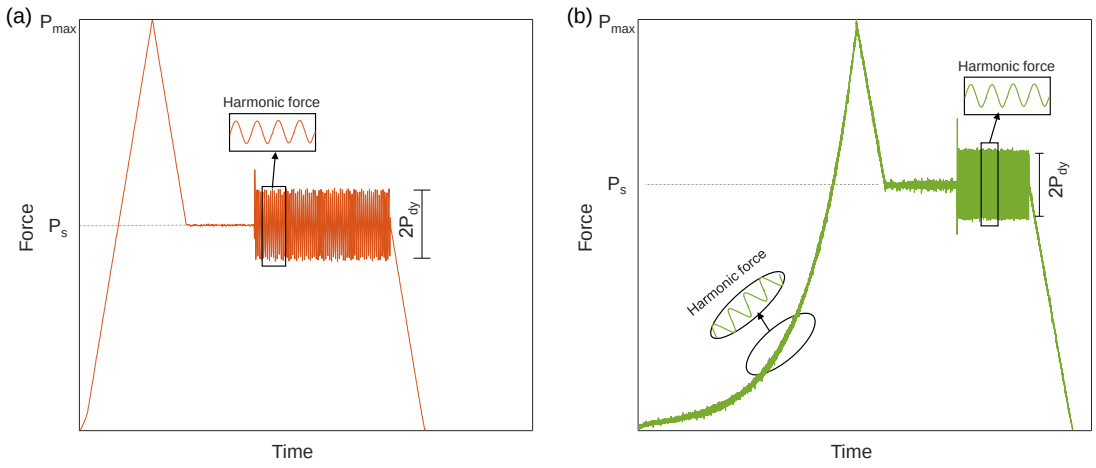

Figure IV.5 – Protocols for viscoelastic properties measurement of (a) CAM method (b) CSM+CAM method

The labeled 'CSM+CAM' method is used to do the comparison between CSM method and CAM method on the same indentation position to avoid the uncertainty from different measured samples or positions. This procedure starts with a typical CSM method and then comes to the same setup using CAM method after the maximum load.

Signal processing and viscoelastic properties determination

A specific signal processing technique was developed to identify the viscoleastic properties from the data recorded during this type of test. The signals of load and displacement as a function of time were extracted from the data files generated by the apparatus. The flow diagram of post-processing for damping identification is drawn in Figure IV.6.

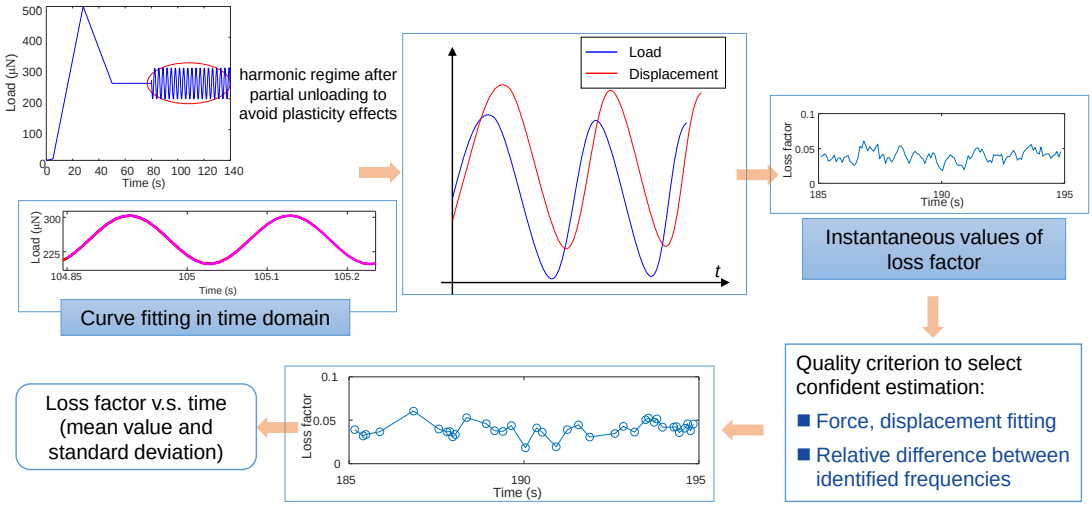

FIGURE IV.6 – Post-processing of the load and displacement for damping identification

The post-processing starts with the estimation of ω through Fast Fourier Transformation on the whole harmonic signal. Then a time interval ($2n\pi/\omega$, n=2) is selected to make a nonlinear fitting of load versus time, and displacement versus time signals using the following functions,

$$P(t) = P_0 + Re(\bar{P}e^{j\omega t}) \tag{IV.10}$$

$$\text{with } \bar{P} = P_R + jP_i \tag{IV.11}$$

$$D(t) = D_0 + Re(\bar{D}e^{j\omega t}) \tag{IV.12}$$

$$\text{with } \bar{D} = D_R + jD_i \tag{IV.13}$$

$$\text{and } f = \frac{1}{T}, \quad \omega = 2\pi f, \quad j = \sqrt{-1} \tag{IV.14}$$

where t is the time, $P(t), D(t)$ are the force and displacement time signal, P_0, P_R, P_i, D_0, D_R, D_i and ω are determined by fitting. Then the phase difference (δ) between the load and displacement can be obtained:

$$\delta = \text{angle}(\frac{\bar{P}}{\bar{D}}), \tag{IV.15}$$

and the stiffness (k_s) can be obtained by,

$$k_s = \left|\frac{\bar{P}}{\bar{D}}\right|, \tag{IV.16}$$

then the storage modulus (E') can be determined by:

$$E' = E_s \cos\delta, \tag{IV.17}$$

where E_s can be determined using the equations IV.6 and IV.7.
Then, the time window is shifted and the whole procedure is repeated. This finally provides the value of the loss factor (tan (δ)) and the stiffness over time. Several quality criteria such as residue on load and displacement fitting, relative difference between identified frequencies on load and displacement, and relative difference between identified phases are used for eliminating erroneous points and analyzing the confidence of the values. Finally, the average values is used as the identified loss factor and their standard deviation is used as error value. For tests realized with the CSM method, the phase difference is automatically computed by the NI software (Indentation® 7.2.5).

All the nanoindentation tests were carried out in force controlled mode at ambient temperature and 50 % relative humidity. The control of humidity was turned off during measurement to avoid noise effect from the machine.

Protocol for GreenPoxy

The tests for pure resin were performed at different temperatures (30, 45, 55, 65 and 80 °C) using the heating source located beneath the specimen. The heating source was set to each expected temperature and hold for at least 5 minutes after the temperature inside the sample (measured using an embeded thermocouple) shows a stable value. The protocol used for the neat resin was the CAM one. The force was increased from 0 mN until the maximum force 500 μN (P_{max}) in 30 s. Then, the force was decreased at the same rate until 250 μN followed by a 60 s hold on at this value. After that, a sinusoidal force was applied for 60 s with a dynamic amplitude of 50 μN (P_{dy}).

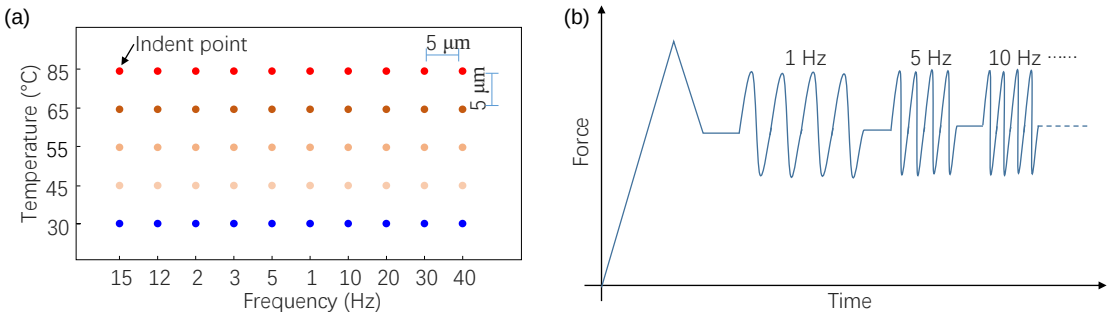

FIGURE IV.7 – Schematic diagram of nanoindentation for (a) GreenPoxy using the CAM protocol at 1 - 40 Hz and 30 - 85 °C (b) suggested protocol inthe future plan

Measurements were made on a frequency range from 1 to 40 Hz in a logarithmic scale value. Only one excitation frequency was used for each position. The distance between the measurement points was around 5 μm, as shown in Figure

IV.7 (a). In addition, a suggested protocol is shown in Figure IV.7 (b) can be also used in the future plan, in order to measure the dynamic mechanical properties under several frequencies at each point.

Protocol for unidirectional flax/GreenPoxy composites

Two FGUD samples were tested under typical 'CSM method' and 'CSM+CAM method', respectively at ambient temperature.

For 'CSM method', the harmonic load was processed during the loading part with a given dynamic amplitude value of 50 μN and a frequency of 5 Hz until the maximum force 500 μN reached. The grid nanoindentation was done in the form of 12 $\times$ 9 indenter points with an interval space value of 5 μm in vertical and horizontal axis, as shown in Figure IV.8 (a).

For 'CSM+CAM method', the protocol started with a harmonic loading which was the same with 'CSM method'. Then the CAM method was processing after reach the peak load, and the P_{max}, P_s and P_{dy} quantities were set at a value of 125, 75 and 15 μN, respectively. The grid nanoindentation with CAM method was carried out in 16 $\times$ 9 indenter points with an interval space values of 4 μm in vertical and horizontal axis at 1 Hz and 5 Hz, as shown in Figure IV.8 (b).

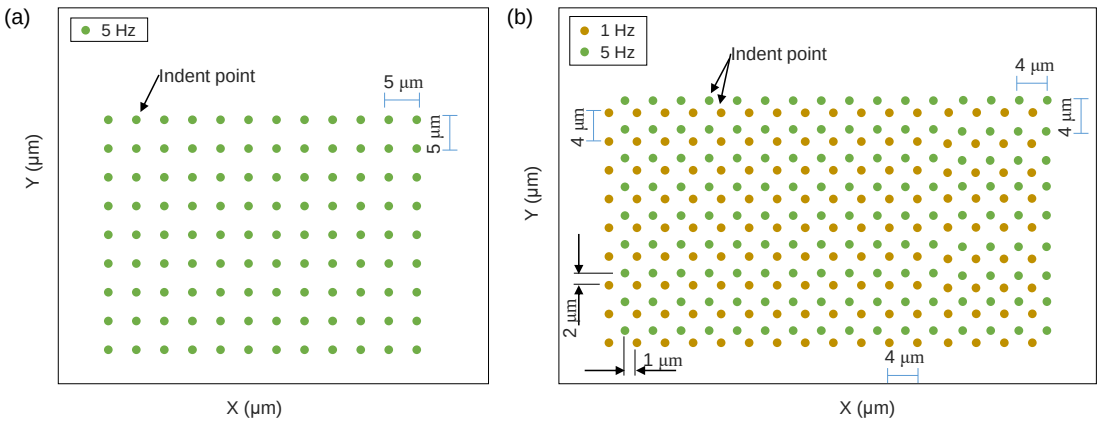

FIGURE IV.8 – Schematic diagram of nanoindentation for FGUD using (a) CSM at 5 Hz and (b) CAM method at 1 Hz and 5 Hz

IV.2.4.c DMA test

DMA of pure resin was processed following ASTM D5026-01 under tensile mode using DMA+300 (Metravib) device. A static displacement of 18 μm and a dynamic displacement of 8 μm were applied to the samples (65 $\times$ 10 $\times$ 2.5 mm^3). The frequency and temperatures range for each test were 1-46.4 Hz and 30-160 °C, respectively. The heating rate was set to 5 °C/min with a 2 minutes hold for each ramp. Other details regarding the setup were detailed in chapter II.2.

IV.3 Results and discussion

IV.3.1 Verification of the effect from instrument on the measurement of storage modulus and loss factor

As mentioned in section 'Experimental setup', the effect of the dynamic stiffness and the damping of the instrument should be taken into account, so this section aims at verifying the influence of these parameters before processing the experiment. The signal provided by the software uses a static correction associated to the stiffness of the measurement head. Therefore, K_i is already accounted for in the signals. Here we quantify the effect of inertia ($m\omega^2$ in IV.18) and damping ($D_i\omega$ in IV.19) on the identified values of stiffness and damping of the material. The two dynamic terms from the sample ($\frac{F_0}{h_0}\cos\delta$, $\frac{F_0}{h_0}\sin\delta$) and the instrument ($m\omega^2$, $-D_i\omega$) are calculated in fiber, matrix, fiber-fiber, and fiber-matrix interface. The effect from the instrument on the measurement of stiffness (dyf_1) and damping (dyf_2) are defined as follows:

$$dyf_1 = \frac{m\omega^2}{\frac{F_0}{h_0}\cos\delta}, \tag{IV.18}$$

$$dyf_2 = \frac{-D_i\omega}{\frac{F_0}{h_0}\cos\delta}. \tag{IV.19}$$

Table IV.1 shows the values from each dynamic terms measured in the different zones. It can be clearly seen that the values of dyf_2 are between 0.15 - 0.55 %, and this term is neglectable on the measurement of damping. Regarding the stiffness term, the values of dyf_1 are around 10^{-4}. Therefore, the term of stiffness from instrument is also neglectable.

Table IV.1 – Comparison of the effect from two terms in fiber, matrix, fiber-fiber (F-F) interface and fiber-matrix (F-M) interface at 5 Hz

	$\frac{F_0}{h_0}\cos\delta$	$m\omega^2$	dyf_1 (%)	$\frac{F_0}{h_0}\sin\delta$	$-D_i\omega$	dyf_2 (%)
Fiber	17242	1.9	1.12×10^{-4}	737	1.14	0.17
Matrix	5739	1.9	3.3×10^{-4}	211	1.14	0.55
F-F interface	17277	1.9	1×10^{-4}	643	1.14	0.19
F-M interface	14615	1.9	1×10^{-4}	789	1.14	0.15

IV.3.2 Damping identification of GreenPoxy using CAM method

The values of loss factor determined by DNI for the Pure GreenPoxy under temperature of 30, 45, 55, and 65 °C are shown in Figure IV.9. The error bar represents the confident identified values.

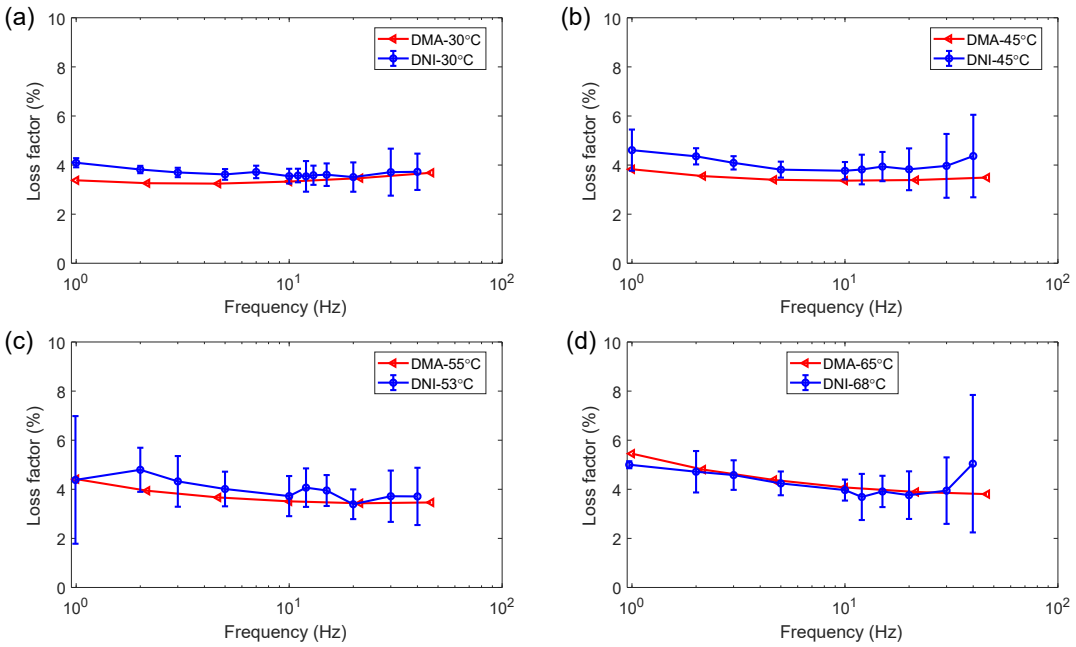

FIGURE IV.9 – Loss factor as a function of frequency (1 - 40 Hz) in GreenPoxy determined using DMA and DNI tests at various temperatures (a) 30 °C, (b) 45 °C, (c) 55 °C and (d) 65 °C

At 30 °C, the loss factor is approximately equal to 4 % on the whole frequency range. A slight and progressive increase up to approximately 5 % is measured at 1 Hz with increasing temperature up to 65 °C. Results are compared to those obtained using DMA tests. It is clear that the loss factor values obtained from dynamic nanoindentation (DNI) and DMA tests are similar on the considered frequency range from 1 Hz to 40 Hz and temperatures. The value measured with the DMA in this chapter is different to the one measured in chapter 2, this is due to the curing process. We can also see that the standard deviations are quite high for DNI measurements (up to 68 %), in particular when increasing the temperature. When doing the comparison, the uncertainty on the loss factor provided by DMA should be also taken into account. Unfortunately, it can not be analyzed since the Metravib does not provide a satisfying way to access to time signals. The values of loss factor identified from DNI and DMA tests show good agreement on the frequency range 1 - 40 Hz and the minimum value of the difference between them is around 2.67 % observed around 2-10 Hz. The maximum difference is observed at 40 Hz and is attributed to the signal noise.

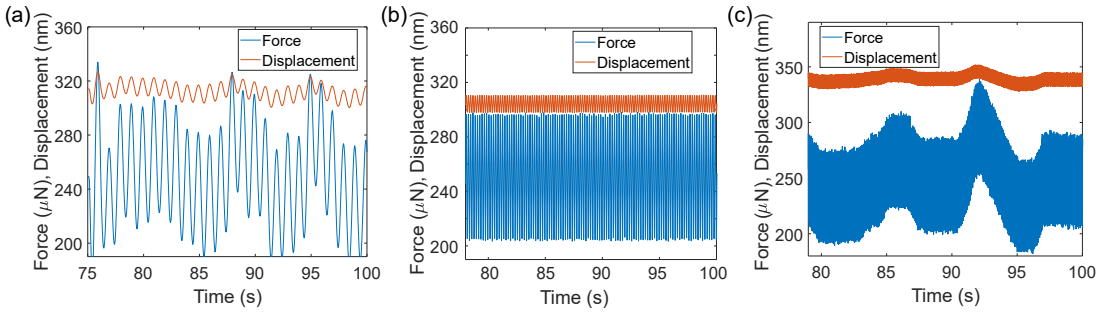

FIGURE IV.10 – Force and displacement signal versus time at (a) 1 Hz, (b) 5 Hz and (c) 40 Hz

The force and displacement signal is shown in the Figure IV.10. The uncertainty in nanoindentation measurements gradually increases as the frequency increases due to the resonance of the instrument causing more noise on the signal. The force signal is not stable accompanied with more than 30 % difference in amplitude, which causes a larger difference between the NI and DMA at 1 Hz and 40 Hz. As shown in Figure IV.10 (b), both load and displacement works in a stable harmonic signal state at 5 Hz. Therefore, it is suggested the experiments are processed at around 5 Hz to decrease the uncertainty from the time signal of the instrument used in this thesis.

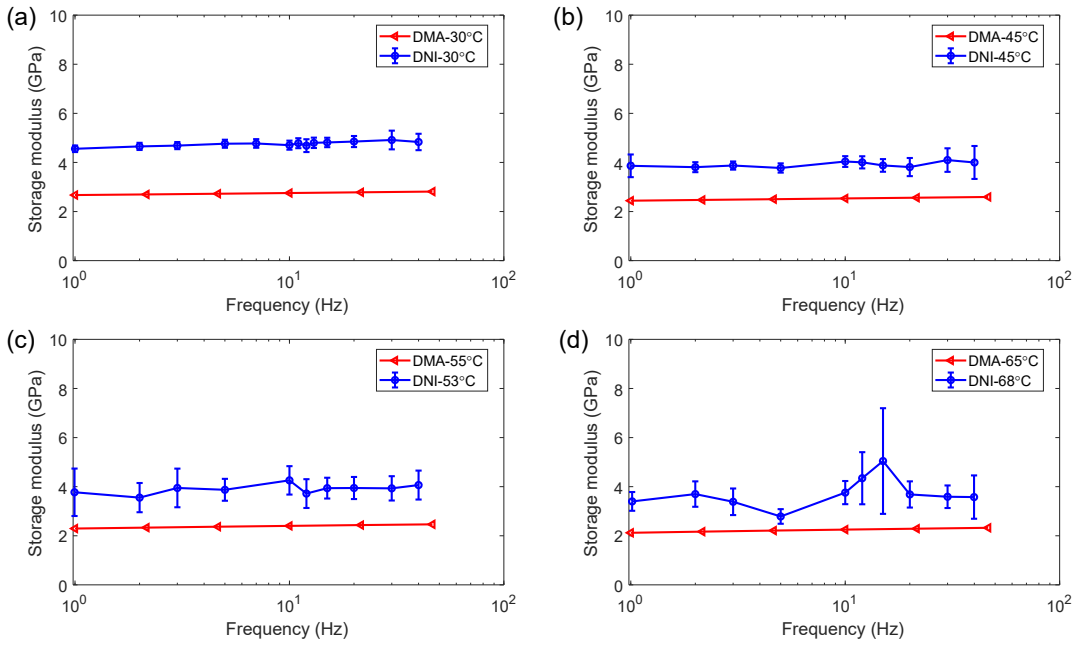

FIGURE IV.11 – Storage modulus as a function of frequency (1 - 40 Hz) in pure resin determined using DMA and DNI tests at various temperatures (a) 30 °C (b) 45 °C (c) 55 °C (d) 65 °C

Figure IV.11 shows the values of storage modulus.The differences between DNI and DMA measurements are up to 67.8 %. It is attributed to several factors. The first is related to the uncertainty induced by the surface polishing. The roughness in the near-surface area and the indentation size effect caused by the blunting of the indenter tip at the apex can lead to an overestimate of the modulus[Shen 06, Nix 98]. In addition, it exists a large difference in the strain rates and ranges between DMA and DNI. In DNI, measurements are made on a plastified material. Plastic deformations are induced by the high-pressure levels below the indenter.

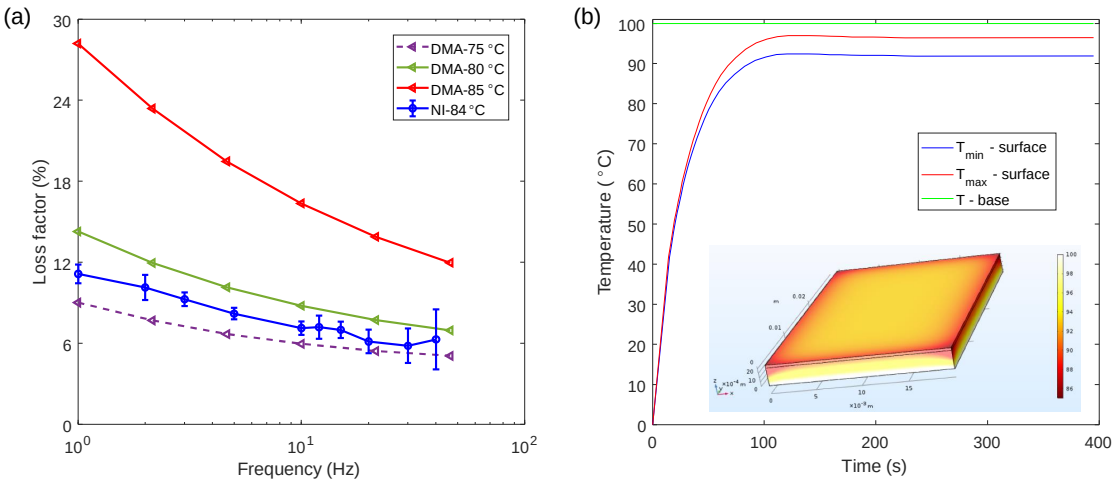

FIGURE IV.12 – (a) Comparison of loss factor in DMA and nanoindentation (NI) tests at the temperature near T_g zone (b) temperature changes based on numerical model

The damping performance of GreenPoxy at a temperature near the glass transition temperature is also studied using the same configuration. Figure IV.12 (a) shows comparison of loss factor in DMA and DNI. The temperature provided by thermocouple is 84 °C. However, unexpected data is found compared with the data from DMA at 85 °C. The curve of NI is between that of DMA at 75 °C and 80 °C. This is supposed to be linked to a heat conduction and convection problem in resin during nanoindentation tests. As the temperature increases, the difference between the resin surface and the bottom will become larger due to the presence of air flow [Maeda 72]. Furthermore, the loss factor will also increase of a value of 0.06 per 1 °C of increasing temperature when approaching the glass transition temperature, hence, requiring a very precise control of the temperature which has to be homogeneous in the sample to provide confident measurement. Figure IV.12 (b) shows the results of thermal simulation for the pure resin when adding a heating source at the bottom. A heterogeneous distribution of temperature in the sample due to the air convection is clearly observed. The minimum and the maximum temperatures in the sample are around 91 °C and 96 °C, respectively, when the temperature of heating source (T-base) is 100 °C. Therefore, precise temperature control is one of

most important issue for this experiment. To work with that, a NI system within a heat chamber should be preferred in the future to do such measurements, instead of the heating device located under the sample which has been used here.

IV.3.3 Damping identification of FGUD using CSM method

In this section, the classical CSM is used to identify the properties of FGUD. The proposed protocol will be applied and discussed in section IV.3.4.

A total of 108 grid indents were processed on the transverse cross-section of FGUD at ambient temperature using CSM method reminded above. The micro structure of FGUD on the cross-section is shown in Figure IV.13 (a). Each point is classified among 4 different component clusters, namely Fiber, Matrix, Interface, Confined resin, as proposed by [Perrier 16]. Figure IV.13 (b) shows the typical curves of load versus penetration depth during the experimental loading-unloading procedure. The descending order of indentation depth is fiber, interface, confined resin, and matrix under the same load because the stiffness of interface and confined resin are significantly affected by neighboring fiber.

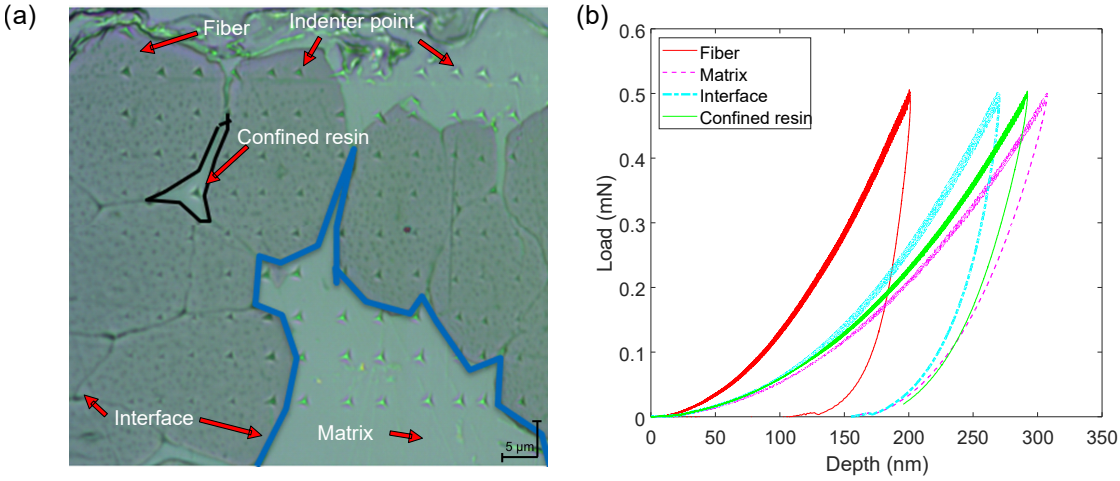

FIGURE IV.13 – Static mechanical properties of FGUD (a) microstructure on the surface (b) experimental loading-unloading curves for different zones (confined resin is in the closed boundary with black line)

IV.3.3.a Evolution of the dynamic properties as a function of the penetration depth

The influence of penetration depth on the dynamic properties has been pointed out several times in literature [Zhang 08]. Then, CSM tests were first processed to quantify the influence of penetration depth on storage modulus (E') and loss factor for the flax fiber composites. The results are shown in Figure IV.14.

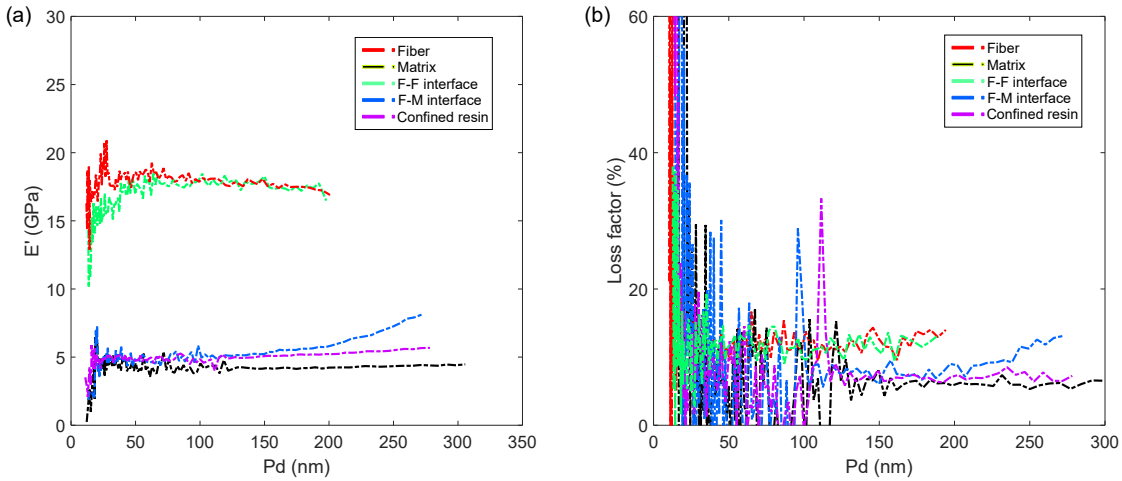

FIGURE IV.14 – Dependence on penetration depth of (a) the storage modulus and (b) loss factor obtained by typical CSM method at 5 Hz.

It can be seen from Figure IV.14 that the measurement of the storage modulus and loss factor is widely changing in the first part of the curves (up to 50 to 100 nm). This is attributed to the contact between the indenter head and the material surface. For the deeper measurements, the viscoelastic properties of the fiber wall, matrix, confined resin and fiber-fiber interface exhibit a quite stable response up to the maximum penetration depth. This result is different from the one observed for wood fiber wall. A non-linear behavior was reported by [Zhang 12] on a penetration depth range from 50 to 400 nm.

For the fiber-matrix interface zone, a slight increase of E' and loss factor with the penetration depth can be observed on after 200 nm. There are two aspects which can explain this phenomenon. Firstly, the surrounding fiber edges are gradually squeezed when the surface area of the indentation increases as the depth increases, and the measurement results begin to be affected by the fibers. Secondly, the polishing process during surface preparation can also cause certain disturbances. A gradient surface is formed due to the difference in the hardness of the fiber and the matrix, which suggests an inherent difficulty when attempting to obtain a stable response [Hardiman 17].

In the following, for each indent, the properties presented for the CSM method will correspond to the mean value measured from the last 60 points measured at maximum depth.

IV.3.3.b Mapping of the viscoelastic properties

Figure IV.15 provides a graphical representation of the viscoleastic properties along an indentation line in the grid. This line moves across areas containing successively fiber walls and matrix.

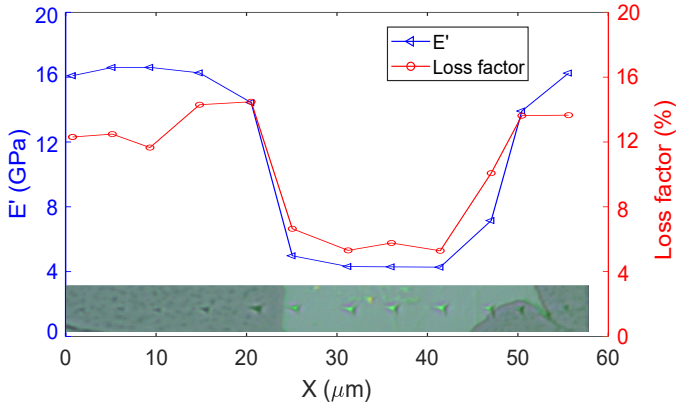

FIGURE IV.15 – Storage modulus and loss factor for each point along a line at 5 Hz

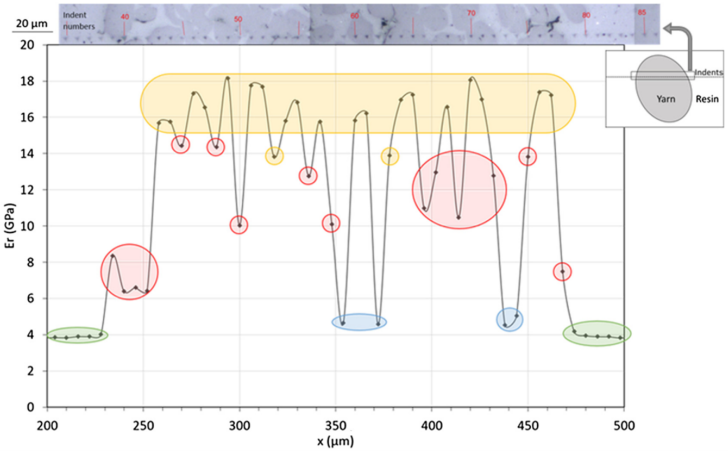

FIGURE IV.16 – Reduced modulus of hemp fiber collected from Ref. [Perrier 16]

Values of 16 GPa and 4 GPa are measured in the fiber wall and in the matrix zone, respectively. The transition from the fiber to the matrix, i.e. through the interface, is also clear. These results are similar to the ones reported in literature for hemp/GreenPoxy composites as shown in Figure IV.16 [Perrier 16]. Interestingly, we can observe on the left side of the figure, that the storage modulus varies non-linearly within the thickness of the fiber wall. The variations can be due to difference in properties between the different cell wall layers [Li 17a, Arnould 17].

The storage modulus of each point versus distance from closer fiber edge is plotted for all the indents in Figure IV.17 (a). The values in the fiber wall are around 16 GPa. The scattering in measurements is significantly higher in the fiber wall than in matrix areas. Again, this can be due to the variation of the viscoelastic properties in the thickness of the wall of the different indented fibers, as well as discrepancies between different individual fibers. In addition, the roughness is also different in the fiber and in matrix.

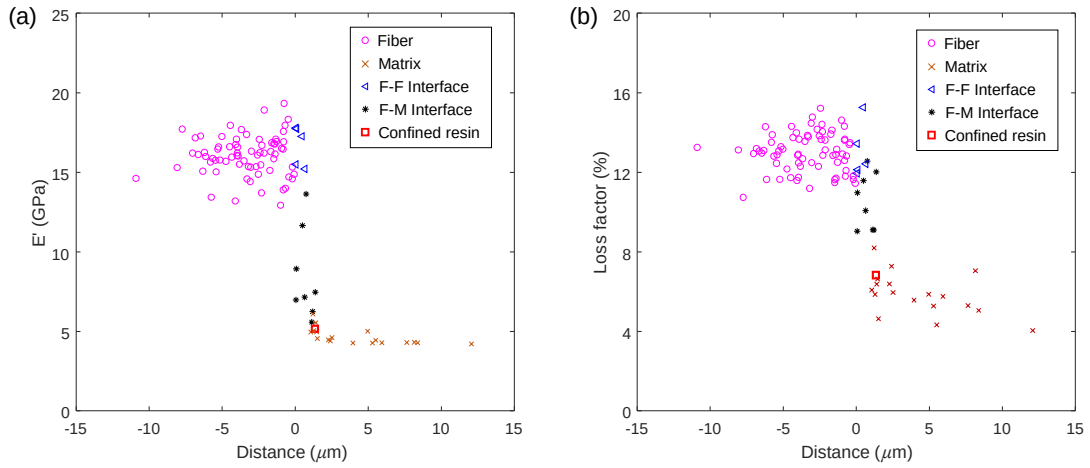

FIGURE IV.17 – (a) Storage modulus and (b) loss factor at 5 Hz versus distance from each fiber edge

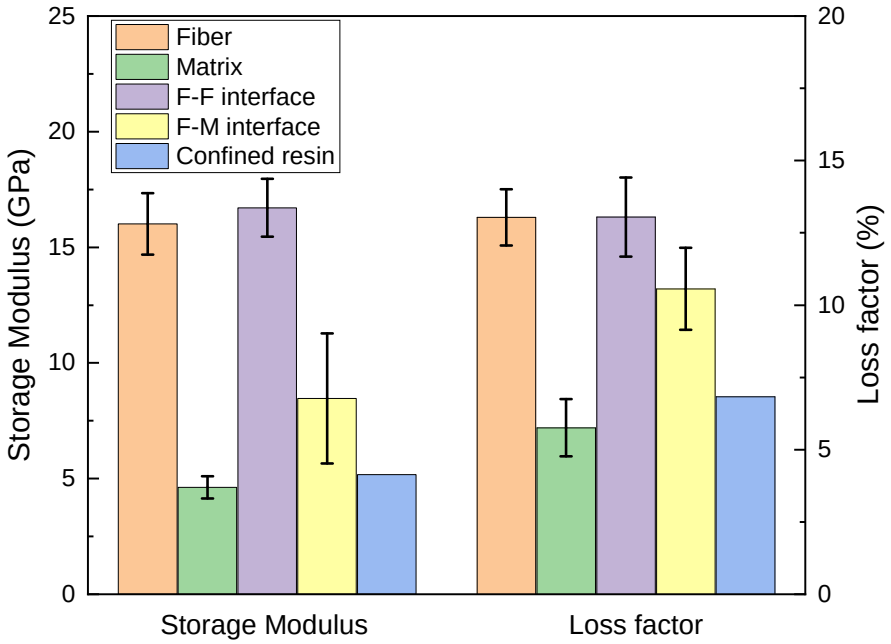

FIGURE IV.18 – Storage modulus and loss factor in each component using CSM method at 5 Hz (single point in confined zone without errorbar)

For the first time, our measurements provide access to the distribution of the loss factor as a function of the spatial position, see Figure IV.17 (b). The distribution of loss factor shows similar trend to that of storage modulus. The loss factor varies from 6 % in the matrix to 12 to 16% in the fiber wall, with a smooth and progressive transition at the interface. A non-linear variation is also observed in the thickness of the fiber wall, see Figure IV.15.

The mean values of storage modulus and loss factor measured for all indents are plotted in Figure IV.18. The error bar shows the standard deviation of the values. As can be seen, E' of fiber (16.0 GPa) is close to that of F-F interface (16.7 GPa), followed with the F-M interface (8.5 GPa), confined resin (5.2 GPa) and matrix (4.6 GPa). The storage modulus in interface zone shows a higher value than that of matrix zone. The measured point in confined resin corresponds to a medium storage modulus between interface zone and matrix zone due to the neighboring fiber.

The mean value of the loss factor in descending order is F-F interface (13 %), fiber (13 %), F-M interface (11 %), confined resin (7 %), matrix (6 %). It is reported that the energy dissipation in fiber zone, F-F interface and F-M interface are caused by friction between micro fiber, friction between elementary fibers, and friction between fiber and matrix, respectively [Duc 14b]. Therefore, the damping produced by the plant fiber and the interface is considerable compared to the matrix. It can also be noticed that the damping value measured in the matrix areas is significantly higher than the one measured on pure matrix using DMA and also on pure matrix using DNI-CAM. This can be due to the fact that the in-situ resin has different properties than resin cured without fibers. It is well know that the presence of fibers can modify the curing process of thermoset resins. It can also be due to the measurement method, i.e. CSM and the potential influence of plasticity during harmonic measurements. The next section will propose a comparison of these results with the CAM method.

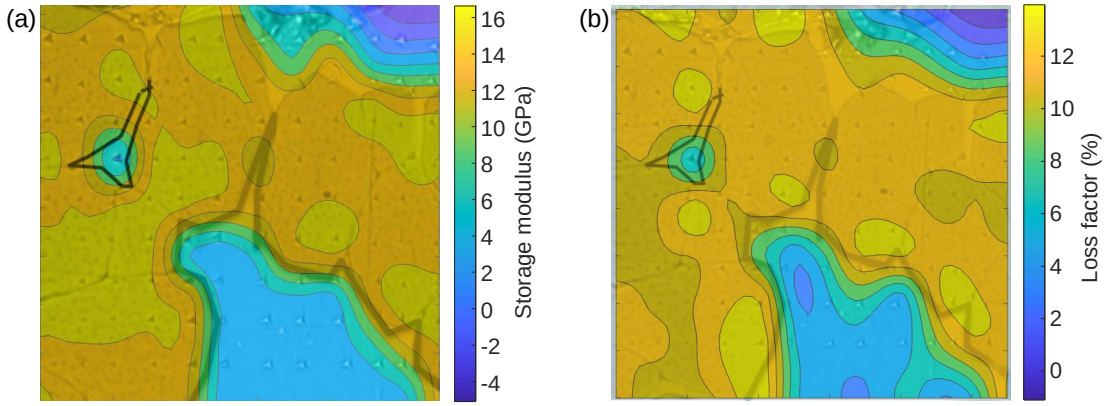

FIGURE IV.19 – Map on the cross section based on results from nanoindentation (a) storage modulus (b) loss factor at 5 Hz with CSM method

The map of storage modulus and loss factor are plotted in Figure IV.19 using biharmonic spline interpolation. It shows a clear correspondence for each component especially in matrix zone, confined resin and F-M interface compared with the cross-section in Figure IV.13 (a). This kind of map reflects the gradient of storage modulus and damping from the matrix to the interface and fiber. Besides, the map of loss factor shows the variation between different fibers attributed to

the intrinsic variabiliy of fibers (related to maturity and processing effect). Some slight differences in storage modulus also appear in the matrix zone, which can be interpreted as a difference in local density [Odegard 05].

This section proposed a discussion related provide the damping properties of the FGUD composites. The experimental results an interesting knowledge for the damping properties in the different constituents including fiber, matrix, F-F or F-M interface and confined resin zone. However, this typical CSM method provides measurements during the loading ramp. The influence of plastic behavior cannot be ignored. Therefore, it is necessary to develop an adapted protocol to tackle this problem.

IV.3.4 Damping identification of FGUD using CSM+CAM method

This section provides the results obtained with the CSM+CAM method. This method was used at 1 Hz and 5 Hz as described in Section IV.2.4. The results of a total of 288 grid indents are obtained as shown in Figure IV.20 (a). The loss factor of each indent was calculated using the post-processing method that is described in Section IV.3.2. The first part of this section is describing the results from CAM method and then the results of CSM and CAM based on 'CSM+CAM method' are compared.

IV.3.4.a Results from CAM method

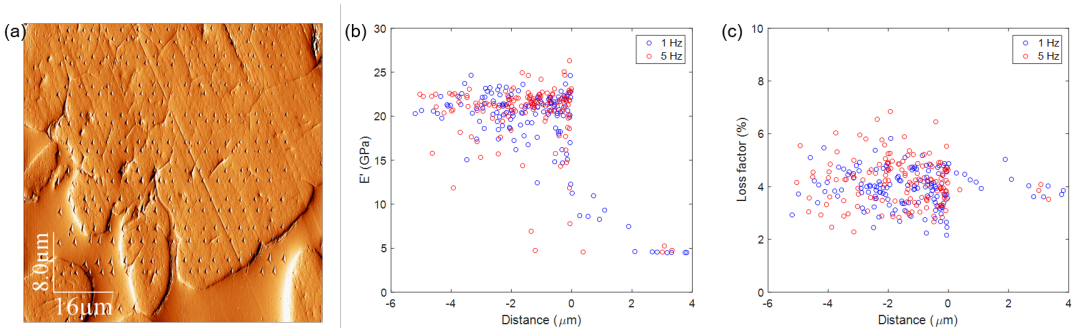

FIGURE IV.20 – (a) Micro-structure on the cross section after nanoindentation tests, (b) storage modulus and (c) loss factor at 1 Hz and 5 Hz versus distance from each fiber edge

As shown in Figure IV.20 (b), the storage modulus varies from the distance between the indent point and fiber edge. Its value mainly distributes between 15 and 25 GPa when the indent point is in the fiber zone. The storage modulus at 1 Hz shows a gradual decrease when the indent point is far from fiber edge (0 μm to 2 μm) due to the disappeared strengthening of adjacent fibers. Then, the storage modulus shows an approximate stable value when the distance is over 2 μm.

Figure IV.20 (c) shows the loss factor distribution for all the components. It is concentrated in the range of 2% to 6%, which is more stable than the result obtained by CSM method. The loss factor variation in the fiber zone is obviously larger than the value in the matrix zone, which is attributed to the intrinsic variability of fibers and within fiber wall. In contrast, the distribution of the loss coefficient is concentrated around 0.04 with a small dispersion level for the matrix. This value of 4 % is similar to the one determined on the pure GreenPoxy at ambient temperature.

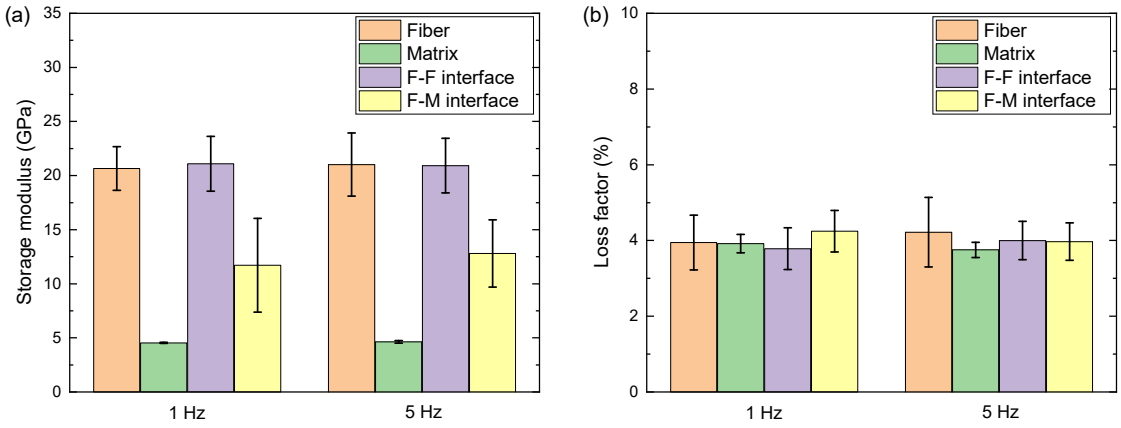

FIGURE IV.21 – (a) Storage modulus and (b) Loss factor in each component at 1 and 5 Hz using CAM method

The mean value of storage modulus and loss factor in each component including fiber, matrix, F-F interface and F-M interface using CAM method is plotted in Figure IV.21. The error bar is shown using the standard deviation of each data series. The storage modulus in fiber zone shows a mean value around 20.6 GPa and the value is closed to that of F-F interface.

IV.3.4.b Comparison of results from different method

The map of storage modulus and loss factor from CSM and CAM measured at 5 Hz in the same sample are compared, as shown in Figure IV.22.

It can be seen from the map that the storage modulus obtained from CSM and CAM are quite similar. For the matrix zone, the values of storage modulus obtained by CSM are between 4.2 - 5.7 GPa and that from CAM are around 4.6 GPa. For the fiber zone, the values extracted from CSM method are between 12 - 23 GPa, and that from CAM are between 14 - 24 GPa. However, the map of loss factor shows a significant different distribution when using CSM and CAM method. The values of loss factor in fiber zone determined using CAM method are between 2 % - 6 % and that from CSM are around 4.4 - 9 %. The overestimation of loss factor using CSM method is due to the viscoplatic effect during the loading procedure, compared to that in CAM method.

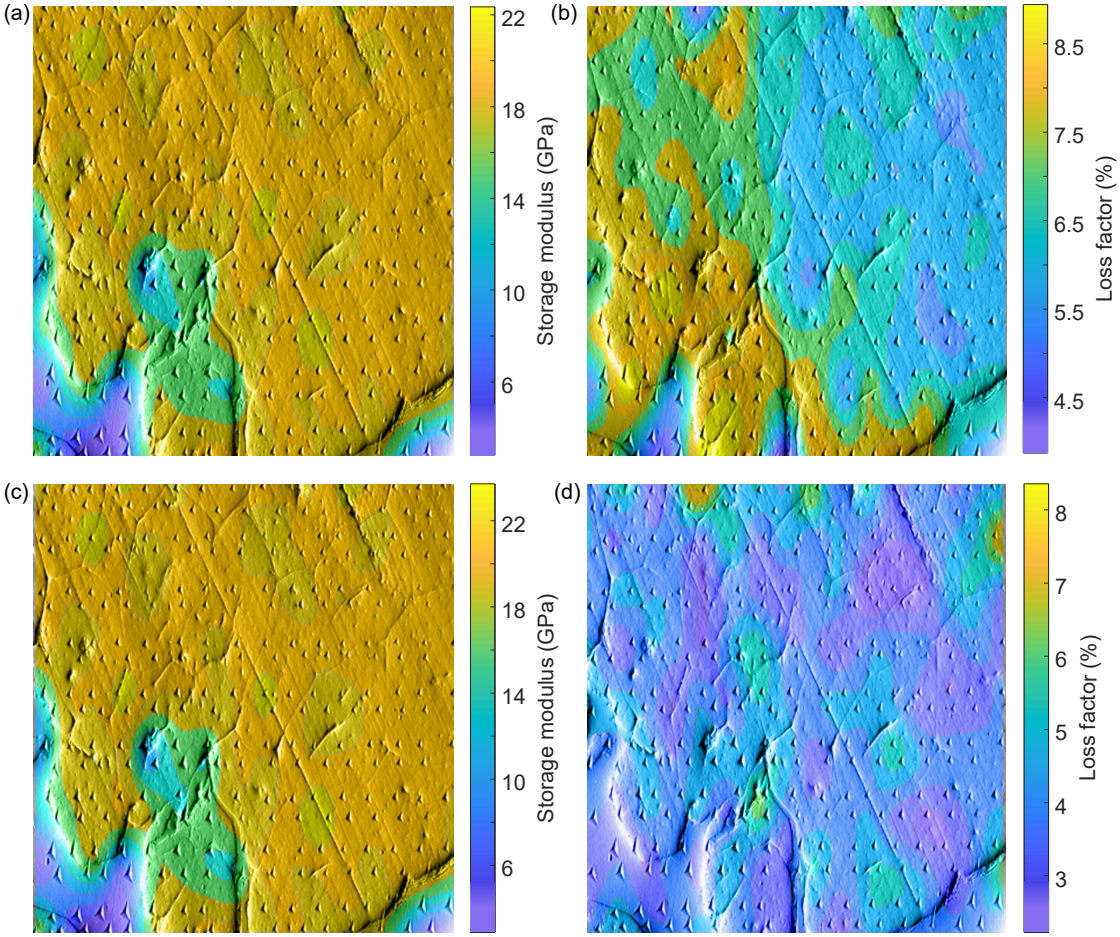

FIGURE IV.22 – Map on the cross section based on the results from storage modulus and loss factor at 5 Hz using (a) - (b) CSM and (c) - (d) CAM method on the same sample

Figure IV.23 shows the average values of storage modulus and loss factor measured in the different zones of the composite cross-section. The errorbar refers to the standard deviation of different indenter points.

The storage modulus of the fiber and matrix zone is equal to 20 GPa and 4.6 GPa with a difference of 5.6 % and 4 %, respectively compared with CSM and CAM method. This indicates that the experimental protocol (CSM or CAM) has no significant effect on the measurement of storage modulus. In addition, it is important to notice the variability in different plant fibers as the average storage modulus mentioned in the previous CSM method is around 16 GPa. However, the loss factor show a higher difference (around 40 % for fiber, 30 % for matrix) when measured with CSM and CAM methods. This is attributed to extra plasticity when the harmonic load is superimposed to the monotonic loading in CSM method. Again, the values of storage modulus and loss factor measured in fiber-fiber and fiber-matrix interface may be not accurate due to the influence of the adjacent fiber and the roughness as mentioned before.

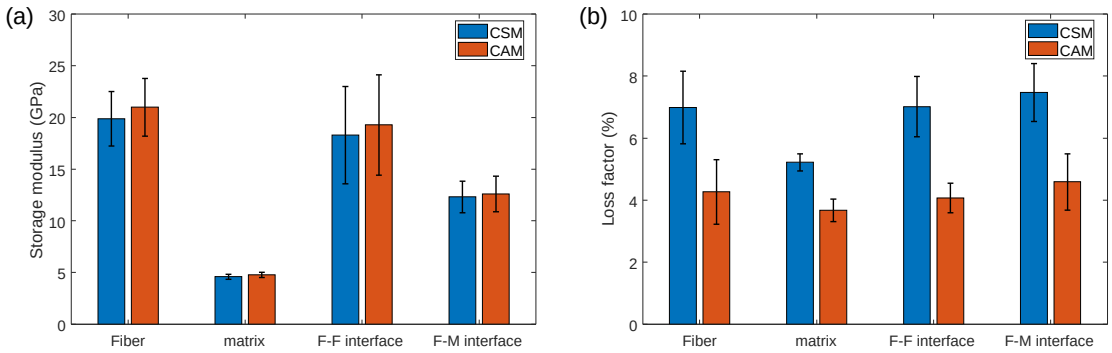

FIGURE IV.23 – Comparison of (a) storage modulus and (b) loss factor at 5 Hz obtained from CSM and CAM method on the same sample

Considering the damping-related results mentioned above, Figure IV.21 shows that the loss factor of each component measured using CAM method are around 4 % and it did not show a particularly significant difference when considering the uncertainty of each component. This can be explained by the fact that the loss factors of fiber, interface, and matrix are close to each other. For the fiber wall, this value of 4 % is comparable with that of cellulose fibers (4 to 4.5 %) measured by Elsayad et al. [Elsayad 20] by Brillouin spectroscopy. This value is also similar to the one obtained in the transverse direction of flax fiber by back-calculation from DMA tests (see chapter II). In addition, the values of loss factor obtained by CAM method are very different from those obtained by CSM method (Figure IV.23).

Figure IV.24 summarizes the reduced modulus measured in the flax fiber wall using both CSM and CAM methods as well as well data from literature obtained for different plant and wood fibers using nanoindentation and tensile tests.

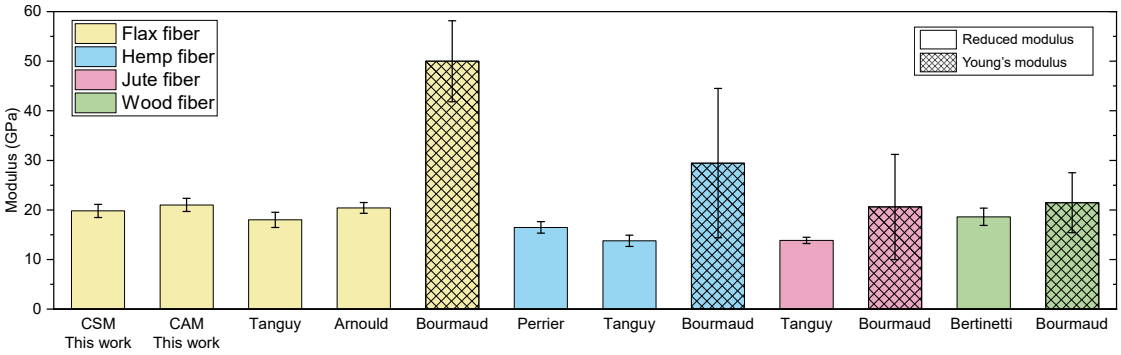

FIGURE IV.24 – Reduced modulus and Young's modulus collected from Refs. [Arnould 17, Bertinetti 15, Perrier 16, Tanguy 16, Bourmaud 18]

It can be clearly seen that the values from nanoindentation and tensile tests have a significant difference whatever the fiber type and who does the measurement. The significance of the elastic modulus from nanoindentation measurements for anisotropic materials such as wood cell walls has already been widely discussed

in literature. In particular, the calculation of the reduced modulus is based on the isotropic assumption, while the matter constituting the fiber wall is strongly anisotropic. Furthermore, the response of the material is submitted to multi-axial loading due to the inclination of the faces of the indenter pyramid. The resulting three-dimensional stress state is governed not only by the longitudinal modulus, but also affected by the much lower transverse modulus, which leads to an underestimation of the longitudinal modulus [Gindl 04a]. Hence, the value from nanoindentation cannot be compared directly to the one obtained in tensile tests on plant fiber. If it is a non-suitable method for the direct determination of the absolute value of the longitudinal elastic modulus of plant fiber cell walls, it is however an appropriate technique for comparisons of mechanical properties of wood and plant fiber cell walls at small scale.

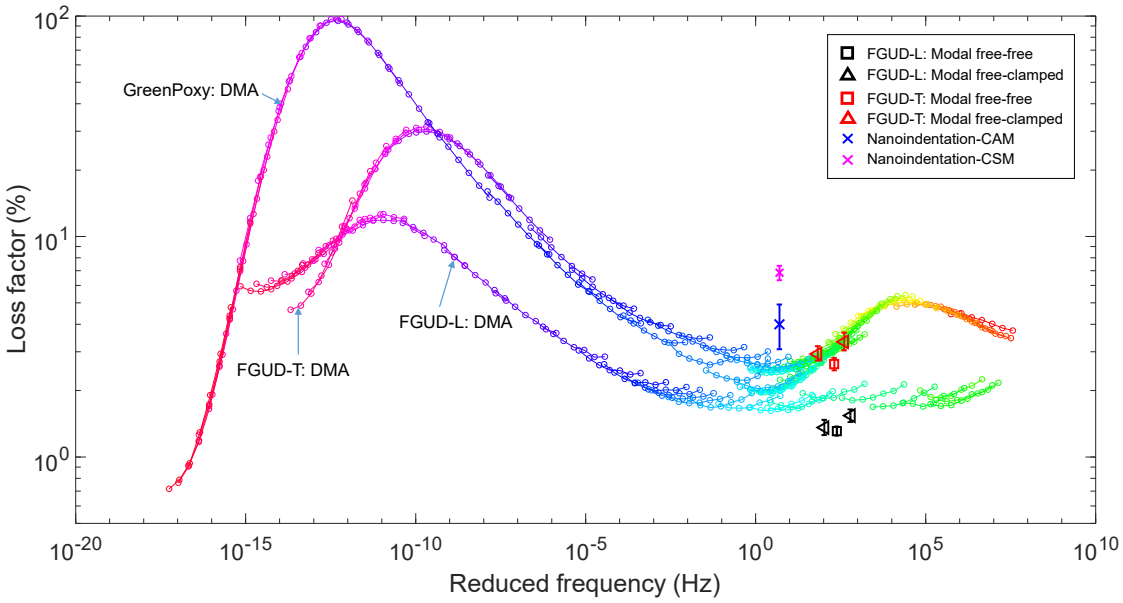

FIGURE IV.25 – Comparison of loss factor in GreenPoxy identified from DMA tests, FGUD identified from DMA and modal tests and fiber zone identified from nanoindentation tests based on CAM and CSM method using the average value

At last, figure IV.25 shows the results of loss factor for FGUD using the three different methods used in this thesis (DMA, modal analysis and DNI). The loss factor on a wide frequency range and at different scales can be compared using this kind of plot. As shown, loss factor in FGUD-T measured in DMA is in accordance with the one obtained from modal tests. The value provided by the modal tests in free-free condition is slightly lower than that obtained free-clamped condition which is expected according to the boundary conditions. For FGUD-L, a higher difference (8 % - 19 %) is found when comparing the value obtained from modal with the one issued from DMA tests due to the stiffness problems of apparatus. The values of loss factor using CAM method are more confident than those obtained using CAM method since it is more closed to those obtained from DMA and modal tests. Although the loss factor from DNI is higher than that from DMA

and modal tests, one has to consider that the measurement is made under high pressure (and then high strain levels) and under multi axial loading, resulting in potential increase of dissipation, which caused the loss factor obtained by DNI is around 60 % - 150 % higher than those obtained by DMA and modal tests.

IV.4 Conclusions

This chapter provides an alternative method for the identification of damping at the nanoscale. The results obtained with the CAM method have been compared to the ones obtained the usual CSM method. Firstly, the damping identification using traditional CSM method has been obtained for FGUD. The loss factor measured in the different constituents of the composite is in descending order: F-F interface, fiber wall, F-M interface, confined resin, matrix. The map of loss factor shows a clear correspondence for each component when compared with the cross section, which refers to their contribution on energy dissipation. However, the influence of the plasticity of the indentation on the measurement using traditional CSM may affect the identification of the damping.

The CAM method for damping identification is proposed, based on the use of harmonic forces performed at constant mean and dynamic amplitudes after loading and partial unloading of the sample. The results of the damping identification are compared with the DMA at ambient temperature and below the T_g. Good consistency is shown with conventional test methods. However, the error increases larger at high frequency (40 Hz) due to the limitations of the device. In addition, accurate temperature control needs to be used when measuring the damping near T_g since the loss factor changes in a larger range even for small temperature changes.

The loss factor in flax fiber walls measured using CAM and CSM method is around 4 % and 13 %, respectively. Obviously, the value from CAM method is in the range of the values of fiber back calculated from DMA tests in longitudinal and transverse directions (2 and 4 %, respectively). This is consistent in particular when considering that the flax fibers are anisotropic material and that the loading is multi axial when using a Berkovich indenter. Hence, CAM method is more preferably used for damping identification.

These are preliminary results. It is recommended to test more different materials using the CAM method mentioned in this chapter and this works has to be continued in the future. The dynamic behavior of the indenter should be thoroughly analyzed and its own damping should be considered in the identification procedures. The same measurements have also to be performed on the other composites (HFRC and FPPC) studied in the previous chapters. Indeed, at this stage, the methodology has been validated and first measurements obtained. More tests are required to study the influence of frequency, temperature and moisture on the full-field measurement of the viscoelastic properties at the nano/microscale.

Conclusions and perspectives

Conclusions

Plant fiber reinforced composites are sought to be a good choice in many sustainable engineering applications due to their moderate cost, easily degradable and lightweight compared to synthetic fiber based composites. They are also considered as a good alternative to provide a good stiffness to damping ratio in such structures. The review of the literature on this topic reveals that the existing knowledge on the damping behavior of PFCs is sometimes deficient or ambiguous.

So, this PhD thesis aims at contributing to a better understanding of the damping behavior of PFCs through a multi-scale damping characterization. Three different experimental methods were used (DMA, modal analysis and dynamic nanoindentation). Several high-grade PFCs were selected as considered as promising for the structural and multifunctional applications targeted in the SSUCHY project. It included continuous flax and hemp fiber reinforcements and thermoset and thermoplastic matrices. The study offered some insights into damping sources in these plant fiber composites, on the effect of fiber or matrix types and provides their damping properties on a wide range of temperature and frequency and also at different scales. The dynamic grid nanoindentation allowed the exploration, for the first time, of the in situ damping properties of the PFCs constituents. The following paragraphs synthesized the main outcomes of each chapter.

Chapter I provided a literature review on the experimental methods and many factors at the meso and microscale and related to the surrounding conditions that affect the damping properties of PFCs. The first outcome of this chapter concerned the construction of the Ashby diagrams based on the values of loss factor and modulus from literature for metal, polymers and organic matrix composites reinforced with synthetic fibers and plant fibers. Based on this literature review, it can be seen that the damping capacity of PFCs, comprised in the range 0.7 - 14 %, is generally much higher than the one of SFCs covering a range from 0.24 to 2.5 %. It confirms the application prospects of PFCs in lightweight sustainable structures and products. The second outcome is a radar plot representing the average values of some mechanical properties and economic parameters (stiffness, strength, loss factor, density and cost) of several material types. It clearly shows that PFCs have average damping levels 5 times higher than some SFCs. The third main contribution is the discussion of the sources of energy dissipation which are specific to PFCs (intra-cell and inter-cell wall friction, intra-yarn and inter-yarn friction, and fiber/matrix sliding) and which add to the common ones in organic matrix composites (viscoelastic nature of the matrix, friction at fiber/matrix interface and in interphase, inelastic and irreversible behaviors such as damage and/or

plasticity). The critical review of the literature on the topic underlines the complexity of damping behavior in such materials, points out contradictory reports and the limitations of the existing knowledge on the damping behavior of PFCs. This work was presented in an international conference (ICCS 22) and submitted to an international peer-reviewed journal.

Chapter II investigated the damping properties of plant fiber composites using DMA tests. In the first section, the influence of the loading mode (bending or tension) in DMA tests on the measurement of dynamic mechanical properties was studied. The tension mode is preferred for the measurement of damping, to limit the effect of friction between the sample and clamp on the measurement of damping. Using the selected experimental configuration, the curing and post-curing process of the GreenPoxy matrix are optimized. Indeed, these manufacturing parameters have a significant effect on the damping properties of the resulting material.

In the second section, the damping properties in the two main directions (longitudinal and transverse direction) of unidirectional flax fiber reinforced composites with thermoset and thermoplastic-based matrices were investigated. PP- based flax fiber UD composites (2.3 %-3.8 %) show generally a higher damping capacity than epoxy-based UD flax fiber composites (1.4 %-2.6 %) at 1 Hz. For unidirectional composites, results also show that the damping properties are mainly driven by the fiber and the matrix in longitudinal and transverse direction, respectively. From these DMA tests, the damping properties of the flax fibers are also identified by inverse method. Values of about 1.6 to 2.2 % are determined in the longitudinal direction when 3.4 to 4 % are identified in the transverse direction.

In the third section, several woven hemp fabrics developed in the SSUCHY project are characterized at the scale of composites made with GreenPoxy and PA12. For the hemp/GreenPoxy composites, and for the considered fabrics, the weave pattern is shown not to be influential on the damping properties of the composites. The loss factor of hemp/GreenPoxy composites is always around 2 % in both material directions even if the yarn density is different. This value of loss factor (2 %) is comparable to that of cross-ply flax composites (1.8 - 1.9 %) in both direction, and the slightly higher value for woven hemp composites is attributed to the fiber waviness induced by crimp. On the wide temperature range studied, flax/petro-based epoxy composites, flax/GreenPoxy composites, and hemp/GreenPoxy composites have shown similar trends in dynamic mechanical behavior with their respective matrices. Results also show that the loss factors of the plant fiber composites studied in this work are higher than that of synthetic fiber composites, which confirms their bright application prospect in sustainable structures.

The master curves of GreenPoxy, flax reinforced GreenPoxy composites and hemp reinforced GreenPoxy composites are also built to obtain the storage modulus and loss factor on a wide frequency range. Regarding the damping properties in a specific reduced frequency range, a non-constant and non-linear evolution is found for both thermosets and thermoplastic based composites. This non-linear behavior as a function of frequency is related to the presence of glass transition and secondary transition in the time-temperature space studied in this work.

At last, the effect of water aging on the damping properties of the unidirectional flax/GreenPoxy composites is studied. The loss factor increases of about 4 times after 5 days aging. So, it is found that the moisture content is the most influential parameter for a given temperature and frequency (1 Hz) among all the parameters studied in this chapter (matrix type, fiber type, reinforcement architecture, lay-up).

Chapter III investigated the damping behavior of several PFC materials including unidirectional composites (FGUD), thermoplastic-based composites (FPPC) and woven fabric reinforced composites (H4) using modal analysis in free-free and free-clamped configurations.

First and foremost, an optimized specimen shape was designed using numerical modeling to minimize the influence of clamping on the damping identification in the free-clamped configuration. The damping properties of the selected materials were then identified in the longitudinal and transverse directions according to the shapes of the eigenmodes. This avoided the mixture of flextural and torsion mode. The loss factors of unidirectional flax/GreenPoxy composites and flax/Polypropylene composites are comprised between 1.3 % - 3.3 % and 1.4 % - 4.6 % on the frequency range of 40 Hz – 1000 Hz, respectively. It indicates the higher damping capacities of PP-based composites when compared to the the thermoset-based (Greenpoxy) ones in transverse direction. Regarding the woven hemp/GreenPoxy composites, the loss factor is between 1.5 %-2.5 % on the frequency range of 40 Hz – 900 Hz. No significant differences were observed between warp (L) and weft (T) directions. This is consistent with the results obtained using DMA at 1 Hz.

In addition, the damping ratio determined from the free-clamped boundary conditions is still higher (maximum 20 %) than that from free-free boundary conditions even if an optimized shape is used. This reminds that the influence of boundary conditions should be taken seriously into account before designing experiments. Thirdly, damping properties of flax/GreenPoxy composites from DMA and modal tests were also compared using the master curves. A good corresponding is found considering a maximum difference of 19 % in longitudinal direction.

At last, the damping ratio of water aged unidirectional flax/GreenPoxy plates is measured at around 2 % in both longitudinal and transverse direction at the saturated mass (14.2 %). The influence of moisture sorption needs to be investigated with more samples since the deformation of the plate during water sorption may have an effect on the modal shape from the numerical model. Furthermore, influence of moisture at different temperatures has to be more thoroughly studied in the future.

Chapter IV offered new light on the damping identification of plant fiber composites at microscale based on dynamic nanoindentation. A new alternative method (Constant Amplitude Method, CAM) for damping identification was first proposed based on the harmonic forces performed at constant mean and dynamic amplitudes after monotonic loading and partial unloading of the sample. Good consistency in loss factor of GreenPoxy was shown at ambient temperature and below the glass transition temperature when compared with the DMA at 1 - 40 Hz.

However, larger uncertainty is found when the dynamic nanoindentation is performed at higher frequency (closed to 40 Hz) due to the limitations of the device and near the glass transition temperature due to temperature control.

Secondly, the damping of flax/GreenPoxy composites was identified using traditional CSM (constant stiffness) method. The map of loss factor shows a clear correspondence for each component (fiber, matrix, fiber-fiber and fiber-matrix interface) when compared with the cross section, which refers to their contribution on energy dissipation. Then, the damping properties obtained by CAM method were compared with those from CSM method. The loss factor in flax fiber walls measured using CAM and CSM method is around 4 % and 7 - 13 %, respectively. Obviously, the value from CAM method is in the range of the values of fiber back calculated from DMA tests in longitudinal and transverse directions (2 and 4 %, respectively). It is considered that the damping value measured using the classical CSM method is overestimated due to the expression of the viscoplasticity. .

Moreover, the results obtained using CAM method are consistent in particular when considering that the flax fibers are anisotropic material and that the loading is multi axial when using a Berkovich indenter. Hence, it is recommended to prefer CAM method to CSM method for damping identification of such materials. At last, the loss factor of flax/GreenPoxy composites obtained by DMA, modal analysis and Nanoindentation are plotted in the same graph to complement the shortcomings of each method. Finally, the damping properties regarding wide temperature, frequency range and different scales can be obtained based on this work.

On-going works and Perspectives

The present research in this thesis explores many aspects that affect the damping properties of plant fiber composites. Damping identification under different methods have been proposed. Some of the measurements were unprecedented and realized using new experimental configurations and/or protocols. Even if a better understanding of the damping behavior of PFCs is provided, many questions are also raised and several aspects definitively deserved to be more thoroughly investigated.

- Matrix is one of the most influential factor in damping properties of plant fiber composites, in particular in the transverse direction of UD laminates. The experiments proposed in this work are mainly focused on two familiar polymers (GreenPoxy and Polypropylene), more types of polymer-based plant fiber composites, such as Polylactic acid, Polymethyl methacrylate and fully bio-based epoxy, are suggested to be characterized, in term of damping performance, in the future.
- The reinforcements used in this thesis are pure unidirectional and quasi-unidirectional flax fabrics. To refine the evaluation of the matrix type in the transverse direction, it is recommend to use the same pure unidirectional fabric to avoid any effect from the transverse filaments or yarns in quasi-UD. Regarding the woven fabrics, damping properties of other weave patterns including plain, basket, cross weaves etc. reinforced composites could also be studied. Furthermore, the yarn density of the fabrics studied in this thesis is closed. Larger ranges of yarn density in warp and weft directions could be considered.
- The analytical model used for back-calculation of damping of plant fiber is based on many idealized hypotheses such as homogeneous composites, perfect interface and no porosity. Therefore, a more complete theoretical model of damping for plant fiber composites needs to be developed, and this work is already in progress. Multi-scale models implemented in FE codes are also under development within the team.
- The dynamic mechanical properties of unidirectional flax fiber composites are reported in this work using DMA test. Unfortunately, the storage modulus in the longitudinal direction is always underestimated due to the frame stiffness limitations of the device and the strain determination method. This problem can be improved by using an equipment with higher stiffness or by using extensometers for the correction of measurements.
- In modal tests, the optimized shape can reduce the influence of boundary conditions on the damping measurement, but the results show that it still cannot completely eliminate its influence. Therefore, other optimized methods can be studied in the future to further reduce the influence of boundary conditions. In addition, damping properties of plant fiber compo-

sites can be measured under extend frequency range by using various beam lengths in free-clamped boundary condition so that the natural frequency can be changed and this work is undergoing.

- Temperature has significant influence on the damping properties of plant fiber composites according to the results from DMA tests. Similar experiments with modal analysis at different temperatures are scheduled.
- Plant fiber composites are more sensitive to water than synthetic fiber composites. Aging experiments in this thesis are always performed on unidirectional Greenpoxy/flax composites. Other types of composite such as woven fabric composites or thermoplastic composites can also be investigated to know the effect of moisture content on damping properties. The effect of relative humidity (indoor condition) on damping is also an interesting issue in addition to water immersion (outdoor condition) for the plant fiber composites. The results of dynamic properties regarding water aging in modal analysis are measured from only one composite plate. More experiments with different plates were originally planned but had been postponed due to the lockdown from COIVD-19 and now it is on the agenda again.
- Preliminary results of damping identification based on dynamic nanoindentation show a good prospect on the measurement of damping at nanoscale. More different materials (thermoplatic-based composites, hemp fabric reinforced composites) are recommended to be tested using the new method (CAM) mentioned in chapter IV and this works have been continued in the my plan. Furthermore, more tests are planed to study the influence of frequency, temperature and moisture on the full-filed measurement of the viscoelastic properties at the nano/microscale.
- Plant fibers can be used as many kinds of reinforcement types such as short or long fibers, nonwoven, non-crimp fabrics, which lead to different microstructure when they are made into plant fiber composites. Although the results related to damping can be found in a small number of existing studies, there are large uncertainties in the comparison due to different types of fibers (flax, sisal or jute), manufacturing processes, suppliers and matrices, etc. It is reluctant or difficult to summarize a correct conclusion based on these researches. Therefore, a more precise comparison is recommended making the fiber be the only variable parameter during the experiment.
- Growth environment is an important factor that affects plant fibers. At present, the main interest in it is mainly focused on static mechanical properties such as Young's modulus, strength, etc., However, dynamic mechanical properties regarding the growth environment are rarely seen. In addition, the difference in the process of production (such as retting or scutching) can also be take into account.

- The damping performance of plant fiber composites with different stacking sequences had been widespread studied in many literature. However, an accurate damping theoretical model is needed to describe the effect of different stacking sequences on damping, especially composite materials mixed with synthetic fibers.
- Fiber treatments including chemical method or enhanced with nanotubes show a significant effect on the damping properties. Existing studies attribute this effect to the changes in the interface. However, how to quantify and characterize the property changes of interface between fiber and matrix is an important issue.
- Fiber volume fraction works is an important factor. Some research conclusions regarding the effect from fiber volume fraction on damping performance (damping is proportional to or inversely proportional to fraction) are conflicting and it can further studied as well as hybrid fiber composites.
- The research of damping properties regarding fiber orientation has enough results in terms of experimental values or theoretical model. However, the research objects are mostly unidirectional plant fiber composite materials, and the fabrics reinforced composites with different fiber orientations are not paid enough attention.
- The influence of interface between fiber and matrix on damping properties is widely accepted by researchers. Although the new method (CAM) is proposed in this thesis, it will always be affected by neighboring fibers or matrix during the experimental measurement, so the value obtained is not accurate. This needs further research for improvement.
- Strain level effect is also an important issue regarding the damping properties of plant fiber composites. The existing experimental technology is difficult to achieve the same strain level that occurred in the nanoindentation experiment. Hence, this comparison is proposed in future research.
- The Ashby diagram of damping regarding stiffness for plant fiber composites is drawn in Chapter 1. Although the relevant dynamic mechanical information can be clearly displayed, it is not sufficient. More comparisons should be made on parameters such as density, price, and strength etc. In addition, the Ashby diagram of damping regarding dynamic stiffness in a wide frequency or temperature range is also recommended to be drawn in the future.

Annexe A
Appendix

A.1 List of Symbols 160
A.2 Verification of measurement in free-free boundary conditions 163

A.1 List of Symbols

ε	Strain
ν_I	Poisson's ratio of the indenter
ν_S	Poisson's ratio of the sample
σ	Stress
A	Projected area of the contact surface
ABS	Acrylonitrile Butadiene Styrene
CNTs	Carbon nanotubes
CAM	Constant amplitude method
CSM	Continuous stiffness measurement
DMA	Dynamic mechanical analysis
DNI	Dynamic nanoindentation method
E^*	Complex Young's modulus of the material
E'	Storage modulus
E''	Loss modulus
E_I	Young's modulus of the indenter
E_r	Reduced modulus
E_S	Young's modulus of the sample
FFRC	Flax fiber reinforced composites
FGCR	Cross-ply flax fiber reinforced GreenPoxy 56 based composites
FGUD	Unidirectional flax reinforced green epoxy composites
FPPC	Flax/polypropylene composites
GE	Pure greenpoxy 56
h	Indentation depth
H	Hardness
h_c	Depth of circle of contact measured from maximum depth
h_f	Depth of the residual indentation
h_{max}	Depth from the original sample surface at load
h_s	Depth of circle of contact measured from specimen free surface

H4	Hemp4 fabric reinforced greenpoxy 56 based composites
H4/PA12	Hemp4 fabric reinforced Nylon plastique 12 composites
H5	Hemp5 fabric reinforced greenpoxy 56 based composites
H6	Hemp6 fabric reinforced greenpoxy 56 based composites
H7	Hemp7 fabric reinforced greenpoxy 56 based composites
HFRC	Hemp fabric reinforced composites
L	Longitudinal direction
L_c	Length of the sample
LDM	Logarithmic decrement measurement method
MFA	Cellulose microfibril angle relative to the longitudinal axis of the fibre
P	Load acting on the sample
PA12	Nylon plastique 12
PBAT	Polybutylene adipate-co-terephthalate
PE	Petro-based epoxy
PFCs	Plant fiber-reinforced composites
PLA	Polylactic acid
PMMA	Polymethyl methacrylate
PP	Polypropylene
S, K_s	Elastic contact stiffness
SFCs	Synthetic fiber-reinforced composites
t	Time
t_c	Thickness of the sample
T	Transverse direction
T_g	Glass transition temperature
t_c	Thickness of the sample
tan (δ), η	Loss factor
TTS	Time-Temperature Superposition
UD	Unidirectional
VBM	Vibration beam

W	Width of the sample
WLF	Williams - Landel - Ferry equation

A.2 Verification of measurement in free-free boundary conditions

The influence of excitation is studied experimentally under amplitude values varying from 0.5 V to 5 V. The damping ratios of the first 6 modes in modal analysis of FGUD in free-free boundary conditions using different excitation amplitudes are compared in Figure A.1 (a).

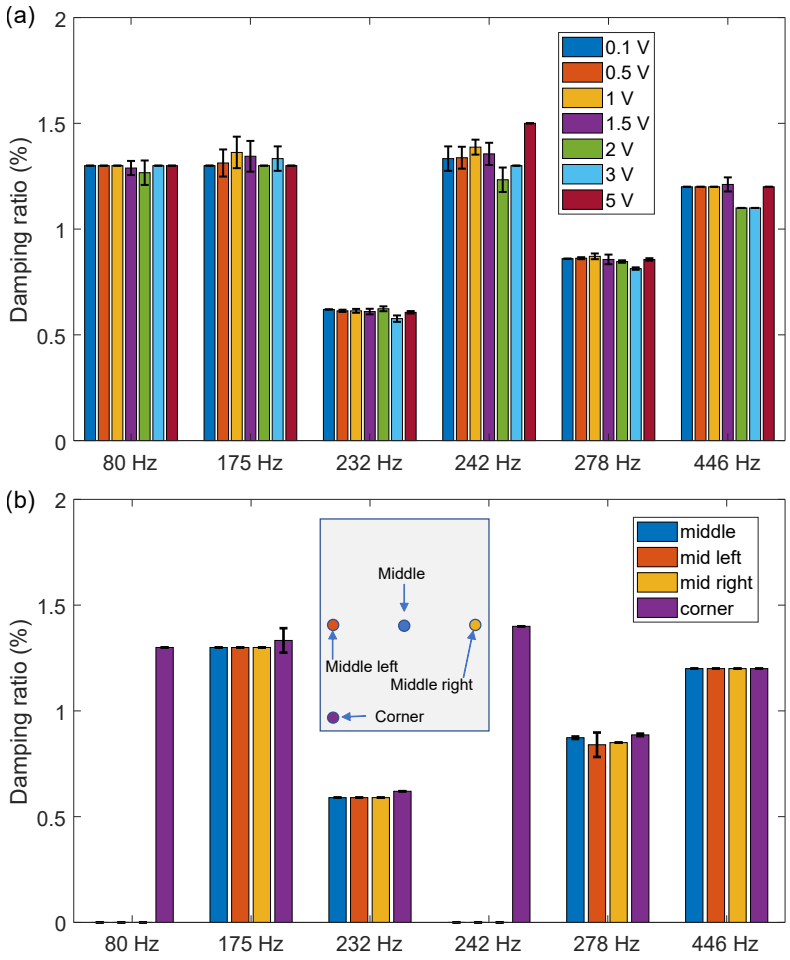

Figure A.1 – Influence of (a) amplitude of excitation and (b) position of measurement on the damping ratio identification under free-free boundary condition

It can be seen clearly that the influence of the amplitude level, for the considered range, on damping identification is very low with the experimental setup used in this study. The difference in damping ratio identified under various excitation amplitudes is indeed extremely low (less than 5 %) except for the damping identified at 242 Hz between 2 V and 5 V with a maximum difference of 17 %. This shows that the measurement uncertainties are quite low and also that the modal

response under the amplitude range of excitation between 0.1 V and 5 V is in the linear viscoelatic range of the tested material. Therefore, 1.5 V was selected as the adequate amplitude of excitation for the rest of the experimental campaign.

Figure A.1 (b) shows the influence of the measurement position on the damping ratio identified for the FGUD plate. The variations are also very low when compared to results usually found in literature [Rahman 17b]. Some values are missing at 80 Hz and 242 Hz as some measurement points were located on nodal lines of specific modes, meaning that the displacement is null and so that the damping properties cannot be identified. Hence, the following tests will measure the response near the corner.

References

[Adams 03] R. D. Adams & M. Maheri. *Damping in advanced polymer–matrix composites*. Journal of Alloys and Compounds, vol. 355, no. 1-2, pages 126–130, 2003.

[Alexander 16] J. Alexander, B. S. Augustine, S. Prudhuvi & A. Paudel. *Hygrothermal effect on natural frequency and damping characteristics of basalt/epoxy composites*. Materials Today: Proceedings, vol. 3, no. 6, pages 1666–1671, 2016.

[Alkbir 16] M. F. Alkbir, S. M. Sapuan, A. A. Nuraini & M. R. Ishak. *Fibre properties and crashworthiness parameters of natural fibre-reinforced composite structure: A literature review*. Composite Structures, vol. 148, pages 59–73, 2016.

[Alkorta 08] J. Alkorta, J. M. Martínez-Esnaola & J. G. Sevillano. *Critical examination of strain-rate sensitivity measurement by nanoindentation methods: Application to severely deformed niobium*. Acta Materialia, vol. 56, no. 4, pages 884–893, 2008.

[Almgren 08] K. M. Almgren, M. Åkerholm, E. K. Gamstedt, L. Salmen & M. Lindström. *Effects of Moisture on Dynamic Mechanical Properties of Wood Fiber Composites Studied by Dynamic FT-IR Spectroscopy*. Journal of Reinforced Plastics and Composites, vol. 27, no. 16-17, pages 1709–1721, nov 2008.

[Amenini 19] F. Amenini, J. Brocail, M. Chauvin & S. Thuillier. *Dynamical properties of flax fibre reinforced PA11 over a large frequency range*. Composites Science and Technology, vol. 171, no. December 2018, pages 234–243, 2019.

[Araújo 09] A. L. Araújo, P. Martins, C. M. Mota Soares, C. A. Mota Soares & J. Herskovits. *Damping optimization of viscoelastic laminated sandwich composite structures*. Structural and Multidisciplinary Optimization, vol. 39, no. 6, pages 569–579, dec 2009.

[Arnould 17] O. Arnould, D. Siniscalco, A. Bourmaud, A. Le Duigou & C. Baley. *Better insight into the nano-mechanical properties of flax fibre cell walls*. Industrial Crops and Products, vol. 97, pages 224–228, 2017.

[Ashworth 16] S. Ashworth, J. Rongong, P. Wilson & J. Meredith. *Mechanical and damping properties of resin transfer moulded jute-carbon hybrid composites*. Composites Part B: Engineering, vol. 105, pages 60–66, 2016.

[Assarar 13] M. Assarar, A. E. Mahi, A. El Mahi & J.-M. Berthelot. *Analysis of the damping of sandwich materials and effect of the characteristics of the constituents Effect of different cyclic signals on three-points-bending behavior of a fibre-glass and epoxy resin composite materials View project ISABEAU View project A*. Rapport technique 2, 2013.

[Assarar 15] M. Assarar, W. Zouari, H. Sabhi, R. Ayad & J. M. Berthelot. *Evaluation of the damping of hybrid carbon-flax reinforced composites*. Composite Structures, vol. 132, pages 148–154, 2015.

[AST 17] *ASTM E756 - 05(2017) Standard Test Method for Measuring Vibration-Damping Properties of Materials*, 2017.

[ASTM-D3171 09] ASTM-D3171. *Standard Test Method for Constituent of Composite Materials*. American Society for Testing and Materials West Conshohocken, PA, 2009.

[Atiqah 19] A. Atiqah, M. Jawaid, S. M. Sapuan & M. R. Ishak. *Dynamic mechanical properties of sugar palm/glass fiber reinforced thermoplastic polyurethane hybrid composites*. Polymer Composites, vol. 40, no. 4, pages 1329–1334, 2019.

[Audibert 18] C. Audibert, A. S. Andreani, É. Lainé & J. C. Grandidier. *Mechanical characterization and damage mechanism of a new flax-Kevlar hybrid/epoxy composite*. Composite Structures, vol. 195, no. March, pages 126–135, 2018.

[Baley 19] C. Baley, M. Gomina, J. Breard, A. Bourmaud & P. Davies. *Industrial Crops & Products Variability of mechanical properties of flax fibres for composite reinforcement . A review*. Industrial Crops & Products, no. September, page 111984, 2019.

[Berges 16] M. Berges, R. Léger, V. Placet, V. Person, S. Corn, X. Gabrion, J. Rousseau, E. Ramasso, P. Ienny & S. Fontaine. *Influence of moisture uptake on the static, cyclic and dynamic behaviour of unidirectional flax fibre-reinforced epoxy laminates*. Composites Part A: Applied Science and Manufacturing, vol. 88, pages 165–177, sep 2016.

[Berthelot 04a] J.-M. Berthelot & Y. Sefrani. *Damping analysis of unidirectional glass and Kevlar fibre composites*. Composites science and technology, vol. 64, no. 9, pages 1261–1278, 2004.

[Berthelot 04b] J. M. Berthelot & Y. Sefrani. *Damping analysis of unidirectional glass and Kevlar fibre composites*. Composites Science and Technology, vol. 64, no. 9, pages 1261–1278, jul 2004.

[Berthelot 07] J. M. Berthelot & Y. Sefrani. *Longitudinal and transverse damping of unidirectional fibre composites*. Composite Structures, vol. 79, no. 3, pages 423–431, jul 2007.

[Berthelot 08] J.-M. M. Berthelot, M. Assarar, Y. Sefrani & A. E. Mahi. *Damping analysis of composite materials and structures*. Composite Structures, vol. 85, no. 3, pages 189–204, oct 2008.

[Bertinetti 15] L. Bertinetti, U. D. Hangen, M. Eder, P. Leibner, P. Fratzl & I. Zlotnikov. *Characterizing moisture-dependent mechanical properties of organic materials: humidity-controlled static and dynamic nanoindentation of wood cell walls*. Philosophical Magazine, vol. 95, no. 16-18, pages 1992–1998, jun 2015.

[Bhudolia 17] S. K. Bhudolia, P. Perrotey & S. C. Joshi. *Enhanced vibration damping and dynamic mechanical characteristics of composites with novel pseudo-thermoset matrix system*. Composite Structures, vol. 179, pages 502–513, 2017.

[Biagiotti 04] J. Biagiotti, D. Puglia & J. M. Kenny. *A review on natural fibre-based composites - Part I: Structure, processing and properties of vegetable fibres*. Journal of Natural Fibers, vol. 1, no. 2, pages 37–68, 2004.

[Bismarck 02] A. Bismarck, I. Aranberri-Askargorta, J. Springer, T. Lampke, B. Wielage, A. Stamboulis, I. Shenderovich & H.-H. Limbach. *Surface characterization of flax, hemp and cellulose fibers ; Surface properties and the water uptake behavior*. Polymer Composites, vol. 23, no. 5, pages 872–894, oct 2002.

[Bogren 06] K. M. Bogren, E. K. Gamstedt, R. C. Neagu, M. AÅkerholm & M. LindstroÖm. *Dynamic–Mechanical Properties of Wood–Fiber Reinforced Polylactide: Experimental Characterization and Micromechanical Modeling*. Journal of Thermoplastic Composite Materials, vol. 19, no. 6, pages 613–637, nov 2006.

[Bourmaud 12a] A. Bourmaud & C. Baley. *Nanoindentation contribution to mechanical characterization of vegetal fibers*. Composites Part B: Engineering, vol. 43, no. 7, pages 2861–2866, oct 2012.

[Bourmaud 12b] A. Bourmaud & C. Baley. *Nanoindentation contribution to mechanical characterization of vegetal fibers.* Composites Part B: Engineering, vol. 43, no. 7, pages 2861–2866, 2012.

[Bourmaud 16] A. Bourmaud, M. Gibaud & C. Baley. *Impact of the seeding rate on flax stem stability and the mechanical properties of elementary fibres.* Industrial Crops and Products, vol. 80, 2016.

[Bourmaud 18] A. Bourmaud, J. Beaugrand, D. U. Shah, V. Placet & C. Baley. *Towards the design of high-performance plant fibre composites.* Progress in Materials Science, vol. 97, no. July 2017, pages 347–408, 2018.

[Brodt 95] M. Brodt & R. S. Lakes. *Composite Materials Which Exhibit High Stiffness and High Viscoelastic Damping.* Journal of Composite Materials, vol. 29, no. 14, pages 1823–1833, 1995.

[Buravalla 01] V. Buravalla, C. Remillat, J. Rongong & G. Tomlinson. *Advances in damping materials and technology.* Smart Materials Bulletin, vol. 2001, no. 8, pages 10–13, aug 2001.

[Butaud 15a] P. Butaud, V. Placet, J. Klesa, M. Ouisse, E. Foltête & X. Gabrion. *Investigations on the frequency and temperature effects on mechanical properties of a shape memory polymer (Veriflex).* Mechanics of Materials, vol. 87, pages 50–60, 2015.

[Butaud 15b] P. Butaud. *Contribution à l'utilisation des polymères à mémoire de forme pour les structures à amortissement contrôlé.* 2015.

[Butaud 16] P. Butaud, E. Foltête & M. Ouisse. *Sandwich structures with tunable damping properties: On the use of Shape Memory Polymer as viscoelastic core.* Composite Structures, vol. 153, pages 401–408, oct 2016.

[Butaud 18] P. Butaud, M. Ouisse, V. Placet, F. Renaud, T. Travaillot, A. Maynadier, G. Chevallier, F. Amiot, P. Delobelle, E. Foltête & C. Rogueda-Berriet. *Identification of the viscoelastic properties of the tBA/PEGDMA polymer from multi-loading modes conducted over a wide frequency–temperature scale range.* Polymer Testing, vol. 69, no. May, pages 250–258, 2018.

[Cadu 18] T. Cadu, M. Berges, O. Sicot, V. Person, B. Piezel, L. Van Schoors, V. Placet, S. Corn, R. Léger, L. Divet, P. Ienny & S. Fontaine. *What are the key parameters to produce a high-grade bio-based composite ? Application to flax/epoxy*

UD laminates produced by thermocompression. Composites Part B: Engineering, vol. 150, no. December 2017, pages 36–46, 2018.

[Carfagni 98] M. Carfagni, E. Lenzi & M. Pierini. *The loss factor as a measure of mechanical damping*. In SPIE proceedings series, pages 580–584, 1998.

[Chandra 99] R. Chandra, S. P. Singh & K. Gupta. *Damping studies in fiber-reinforced composites - a review*. Composite Structures, vol. 46, no. 1, pages 41–51, sep 1999.

[Chang 19] J.-j. Chang, Y.-y. Li, X.-f. Zeng, H.-y. Zhong, T.-l. Wan & C. Lu. *Study on the Viscoelasticity Measurement of Materials Based on Surface Reflected Waves*. Materials, vol. 12, no. 11, page 1875, 2019.

[Cheour 16] K. Cheour, M. Assarar, D. Scida, R. Ayad & X.-L. L. Gong. *Effect of water ageing on the mechanical and damping properties of flax-fibre reinforced composite materials*. Composite Structures, vol. 152, pages 259–266, sep 2016.

[Chilali 17] A. Chilali, M. Assarar, W. Zouari, H. Kebir & R. Ayad. *Effect of geometric dimensions and fibre orientation on 3D moisture diffusion in flax fibre reinforced thermoplastic and thermosetting composites*. Composites Part A: Applied Science and Manufacturing, vol. 95, pages 75–86, 2017.

[Chua 87] P. S. Chua. *Dynamic mechanical analysis studies of the interphase*. Polymer Composites, vol. 8, no. 5, pages 308–313, oct 1987.

[Chung 03] D. Chung. *Structural composite materials tailored for damping*. Journal of Alloys and Compounds, vol. 355, no. 1-2, pages 216–223, 2003.

[Cihan 19] M. Cihan, A. J. Sobey & J. I. Blake. *Mechanical and dynamic performance of woven flax/E-glass hybrid composites*. Composites Science and Technology, vol. 172, no. December 2018, pages 36–42, 2019.

[Cisse 15] O. Cisse, V. Placet, V. Guicheret-Retel, F. Trivaudey & M. L. Boubakar. *Creep behaviour of single hemp fibres. Part I: viscoelastic properties and their scattering under constant climate*. Journal of Materials Science, vol. 50, no. 4, pages 1996–2006, 2015.

[Corbin 20a] A.-C. Corbin, M. Ferreira, A. R. Labanieh & D. Soulat. *Natural fiber composite manufacture using wrapped hemp roving with PA12*. Materials Today: Proceedings, 2020.

[Corbin 20b] A.-C. Corbin, D. Soulat, M. Ferreira, A.-R. Labanieh, X. Gabrion, P. Malécot & V. Placet. *Towards hemp fabrics for high-performance composites: Influence of weave pattern and features*. Composites Part B: Engineering, vol. 181, page 107582, 2020.

[D5026 13] A. D5026. *Standard Test Method for Plastics: Dynamic Mechanical Properties: In Tension*, 2013.

[Daoud 16] H. Daoud, J. L. Rebière, A. Makni, M. Taktak, A. El Mahi & M. Haddar. *Numerical and experimental characterization of the dynamic properties of flax fiber reinforced composites*. International Journal of Applied Mechanics, vol. 8, no. 5, jul 2016.

[Daoud 17] H. Daoud, A. El Mahi, J. L. Rebière, M. Taktak & M. Haddar. *Characterization of the vibrational behaviour of flax fibre reinforced composites with an interleaved natural viscoelastic layer*. Applied Acoustics, vol. 128, pages 23–31, 2017.

[Datta 02] C. Datta, D. Basu & A. Banerjee. *Mechanical and dynamic mechanical properties of jute fibers-novolac-epoxy composite laminates*. Journal of Applied Polymer Science, vol. 85, no. 14, pages 2800–2807, sep 2002.

[Datta 17] J. Datta & M. Włoch. *Preparation, morphology and properties of natural rubber composites filled with untreated short jute fibres*. Polymer Bulletin, vol. 74, no. 3, pages 763–782, 2017.

[Dayo 18] A. Q. Dayo, A. Zegaoui, A. A. Nizamani, S. Kiran, J. Wang, M. Derradji, W. an Cai & W. bin Liu. *The influence of different chemical treatments on the hemp fiber/polybenzoxazine based green composites: Mechanical, thermal and water absorption properties*. Materials Chemistry and Physics, vol. 217, no. June, pages 270–277, 2018.

[Della 07] C. N. Della & D. Shu. *Vibration of delaminated composite laminates: A review*. Applied Mechanics Reviews, vol. 60, no. 1, pages 1–20, 2007.

[Deuschle 07] J. Deuschle, S. Enders & E. Arzt. *Surface detection in nanoindentation of soft polymers*. Journal of Materials Research, vol. 22, no. 11, pages 3107–3119, 2007.

[dos Santos Silva 19] G. dos Santos Silva, C. Capela & M. Gaspar. *Developing Sustainable Materials for Marine Environments: Algae as Natural Fibers on Polymer Composites*. In International Conference of Progress in Digital and Physical Manufacturing, pages 198–205. Springer, 2019.

[Duc 14a] F. Duc, P. E. Bourban & J. A. E. Månson. *The role of twist and crimp on the vibration behaviour of flax fibre composites*. Composites Science and Technology, vol. 102, pages 94–99, 2014.

[Duc 14b] F. Duc, P. E. Bourban, C. J. G. Plummer & J. A. E. Månson. *Damping of thermoset and thermoplastic flax fibre composites*. Composites Part A: Applied Science and Manufacturing, vol. 64, pages 115–123, 2014.

[Duc 14c] F. Duc, P. E. Bourban & J. A. E. Månson. *Dynamic mechanical properties of epoxy/flax fibre composites*. Journal of Reinforced Plastics and Composites, vol. 33, no. 17, pages 1625–1633, 2014.

[Duval 15] A. Duval, V. Marcel, L. Dejaeger, F. Lhuillier & M. Khalfallah. *Vibro-acoustic properties of a very long flax fibers reinforced thermoset "flaxpreg" light sandwich*. In SAE Technical Papers, volume 2015-June. SAE International, jun 2015.

[Eder 13] M. Eder, O. Arnould, J. W. Dunlop, J. Hornatowska & L. Salmén. *Experimental micromechanical characterisation of wood cell walls*. Wood Science and Technology, vol. 47, no. 1, pages 163–182, 2013.

[Ege 09] K. Ege, X. Boutillon & B. David. *High-resolution modal analysis*. Journal of Sound and Vibration, vol. 325, no. 4-5, pages 852–869, sep 2009.

[Ehrenstein 12] G. W. Ehrenstein, G. Riedel & P. Trawiel. Thermal analysis of plastics: theory and practice. Carl Hanser Verlag GmbH Co KG, 2012.

[El-Hafidi 17] A. El-Hafidi, P. B. Gning, B. Piezel, M. Belaïd & S. Fontaine. *Determination of dynamic properties of flax fibres reinforced laminate using vibration measurements*. Polymer Testing, vol. 57, pages 219–225, 2017.

[Elsayad 20] K. Elsayad, G. Urstöger, C. Czibula, C. Teichert, J. Gumulec, J. Balvan, M. Pohlt & U. Hirn. *Mechanical Properties of cellulose fibers measured by Brillouin spectroscopy*. Cellulose, pages 1–12, 2020.

[Essabir 13] H. Essabir, A. Elkhaoulani, K. Benmoussa, R. Bouhfid, F. Z. Arrakhiz & A. Qaiss. *Dynamic mechanical thermal behavior analysis of doum fibers reinforced polypropylene composites*. Materials and Design, vol. 51, pages 780–788, 2013.

[Essabir 15] H. Essabir, M. E. Achaby, E. M. Hilali, R. Bouhfid & A. E. Qaiss. *Morphological, Structural, Thermal and Tensile Properties of High Density Polyethylene Composites*

Reinforced with Treated Argan Nut Shell Particles. Journal of Bionic Engineering, vol. 12, no. 1, pages 129–141, 2015.

[Etaati 14] A. Etaati, S. A. Mehdizadeh, H. Wang & S. Pather. *Vibration damping characteristics of short hemp fibre thermoplastic composites*. Journal of Reinforced Plastics and Composites, vol. 33, no. 4, pages 330–341, 2014.

[Fay 91] J. J. Fay, C. J. Murphy, D. A. Thomas & L. H. Sperling. *Effect of morphology, crosslink density, and miscibility on interpenetrating polymer network damping effectiveness*. Polymer Engineering & Science, vol. 31, no. 24, pages 1731–1741, 1991.

[Ferry 80] J. D. Ferry. Viscoelastic properties of polymers. John Wiley & Sons, 1980.

[Fiore 15] V. Fiore, G. Di Bella & A. Valenza. *The effect of alkaline treatment on mechanical properties of kenaf fibers and their epoxy composites*. Composites Part B: Engineering, vol. 68, pages 14–21, 2015.

[Fiore 20] V. Fiore, C. Sanfilippo & L. Calabrese. *Dynamic Mechanical Behavior Analysis of Flax/Jute Fiber-Reinforced Composites under Salt-Fog Spray Environment*. Polymers, vol. 12, no. 3, page 716, mar 2020.

[Fischer-Cripps 11] A. C. Fischer-Cripps. *Applications of Nanoindentation*, 2011.

[Fraga 03] A. N. Fraga, V. A. Alvarez, A. Vázquez & O. De La Osa. *Relationship between dynamic mechanical properties and water absorption of unsaturated polyester and vinyl ester glass fiber composites*. Journal of Composite Materials, vol. 37, no. 17, pages 1553–1574, 2003.

[Fu 01] W. Fu & D. D. L. Chung. *Vibration reduction ability of polymers, particularly polymethylmethacrylate and polytetrafluoroethylene*. Polymers and Polymer Composites, vol. 9, no. 6, pages 423–426, 2001.

[Gao 11a] Y. Gao, Y. Li, Y. Hong, H. Zhang & X. He. *Modeling of the Damping Properties of Unidirectional Carbon Fibre Composites*. Polymers and Polymer Composites, vol. 19, no. 2-3, pages 119–122, 2011.

[Gao 11b] Y. Gao, Y. Li, Y. Hong, H. Zhang & X. He. *Modeling of the damping properties of unidirectional carbon fibre composites*. Polymers and Polymer Composites, vol. 19, no. 2-3, pages 119–122, 2011.

[Gassan 99] J. Gassan & A. K. Bledzki. *Possibilities for improving the mechanical properties of jute/epoxy composites by alkali treatment of fibres.* Composites Science and Technology, vol. 59, no. 9, pages 1303–1309, jul 1999.

[Geethamma 95] V. G. Geethamma, R. Joseph & S. Thomas. *Short coir fiber-reinforced natural rubber composites: Effects of fiber length, orientation, and alkali treatment.* Journal of Applied Polymer Science, vol. 55, no. 4, pages 583–594, 1995.

[Geethamma 05] V. G. Geethamma, G. Kalaprasad, G. Groeninckx & S. Thomas. *Dynamic mechanical behavior of short coir fiber reinforced natural rubber composites.* Composites Part A: Applied Science and Manufacturing, vol. 36, no. 11, pages 1499–1506, nov 2005.

[Gerald Arul Selvan 16] M. Gerald Arul Selvan & A. Athijayamani. *Mechanical properties of fragrant screwpine fiber reinforced unsaturated polyester composite: Effect of fiber length, fiber treatment and water absorption.* Fibers and Polymers, vol. 17, no. 1, pages 104–116, jan 2016.

[Ghasemzadeh 09] S. Ghasemzadeh, V. Haddadi-Asl, S. Kajorncheappunngam, H. V. GangaRao & R. K. Gupta. *Dynamic mechanical study of epoxy, epoxy/glass, and glass/epoxy/wood hybrid composites aged in various media.* Polymer Composites, vol. 30, no. 12, pages 1761–1770, dec 2009.

[Gibson 91] R. Gibson, S. Hwang & H. Kwak. *Micromechanical modeling of damping in composites including interphase effects.* In 36th Intern. SAMPE Symposium, Soc. for the Adv. of Mat. and Process Eng., Covina, pages 592–606, 1991.

[Gibson 92] R. F. Gibson. *Damping characteristics of composite materials and structures.* Journal of Materials Engineering and Performance, vol. 1, no. 1, pages 11–20, feb 1992.

[Gibson 00] R. F. Gibson. *Modal vibration response measurements for characterization of composite materials and structures.* Composites Science and Technology, vol. 60, no. 15, pages 2769–2780, 2000.

[Gibson 14] R. F. Gibson. *A review of recent research on nanoindentation of polymer composites and their constituents.* Composites Science and Technology, vol. 105, pages 51–65, 2014.

[Gindl 04a] W. Gindl & T. Schöberl. *The significance of the elastic modulus of wood cell walls obtained from nanoindentation measurements.* Composites Part A: Applied Science and Manufacturing, vol. 35, no. 11, pages 1345–1349, 2004.

[Gindl 04b] W. Gindl & T. Schöberl. *The significance of the elastic modulus of wood cell walls obtained from nanoindentation measurements*. Composites Part A: Applied Science and Manufacturing, vol. 35, no. 11, pages 1345–1349, 2004.

[Gopalan 19] V. Gopalan, V. Suthenthiraveerappa & V. Pragasam. *Experimental and numerical investigation on the dynamic characteristics of thick laminated plant fiber-reinforced polymer composite plates*. Archive of Applied Mechanics, vol. 89, no. 2, pages 363–384, 2019.

[Gorshkova 10] T. Gorshkova, O. Gurjanov, P. Mikshina, N. Ibragimova, N. Mokshina, V. Salnikov, M. Ageeva, S. Amenitskii, T. Chernova & S. Chemikosova. *Specific type of secondary cell wall formed by plant fibers*. Russian Journal of Plant Physiology, vol. 57, no. 3, pages 328–341, 2010.

[Goubet 02] F. Goubet, P. Jackson, M. J. Deery & P. Dupree. *Polysaccharide analysis using carbohydrate gel electrophoresis. A method to study plant cell wall polysaccharides and polysaccharide hydrolases*. Analytical Biochemistry, vol. 300, no. 1, pages 53–68, jan 2002.

[Grunenfelder 17] L. K. Grunenfelder, A. Dills, T. Centea & S. Nutt. *Effect of prepreg format on defect control in out-of-autoclave processing*. Composites Part A: Applied Science and Manufacturing, vol. 93, pages 88–99, 2017.

[Gu 09] H. Gu. *Dynamic mechanical analysis of the seawater treated glass/polyester composites*. Materials and Design, vol. 30, no. 7, pages 2774–2777, 2009.

[Hadiji 20] H. Hadiji, M. Assarar, W. Zouari, F. Pierre, K. Behlouli, B. Zouari & R. Ayad. *Damping analysis of nonwoven natural fibre-reinforced polypropylene composites used in automotive interior parts*. Polymer Testing, page 106692, 2020.

[Haggui 19] M. Haggui, A. El Mahi, Z. Jendli, A. Akrout & M. Haddar. *Static and fatigue characterization of flax fiber reinforced thermoplastic composites by acoustic emission*. Applied Acoustics, vol. 147, no. June 2017, pages 100–110, 2019.

[Hagnell 19] M. Hagnell & M. Åkermo. *The economic and mechanical potential of closed loop material usage and recycling of fibre-reinforced composite materials*. Journal of Cleaner Production, vol. 223, pages 957–968, jun 2019.

[Hamid 12] M. R. Y. Hamid, M. H. Ab Ghani & S. Ahmad. *Effect of antioxidants and fire retardants as mineral fillers on the physical and mechanical properties of high loading hybrid*

biocomposites reinforced with rice husks and sawdust. Industrial Crops and Products, vol. 40, no. 1, pages 96–102, nov 2012.

[Hardiman 17] M. Hardiman, T. J. Vaughan & C. T. McCarthy. *A review of key developments and pertinent issues in nanoindentation testing of fibre reinforced plastic microstructures*. Composite Structures, vol. 180, pages 782–798, 2017.

[Harris 93] B. Harris, O. G. Braddell, D. P. Almond, C. Lefebvre & J. Verbist. *Study of carbon fibre surface treatments by dynamic mechanical analysis*. Journal of Materials Science, vol. 28, no. 12, pages 3353–3366, jun 1993.

[Hassan 16] M. K. Hassan, S. J. Tucker, A. Abukmail, J. S. Wiggins & K. A. Mauritz. *Polymer chain dynamics in epoxy based composites as investigated by broadband dielectric spectroscopy*. Arabian Journal of Chemistry, vol. 9, no. 2, pages 305–315, 2016.

[Herbert 08] E. G. Herbert, W. C. Oliver & G. M. Pharr. *Nanoindentation and the dynamic characterization of viscoelastic solids*. 2008.

[Hine 19] P. Hine & A. Gusev. *Validating a micromechanical modelling scheme for predicting the five independent viscoelastic constants of unidirectional carbon fibre composites*. International Journal of Engineering Science, vol. 144, page 103133, nov 2019.

[Hiroshi Mizumachi 70] H. M. Hiroshi Mizumachi. *Study of Polymer Blends as a Vibration Damper*. The Journal of Adhesion, vol. 2, no. 4, pages 292–298, oct 1970.

[Hosseinaei 11] O. Hosseinaei, S. Wang, T. G. Rials, C. Xing & Y. Zhang. *Effects of decreasing carbohydrate content on properties of wood strands*. Cellulose, vol. 18, no. 3, pages 841–850, jun 2011.

[Huang 06] G. Huang & H. Lu. *Measurement of Young's relaxation modulus using nanoindentation*. Mechanics of time-dependent materials, vol. 10, no. 3, pages 229–243, 2006.

[Huda 06] M. S. Huda, L. T. Drzal, M. Misra & A. K. Mohanty. *Wood-fiber-reinforced poly(lactic acid) composites: Evaluation of the physicomechanical and morphological properties*. Journal of Applied Polymer Science, vol. 102, no. 5, pages 4856–4869, 2006.

[Hwang 92] S. Hwang & R. Gibson. *Contribution of interlaminar stresses to damping in thick laminated composites under uniaxial extension*. Composite Structures, vol. 20, no. 1, pages 29–35, jan 1992.

[Ismail 19] A. S. Ismail, M. Jawaid & J. Naveen. *Void content, tensile, vibration and acoustic properties of kenaf/bamboo fiber reinforced epoxy hybrid composites*. Materials, vol. 12, no. 13, 2019.

[ISO 01] E. ISO*et al. Plastics—Determination of dynamic mechanical properties. Part 1: General principles*. ISO, 2001.

[J. George 96] S. J. George, S. S. Bhagawan, S. Thomas, J. George, S. S. Bhagawan & S. Thomas. *Thermogravimetric and dynamic mechanical thermal analysis of pineapple fibre reinforced polyethylene composites*. Journal of Thermal Analysis, vol. 47, no. 1, pages 1121–1140, 1996.

[Jawaid 11] M. Jawaid & H. A. Khalil. *Cellulosic/synthetic fibre reinforced polymer hybrid composites: A review*. Carbohydrate polymers, vol. 86, no. 1, pages 1–18, 2011.

[Jawaid 13] M. Jawaid, H. P. Abdul Khalil, A. Hassan, R. Dungani & A. Hadiyane. *Effect of jute fibre loading on tensile and dynamic mechanical properties of oil palm epoxy composites*. Composites Part B: Engineering, vol. 45, no. 1, pages 619–624, 2013.

[Jeannin 19a] T. Jeannin, M. Berges, X. Gabrion, R. Léger, V. Person, S. Corn, B. Piezel, P. Ienny, S. Fontaine & V. Placet. *Influence of hydrothermal ageing on the fatigue behaviour of a unidirectional flax-epoxy laminate*. Composites Part B: Engineering, vol. 174, page 107056, oct 2019.

[Jeannin 19b] T. Jeannin, X. Gabrion, E. Ramasso & V. Placet. *About the fatigue endurance of unidirectional flax-epoxy composite laminates*. Composites Part B: Engineering, vol. 165, pages 690–701, may 2019.

[Jonoobi 10] M. Jonoobi, J. Harun, A. P. Mathew & K. Oksman. *Mechanical properties of cellulose nanofiber (CNF) reinforced polylactic acid (PLA) prepared by twin screw extrusion*. Composites Science and Technology, vol. 70, no. 12, pages 1742–1747, oct 2010.

[Joseph 92] K. Joseph, S. Thomas & C. Pavithran. *Viscoelastic properties of short-sisal-fiber-filled low-density polyethylene composites: effect of fiber length and orientation*. Materials Letters, vol. 15, no. 3, pages 224–228, nov 1992.

[Joseph 93] K. Joseph, S. Thomas, C. Pavithran & M. Brahmakumar. *Tensile properties of short sisal fiber-reinforced polyethylene composites*. Journal of Applied Polymer Science, vol. 47, no. 10, pages 1731–1739, 1993.

[Joseph 10] S. Joseph, S. P. Appukuttan, J. M. Kenny, D. Puglia, S. Thomas & K. Joseph. *Dynamic mechanical properties of oil palm microfibril-reinforced natural rubber composites*. Journal of Applied Polymer Science, vol. 117, no. 3, pages 1298–1308, aug 2010.

[Joshi 04] S. V. Joshi, L. T. Drzal, A. K. Mohanty & S. Arora. *Are natural fiber composites environmentally superior to glass fiber reinforced composites ?* Composites Part A: Applied Science and Manufacturing, vol. 35, no. 3, pages 371–376, apr 2004.

[Karaduman 14] Y. Karaduman, M. M. A. Sayeed, L. Onal & A. Rawal. *Viscoelastic properties of surface modified jute fiber/polypropylene nonwoven composites*. Composites Part B: Engineering, vol. 67, pages 111–118, 2014.

[Keryvin 15a] V. Keryvin, M. Lan, A. Bourmaud, T. Parenteau, L. Charleux & C. Baley. *Analysis of flax fibres viscoelastic behaviour at micro and nano scales*. Composites Part A: Applied Science and Manufacturing, vol. 68, pages 219–225, 2015.

[Keryvin 15b] V. Keryvin, M. Lan, A. Bourmaud, T. Parenteau, L. Charleux & C. Baley. *Analysis of flax fibres viscoelastic behaviour at micro and nano scales*. Composites Part A: Applied Science and Manufacturing, vol. 68, pages 219–225, 2015.

[Khalfallah 14] M. Khalfallah, B. Abbès, F. Abbès, Y. Q. Guo, V. Marcel, A. Duval, F. Vanfleteren & F. Rousseau. *Innovative flax tapes reinforced Acrodur biocomposites: A new alternative for automotive applications*. Materials and Design, vol. 64, 2014.

[Khelfa 15] H. Khelfa. *Identification des propriétés d'élasticité et d'amortissement d'une fibre isolée anisotrope par ultrasons laser: ouverture au cas des fibres naturelles*. PhD thesis, Le Mans, 2015.

[Kishi 04] H. Kishi, M. Kuwata, S. Matsuda, T. Asami & A. Murakami. *Damping properties of thermoplastic-elastomer interleaved carbon fiber-reinforced epoxy composites*. Composites Science and Technology, vol. 64, no. 16, pages 2517–2523, dec 2004.

[Kollia 19] A. Kollia, L. C. Kontaxis, G. C. Papanicolaou & S. P. Zaoutsos. *Effect of thermal shock cycling on the quasi-static and dynamic flexural properties of flax fabric-epoxy matrix laminates*. Journal of Applied Polymer Science, vol. 48529, pages 1–9, 2019.

[Koruk 12] H. Koruk & K. Y. Sanliturk. *Identification and removal of adverse effects of non-contact electromagnetic excitation in Oberst Beam Test Method.* Mechanical Systems and Signal Processing, vol. 30, pages 274–295, jul 2012.

[Kramer 01] A. A. Kramer Volinsky, N. Moody & W. Gerberich. *Substrate effects on indentation plastic zone development in thin soft films. J. Mater. Res. 16, 3150-3157.* J. Mater. Res, vol. 16, no. 11, 2001.

[Kuzak 99] S. G. Kuzak & A. Shanmugam. *Dynamic mechanical analysis of fiber-reinforced phenolics.* Journal of Applied Polymer Science, vol. 73, no. 5, pages 649–658, 1999.

[Lakes 98] R. S. Lakes. Viscoelastic solids, volume 9. CRC press, 1998.

[Landel 93] R. F. Landel & L. E. Nielsen. Mechanical properties of polymers and composites. CRC press, 1993.

[Launay 13] A. Launay, Y. Marco, M. H. Maitournam & I. Raoult. *Modelling the influence of temperature and relative humidity on the time-dependent mechanical behaviour of a short glass fibre reinforced polyamide.* Mechanics of Materials, vol. 56, pages 1–10, jan 2013.

[Le Duigou 14] A. Le Duigou, A. Bourmaud, P. Davies & C. Baley. *Long term immersion in natural seawater of Flax/PLA biocomposite.* Ocean Engineering, vol. 90, pages 140–148, 2014.

[le Duigou 17] A. le Duigou, J. Merotte, A. Bourmaud, P. Davies, K. Belhouli & C. Baley. *Hygroscopic expansion: A key point to describe natural fibre/polymer matrix interface bond strength.* Composites Science and Technology, vol. 151, pages 228–233, oct 2017.

[Le Guen 16] M. J. Le Guen, R. H. Newman, A. Fernyhough, G. W. Emms & M. P. Staiger. *The damping-modulus relationship in flax-carbon fibre hybrid composites.* Composites Part B: Engineering, vol. 89, pages 27–33, 2016.

[Leitner 17] A. Leitner, V. Maier-Kiener & D. Kiener. *Dynamic nanoindentation testing: is there an influence on a material's hardness ?* Materials Research Letters, vol. 5, no. 7, pages 486–493, 2017.

[Li 02] X. Li & B. Bhushan. *A review of nanoindentation continuous stiffness measurement technique and its applications.* Materials characterization, vol. 48, no. 1, pages 11–36, 2002.

[Li 05] Z. Li & M. J. Crocker. *A review on vibration damping in sandwich composite structures.* International Journal of Acoustics and Vibration, vol. 10, no. 4, pages 159–169, 2005.

[Li 07] X. Li, L. G. Tabil & S. Panigrahi. *Chemical treatments of natural fiber for use in natural fiber-reinforced composites: A review.* Journal of Polymers and the Environment, vol. 15, no. 1, pages 25–33, jan 2007.

[Li 16] Y. Li & B. Xue. *Hydrothermal ageing mechanisms of unidirectional flax fabric reinforced epoxy composites.* Polymer degradation and stability, vol. 126, pages 144–158, 2016.

[Li 17a] Q. Li, Y. Li & L. Zhou. *Nanoscale evaluation of multilayer interfacial mechanical properties of sisal fiber reinforced composites by nanoindentation technique.* Composites Science and Technology, vol. 152, pages 211–221, 2017.

[Li 17b] Q. Li, Y. Li & L. Zhou. *Nanoscale evaluation of multilayer interfacial mechanical properties of sisal fiber reinforced composites by nanoindentation technique.* Composites Science and Technology, vol. 152, pages 211–221, nov 2017.

[Li 17c] Y. Li, S. Cai & X. Huang. *Multi-scaled enhancement of damping property for carbon fiber reinforced composites.* Composites Science and Technology, vol. 143, pages 89–97, 2017.

[Li 18] Y. Li, X. Yi, T. Yu & G. Xian. *An overview of structural-functional-integrated composites based on the hierarchical microstructures of plant fibers.* Advanced Composites and Hybrid Materials, vol. 1, no. 2, pages 231–246, 2018.

[Liang 10] Z. Liang, P. Pan, B. Zhu, T. Dong & Y. Inoue. *Mechanical and thermal properties of poly(butylene succinate)/plant fiber biodegradable composite.* Journal of Applied Polymer Science, vol. 115, no. 6, pages 3559–3567, mar 2010.

[Liang 14] S. Liang, P.-B. Gning & L. Guillaumat. *Properties evolution of flax/epoxy composites under fatigue loading.* International Journal of Fatigue, vol. 63, pages 36–45, 2014.

[Liao 18] G. Liao, Z. Li, Y. Cheng, D. Xu, D. Zhu, S. Jiang, J. Guo, X. Chen, G. Xu & Y. Zhu. *Properties of oriented carbon fiber/polyamide 12 composite parts fabricated by fused deposition modeling.* Materials & Design, vol. 139, pages 283–292, 2018.

[Liu 18] J. Liu, W. Zhu, Z. Yu & X. Wei. *Dynamic shear-lag model for understanding the role of matrix in energy dissipation in fiber-reinforced composites.* Acta Biomaterialia, vol. 74, pages 270–279, 2018.

[Lomov 11] S. V. Lomov. Non-crimp fabric composites: manufacturing, properties and applications. Elsevier, 2011.

[López-Aenlle 19] M. López-Aenlle, A. Noriega & F. Pelayo. *Mechanical characterization of polyvinil butyral from static and modal tests on laminated glass beams.* Composites Part B: Engineering, vol. 169, no. February, pages 9–18, 2019.

[Lu 97] Y. Lu & D. Shinozaki. *Microindentation testing of inhomogeneous microstructures in welded polyethylene.* Polymer Engineering & Science, vol. 37, no. 11, pages 1815–1824, 1997.

[Lu 19] M. M. Lu & A. W. Van Vuure. *Improving moisture durability of flax fibre composites by using non-dry fibres.* Composites Part A: Applied Science and Manufacturing, vol. 123, pages 301–309, aug 2019.

[Machado 16] J. S. Machado, S. Santos, F. F. S. Pinho, F. Luís, A. Alves, R. Simões, C. Rodrigues & J. C. Rodrigues. *Impact of high moisture conditions on the serviceability performance of wood plastic composite decks.* Materials and Design, vol. 103, pages 122–131, aug 2016.

[Madera-Santana 09] T. J. Madera-Santana, M. Misra, L. T. Drzal, D. Robledo & Y. Freile-Pelegrin. *Preparation and characterization of biodegradable agar/poly(butylene adipateco-terephatalate) composites.* Polymer Engineering and Science, vol. 49, no. 6, pages 1117–1126, jun 2009.

[Maeda 72] M. Maeda. Heat conduction, volume 16. CRC Press, sep 1972.

[Mahmoudi 19] S. Mahmoudi, A. Kervoelen, G. Robin, L. Duigou, E. M. Daya & J. M. Cadou. *Experimental and numerical investigation of the damping of flax–epoxy composite plates.* Composite Structures, vol. 208, no. April 2018, pages 426–433, 2019.

[Mallick 07] P. Mallick. Fiber-reinforced composites: materials, manufacturing, and design. CRC Press, Boca Raton, third edit edition, 2007.

[Marchetti 20] F. Marchetti, K. Ege, Q. Leclere & N. B. Roozen. *On the structural dynamics of laminated composite plates and sandwich structures ; a new perspective on damping identification.* Elsevier, 2020.

[Margem 10] F. M. Margem, S. N. Monteiro, J. B. Neto, R. J. S. Rodriguez & B. G. Soares. *The dynamic-Mechanical behavior of epoxy matrix composites reinforced with ramie fibers*. 65th ABM International Congress, 18th IFHTSE Congress and 1st TMS/ABM International Materials Congress 2010, vol. 6, no. 2, pages 5003–5011, 2010.

[Martin 16] N. Martin, P. Davies & C. Baley. *Evaluation of the potential of three non-woven flax fiber reinforcements: Spunlaced, needlepunched and paper process mats*. Industrial Crops and Products, vol. 83, pages 194–205, 2016.

[Martínez-Hernández 07] A. L. Martínez-Hernández, C. Velasco-Santos, M. De-Icaza & V. M. Castaño. *Dynamical-mechanical and thermal analysis of polymeric composites reinforced with keratin biofibers from chicken feathers*. Composites Part B: Engineering, vol. 38, no. 3, pages 405–410, 2007.

[Matter 09] M. Matter, T. Gmür, J. Cugnoni & A. Schorderet. *Numerical-experimental identification of the elastic and damping properties in composite plates*. Composite Structures, vol. 90, no. 2, pages 180–187, 2009.

[Mazuki 11] A. A. M. Mazuki, H. M. Akil, S. Safiee, Z. A. M. Ishak & A. A. Bakar. *Degradation of dynamic mechanical properties of pultruded kenaf fiber reinforced composites after immersion in various solutions*. Composites Part B: Engineering, vol. 42, no. 1, pages 71–76, 2011.

[Melelli 19] A. Melelli, O. Arnould, G. Roselli, G. Di Girolami, F. Jamme, J. Beaugrand & A. Bourmaud. *Investigation of flax yarns from italian paintings using AFM mechanical characterization*. 2019.

[Menard 08] K. P. Menard. Dynamic Mechanical Analysis. CRC Press, may 2008.

[Menrad 08] K. Menrad. *Dynamic Mechanical Analysis: A Practical Introduction*. 2008.

[Mishra 12] I. Mishra & S. K. Sahu. *An experimental approach to free vibration response of woven fiber composite plates under free-free boundary condition*. International Journal of Advanced Technology in Civil Engineering, vol. 1, no. 2, pages 67–72, 2012.

[Mizumachi 70] H. Mizumachi. *Study of Polymer Blends as a Vibration Damper*. The Journal of Adhesion, vol. 2, no. 4, pages 292–298, 1970.

[Mofokeng 12] J. P. Mofokeng, A. Luyt, T. Tábi & J. Kovács. *Comparison of injection moulded, natural fibre-reinforced composites with PP and PLA as matrices.* Journal of Thermoplastic Composite Materials, vol. 25, no. 8, pages 927–948, 2012.

[Mohanty 06] S. Mohanty, S. K. Verma & S. K. Nayak. *Dynamic mechanical and thermal properties of MAPE treated jute/HDPE composites.* Composites Science and Technology, vol. 66, no. 3-4, pages 538–547, mar 2006.

[Montazeri 12] A. Montazeri, K. Pourshamsian & M. Riazian. *Viscoelastic properties and determination of free volume fraction of multi-walled carbon nanotube/epoxy composite using dynamic mechanical thermal analysis.* Materials and Design, vol. 36, pages 408–414, apr 2012.

[Monti 16] A. Monti, A. El Mahi, Z. Jendli & L. Guillaumat. *Mechanical behaviour and damage mechanisms analysis of a flax-fibre reinforced composite by acoustic emission.* Composites Part A: Applied Science and Manufacturing, vol. 90, pages 100–110, nov 2016.

[Monti 17] A. Monti, A. El Mahi, Z. Jendli & L. Guillaumat. *Experimental and finite elements analysis of the vibration behaviour of a bio-based composite sandwich beam.* Composites Part B: Engineering, vol. 110, pages 466–475, 2017.

[Mukherjee 84] P. S. Mukherjee & K. G. Satyanarayana. *Structure and properties of some vegetable fibres - Part 1 Sisal fibre.* Journal of Materials Science, vol. 19, no. 12, pages 3925–3934, dec 1984.

[Multiphysics 98] C. Multiphysics. *Introduction to COMSOL multiphysics®.* COMSOL Multiphysics, Burlington, MA, accessed Feb, vol. 9, page 2018, 1998.

[Munde 19] Y. S. Munde, R. B. Ingle & I. Siva. *A comprehensive review on the vibration and damping characteristics of vegetable fiber-reinforced composites.* Journal of Reinforced Plastics and Composites, vol. 38, no. 17, pages 822–832, 2019.

[Mylsamy 11] K. Mylsamy & I. Rajendran. *The mechanical properties, deformation and thermomechanical properties of alkali treated and untreated Agave continuous fibre reinforced epoxy composites.* Materials and Design, vol. 32, no. 5, pages 3076–3084, 2011.

[Navin 94] C. Navin, P. K. Rohatgi*et al.* Natural fibres and their composites. Periodical Experts Book Agency, 1994.

[Nelson 78] D. J. Nelson & J. W. Hancock. *Interfacial slip and damping in fibre reinforced composites*. Journal of Materials Science, vol. 13, no. 11, pages 2429–2440, nov 1978.

[Nguyen 16] X. T. Nguyen, S. Hou, T. Liu & X. Han. *A potential natural energy absorption material – Coconut mesocarp: Part A: Experimental investigations on mechanical properties*. International Journal of Mechanical Sciences, vol. 115-116, pages 564–573, sep 2016.

[Nix 98] W. D. Nix & H. Gao. *Indentation size effects in crystalline materials: a law for strain gradient plasticity*. Journal of the Mechanics and Physics of Solids, vol. 46, no. 3, pages 411–425, 1998.

[Oberst 52] H. Oberst & K. Frankenfeld. *Über die Dämpfung der Biegeschwingungen dünner Bleche durch fest haftende Beläge*. Acta Acustica united with Acustica, vol. 2, no. 6, pages 181–194, 1952.

[Odegard 05] G. M. Odegard, T. S. Gates & H. M. Herring. *<CHARACTERIZATION OF VISCOELASTIC PROPERTIES OF POLYMERIC MATERIALS THROUGH NANOINDENTATION.pdf>*. vol. 45, no. 2, pages 130–136, 2005.

[Oliver 92] W. C. Oliver & G. M. Pharr. *An improved technique for determining hardness and elastic modulus using load and displacement sensing indentation experiments*. Journal of materials research, vol. 7, no. 6, pages 1564–1583, 1992.

[Otaigbe 91] J. U. Otaigbe. *Dynamic mechanical response of a thermoplastic sheet molding compound-glass fiber composite*. Polymer Engineering & Science, vol. 31, no. 2, pages 104–109, 1991.

[Ouisse 19] M. Ouisse, D. Renault, P. Butaud, E. Sadoulet & E. Sadoulet-Reboul. *Damping control for improvement of acoustic black hole effect*. Journal of Sound and Vibration, pages 63–72, 2019.

[Pan 08] P. Pan, B. Zhu, T. Dong, S. Serizawa, M. Iji & Y. Inoue. *Kenaf fiber/poly(ε-caprolactone) biocomposite with enhanced crystallization rate and mechanical properties*. Journal of Applied Polymer Science, vol. 107, no. 6, pages 3512–3519, mar 2008.

[Peeters Bart 04] G. P. L. J. Peeters Bart Van der Auweraer Herman. *The PolyMAX frequency-domain method: a new standard for modal parameter estimation ?* Shock and Vibration, vol. 11, no. 3,4, pages 395–409, 2004.

[Péron 19] M. Péron, A. Célino, M. Castro, F. Jacquemin & A. L. Duigou. *Study of hygroscopic stresses in asymmetric biocomposite laminates*. Composites Science and Technology, vol. 169, no. September 2018, pages 7–15, 2019.

[Perrier 16] A. Perrier, E. Le Bourhis, F. Touchard & L. Chocinski-Arnault. *Effect of water ageing on nanoindentation response of single hemp yarn/epoxy composites*. Composites Part A: Applied Science and Manufacturing, vol. 84, pages 216–223, 2016.

[Perrier 17] A. Perrier, F. Touchard, L. Chocinski-Arnault & D. Mellier. *Influence of water on damage and mechanical behaviour of single hemp yarn composites*. Polymer Testing, vol. 57, pages 17–25, feb 2017.

[Pertegás 16] S. L. Pertegás, A. Anusic, K. Resch & R. Schledjewski. *Green Composites: Challenges to reach high performance components*. In 17th European Conference on Composite Materials. ECCM17, 2016.

[Pethica 88] J. Pethica & W. Oliver. *Mechanical properties of nanometre volumes of material: use of the elastic response of small area indentations*. MRS Online Proceedings Library Archive, vol. 130, 1988.

[Pinto 20] F. Pinto, L. Boccarusso, D. De Fazio, S. Cuomo, M. Durante & M. Meo. *Carbon/hemp bio-hybrid composites: Effects of the stacking sequence on flexural, damping and impact properties*. Composite Structures, vol. 242, page 112148, jun 2020.

[Piranda 94] J. Piranda. *Manuel d'utilisation du logiciel MODAN*. Laboratoire de Mécanique Appliquée R. Chaléat, Université de Franche-Comté, Besançon, vol. 35, page 134, 1994.

[Placet 09] V. Placet. *Characterization of the thermo-mechanical behaviour of Hemp fibres intended for the manufacturing of high performance composites*. Composites Part A: Applied Science and Manufacturing, vol. 40, no. 8, pages 1111–1118, 2009.

[Placet 10a] V. Placet & E. Foltête. *Is dynamic mechanical analysis (DMA) a non-resonance technique ?* EPJ Web of Conferences, vol. 6, page 41004, jun 2010.

[Placet 10b] V. Placet. *Tensile behaviour of natural fibres. Effect of loading rate, temperature and humidity on the "accommodation" phenomena*. In EPJ Web of Conferences, volume 6, page 20001. EDP Sciences, 2010.

[Poon 08] B. Poon, D. Rittel & G. Ravichandran. *An analysis of nanoindentation in linearly elastic solids*. International Journal of Solids and Structures, vol. 45, no. 24, pages 6018–6033, 2008.

[Pothan 03] L. A. Pothan, Z. Oommen & S. Thomas. *Dynamic mechanical analysis of banana fiber reinforced polyester composites*. Composites Science and Technology, vol. 63, no. 2, pages 283–293, feb 2003.

[Pothan 08] L. A. Pothan, Y. Mai, S. Thomas & R. Li. *Tensile and flexural behavior of sisal fabric/polyester textile composites prepared by resin transfer molding technique*. Journal of Reinforced Plastics and Composites, vol. 27, no. 16-17, pages 1847–1866, 2008.

[Rahman 17a] M. Z. Rahman, K. Jayaraman & B. R. Mace. *Vibration damping of flax fibre-reinforced polypropylene composites*. Fibers and Polymers, vol. 18, no. 11, pages 2187–2195, 2017.

[Rahman 17b] M. Rahman, K. Jayaraman & B. Mace. *Vibration damping of flax fibre-reinforced polypropylene composites*. Fibers and Polymers, vol. 18, no. 11, pages 2187–2195, 2017.

[Rajesh 16a] M. Rajesh & J. Pitchaimani. *Dynamic mechanical analysis and free vibration behavior of intra-ply woven natural fiber hybrid polymer composite*. Journal of Reinforced Plastics and Composites, vol. 35, no. 3, pages 228–242, 2016.

[Rajesh 16b] M. Rajesh & J. Pitchaimani. *Polyvinyl Alcohol-Modified Pithecellobium Clypearia Benth Herbal Residue FiberPolypropylene Composites*. Polymer Composites, vol. 37, no. 1, pages 915–924, 2016.

[Rajeshkumar 14] G. Rajeshkumar & V. Hariharan. *Free vibration characteristics of Phoenix Sp fiber reinforced polymer matrix composite beams*. Procedia Engineering, vol. 97, pages 687–693, 2014.

[Ramesh 19] M. Ramesh. *Flax (Linum usitatissimum L.) fibre reinforced polymer composite materials: A review on preparation, properties and prospects*. Progress in Materials Science, vol. 102, no. December 2018, pages 109–166, 2019.

[Rao 97] M. D. Rao, R. Echempati & S. Nadella. *Dynamic analysis and damping of composite structures embedded with viscoelastic layers*. Composites Part B: Engineering, vol. 28, no. 5-6, pages 547–554, 1997.

[Ray 02] D. Ray, B. K. Sarkar, S. Das & A. K. Rana. *Dynamic mechanical and thermal analysis of vinylester-resin-matrix composites reinforced with untreated and alkali-treated jute fibres*. Composites Science and Technology, vol. 62, no. 7-8, pages 911–917, 2002.

[Reinders] M. Reinders. *HempFlax Non-Wovens*. https://www.hempflax.com/en/applications/industrialapplications/non-wovens.

[Rezaei 09] F. Rezaei, R. Yunus & N. Ibrahim. *Effect of fiber length on thermomechanical properties of short carbon fiber reinforced polypropylene composites*. Materials & Design, vol. 30, no. 2, pages 260–263, 2009.

[Rong 01] M. Z. Rong, M. Q. Zhang, Y. Liu, G. C. Yang & H. M. Zeng. *The effect of fiber treatment on the mechanical properties of unidirectional sisal-reinforced epoxy composites*. Composites Science and Technology, vol. 61, no. 10, pages 1437–1447, aug 2001.

[Rouf 17] K. Rouf, N. L. Denton & R. M. French. *Effect of fabric weaves on the dynamic response of two-dimensional woven fabric composites*. Journal of Materials Science, vol. 52, no. 17, pages 10581–10591, 2017.

[Rueppel 17] M. Rueppel, J. Rion, C. Dransfeld, C. Fischer & K. Masania. *Damping of carbon fibre and flax fibre angle-ply composite laminates*. Composites Science and Technology, vol. 146, pages 1–9, 2017.

[Saba 16] N. Saba, M. Jawaid, O. Y. Alothman & M. T. Paridah. *A review on dynamic mechanical properties of natural fibre reinforced polymer composites*. Construction and Building Materials, vol. 106, pages 149–159, mar 2016.

[Saha 99] A. K. Saha, S. Das, D. Bhatta & B. C. Mitra. *Study of Jute Fiber Reinforced Polyester Composites by Dynamic Mechanical Analysis*. Journal of Applied Polymer Science, vol. 71, no. 9, pages 1505–1513, feb 1999.

[Sala 20] B. Sala & V. G.-R. V. P. Xavier Gabrion Frederique Trivaudey. *Influence of the stress level and hygrothermal conditions on the creep/recovery behaviour of high-grade flax and hemp fibre reinforced GreenPoxy matrix composites*. Composites Part A: Applied Science and Manufacturing, vol. 00, pages 000–000, 2020.

[Salleh 14] F. M. Salleh, A. Hassan, R. Yahya & A. D. Azzahari. *Effects of extrusion temperature on the rheological, dynamic mechanical and tensile properties of kenaf fiber/HDPE composites*. Composites Part B: Engineering, vol. 58, pages 259–266, 2014.

[Saravana Bavan 10] D. Saravana Bavan & G. Mohan Kumar. *Potential use of natural fiber composite materials in India*. Journal of Reinforced Plastics and Composites, vol. 29, no. 24, pages 3600–3613, dec 2010.

[Sargianis 13] J. J. Sargianis, H. I. Kim, E. Andres & J. Suhr. *Sound and vibration damping characteristics in natural material based sandwich composites*. Composite Structures, vol. 96, pages 538–544, 2013.

[Sathishkumar 14] T. Sathishkumar, J. Naveen, & S. Satheeshkumar. *Hybrid fiber reinforced polymer composites–a review*. Journal of Reinforced Plastics and Composites, vol. 33, no. 5, pages 454–471, 2014.

[Sathishkumar 17] T. P. Sathishkumar, J. Naveen, P. Navaneethakrishnan, S. Satheeshkumar & N. Rajini. *Characterization of sisal/cotton fibre woven mat reinforced polymer hybrid composites*. Journal of Industrial Textiles, vol. 47, no. 4, pages 429–452, nov 2017.

[Sathishkumar 18] G. Sathishkumar, S. Sivabalan, S. Joseph Irudaya Raja & S. Sivaganesan. *Vibration and viscoelastic characteristics of sisal fiber reinforced polyester composite*. International Journal of Mechanical and Production Engineering Research and Development, vol. 2018, no. Special Issue, pages 329–338, 2018.

[Saxena 11] M. Saxena, A. Pappu, R. Haque & A. Sharma. *Sisal Fiber Based Polymer Composites and Their Applications*. In Cellulose Fibers: Bio- and Nano-Polymer Composites, pages 589–659. Springer Berlin Heidelberg, 2011.

[Schrank 17] V. Schrank, M. Beer, M. Beckers & T. Gries. Polymer-optical fibre (pof) integration into textile fabric structures. Elsevier, 2017.

[Senthil Kumar 14] K. Senthil Kumar, I. Siva, P. Jeyaraj, J. T. Winowlin Jappes, S. C. Amico & N. Rajini. *Synergy of fiber length and content on free vibration and damping behavior of natural fiber reinforced polyester composite beams*. Materials and Design, vol. 56, pages 379–386, 2014.

[Senthil Kumar 16] K. Senthil Kumar, I. Siva, N. Rajini, J. T. Winowlin Jappes & S. C. Amico. *Layering pattern effects on vibrational behavior of coconut sheath/banana fiber hybrid composites*. Materials and Design, vol. 90, pages 795–803, jan 2016.

[Senthilkumar 17] K. Senthilkumar, I. Siva, M. T. H. Sultan, N. Rajini, S. Siengchin, M. Jawaid & A. Hamdan. *Static and dynamic properties of sisal fiber polyester composites - Effect of interlaminar fiber orientation*. BioResources, vol. 12, no. 4, pages 7819–7833, nov 2017.

[Senthilrajan 19a] S. Senthilrajan & N. Venkateshwaran. *Ageing and Its Influence on Vibration Characteristics of Jute/Polyester Composites*. Journal of Polymers and the Environment, vol. 27, no. 10, pages 2144–2155, 2019.

[Senthilrajan 19b] S. Senthilrajan & N. Venkateshwaran. *Ageing and Its Influence on Vibration Characteristics of Jute/Polyester Composites*. Journal of Polymers and the Environment, vol. 27, no. 10, pages 2144–2155, 2019.

[Shah 13] D. U. Shah. *Developing plant fibre composites for structural applications by optimising composite parameters: a critical review*. Journal of materials science, vol. 48, no. 18, pages 6083–6107, 2013.

[Shah 14] D. U. Shah. *Natural fibre composites: Comprehensive Ashby-type materials selection charts*. Materials and Design, vol. 62, pages 21–31, oct 2014.

[Shen 04] L. Shen, I. Y. Phang, T. Liu & K. Zeng. *Nanoindentation and morphological studies on nylon 66/organoclay nanocomposites. II. Effect of strain rate*. Polymer, vol. 45, no. 24, pages 8221–8229, 2004.

[Shen 06] L. Shen, L. Wang, T. Liu & C. He. *Nanoindentation and morphological studies of epoxy nanocomposites*. Macromolecular Materials and Engineering, vol. 291, no. 11, pages 1358–1366, 2006.

[Shen 12] L. Shen, W. C. D. Cheong, Y. L. Foo & Z. Chen. *Nanoindentation creep of tin and aluminium: A comparative study between constant load and constant strain rate methods*. Materials Science and Engineering: A, vol. 532, pages 505–510, 2012.

[Shinoj 11] S. Shinoj, R. Visvanathan, S. Panigrahi & N. Varadharaju. *Dynamic mechanical properties of oil palm fibre (OPF)-linear low density polyethylene (LLDPE) biocomposites and study of fibre-matrix interactions*. Biosystems Engineering, vol. 109, no. 2, pages 99–107, 2011.

[Shinozaki 97] D. Shinozaki & Y. Lu. *Micro-indentation relaxation measurements in polymer thin films.* Journal of Electronic Materials, vol. 26, no. 7, pages 852–858, 1997.

[Singh 08] S. P. Singh, J. F. Smith & R. P. Singh. *Characterization of the damping behavior of a nanoindentation instrument for carrying out dynamic experiments.* Experimental Mechanics, vol. 48, no. 5, pages 571–583, 2008.

[Song 12] Y. S. Song, J. T. Lee, D. S. Ji, M. W. Kim, S. H. Lee & J. R. Youn. *Viscoelastic and thermal behavior of woven hemp fiber reinforced poly lactic acid composites.* Composites Part B, vol. 3, no. 43, pages 856–860, 2012.

[Sreenivasan 15] V. S. Sreenivasan, N. Rajini, A. Alavudeen & V. Arumugaprabu. *Dynamic mechanical and thermo-gravimetric analysis of Sansevieria cylindrica/polyester composite: Effect of fiber length, fiber loading and chemical treatment.* Composites Part B: Engineering, vol. 69, pages 76–86, 2015.

[Su 09] H. Su. *Acoustic emission analysis of compressive properties of multidirectional filament wound composite material tubes.* In Proceedings - 2009 International Conference on Information Engineering and Computer Science, ICIECS 2009, 2009.

[Subramanian 11] C. Subramanian, S. B. Deshpande & S. Senthilvelan. *Effect of reinforced fiber length on the damping performance of thermoplastic composites.* Advanced Composite Materials, vol. 20, no. 4, pages 319–335, 2011.

[Suresh Kumar 14] S. M. Suresh Kumar, D. Duraibabu & K. Subramanian. *Studies on mechanical, thermal and dynamic mechanical properties of untreated (raw) and treated coconut sheath fiber reinforced epoxy composites.* Materials and Design, vol. 59, pages 63–69, 2014.

[Tahan Latibari 13] S. Tahan Latibari, M. Mehrali, L. Mottahedin, A. Fereidoon & H. S. C. Metselaar. *Investigation of interfacial damping nanotube-based composite.* Composites Part B: Engineering, vol. 50, pages 354–361, 2013.

[Tajvidi 10] M. Tajvidi, N. Motie, G. Rassam, R. H. Falk & C. Felton. *Mechanical performance of hemp fiber polypropylene composites at different operating temperatures.* Journal of Reinforced Plastics and Composites, vol. 29, no. 5, pages 664–674, 2010.

[Tanguy 16] M. Tanguy, A. Bourmaud & C. Baley. *Plant cell walls to reinforce composite materials: Relationship between nanoindentation and tensile modulus.* Materials Letters, vol. 167, pages 161–164, 2016.

[Theotokoglou 15] E. E. Theotokoglou, I. Giannopoulos & E. Sideridis. *Analytical, experimental and numerical approach of storage and loss moduli of fibre reinforced epoxy composites.* ICCM International Conferences on Composite Materials, vol. 2015-July, no. July, pages 19–24, 2015.

[Thiruchitrambalam 12] M. Thiruchitrambalam, A. Alavudeen & N. Venkateshwaran. *Review on kenaf fiber composites.* Reviews on Advanced Materials Science, vol. 32, no. 2, pages 106–112, 2012.

[Towo 08] A. N. Towo & M. P. Ansell. *Fatigue evaluation and dynamic mechanical thermal analysis of sisal fibre-thermosetting resin composites.* Composites Science and Technology, vol. 68, no. 3-4, pages 925–932, 2008.

[Treviso 15] A. Treviso, B. Van Genechten, D. Mundo & M. Tournour. *Damping in composite materials: Properties and models.* Composites Part B: Engineering, vol. 78, pages 144–152, aug 2015.

[Tung 92] C.-J. Tung & T.-C. J. Hsu. *Vibration damping with urethane/acrylate simultaneous semi-interpenetrating polymer networks.* Journal of Applied Polymer Science, vol. 46, no. 10, pages 1759–1773, 1992.

[Tze 07] W. T. Tze, S. Wang, T. G. Rials, G. M. Pharr & S. S. Kelley. *Nanoindentation of wood cell walls: Continuous stiffness and hardness measurements.* Composites Part A: Applied Science and Manufacturing, vol. 38, no. 3, pages 945–953, 2007.

[Ungar 62] E. E. Ungar & E. M. Kerwin Jr. *Loss factors of viscoelastic systems in terms of energy concepts.* The Journal of the acoustical Society of America, vol. 34, no. 7, pages 954–957, 1962.

[Väisänen 17] T. Väisänen, O. Das & L. Tomppo. *A review on new bio-based constituents for natural fiber-polymer composites.* Journal of Cleaner Production, vol. 149, pages 582–596, 2017.

[Van Hazendonk 96] J. M. Van Hazendonk, E. J. Reinerik, P. De Waard & J. E. Van Dam. *Structural analysis of acetylated hemicellulose polysaccharides from fibre flax (Linum usitatissimum L.).* Carbohydrate Research, vol. 291, pages 141–154, sep 1996.

[Viala 18] R. Viala, V. Placet & S. Cogan. *Identification of the anisotropic elastic and damping properties of complex shape composite parts using an inverse method based on finite element model updating and 3D velocity fields measurements (FEMU-3DVF): Application to bio-based composite violin soundboards.* Composites Part A: Applied Science and Manufacturing, vol. 106, pages 91–103, mar 2018.

[Wang 00] B. Wang & M. Yang. *Damping of honeycomb sandwich beams.* Journal of Materials Processing Technology, vol. 105, no. 1, pages 67–72, sep 2000.

[Wang 19] X. Wang & M. Petru. *Effect of hygrothermal aging and surface treatment on the dynamic mechanical behavior of flax fiber reinforced composites.* Materials, vol. 12, no. 15, page 2376, 2019.

[Wielage 03] B. Wielage, T. Lampke, H. Utschick & F. Soergel. *Processing of natural-fibre reinforced polymers and the resulting dynamic-mechanical properties.* Journal of Materials Processing Technology, vol. 139, no. 1-3 SPEC, pages 140–146, aug 2003.

[Wingard 90] C. D. Wingard & C. L. Beatty. *Crosslinking of an epoxy with a mixed amine as a function of stoichiometry. II. Final properties via dynamic mechanical spectroscopy.* Journal of Applied Polymer Science, vol. 41, no. 1112, pages 2539–2554, jan 1990.

[Yadav 19] A. Yadav & M. K. Gupta. *Development and characterization of jute composites for sustainable product: Effect of chemical treatments and polymer coating.* Materials Research Express, nov 2019.

[Yan 14] L. Yan, N. Chouw & K. Jayaraman. *Flax fibre and its composites - A review.* Composites Part B: Engineering, vol. 56, pages 296–317, 2014.

[Yan 16] L. Yan, B. Kasal & L. Huang. *A review of recent research on the use of cellulosic fibres, their fibre fabric reinforced cementitious, geo-polymer and polymer composites in civil engineering.* Composites Part B: Engineering, vol. 92, pages 94–132, may 2016.

[Yu 10] T. Yu, J. Ren, S. Li, H. Yuan & Y. Li. *Effect of fiber surface-treatments on the properties of poly(lactic acid)/ramie composites.* Composites Part A: Applied Science and Manufacturing, vol. 41, no. 4, pages 499–505, apr 2010.

[Zahari 15] W. Zahari, R. Badri, H. Ardyananta, D. Kurniawan & F. Nor. *Mechanical Properties and Water Absorption Behavior of Polypropylene / Ijuk Fiber Composite by Using Silane Treatment*. Procedia Manufacturing, vol. 2, pages 573–578, 2015.

[Zai 09] B. A. Zai, M. K. Park, H. S. Choi, H. Mehboob & R. Ali. *Effect of moisture absorption on damping and dynamic stiffness of carbon fiber/epoxy composites*. Journal of Mechanical Science and Technology, vol. 23, no. 11, pages 2998–3004, nov 2009.

[Zeng 01] X. Zeng, J. Rose & J. Rice. *Stiffness and Damping Ratio of Rubber-Modified Asphalt Mixes: Potential Vibration Attenuation for High-Speed Railway Trackbeds*. Journal of Vibration and Control, vol. 7, no. 4, pages 527–538, may 2001.

[Zhang 01] P. Q. Zhang, J. H. Ruan & W. Z. Li. *Influence of some factors on the damping property of fiber-reinforced epoxy composites at low temperature*. Cryogenics, vol. 41, no. 4, pages 245–251, 2001.

[Zhang 05] M. Q. Zhang, M. Z. Rong & X. Lu. *Fully biodegradable natural fiber composites from renewable resources: All-plant fiber composites*. Composites Science and Technology, vol. 65, no. 15-16 SPEC. ISS., pages 2514–2525, 2005.

[Zhang 08] Y.-F. Zhang, S.-L. Bai, D.-Y. Yang, Z. Zhang & S. Kao-Walter. *Study on the viscoelastic properties of the epoxy surface by means of nanodynamic mechanical analysis*. Journal of Polymer Science Part B: Polymer Physics, vol. 46, no. 3, pages 281–288, 2008.

[Zhang 12] T. Zhang, S. L. Bai, Y. F. Zhang & B. Thibaut. *Viscoelastic properties of wood materials characterized by nanoindentation experiments*. Wood science and technology, vol. 46, no. 5, pages 1003–1016, 2012.

[Zhang 19] J. Zhang, A. A. Khatibi, E. Castanet, T. Baum, Z. Komeily-Nia, P. Vroman & X. Wang. *Effect of natural fibre reinforcement on the sound and vibration damping properties of bio-composites compression moulded by nonwoven mats*. Composites Communications, vol. 13, no. January, pages 12–17, 2019.

[Zhao 19] D. Zhao, H. Hamada & Y. Yang. *Influence of polyurethane dispersion as surface treatment on mechanical, thermal and dynamic mechanical properties of laminated woven*

carbon-fiber-reinforced polyamide 6 composites. Composites Part B: Engineering, vol. 160, no. December 2018, pages 535–545, 2019.

[Zhou 14] F. Zhou, G. Cheng & B. Jiang. *Effect of silane treatment on microstructure of sisal fibers*. Applied Surface Science, vol. 292, pages 806–812, feb 2014.

[Zierdt 15] P. Zierdt, T. Theumer, G. Kulkarni, V. Däumlich, J. Klehm, U. Hirsch & A. Weber. *Sustainable wood-plastic composites from bio-based polyamide 11 and chemically modified beech fibers*. Sustainable Materials and Technologies, vol. 6, pages 6–14, 2015.

[Zoghaib 15] L. Zoghaib & P.-O. Mattei. *Damping analysis of a free aluminum plate*. Journal of Vibration and Control, vol. 21, no. 11, pages 2083–2098, aug 2015.

Figures List

1 Partners in SSUCHY project 2
2 Technology roadmap of SSUCHY project 2
3 Five core objectives in SSUCHY project 3
4 Classification of plant fibers 7
5 (a) Absolute tensile properties of different series of fiber [Shah 14] (b) The schematic representation of the flax and hemp fiber structure 7
6 Different reinforcements and micro-structures of (a) short fiber [Datta 17] (b) non-crimp [Schrank 17, Liang 14](c) non-woven [Reinders , Martin 16] and (d) woven fabric [Song 12, Corbin 20b] 8
7 Schematic diagram of the thesis. 10

I.1 Ashby diagram: loss factor v.s. modulus at ambient temperature (summarized from refs.[Araújo 09, Duc 14b, Margem 10, Joseph 10, Jawaid 13, Towo 08, Saha 99, Mylsamy 11, Suresh Kumar 14, Sreenivasan 15, Ray 02, Pothan 03, Daoud 17, Shinoj 11, Karaduman 14, Mohanty 06, Etaati 14, Amenini 19, Mahmoudi 19, Li 17c, Ashworth 16, Cihan 19, Zhang 19, Essabir 13, El-Hafidi 17, Liang 10, Le Guen 16, Assarar 15, Rueppel 17, Madera-Santana 09, Mazuki 11]) 18
I.2 Energy dissipation in PFCs. 19
I.3 Mechanical properties of unidirectional (UD) fiber reinforced epoxy composites in the longitudinal direction (measured by DMA tests at 1 Hz and ambient temperature), summarized from refs. [Duc 14b, Mylsamy 11, Towo 08] 25
I.4 Variation of loss factor as function of fiber orientation in UD composites in longitudinal direction using modal tests (a) Flax/GP56, (b) Flax/PP, (c) Flax/Epoxy, (d) Glass/Epoxy [Daoud 17, Rueppel 17, Rahman 17b, Gao 11b]. 29
I.5 Loss factor and modulus of different polymers at 1 Hz and ambient temperature summarized from [Duc 14b, Margem 10, Ray 02, Shinoj 11, Madera-Santana 09, Martínez-Hernández 07, dos Santos Silva 19] (Polylactic acid 2, 4 (PLA 2, 4), and Polypropylene (PP), Polybutylene adipate-co-terephthalate (PBAT), Polymethyl methacrylate (PMMA)) 30

I.6 Young's modulus and loss factor of flax composites in the longitudinal direction and pure matrix measured by DMA at 1 Hz and ambient temperature (summarized from ref. [Duc 14b]) 31

I.7 Parameters related to the interface properties 31

I.8 Different kinds of composites 34

I.9 Young's modulus and loss factor of (a) wood fiber composites and (b) different kinds of composites based on DMA tests at 1 Hz and ambient temperature with respect to relative humidity and after water absorption (summarized from ref. [Bogren 06, Gu 09, Cheour 16] 34

I.10 Ashby diagrams of PFCs and SFCs: loss factor v.s. modulus (triangles are measured by modal tests at first mode and ambient temperature, circles are measured by DMA tests at 1 Hz and ambient temperature, empty symbols and full symbols mean horizontal axis are using storage modulus and Young's modulus, respectively. (summarized from refs. [Shah 13, Araújo 09, Duc 14b, Margem 10, Joseph 10, Jawaid 13, Towo 08, Saha 99, Mylsamy 11, Suresh Kumar 14, Sreenivasan 15, Ray 02, Pothan 03, Daoud 17, Shinoj 11, Karaduman 14, Mohanty 06, Etaati 14, Amenini 19, Mahmoudi 19, Li 17c, Ashworth 16, Cihan 19, Zhang 19, Essabir 13, El-Hafidi 17, Liang 10, Le Guen 16, Assarar 15, Rueppel 17, Madera-Santana 09, Mazuki 11]). 39

II.1 Mechanics of viscoelastic material under alternating stress: (a) Stress and strain curve, (b) Hysteresis loop 46

II.2 Typical dynamic mechanical properties of epoxy based composites . . 48

II.3 Main assets in Metravib® DMA+300 49

II.4 (a) Force measurement and (b) displacement measurement technologies in the used device. 49

II.5 Excitation in DMA tests 51

II.6 Verification of the excitation setup in DMA tests (a) Response of stress-strain under quasi-static tension (b) Storage modulus and loss factor with different static and dynamic forces under tension mode . . 51

II.7 Protocol changes during temperature sweep in DMA tests 52

II.8 Reinforcements used in this work: (a) Unidirectional flax tape, (b) Hemp4 - Satin fabric and Hemp6 - Twill fabric [Corbin 20b], (c) non-crimp flax/PP prepreg, (d) H4/PA12 prepreg (H4/PA12 refers to Hemp4 reinforced Polyamide 12 composites) 54

II.9 Temperature and pressure during fabrication of (a) (1) pure GreenPoxy and plant fiber/GreenPoxy composites (2) Pure petro-based epoxy and plant fiber/petro-based epoxy composites, (b) Hemp/PA12 composites. 56

II.10 Water aging test process 58

II.11 (a) Storage modulus and (b) loss factor of FGUD-L obtained from DMA test in bending and tension mode at 1 Hz (E-Static refers to monotonic test in tension). 59

II.12 Temperature cycle during DMA test 60

II.13 (a) Storage modulus and (b) loss factor of FGUD (post-curing at 130 °C and 1h) in transverse direction for each temperature cycles at 1 Hz. 61

II.14 Comparison of storage modulus and loss factor of pure GreenPoxy at 1 Hz and ambient temperature using the optimized curing time and the datasheet from Sicomin® (C60-1h refers to sample curing at 60 °C and 1 hour with post-curing at 130 °C and 1 hour, C60-16h refers to sample curing at 60 °C and 16 hour with post-curing at 100 °C and 1 hour) 62

II.15 Dynamic mechanical properties of GreenPoxy from -100 to 160 °C at 5 Hz. 63

II.16 (a) Storage modulus and (b) loss factor of pure matrix and Flax reinforced composites measured by DMA tests at 1 Hz and ambient temperature (value of Pure PP is refer to [Duc 14b]) 64

II.17 Loss factor of hemp fiber reinforced composites measured by DMA tests at 1 Hz and ambient temperature 68

II.18 Comparison between balanced hemp fabric/GreenPoxy composites and FGCR in (a) storage modulus and (b) loss factor at 1 Hz and ambient temperature 69

II.19 Mesostructure of H4/PA12 70

II.20 (a) Normalized storage modulus, (b) loss modulus, (c) loss factor of FFRC and pure matrix at 1 Hz and 30 - 160 °C 71

II.21 (a) Normalized storage modulus, (b) loss modulus, (c) loss factor of HFRC at 1 Hz and 30 - 160 °C (PA12 is collected from Ref. [Liao 18]) 73

II.22 (a) Storage modulus, (b) loss modulus, (c) loss factor of FGUD-T at 1-50 Hz and 30 - 160 °C, (e) Storage modulus, (f) loss modulus, (g) loss factor of H4-T at 1-50 Hz and 30 - 160 °C 75

II.23 Loss factor of FGUD, FPPC and Hemp4 at 0.01-100 Hz and ambient temperature 76

II.24 Master curve of loss factor for pure GE (reference temperature = 25 °C) . . . 77
II.25 Master curves of storage modulus and loss factor for GE, FGUD and H4 with T_{ref} = 25 °C. . . . 78
II.26 Cole-cole curve of (a) GE, (b) FGUD-T, (c) FGUD-L and (d) H4-L . 79
II.27 Mass gained versus water aging time in longitudinal and transverse direction. . . . 80
II.28 Mean curve of storage modulus and loss factor versus water aging time in (a) longitudinal direction(L) and in (b) transverse direction(T) 'M*i*-L(T)-1(2)', '*i*' refers to water aging day,'H' and 'C' means the heating and cooling process in DMA tests, respectively . . . 81
II.29 Changes in storage modulus and loss factor versus water aging time at 1 Hz and 30 °C in (a) longitudinal direction(L) and in (b) transverse direction(T) . . . 82
II.30 Ashby diagram using loss factor and Young's modulus measured at 1 Hz in this thesis (black, red and blue points are thermoset, thermoplastic based composites and water aged FGUD, respectively) 84

III.1 Method of damping calculation using (a) logarithmic decrement (b) half-power bandwidth. . . . 94
III.2 The shape of the sample for modal test in (a) free-free and (b) free-clamped boundary conditions (unit: mm) (Values are given in the Table III.3.2.a) . . . 95
III.3 Experimental setup in (a) free-free and (b) free-clamped boundary condition . . . 97
III.4 Schematic diagram of the experimental system . . . 97
III.5 Water aging test at ambient temperature . . . 98
III.6 Geometry of the sample for clamped boundary conditions (Unit: mm) . . . 100
III.7 The influence of lb and lc on modes 1-6 when la=4 (Different curve refers to different value of lb) . . . 102
III.8 The influence of la and lc on mode 1-6 when lb=40 (Different curve refers to different value of la) . . . 103
III.9 The influence of la and lb on modes 1-6 when lc=20 (Different curve refers to different value of la) . . . 103
III.10 Difference of loss factor under various values of la, lb and lc in modes 1-6 ((a)-(g)) (the blue points refer to difference (*err*) is less than 10 %, ■ refers to the final selected value) . . . 104

III.11Standard deviation on loss factor obtained 5 % variation around the nominal value of the parameters in experimental setup (tick: thickness of the sample, ρ: density of the composites, E_t and E_l: Young's modulus in transverse and longitudinal direction, υ_t and υ_l: Possion's ratio in transverse and longitudinal direction, G: shear modulus) 105

III.12(a) FRF results of numerical model and experiment, and (b) modal shape simulated by numerical model for FGUD in free-free conditions 106

III.13Comparison of the loss factor values determined for FUGD material in DMA and modal tests. (The resutls from DMA test is at 1 Hz and modal tests are obtained from the flexual modes in longitudinal direction (around 244 Hz) and transverse direction (204 Hz)) 107

III.14(a) FRF from numerical model and experiment, and (b) modal shape in numerical model for FPPC in free-free conditions 108

III.15(a) FRF from numerical model and experiment, and (b) modal shape in numerical model for H4 in free-free condition 110

III.16Modal response of FGUD in (a) longitudinal direction, and (b) transverse direction 111

III.17Modal response of FPPC in longitudinal direction 112

III.18Modal response of H4 in (a) longitudinal direction, and (b) transverse direction 113

III.19Damping ratios measured under free-free and free-clamped boundary conditions. 115

III.20Loss factor in Modal and DMA tests. (Modal-clamp and modal-free refer to modal tests under free-clamped and free-free boundary conditions) 116

III.21Superimposition of the loss factor master curves identified from DMA tests and loss factor values identified from modal tests for FUGD 116

III.22Results of water aging tests for gained mass as a function of square root of time. 117

III.23Results of water aging tests for (a) normalized storage modulus and (b) loss factor as a function of gained mass in L and T direction 117

III.24The deformation of the tested plate during water aging 118

IV.1 (a) Typical loading-unloading curves (P_{max} is the maximum load during nanoindentation, h_f is the depth of the residual indentation, h_{max} is the depth from the original sample surface at load P_{max}) (b) Profile change after indentation (h_s is the distance from the edge of the contact to the surface, $h_s + h_c = h_{max}$, h_c is the contact depth measured from maximum depth h_{max}) 126

IV.2 Protocols for viscoelastic properties measurement from (a) creep and relaxation tests (b) CSM method 127

IV.3 Sample for nanoindentation tests of (a),(b) neat resin and (c) FGUD 129

IV.4 (a) Anton Paar Nanoindentation Instrument (b) Dynamic mechanical model of viscoelastic material in the test system (c) Shape of Berkovich indenter [Fischer-Cripps 11] 130

IV.5 Protocols for viscoelastic properties measurement of (a) CAM method (b) CSM+CAM method. 131

IV.6 Post-processing of the load and displacement for damping identification 132

IV.7 Schematic diagram of nanoindentation for (a) GreenPoxy using the CAM protocol at 1 - 40 Hz and 30 - 85 °C (b) suggested protocol inthe future plan 133

IV.8 Schematic diagram of nanoindentation for FGUD using (a) CSM at 5 Hz and (b) CAM method at 1 Hz and 5 Hz 134

IV.9 Loss factor as a function of frequency (1 - 40 Hz) in GreenPoxy determined using DMA and DNI tests at various temperatures (a) 30 °C, (b) 45 °C, (c) 55 °C and (d) 65 °C 136

IV.10 Force and displacement signal versus time at (a) 1 Hz, (b) 5 Hz and (c) 40 Hz 137

IV.11 Storage modulus as a function of frequency (1 - 40 Hz) in pure resin determined using DMA and DNI tests at various temperatures (a) 30 °C (b) 45 °C (c) 55 °C (d) 65 °C 137

IV.12 (a) Comparison of loss factor in DMA and nanoindentation (NI) tests at the temperature near T_g zone (b) temperature changes based on numerical model. 138

IV.13 Static mechanical properties of FGUD (a) microstructure on the surface (b) experimental loading-unloading curves for different zones (confined resin is in the closed boundary with black line) 139

IV.14 Dependence on penetration depth of (a) the storage modulus and (b) loss factor obtained by typical CSM method at 5 Hz. 140

IV.15 Storage modulus and loss factor for each point along a line at 5 Hz . . 141

IV.16 Reduced modulus of hemp fiber collected from Ref. [Perrier 16] 141

IV.17(a) Storage modulus and (b) loss factor at 5 Hz versus distance from each fiber edge 142

IV.18Storage modulus and loss factor in each component using CSM method at 5 Hz (single point in confined zone without errorbar) 142

IV.19Map on the cross section based on results from nanoindentation (a) storage modulus (b) loss factor at 5 Hz with CSM method. 143

IV.20(a) Micro-structure on the cross section after nanoindentation tests, (b) storage modulus and (c) loss factor at 1 Hz and 5 Hz versus distance from each fiber edge 144

IV.21(a) Storage modulus and (b) Loss factor in each component at 1 and 5 Hz using CAM method. 145

IV.22Map on the cross section based on the results from storage modulus and loss factor at 5 Hz using (a) - (b) CSM and (c) - (d) CAM method on the same sample 146

IV.23Comparison of (a) storage modulus and (b) loss factor at 5 Hz obtained from CSM and CAM method on the same sample 147

IV.24Reduced modulus and Young's modulus collected from Refs. [Arnould 17, Bertinetti 15, Perrier 16, Tanguy 16, Bourmaud 18] 147

IV.25Comparison of loss factor in GreenPoxy identified from DMA tests, FGUD identified from DMA and modal tests and fiber zone identified from nanoindentation tests based on CAM and CSM method using the average value 148

A.1 Influence of (a) amplitude of excitation and (b) position of measurement on the damping ratio identification under free-free boundary condition 163

Tables List

I.1 Main features in mesoscale parameters. 24

I.2 Main features in micro scale parameters 32

I.3 Main features in surrounding conditions 36

II.1 Dynamic mechanical parameters in DMA tests 47

II.2 Configrations for each materials in DMA tests (D_{DMA}: Dimension, F_{sta}: Static force, F_{dyn}: Dynamic force, T_{DMA}: temperature range, f_{DMA}: frequency range, FGUD: UD Flax/GreePoxy composites, FPGE: Flax/Petro-based epoxy composites, FPPC: Flax/Polypropylene composites, HFRC: Hemp fabric composites, H4: Hemp4/GreenPoxy composites, L and T refer to longitudinal and transverse direction) . . 52

II.3 Hemp fabric with different woven patterns 53

II.4 Components in each product 55

II.5 Static mechanical properties of different type PFCs (mean value + standard deviation) 58

II.6 T_g of FGUD-T as a funtion of temperature cycle in DMA tests (T_g 1: T_g in the first loop, T_g 8: T_g in the last loop, difference=T_g 8 - T_g 1) 61

II.7 Values of storage modulus (E′) determined at 1 Hz using DMA tests and Young's modulus determined using monotonic tests (E_{static}) (FGCR refers to cross-ply flax/GreenPoxy composites) 65

II.8 Dynamic mechanical properties at 1 Hz, 30 °C and T_g (E′ and loss factor are measured at 30 °C, E′_T_g and loss factor-T_g are measured at T_g) 74

III.1 Dimensions of the different plates and specimens used for modal tests in free-free and free-clamped configurations (Unit: mm) 96

III.2 Mechanical properties of different materials 100

III.3 Mechanical properties of different materials 101

III.4 Selected lc for modes 1-6 when la=4. 102

III.5 Selected la for modes 1-6 when lb=40 102

III.6 Selected range of la for modes 1-6 when lc=20. 104

III.7 Results of modal analysis of FGUD in free-free conditions (f_{exp} and f_{num} refers to natural frequency from experiment and numerical model, respectively, 'Tor' and 'Fle' refer to torsion and flexural mode, L and T refer to longitudinal and transverse direction, respectively) . 107

III.8 Results of modal analysis of FPPC in free-free conditions (f_{exp} and f_{num} refers to natural frequency from experiment and numerical model, respectively) 109

III.9 Results of modal analysis of H4 in free-free conditions (f_{exp} and f_{num} refers to natural frequency from experiment and numerical model, respectively) 110

III.10 Results of modal analysis of FGUD in free-clamped conditions (f_{exp} and f_{num} refers to natural frequency from experiment and numerical model, respectively) (The results from experiment are using the average values of three samples, std refer to their standard deviation) 112

III.11 Results of modal analysis of FPPC in free-clamped conditions (f_{exp} and f_{num} refers to natural frequency from experiment and numerical model, respectively). (The results from experiment are using the average values of three samples, std refer to their standard deviation). 113

III.12 Results of modal analysis of H4 in free-clamped conditions (f_{exp} and f_{num} refers to natural frequency from experiment and numerical model, respectively) (The results from experiment are using the average values of three samples, std refer to their standard deviation) 114

IV.1 Comparison of the effect from two terms in fiber, matrix, fiber-fiber (F-F) interface and fiber-matrix (F-M) interface at 5 Hz. 135

sPIM

Titre : Caractérisation multi-échelle de l'amortissement des matériaux composites à fibres végétales

Mots clefs: Propriétés d'amortissement, identification de l'amortissement, composites de fibres végétales, méthode multi-échelles

Résumé : Les vibrations et le bruit sont des problèmes inévitables dans les produits d'ingénierie et la vie quotidienne. Il est donc indispensable de connaître les performances d'amortissement des matériaux d'ingénierie et les facteurs qui affectent les dites propriétés. Les composites à base de fibres végétales (PFC) sont devenus une nouvelle option lorsqu'il s'agit de trouver un compromis entre l'amortissement et la rigidité. Les recherches actuelles sur l'amortissement sont principalement menées à l'échelle macro scopique et les sources et les mécanismes d'amortissement des composites de fibres végétales sont complexes et encore mal compris.
Ainsi, l'objectif de cette de proposer une caractérisation fine et une meilleure compréhension de l'amortissement dans les composites biosourcés à l'aide d'une approche expérimentale multi-échelle. Cette thèse commence par une revue de la littérature sur le comportement d'amortissement des PFC. Ensuite, les influences de nombreux paramètres, y compris les types de matrice et de fibres, l'architecture du renfort, la température, la fréquence et la teneur en humidité sur les propriétés d'amortissement des PFC, sont étudiées sur la base d'une analyse mécanique dynamique (DMA) et d'une analyse modale. Les propriétés d'amortissement des constituants sont également déterminées in situ grâce des des essais en nanoindentation dynamique. Un protocole de chargement à amplitude constant est proposé en alternative à la méthode dynamique traditionnelle de raideur de contact (CSM). Les résultats sont comparés à ceux obtenus par l'analyse mécanique dynamique et méthodes de test modal. Les résultats montrent la contribution de chaque composant (fibre, matrice et interface) sur la dissipation d'énergie. En fin, les propriétés d'amortissement déterminées à ces différentes échelles à l'aide de ces trois techniques expérimentales sont tracées sur une concernant la large gamme de fréquences et de températures.

Title : Multi-scale damping characterization of plant fiber composite materials

Keywords : Damping properties, Damping identification, Plant fiber composites, Multiscale method

Abstract : Vibration and noise are unavoidable problems in engineering products and daily life. Thus, the knowledge of the damping performances of engineering materials and the factors that affect these properties are highly required. Plant fiber composites (PFCs) have become a new option when considering the compromise between damping and stiffness. Current researches on damping are mainly work at the macroscale and the damping sources and mechanisms in plant fiber composites are complex and not fully revealed.
Thus, the main objective of this thesis is to provide a better characterization and understanding of damping in PFCs using various experimental techniques at different scales and on a wide range of frequency. This thesis starts with the review of literature on the damping behavior of PFCs. Then, the influences of many parameters including matrix types, fiber architecture, woven pattern, temperature, frequency and moisture content on the damping properties of PFCs are investigated based on dynamic mechanical analysis (DMA) and modal analysis. Furthermore, a constant amplitude method as well as constant stiffness method are used to map the in situ damping properties at the microscale based on grid dynamic Nanoindentation (DNI). These results are then compared to those obtained from dynamic mechanical analysis and modal test methods. The results from DNI show the contribution of each component (fiber, matrix and interface) on energy dissipation. Finally, the damping properties measured using these three experimental techniques at the three different scales are plotted on a wide frequency and temperature range.

UBFC UNIVERSITÉ BOURGOGNE FRANCHE-COMTÉ
Université Bourgogne Franche-Comté
32, avenue de l'Observatoire
25000 Besançon